Resolving Relationships between Deep-sea Benthic Diversity and Multi-scale Topographic Heterogeneity

by

Cherisse Du Preez
B.Sc., University of Victoria, 2008

A Dissertation Submitted in Partial Fulfillment of the
Requirements for the Degree of

DOCTOR OF PHILOSOPHY

in the Department of Biology

Supervisory Committee

Resolving Relationships between Deep-sea Benthic Diversity
and Multi-scale Topographic Heterogeneity

by

Cherisse Du Preez
B.Sc., University of Victoria, 2008

Supervisory Committee

Dr. Verena Tunnicliffe, Supervisor
(Department of Biology)

Dr. Henry Reiswig, Member
(Department of Biology)

Dr. Kim Juniper, Member
(Department of Biology)

Dr. Rosaline Canessa, Outside Member
(Department of Geography)

Abstract

Supervisory Committee

Dr. Verena Tunnicliffe, Supervisor
(Department of Biology)

Dr. Henry Reiswig, Member
(Department of Biology)

Dr. Kim Juniper, Member
(Department of Biology)

Dr. Rosaline Canessa, Outside Member
(Department of Geography)

Resolving diversity patterns and their underlying drivers has application for both ecological theory and ocean management. Because seafloor characteristics are often used to assess bottom habitat, I examined the relationship between deep-sea benthic (bottom-living) diversity and multi-scale topographic heterogeneity. Most work occurred on the Canadian Pacific continental shelf at Learmonth Bank with additional sites in Strait of Georgia (BC) and Gulf of Maine (Atlantic shelf). High-resolution species distribution and seafloor data were annotated from remotely operated vehicle benthic imagery surveys while large-scale seafloor data were derived from multibeam sonar.

New method development to address problems of current methods and to facilitate comparison among ecosystems is a major outcome. My new MiLS method (microtopographic laser scanning) can profile the deep seafloor at a resolution of ~1-2 cm with high accuracy and precision. I also developed a new ACR (arc-chord ratio) rugosity index as a measure of 3-D topographic heterogeneity that is simple, accurate and highly versatile.

Model systems and scales vary among my studies but results consistently yield a positive relationship between diversity and topographic heterogeneity and identify bottom hydrodynamics as an important underlying driver. Rockfish *Sebastes* spp. associate with higher seafloor rugosity non-randomly and select for deep-sea corals and

sponges over inert substrata alone. Data indicate that degradation of biogenic structures is a long-term detriment to rockfish species. Gorgonian coral- and sponge-dominant biotopes strongly associate with a single substratum type. These relationships were used to map coral and sponge distributions. This work, which collectively adds new information on the ecological relevance and distribution of corals and sponges, is pertinent to the conservation and management of fish stocks and vulnerable marine ecosystems. Epibenthic community variables abundance, richness, and Shannon diversity positively correlated with both the local microtopographic heterogeneity on a scale of 10 m^2 and with the surrounding regional large-scale topographic heterogeneity on scales of 25 to 250,000 m^2. Relationships were strongest between epibenthic community variables and the largest scale rugosity and were used to generate and test predictive diversity models. Where management strategies rely on surrogate measures in data-poor areas, mapping benthic diversity using ACR rugosity will provide good indicators.

Although bottom hydrodynamics is consistently identified as an underlying driver of epibenthic patterns related to topographic heterogeneity, data suggest the nature of the relationship varies across spatial scales. At small scales, high topographic heterogeneity likely increases diversity by increasing the number of available niches (including hydrodynamic gradients; e.g., the abrupt vertical rugosity created by tall corals and sponges provides rockfish refuge from currents) while at large scales, high topographic heterogeneity increases local diversity less directly through distant hydraulic events that alter bottom flow hydrodynamics.

Table of Contents

List of Tables

List of Figures

Acknowledgments

I cannot thank my supervisor and mentor, Verena Tunnicliffe, enough for the privilege of being her graduate student. From day one Verena implored me to "enjoy the experience" and I can honestly say I have never enjoyed anything more —it has been the adventure of a lifetime. Thank for the amazing opportunities and for the freedom to make it my own.

I would like to thank Kim Juniper, Henry Reiswig, and Rosaline Canessa for their direction, support and advice throughout this project. I am extremely thankful to Rosaline Canessa for going over and above in introducing me to the wonderful world of GIS. Additional thanks to Frédéric Guichard for his valuable input as my external examiner.

I am very grateful to the Tunnicliffe Lab past and present (like siblings, you survived together): Jonathan Rose, Candice St. Germain, Heidi Gartner, Jen Tyler, Jackson Chu, Lara Puetz; and to my departmental peers (the academic equivalent of cousins, you understand the crazy): Nathalie Forget, Sheryl Murdock, Steve Leaver, Valerie Ethier, Anne Mchale, Jacques St Laurent, and Lianna Teeter.

I am extremely grateful to have been part of the Canadian Healthy Oceans Network (CHONe). It enriched my graduate research and my experience immeasurably. Special thanks to Paul Snelgrove, Peter Lawton, Evan Edinger, Joan Atkinson, Susan Curtis, Philippe Archambault, and Anna Metaxas.

Exploring the deep sea requires a great deal of support and infrastructure and my research would not have been possible without CHONe, NSERC, the University of Victoria, DFO, ArcticNet, J. Vaughn Barrie, personnel of the Canadian Scientific Submersible Facility, and the CCGS Hudson and Tully. I would like to especially thank DFO personnel Jim Boutilier, James Pegg, and Janelle Curtis for their interest in my research.

To my family for all their love and support, and for inspiring me daily: Yvonne, Angel, and Shelton Du Preez. I'm not entirely sure which of us loves the ocean more but if the competition is judge on years invested: I win. My sincere thanks to Rick and Phillipa Hudson for threatening my life if I didn't go back to school.

If I managed to keep a smig of sanity through this its owing in large to my wonderful distractions: Courtney Sims, the Velox Valkryies, rugby, crossfit and my Pops.

Dedications

For Dr. Verena Tunnicliffe.

“If I have seen further it is by standing on the shoulders of Giants”

~Isaac Newton

For my family, who challenge and inspire me to live an extraordinary life.

For three old men of the sea.

My father Lawrence Du Preez,

my grandfather Denise Glazer &

my friend Mr Yousuf Ebrahim.

Chapter 1: Introduction

Background

Management of marine ecosystems often requires more comprehensive information than existing biological data can provide. In such situations it is extremely valuable to have identified robust ecological patterns that can be extrapolated to predict baseline information for data-poor areas. For conservation and management efforts, diversity is the single most assessed biological component of marine ecosystems (Corrigan and Kershaw, 2008). Not only is diversity an index of biological variability but strong scientific evidence has indicated marine diversity has positive linkages with ecosystem functions, services, stability, and recovery potential (Worm et al., 2006). There are many suspected driving forces behind diversity (e.g., productivity, predation, competition, disturbance). The hypothesis of a positive relationship between diversity and topographic heterogeneity originated in terrestrial restoration (Larkin et al., 2006) but is now a widely accepted ecological pattern in terrestrial and aquatic ecosystems (e.g., forest, wetland, intertidal, marine, freshwater; Levin, 1974; Huston, 1979; Beatty 1984; Cusson and Bourget, 1997; Beck 1998; Levin et al., 2001; Gratwicke and Speight, 2005; Dufour et al., 2006; Larkin et al., 2006; Moser et al., 2007; Schlacher et al., 2007; Shumway et al., 2007; Walker et al., 2009; Bridge et al., 2011). Topographic heterogeneity is defined as a variation in elevation over a specific area and accounts for characteristics that are both vertical (e.g., the minimum and maximum elevation) and horizontal (e.g., frequencies in elevation changes; Larkin et al. 2006). The general hypothesis is that topographic heterogeneity increases overall diversity by increasing the number of available niches,

increasing ways of exploiting environmental resources and decreasing species exclusion through reduced interspecific competition (Levin, 1974; Huston, 1979; Larkin et al., 2006). Topographic heterogeneity has long been recognized as a key ecological variable (e.g., Watson, 1835) and, over the years, has been referred to as several interchangeable terms, including topographic roughness, complexity, variability, and rugosity.

Topographic heterogeneity as a surrogate for marine benthic diversity

A surrogate is a relatively easily measurable component of an ecosystem that effectively indicates a more difficult to measure pattern. Once a potential surrogate is identified and studied to sufficient detail, a statistical model of the surrogacy relationship is generated, validated, and used to extrapolate data. Topographic heterogeneity is a promising abiotic surrogate for marine benthic diversity (McArthur et al., 2010) with other potential surrogates including both biological and physical variables (e.g., higher-taxa, foundation species, depth, slope, temperature, oxygen-level; McArthur et al., 2010; Mellin et al., 2011).

In marine ecosystems, topographic heterogeneity is created by geologic (e.g., canyons and seamounts), hydraulic (e.g., sand dunes and wave-cut terraces), and biotic (e.g., reefs and mounds) processes (Larkin et al., 2006), and affects benthic diversity patterns by influencing the available surface for settlement and growth, access to nutrients, disturbance (in mobile sediment), protection from predation, juvenile nursery grounds, and exposure or shelter. The relationship between diversity and topographic heterogeneity is so well established on tropical coral reefs that measuring local *in situ* topographic heterogeneity is part of ecological reef monitoring programs worldwide (Hill and Wilkinson, 2004). But studies on fish communities and coral reefs constitute the majority of empirical research demonstrating this relationship (e.g., Gratwicke and

Speight, 2005; Walker et al., 2009) even though, on a global scale, tropical coral reefs are a rare habitat (<<1 % the ocean floor; Spalding et al., 2001). Coral reef based studies represent a bias in research on the relationship between diversity and topographic heterogeneity towards easily accessible marine habitats (where intertidal and other shallow subtidal habitats are also relatively well studied; e.g., Cusson and Bourget, 1997; Beck 1998) while the relationship remains poorly documented in the deepsea.

Of the few studies that document faunal distributions in relation to small-scale topographic structures in deeper marine ecosystems, the majority focus on the heterogeneity created by discrete categories of biogenic structures (e.g., Levin et al., 1986; Bett and Rice, 1992; Buhl-Mortensen et al., 2010). From these studies, it is difficult, if not impossible, to discern whether it is a biologic or abiotic quality of these structures which results in the high diversity patterns observed. At larger scales in the deepsea it has long been recognized that complex topographic features, such as seamounts (Stocks and Hart, 2008) and canyons (De Leo et al., 2014), support enhanced diversity but research to identify and understand the drivers is ongoing.

Generic issues related to scale and spatial analyses have further limited research on the relationship between marine benthic diversity and topographic heterogeneity. In spatial ecology, scale refers to the resolution (grain size) and the extent (area) of a study (Wu, 2004). The scale-dependence of detecting spatial patterns has long been recognized (Wu, 2004) yet often studies will often use single-scale values (resolution and extent) arbitrarily set by a sampling method with no ecological relevance (Chave, 2013). This lack of comprehensive investigation into scale-dependent variation undermines the interpretation and usefulness of such studies (Wu, 2004). In measuring topographic

heterogeneity, roughness metric such as rugosity are predicted to decrease with decreasing resolution (i.e., increasing grain size) while it is more difficult to predict the effect of changing extent (Wu, 2004). In trying to detect diversity patterns, it is suggested the size (extent) of the organisms may be the most relevant to investigate (Jumars, 1976) but ecological processes act at a variety of spatial and temporal scales and generate patterns at scales that may differ from that at which the processes act (Levin, 1992). This cross-scale relationship works in both directions; for example, topographic heterogeneity at one scale can lead to biological responses measurable over larger or smaller scale (e.g., Netto et al., 1999; Barros et al., 2004). Multi-scale (resolution and extent) studies are thus crucial to resolve the relationship between marine benthic diversity and topographic heterogeneity.

The limited scope of marine research on this relationship to date warrants caution when considering topographic heterogeneity as a surrogate for marine benthic diversity. Generalizing and extrapolating patterns is a ubiquitous problem in ecology—biological and environmental processes, hence the underlying causes of a relationship, differ among species assemblages, ecosystems, and temporal and spatial scales (Chave, 2013; Levin, 1992). Cases of no detectable relationship between benthic diversity and topographic heterogeneity (e.g., gastropods in mangrove habitats, Beck 1998; macroinvertebrates in reef habitats, Alexander et al., 2009) support the need for more comprehensive research on the relationship in a wider range of marine habitats prior to using topographic heterogeneity as a surrogate for marine benthic diversity.

Application in deep continental shelf ecosystems

Deep continental shelf ecosystems represent a pertinent example of the need to expand the scope of studies validating and resolving the relationship between marine benthic

diversity and topographic heterogeneity. Conservation and management efforts for deep continental shelf ecosystems (e.g., deep-sea sponge and coral ecosystems) would greatly benefit from the ability to use topographic heterogeneity reliably as a surrogate for marine benthic diversity. These ecosystems are limited in existing biological data but are in need of greater conservation and management efforts owing to increasing anthropogenic influences (notably global warming and habitat alteration) and vulnerability to exploitation (Pauly et al., 2003; Ardron et al., 2007; Levin et al., 2010; Ramirez-Llodra et al., 2011). In contrast to existing biological data, there is a great deal of seafloor topographic data from continental shelves as remote sensing techniques that can be used to map topography at relatively large-scales with high-resolution (e.g., multibeam bathymetric sonar).

Microtopographic heterogeneity and biogenic structures

Understanding the relationship between marine benthic diversity and topographic heterogeneity has application in marine conservation and management apart from the potential use of topographic heterogeneity as an abiotic surrogate. Establishing the effect of microtopographic (small-scale) heterogeneity on diversity has application in restoration projects (e.g., designing optimal artificial reefs and structures; Spieler et al., 2001; Sherman et al., 2002) and in managing fishing activities. Mobile bottom-contact fishing gear (e.g., bottom trawls) degrades microtopographic heterogeneity by flattening the sediment and by removing biogenic structures (Ardron et al., 2007; Heifetz et al., 2009; Ramirez-Llodra et al., 2011). Individual biogenic structures, such as deep-sea sponges and corals, add microtopographic heterogeneity to the underlying abiotic substrate while reef-forming species can create seafloor structures at scales of 100s of meters to kilometers (Levin et al., 2010). The functional significance of the

microtopographic heterogeneity created by biogenic structures to associated benthic fauna remains unclear but resolving the importance of the topographic heterogeneity they create may have implications in managing the negative effect of mobile fishing gear. Examples of benthic fauna that associate with deep-sea sponges and corals include both commercial and endangered rockfish *Sebastes* spp. (Family Scorpaenidae; Krieger and Ito, 1999; Husebø et al., 2002; Krieger and Wing, 2002; Freese and Wing, 2003).

Hydrodynamics as a potential underlying driver

To demonstrate effectively the validity of an ecological pattern requires an understanding of the underlying drivers (Levin, 1992; Chave, 2013). Hydrodynamic processes are major controlling factors of life in an aquatic ecosystems (Schrohenloher, 1981). Bottom flow hydrodynamics at local and regional scales affect benthic diversity through many processes, including larval delivery and recruitment, delivery of oxygen and nutrients (e.g., particulate organic matter flux and bacterial production), feeding opportunities, removal of waste, the passive collection or dispersal of organisms, suspension and deposition of sediment (i.e., available substrate and turbidity), scouring and erosion of sediment and of organisms, and levels of biotic and abiotic disturbance (Schrohenloher, 1981; Butman, 1987; Levin et al., 2001; McArthur et al., 2010; Bianchi et al., 2011; Levin and Sibuet, 2012; Elahi et al., 2014). In the intertidal, a few studies have successfully demonstrated a link between microtopographic heterogeneity, flow velocity, and the benthos community structure (Cusson and Bourget, 1997; Guichard and Bourget, 1998; Guichard et al., 2001; Barros et al., 2004). In the shallow subtidal, study results are not as conclusive but still suggest the relationship between infaunal assemblage structure and topography is mediated by hydrodynamic regimes (Netto et al., 1999; Barros et al., 2004). If topographic heterogeneity is an indicator of hydrodynamic

regime, the landscape metric is a temporally integrated measure of the local variation in current speed and direction (e.g., tidal driven currents).

Identifying the underlying drivers of the relationship between marine benthic diversity and topographic heterogeneity may be another benefit to expanding the scope of studies into the deepsea. In comparison to shallow-water fauna, deep-sea organisms are more strongly linked to the seafloor, relatively fixed in space, and in low densities (Snelgrove and Smith, 2002). Accurately surveying sessile and sedentary fauna is substantially easier than surveying mobile fauna and, at low densities, subtle differences in species' preferences may be more effective at distributing species into patterns than at high densities, when populations would overflow onto less preferred areas (Huston, 1979).

Research objectives

My thesis work is part of the Canadian Healthy Oceans Network (CHONe), a nationwide diversity initiative to develop scientific approaches for the sustainability of Canada's oceans. The main objective of my thesis was to resolve the relationship between marine benthic diversity and multi-scale topographic heterogeneity in deep continental shelf ecosystems, thereby to ultimately inform conservation and management decisions. My major research objectives were:

1. to develop a method to measure microtopography (high resolution small-scale topography) in remote deep-sea environments (Chapter 2),
2. to develop a new rugosity index for quantifying three-dimensional topographic heterogeneity (Chapter 3),

3. to test the hypothesis of a positive relationship between marine benthic diversity and topographic heterogeneity in the deepsea and explore hydrodynamics as an underlying driver:
    a. by investigating the distribution of benthic fish in response to substratum type, biogenic structures, and trawling in a deep continental shelf environment (Chapter 4), and
    b. by investigating the relationship between local epibenthic diversity and multiple scales (resolution and extent) of topographic heterogeneity within several deep continental shelf environments (Chapter 5).

Methodological approach

Study site

All my research study sites are in deep-sea ecosystems on the Canadian continental shelf. Two are in the Gulf of Maine off the Atlantic coast, in the Jordan Basin (43°19'N, 67°03'W) and the Northeast Channel (41°59'N, 65°38'W). One is in the Strait of Georgia off the Pacific coast, on Coral Knoll (49°22'N, 123°53'W). One is in Dixon Entrance north of Haida G'waii, and covers an extensive area on and around Learmonth Bank (54°29'N, 133°00'W). The first three study sites are included only in Chapter 5 while Learmonth Bank is included in all of my research chapters.

Learmonth Bank offers unique research opportunities to marine scientists interested in marine benthic diversity. Approximately half of the Learmonth Bank area is regarded as a 'hotspot' for bottom trawling (Sinclair et al., 2005) while the other half remains unfished and pristine owing to a maritime boundary dispute between Canada and the USA (Gray, 1997) thus the Bank hosts a rare juxtaposition of these two levels of trawling activity.

Learmonth Bank has a range of glaciated bathymetric features with high abundance of deep-sea sponges, corals, and rockfish.

Biological summary statistics

The concept of diversity is ubiquitous in ecology but it has many definitions and is represented by a variety of summary statistics (Ricotta, 2005). In general, a species diversity index represents the number of species present in a community and the relative proportion of their abundances (Pielou, 1977). All diversity statistics suffer from the defect that they are not sufficiently widely applicable (Pielou, 1977) but the most widely used diversity index, and the one I use in my thesis research, is the Shannon diversity index (also known as the Shannon-Weaver index, the Shannon-Wiener index, the Shannon's diversity index, and Shannon entropy). My rational for selecting the most common index is to increases the comparability of my findings with other studies and with different habitats.

The Shannon diversity index is a function of richness and evenness: $H' = \sum_{i=1}^{R} p_i \ln p_i$ where p_i is the proportion of species i. The Shannon index has values 0 and higher, where 0 represents no uncertainty in predicting the identification in a randomly selected individual and values >> 0 represent a higher diversity. I calculate and analyse both alpha diversity (α-diversity) and beta diversity (β-diversity). I present α-diversity as the mean diversity in a site and β-diversity (turnover) as the extent to which diversity of the entire site (gamma diversity; γ-diversity) is greater than the diversity of an average sample (Magurran, 2004).

Even though the objective of a diversity index is to summarize the biological characteristics of a community, diversity indices are heavily criticised for their inherent

loss of information. For this reason, throughout my chapters, I retain and analyse abundance and richness data. I present abundance (*N*) as the sum of discrete counts of all organisms and richness (*S*) as the total number of species.

Terminology

The term used in reference to topographic heterogeneity differs among some of my research chapters and appendices. The terms are interchangeable in the scientific literature and include rugosity, roughness, abrupt vertical relief, and structural complexity. Five of my chapters and appendices are published or submitted manuscripts in different peer-reviewed journals and technical reports. The term used in each manuscript reflects the publication's target audience. Within this thesis, these terms should be considered synonymous with topographic heterogeneity.

Rugosity: a measure of topographic heterogeneity

There are many indices and methods used to measure topographic heterogeneity, ranging from descriptive to counts of discrete structures, from categorical to quantitative (McCormick, 1994). An advantage of quantified indices is their comparability between different habitats and studies (Beck, 1998). Where limited topographic data were available for my research project detailed in Chapter 4, I used a simple measure of vertical relief. Where topographic data (2-D or 3-D) were available, I used rugosity as a measure of topographic heterogeneity. Rugosity is the most common technique in marine studies (e.g., Hills and Thomason, 1996; Brock et al., 2004; Dolan et al., 2008; Dunn and Halpin, 2009; Walker et al., 2009); Risk's (1972) 'chain and tape' method is the common method to measure rugosity. Two-dimensional rugosity is defined as the ratio between the surface contour distance and the linear distance between two points (Risk, 1972) and is synonymous with the term tortuosity or the arc-chord ratio (Moser et al., 2007).

Rugosity encompasses and combines both structural relief and roughness (Moser et al., 2007), where a flat surface has a value of 1 and a high rugose surface yields value >>1. Rugosity can also be calculated for three-dimensional surfaces although there is no consensus of a standard calculation at present. The most common calculation defines three-dimensional rugosity as a ratio between the contour area of the surface and the area of the surface orthogonally projected onto a horizontal plane (e.g., Jenness, 2004). I present a refined approach in Chapter 3.

New methodological approaches

The deepsea is a challenging place to conduct research owing to its remoteness and extreme conditions. Sampling techniques that are relatively easy in terrestrial or shallow aquatic habitats usually require significant modification, or complete renovation, for application in the deepsea. A large component of my thesis research was developing new methods in deep-sea research. In Chapters 2 and 3 and in Appendix E, I present new methods in deep-sea research that I developed to enable my own research and to aid future research. Although these methods were developed for use in the deepsea, each is adaptable for use in nearly any terrestrial and aquatic habitat.

Microtopographic laser scanning (MiLS)

Chapter 2 describes the new video survey method of microtopographic laser scanning (MiLS) that essentially profiles substratum microtopography using a low-flying platform with an attached optical camera-laser array. The resulting high-resolution profile can be analysed in a variety of ways but we demonstrate how it can be analysed for microtopographic heterogeneity measured as rugosity. In two case studies we demonstrate the usage and advantage of the MiLS method, including how it can be used

in sensitive deep-sea research to noninvasively measure the *in situ* rugosity of fragile deep-sea sponges and corals. This chapter was published in the peer-reviewed journal *Limnology and Oceanography: Methods* (Du Preez and Tunnicliffe, 2012) with a web appendix of a workable spreadsheet to aid in analysis (*see* Appendix B).

Arc-chord ratio (ACR) rugosity

Chapter 3 describes the new arc-chord ratio (ACR) rugosity index. Not long into my graduate program I became aware of significant issues with how three-dimensional rugosity is presently measured. For my research I required a rugosity index that overcame these issues. The ACR rugosity index builds on the two-dimensional rugosity definition and equation I use in Chapter 2 and is simple, accurate, and extremely versatile. In Chapter 3 I describe the ACR method in general, so that it may be applied to a range of rugosity analyses. I detail its application for the three most common analyses. I also provide ArcGIS® resources (i.e., systematic instructions and automated geoprocessing models in Appendix C-D).

This chapter is published in the peer-reviewed journal *Landscape Ecology* (Du Preez, 2014).

Benthic imagery surveys

All of my thesis research projects used remotely operated vehicles (ROVs) to conduct deep-sea benthic imagery surveys. An ROV is an unmanned submersible, controlled remotely from a ship via a tethering cable. Throughout my chapters I detail new ROV survey methods I developed for specific research projects. During my graduate program I joined the scientific crew on over a dozen ROV cruises and most were not for my own thesis research. While aboard I learnt many best practices that are very valuable but had no place in my thesis. In Appendix E I summarize these best practices and tips in a

scientist's guide to using ROVs for benthic imagery surveys. This appendix has been submitted as a method article for the *Department of Fisheries and Oceans Technical Report* "Recent research studies on seabed structure and benthic diversity relationships in Canadian Marine habitats" (Du Preez et al., *in review*).

Major research questions

Benthic fish and biogenic structures

In Chapter 2, I examine the distribution of Scorpaenidae benthic fish in response to substratum, biogenic structures and trawling at Learmonth Bank. I indentify the importance of the microtopographic heterogeneity created by deep-sea sponges and corals for rockfish *Sebastes* spp. abundance and species richness and highlight the importance of managing activities that degrade small-scale topographic heterogeneity (e.g., bottom-contact fishing).

This chapter was published in the peer-reviewed journal *Marine Ecology Progress Series* (Du Preez and Tunnicliffe, 2011). A version of this work was presented at a Canadian Science Advisory Secretariat concerning corals, sponges, and hydrothermal vents in Canadian waters, which ultimately informed Fisheries and Oceans Canada policy to manage impacts of fishing on sensitive benthic areas (DFO, 2010). The methods section of this research was also included and described as a new tool for acquisition and analysis of seabed imagery in a feature article written by a number of CHONe principal investigators (Snelgrove et al., 2012).

The work highlighted the importance of deep-sea sponges and coral to benthic fish species and the unique conservation opportunity Learmonth Bank and its border dispute presents. It has been proposed that Learmonth Bank become a coral-sponge protected

area (Ardron, 2005). To provide more information on the distribution of the coral and sponge habitats, I collaborated with CHONe colleagues from Memorial University of Newfoundland to map coral and sponges habitats on Learmonth Bank. This work was published in the peer-reviewed journal *Deep-Sea Research II* (Neves et al., 2014) and appears in Appendix F.

Marine benthic diversity and topographic heterogeneity

In Chapter 5, I investigate the relationship between deep-sea epibenthic diversity at a local scale and topographic heterogeneity at multiple local and regional scales. I test the hypothesis of a positive relationship at all scales and I investigate the potential role of bottom flow hydrodynamics as a link between diversity and topographic heterogeneity. By sampling and analysing geographically diverse ecosystems I aim to elucidate the role of microtopographic heterogeneity as a common driver of diversity patterns on continental shelves.

This is the single largest research project of my thesis and includes all the aforementioned study sites on the Canadian Pacific and Atlantic continental shelf. It uses arc-chord ratio (ACR) rugosity as a measure of topographic heterogeneity and employs all the methods and analyses I developed.

Literature cited

Ardron, J. 2005. Protecting British Columbia's coral and sponges. Living Oceans Society report (v. 1.0), Sointula, B.C.

_____, Jamieson, G.S., and Hangaard, D. 2007. Spatial identification of closures to reduce the by-catch of corals and sponges in the groundfish trawl fishery, British Columbia, Canada. Bulletin of Marine Science **81**: 157-167.

Alexander, T.J., Barrett, N., Haddon, M., and Edgar, G. 2009. Relationships between mobile macroinvertebrates and reef structure in a temperate marine reserve. Marine Ecology Progress Series **389**: 31-44.

Barros, F., Underwood, A.J., and Archambault, P. 2004. The influence of troughs and crests of ripple marks on the structure of subtidal benthic assemblages around rocky reefs. Estuarine, Coastal and Shelf Science **60**: 781-790.

Beatty, S.W. 1984. Influence of microtopography and canopy species on spatial patterns of forest understory plants. Ecology **65**: 1406-1419. doi:10.2307/1939121.

Beck, M.W. 1998. Comparison of the measurement and effects of habitat structure on gastropods in rocky intertidal and mangrove habitats. Marine Ecology Progress Series **169**: 165-178.

Bett, B.J., and Rice, A.L. 1992. The influence of hexactinellid sponge (*Pheronema carpenteri*) spicules on the patchy distribution of macrobenthos in the Porcupine Seabight (Bathyal NE Atlantic). Ophelia **36**: 217-226.

Bianchi, C.N., Dando, P.R. and Morri, C. 2011. Increased diversity of sessile epibenthos at subtidal hydrothermal vents: seven hypotheses based on observations at Milos Island, Aegean Sea. Advances in Oceanography and Limnology **2**: 1-31.

Bridge, T. C. L., Done, T. J., Beaman, R. J., Friedman, A., Williams, S. B., Pizarro, O., and Webster, J.M. 2010. Topography, substratum and benthic macrofaunal relationships on a tropical mesophotic shelf margin, central Great Barrier Reef, Australia. Coral Reefs **30**: 143-153.

Brock, J.C., Wright, C.W., Clayton, T.D., and Nayegandhi, A. 2004. LIDAR optical rugosity of coral reefs in Biscayne National Park, Florida. Coral Reefs **23**: 48-59.

Buhl-Mortensen, L., Vanreusel, A., Gooday, A.J., Levin, L.A., Priede, I.G., Buhl-Mortensen, P., Gheerardyn, H., King, N.J., and Raes, M. 2010. Biological structures as a source of habitat heterogeneity and biodiversity on the deep ocean margins. Marine Ecology **31**: 21-50.

Butman, C.A. 1987. Larval settlement of soft-sediment invertebrates - the spatial scales of pattern explained by active habitat selection and the emerging role of hydrodynamical processes. Oceanography and Marine Biology **25**: 113-165.

Chave, J. 2013. The problem of pattern and scale in ecology: what have we learned in 20 years? Ecology Letters. doi:10.1111/ele.12048.

Corrigan, C., and Kershaw, F. 2008. Working toward high seas marine protected areas: an assessment of progress made and recommendations for collaboration. UNEP-WCMC, Cambridge, UK.

Cusson, M., and Bourget, E. 1997. Influence of topographic heterogeneity and spatial scales on the structure of the neighbouring intertidal endobenthic macrofaunal community. Marine Ecology Progress Series **150**: 181-193.

De Leo, F. C., Vetter, E. W., Smith, C. R., Rowden, A. A., and McGranaghan, M. 2014. Spatial scale-dependent habitat heterogeneity influences submarine canyon macrofaunal abundance and diversity off the Mainand Northwest Hawaiian Islands. Deep Sea Research II **104**: 267-290.

DFO. 2010. National Science Advisory Process concerning corals, sponges, and hydrothermal vents in Canadian waters; March 9–12, 2010. DFO Canadian Science Advisory Secretariat Proceedings Series 2010/027.

Dolan, M.F.J., Grehan, A.J., Guinan, J.C., and Brown, C. 2008. Modelling the local distribution of cold-water corals in relation to bathymetric variables: Adding spatial context to deep-sea video data. Deep-Sea Research I **55**: 1564-1579.

Du Preez, C. 2014. A new arc-chord ratio (ACR) rugosity index for quantifying three-dimensional landscape structural complexity. Landscape Ecology. doi: 10.1007/s10980-014-0118-8.

_____, and Tunnicliffe, V. 2011. Shortspine thornyhead and rockfish (Scorpaenidae) distribution in response to substratum, biogenic structures and trawling. Marine Ecology Progress Series **425**: 217-231.

_____, and _____. 2012. A new video survey method of microtopographic laser scanning (MiLS) to measure small-scale seafloor bottom roughness. Limnology and Oceanography: Methods **10**: 899-909.

_____, Chu, J.W.F., and Rose, J. *In review*. A scientist's guide to using remotely operated vehicles (ROVs) for benthic imagery surveys. *In* Recent research studies on seabed structure & benthic biodiversity relationships in Canadian Marine habitats. *Edited by* P. Lawton and E. Edinger. Canadian Technical Report of Fisheries and Aquatic Sciences XXXX: XX + XX p.

Dufour, A., Gadallah, F., Wagner, H.H., Guisan, A., and Buttler, A. 2006. Plant species richness and environmental heterogeneity in a mountain landscape: effects of variatility and spatial configuration. Ecography **29**: 573-584.

Dunn, D.C., and Halpin, P.N. 2009. Rugosity-based regional modeling of hard-bottom habitat. Marine Ecology Progress Series **377**: 1-11.

Elahi, R., Dwyer, T.R., and Sebens, K.P. 2014. Mesoscale variability in oceanographic retention sets the abiotic stage for subtidal benthic diversity. Marine Ecology Progress Series **498**: 117-132.

Freese, J.L., and Wing, B.L. 2003. Juvenile red rockfish, *Sebastes* sp., associations with sponges in the Gulf of Alaska. Marine Fisheries Review **65**(3): 38-42.

Gratwicke, B., and Speight, M.R. 2005. The relationship between fish species richness, abundance and habitat complexity in a range of shallow tropical marine habitats. Journal of Fish Biology **66**: 650-667. doi:10.1111/j.1095-8649.2005.00629.x.

Gray, D.H. 1997. Canada's unresolved maritime boundaries. Boundary and Security Bulletin **5**(3): 61-71.

Guichard, F., and Bourget, E. 1998. Topographic heterogeneity, hydrodynamics and benthic community structure: a scale-dependent cascade. Marine Ecology Progress Series **171**: 59-70.

_____, _____, and Robert, J.-L. 2001. Scaling the influence of topographic heterogeneity on intertidal benthic communities: alternate trajectories mediated by hydrodynamics and shading. Marine Ecology Progress Series **217**: 27-41.

Heifetz, J., Stone, R.P., and Shotwell, S.K. 2009. Damage and disturbance to coral and sponge habitat of the Aleutian Archipelago. Marine Ecology Progress Series **397**: 295-303.

Hill, J., and Wilkinson, C. 2004. Methods for ecological monitoring of coral reef. Australian Institute of Marine Science, Townsville (Australia).

Hill, J.M., and Thomason, J.C. 1996. A multi-scale analysis of settlement density and pattern dynamics of the barnacle *Semibalanus balanoides*. Marine Ecology Progress Series **138**: 103-115.

Husebø, A., Nøttestad, L., Fosså, J.H., Furevik, D.M., and Jørgensen, S.B. 2002. Distribution and abundance of fish in deep-sea coral habitats. Hydrobiologia **471**: 91-99.

Huston, M. 1979. A general hypothesis of species diversity. The American Naturalist **113**(1): 81-101.

Jenness, J.S. 2004. Calculating landscape surface area from digital elevation models. Wildlife Society Bulletin **32**: 829-839.

Jumars, P.A. 1976. Deep-sea species diversity: does it have a characteristic scale? Journal of Marine Research **34**(2): 217-246.

Krieger, K.J., and Ito, D.H. 1999. Distribution and abundance of shortraker rockfish, *Sebastes borealis*, and rougheye rockfish, *S. aleutianus*, determined from a manned submersible. Fishery Bulletin **97**: 264-272.

_____, and Wing, B.L. 2002. Megafauna associations with deepwater corals (*Primnoa* spp.) in the Gulf of Alaska. Hydrobiologia **47**: 83-90.

Larkin, D., Vivian-Smith, G., and Zedler, J.B. 2006. Topographic heterogeneity theory and ecological restoration. *In* Foundations of restoration ecology. *Edited by* A. Donald, M.P. Falk, and J. Zedler. Island Press, Washington, D.C. pp. 142-152.

Levin, L.A., and Sibuet, M. 2012. Understanding continental margin biodiversity: a new imperative. Annual Review of Marine Science **4**: 79-112.

_____, DeMaster, D.J., McCann, L.D., and Thomas, C.L. 1986. Effects of giant protozoans (Class: Xenophyophorea) on deep-seamount benthos. Marine Ecology Progress Series **29**: 99-104.

_____, Sibuet, M., Gooday, A.J., Smith, C.R., and Vanreusel, A. 2010. The roles of habitat heterogeneity in generating and maintaining biodiversity on continental margins: an introduction. Marine Ecology **31**: 1-5.

_____, Etter, R.J., Rex, M.A., Gooday, A.J., Smith, C.R., Pineda, J., Stuart, C.T., Hessler, R.R., and Pawson, D. 2001. Environmental influences on regional deep-sea species diversity. Annual Review of Ecology and Systematics **32**: 51-93.

Levin, S.A. 1974. Dispersion and population interactions. The American Naturalist **108**: 207-228.

_____. 1992. The problem of pattern and scale in ecology. Ecology **73**: 1943-1967.

Netto, S.A., Attrill, M.J., and Warwick, R.M. 1999. Sublittoral meiofauna and macrofauna of Rocas Atoll (NE Brazil): indirect evidence of a topographically controlled front. Marine Ecology Progress Series. **179**: 175-186.

Magurran, A.E. 2004. Measuring biological diversity. Blackwell Science Ltd., Oxford.

McArthur, M.A., Brooke, B.P., Przeslawski, R., Ryan, D.A., Lucieer, V.L., Nichol, S., McCallum, A.W., Mellin, C., Cresswell, I.D., and Radke, L.C. 2010. On the use of abiotic surrogates to describe marine benthic biodiversity. Estuarine, Coastal and Shelf Science **88**: 21-32.

McCormick, M.I. 1994. Comparison of field methods for measuring surface topography and their associations with a tropical reef fish assemblage. Marine Ecology Progress Series **112**: 87-96.

Mellin, C., Delean, S., Caley, J., Edgar, G., Meekan, M., Pitcher, R., Przeslawski, R., Williams, A., and Bradshaw, C. 2011. Effectiveness of biological surrogates for predicting patterns of marine biodiversity: a global meta-analysis. PLoS ONE **6**(6): e20141. doi:10.1371/journal.pone.0020141.

Moser, K., Ahn, C., and Noe, G. 2007. Characterization of microtopography and its influence on vegetation patterns in created wetlands. Wetlands **27**: 1081-1097.

Neves, B.M., Du Preez, C., and Edinger, E. 2014. Mapping coral and sponge habitats on a shelf-depth environment using multibeam sonar and ROV video observations: Learmonth Bank, northern British Columbia, Canada. Deep-Sea Research II **99**: 169-183.

Pauly, D., Alder, J., Bennett, E., Christensen, V., Tyedmers, P., and Watson, R. 2003. The future for fisheries. Science **302**: 1359-1361.

Pielou, E.C. 1977. Mathematical ecology. John Wiley & Sons, New York, N.Y.

Ramirez-Llodra, E., Tyler, P.A., Baker, M.C., Bergstad, O.A., Clark, M.R., Escobar, E., Levin, L.A., Menot, L., Rowden, A.A., Smith, C.R., and Dover, C.L.V. 2011. Man and the last great wilderness: human impact on the deep sea. PLoS ONE **6**: e22588.

Ricotta, C. 2005. Through the jungle of biological diversity. Acta Biotheoretica **53**: 29-38.

Risk, M.J. 1972. Fish diversity on a coral reef in the Virgin Islands. Atoll Research Bulletin **193**: 1-6.

Schlacher, T. A., Schlacher-Hoenlinger, M. A., Williams, A., Althaus, F., Hooper, J. N. A., and Kloser, R. 2007. Richness and distribution of sponge megabenthos in continental margin canyons off southeastern Australia. Marine Ecology Progress Series **340**: 73-88.

Schrohenloher, S.A. 1981. Life in moving fluids: the physical biology of flow. Willard Grant Press, Boston, Massachusetts.

Sherman, R.L., Gilliam, D.S., and Spieler, R.E. 2002. Artificial reef design: void space, complexity, and attractants. ICES Journal of Marine Science **59**: S196-S200.

Shumway, C.A., Hofmann, H.A., and Dobberfuhl, A.P. 2007. Quantifying habitat complexity in aquatic ecosystems. Freshwater Biology **52**(6): 1065-1076. doi:10.1111/j.1365-2427.2007.01754.x.

Sinclair, A.F., Conway, K.W., and Crawford, W.R. 2005. Associations between bathymetric, geologic and oceanographic features and the distribution of the British Columbia bottom trawl fishery. ICES CM 2005/L:25: 1-31.

Snelgrove, P.V.R., Archambault, P., Juniper, K., Lawton, P., Metaxas, A., Pepin, P., Rice, J.C., and Tunnicliffe, V. 2012. Canadian Healthy Oceans Network (CHONe): An Academic–Government Partnership to Develop Scientific Guidelines for Conservation and Sustainable Usage of Marine Biodiversity. Fisheries **37**: 296-304.

_____, and Smith, C.R. 2002. A riot of species in an environment calm: the paradox of the species-rich deep-sea floor. Oceanography and Marine Biology - An Annual Review **40**: 311-342.

Spalding, M.D., Ravilious, C., and Green, E.P. 2001. World atlas of coral reefs. University of California Press., Berkeley, CA.

Spieler, R.E., Gilliam, D.S., and Sherman, R.L. 2001. Artificial substrate and coral reef restoration: what do we need to know to know what we need. Bulletin of Marine Science **69**(2): 1013-1030.

Stocks, K.I., and Hart, P.J.B. 2007. Biogeography and biodiversity of seamounts. *In* Seamounts: ecology, fisheries and conservation. *Edited by* T.J. Pitcher, T. Morato, P.J.B. Hart, M.R. Clark, N. Haggan, and R.S. Santos. Blackwell Publishing Ltd, Oxford, U.K. pp. 252-281. doi: 10.1002/9780470691953.ch13.

Walker, B.K., Jordan, L.K.B., and Spieler, R.E. 2009. Relationship of reef fish assemblages and topographic complexity on southeastern Florida coral reef habitats. Journal of Coastal Research **53**: 39-48.

Watson, H.C. 1835. Remarks on the geographical distribution of British plants: Chiefly in connection with latitude, elevation, and climate. Printed for Longman, Rees, Orme, Brown, Green, and Longman, London, U.K.

Worm, B., Barbier, E.B., Beaumont, N., Duffy, J.E., Folke, C., Halpern, B.S., Jackson, J.B.C., Lotze, H.K., Micheli, F., Palumbi, S.R., Sala, E., Selkoe, K.A., Stachowicz, J.J., and Watson, R. 2006. Impacts of biodiversity loss on ocean ecosystem services. Science **314**: 787-790.

Wu, J. 2004. Effects of changing scale on landscape pattern analysis: scaling relations. Landscape Ecology **19**:125–138.

Chapter 2: A new video survey method of microtopographic laser scanning (MiLS) to measure small-scale seafloor bottom roughness

Preface

Chapter 2 is a methods article published in the peer-reviewed journal *Limnology and Oceanography*: *Methods*: Du Preez, C., and Tunnicliffe, V. (2012) A new video survey method of microtopographic laser scanning (MiLS) to measure small-scale seafloor bottom roughness. *Limnology and Oceanography: Methods* **10**: 899-909. Post-publication, I realise that the term "fractal" is not used correctly. Thus a replacement term is shown in square brackets in this thesis version. Dr. Verena Tunnicliffe (Thesis supervisor, University of Victoria) provided the resources for this work and assisted with the writing of this article. My contribution was developing the method, collecting and analysing the case study data, and writing the article.

Abstract

A novel video survey method measures small-scale seafloor bottom roughness in fragile and deep-sea habitats called microtopographic laser scanning (MiLS). Using a controlled submersible platform, an attached downward-facing video camera with a single optical laser can return imagery to detail the bottom profile at a resolution of ~1-2 cm. The method compares the position of the underlying substratum and laser dot between successive video frames to determine distance traveled in the forward direction and substratum height. The video imagery is processed using photogrammetry to calculate small-scale topography (horizontal and vertical axes). MiLS is adaptable for

most aquatic habitats as it can be executed using any platform that can move forward with a constant slope over the desired transect. Traditional techniques of measuring small-scale roughness are largely restricted to easily accessible habitats and often yield measurements that are relative and not comparable among different habitats and studies. Quantifying roughness in ways that permit comparisons is critical to understanding effects of bottom roughness and would benefit many fields of aquatic science. With its versatility, ability to access remote locations and output of quantified measurements, MiLS has the potential to fill this need. It is also likely this method will be useful in subaerial habitats such as wetlands. Here, we describe the MiLS equipment, theory, and method in detail, and then demonstrate its application in a lab trial and in a field study in a deep-sea (≤450 m depth) sponge and coral habitat where its high resolution, accuracy, and precision is made evident.

Introduction

Small-scale roughness is regarded by limnologists and oceanographers as an important characteristic of the bottom boundary and is relevant to many fields of study including sediment transport, coral reef restoration, fluid dynamics, benthic species distribution, and biodiversity patterns (Boudreau and Jørgensen 2001; Spieler et al. 2001; Snelgrove and Smith 2002; Courtwright and Findlay 2011). Small-scale or ‘organism-sized’ surface structure is known as microtopography and roughness is the degree to which a surface is uneven, irregular, or coarse (Thomas 1999). We have traditionally used handheld instruments to make quantified field measurements of small-scale roughness, including conventional surveying equipment (Beck 1998; Moser et al. 2007) and devices

such as the chain-and-tape method (Risk 1972), falling-rod gauges (Leatherman 1987) and moulds (Sanson et al. 1995). These instruments require hands-on operation, hence the majority of small-scale bottom roughness studies are conducted in relatively accessible habitats, such as intertidal (Beck 1998; Lund-Hansen et al. 2004) and shallow submarine using SCUBA (Risk 1972; Walker et al. 2009) while in deeper water habitat, small-scale roughness is often documented using habitat-specific categories.

Airborne lidar (light detection and ranging) and ship-based sonar (sound navigation and ranging) are remote-sensing techniques that quantify submarine topography. Both techniques can potentially resolve bottom surface features at scales ranging from tens of centimeters to meters (Wright and Brock 2002; Caress et al. 2008), but lidar is restricted to shallow coastal waters (0 to 10 m depth; Wright and Brock 2002) and the resolution of sonar decreases as the distance between the sensor and the bottom increases. Sonar sensors can be attached to submersible platforms to operate in deeper water with increased resolution, but this can be logistically and financially taxing. Another drawback of lidar and sonar is specialization of the instruments that are limited in events they can detect.

Bottom photographic or video image surveys can be processed for many types of visual phenomena including small-scale roughness. Surface texture (Haralick et al. 1973) and optical intensity analysis (Shumway et al. 2007) are techniques used to quantify small-scale roughness from image characteristics but the measurements are relevant only within the study. Quantifying roughness in ways that permit comparisons among different habitats and studies is critical to defining common consequences of bottom roughness

(McCoy et al. 1991; Sanson et al. 1995). One approach is to develop a roughness index that is comparable across studies.

Photogrammetry is a technique of extracting spatial and geometric data from images. In topography, photogrammetry is used to generate a surface profile from which roughness can be mathematically characterized as an index, enabling the comparability of results. Briggs (1989) used the photogrammetry technique of stereoscopy to profile and quantify smallscale roughness in a continental shelf environment. The stereoscopic camera was deployed in depths up to 50 m as a ship-based "dropcam" (Briggs 1989). This technique required repeated contact with the bottom, which can be destructive, especially in habitats vulnerable to physical contact such as deep-sea sponge and coral habitats. 'Off-bottom' surveys are less invasive but the roughness data annotated are usually categorical and of low resolution.

Here, we describe and assess a new off-bottom video survey method called microtopographic laser scanning (MiLS). Any submersible platform that can move forward at a constant slope equipped with a downward-facing video camera and optical laser can return imagery to detail the bottom profile at a resolution of ~1-2 cm. "Constant slope" means that the inclination of the vehicle does not change as it moves over the seafloor upward, downward, or with no depth change. We use photogrammetry based on simple scale equations to output a microtopographic profile (x- and y-axes) and, with ~~fractal~~ trigonometry, we calculate an index of bottom roughness. Several indices are possible, including rugosity, relief, and height or angle variations (McCormick 1994). Our objective in developing MiLS was to provide a rigorous yet versatile method to measure smallscale bottom roughness that can be executed in most aquatic habitats, even

those vulnerable to physical contact, and that can yield results comparable among different habitats and studies.

We describe the MiLS equipment, theory, and method in detail, and then demonstrate application with a lab trial, a field study in a deep-sea sponge and coral habitat.

Materials and procedures

The microtopographic laser scanning (MiLS) system consists of two main components: a submersible platform and an attached underwater camera-laser array. Platform options include remotely operated vehicles (ROVs; Fig. 2.1A), SCUBA divers (Fig. 2.1B), autonomous underwater vehicles (AUVs; Fig. 2.1C), towed platforms, and manned submersibles. The major criterion in selecting a platform is that it be able to move forward at a constant slope over the desired transect (Fig. 2.1). If the platform's slope is available in realtime, through the monitoring of its vertical and horizontal movement from the position system or sensors (e.g., depth gauge), then protocol corrections will return a better survey. The distance over which the platform can maintain a constant slope maybe a limiting factor in transect length; however, data can be post-processed to select, and potentially assemble, the segments of constant slope. Attainable segment length may range from centimeters to tens of meters and is dependent on the platform and environmental conditions. Platform lights to illuminate the seafloor are required except in shallow water where ambient light can be sufficient.

The camera-laser array is attached to the platform facing downward; Fig. 2.2A shows a schematic overview of the array. The components can be contained in separate underwater housings but the array is configured on a single mount. The laser is

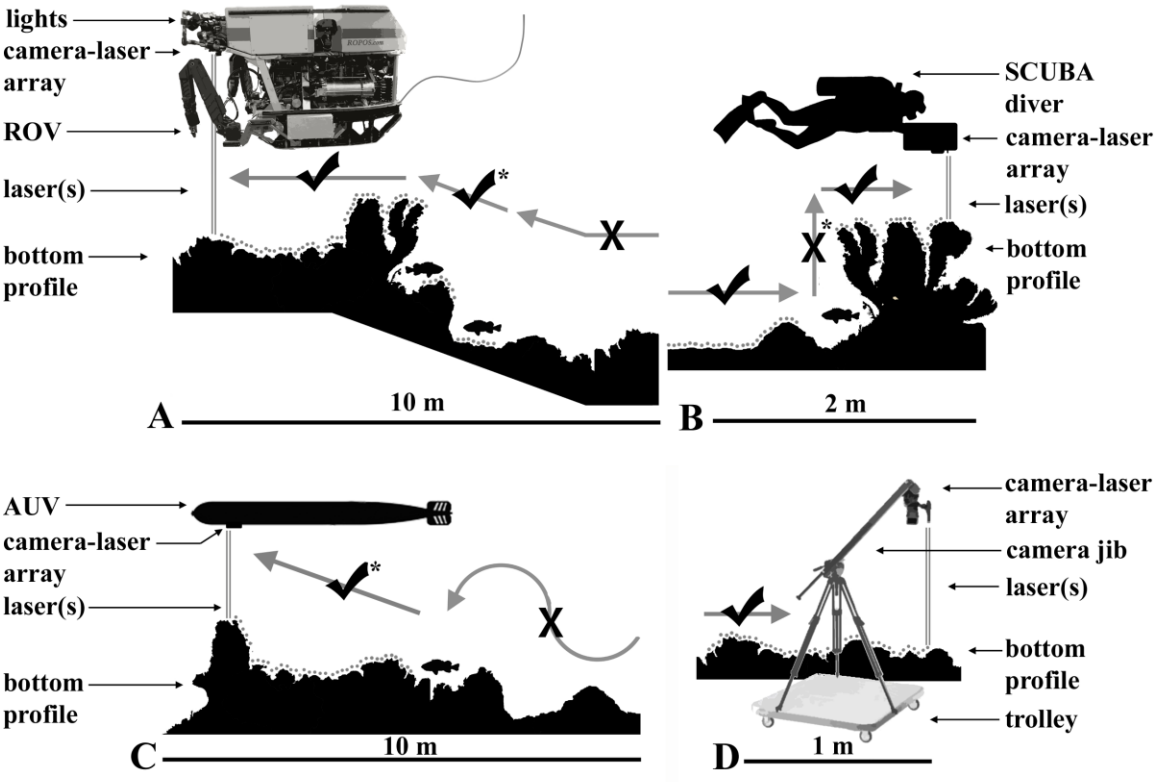

Figure 2.1. Four platforms with downward-facing camera-laser arrays conducting microtopographic laser scanning (MiLS): (A) an ROV, (B) a SCUBA diver, (C) an AUV, and (D) a trolley platform (subaerial use). The present article includes assessment examples using the ROV *ROPOS* and trolley. The gray arrows represent various flight paths and indicate which have a forward-moving constant slope and are appropriate for MiLS (✓) and which are not (x). When a change of depth is required (flight paths with *), it can be made during transecting (A & C) or the platform can be adjusted vertically and then continue forward at a new constant depth (B). Note that if the array mount can be tilted 90°, forward-facing, the vertical flight path illustrated by the SCUBA diver would be appropriate for MiLS of the vertical feature (see text for details). The gray dots over the substratum represent the x- and y-axis data calculated using photogrammetry of the video imagery.

positioned to one side of the camera lens, parallel with the camera's optical axis and preferably with no set-back from the center of the lens. Note only one laser is required for MiLS but two lasers, mounted in parallel, project a multipurpose scale commonly used in video surveys (as in Du Preez and Tunnicliffe 2011 [Chapter 4]). In our assessment

studies, two parallel lasers were positioned 5 cm on either side of the center of the camera lens, and we designated the right laser for MiLS (line *AB* in Fig. 2.2A). The array configuration can be adapted, but it is important to record the distances between the instruments and to have them aligned parallel; thus, ground distances between the

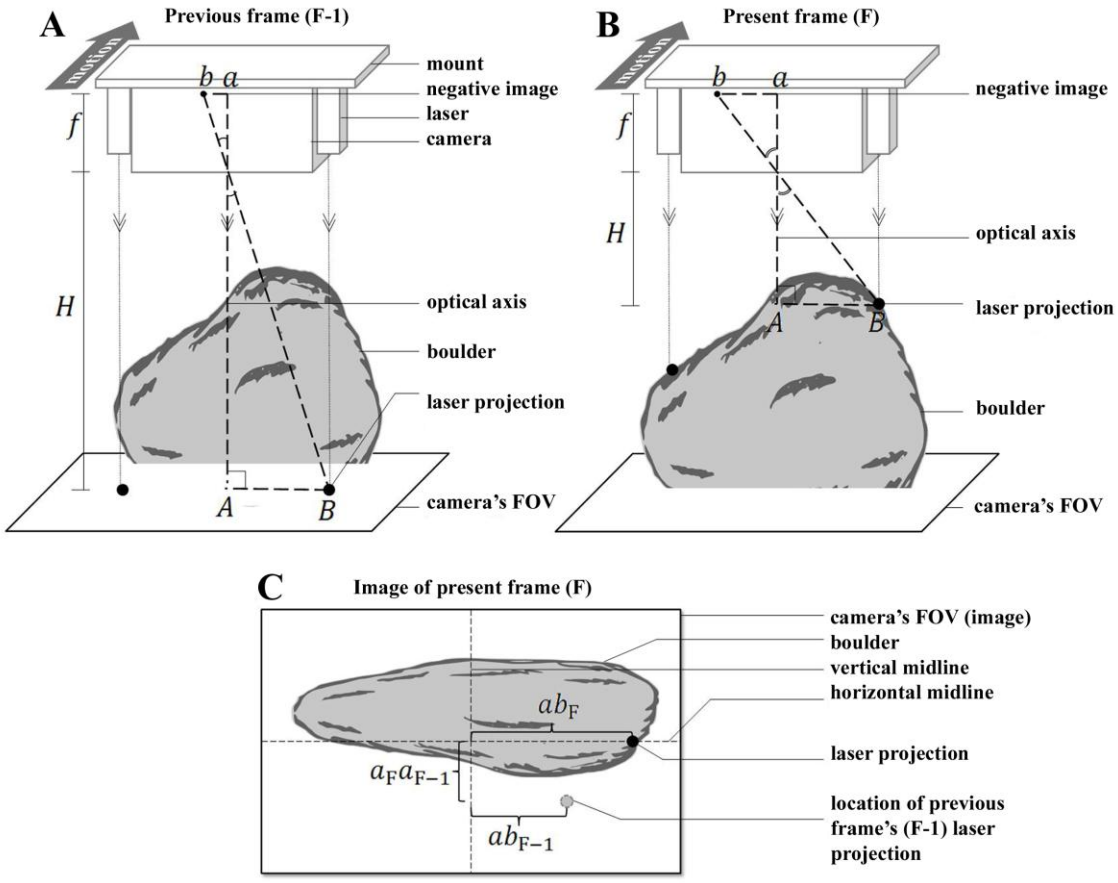

Figure 2.2. Schematic diagrams from behind the camera-laser array during two successive frames: (A) the previous frame, F-1, and (B) present frame, F; and (C) the still frame image from the latter. (A & B) For both diagrams, the photogrammetric trigonometry is imposed (dashed lines) with *H* = distance between camera lens and line *AB*, *AB* = distance between the laser dot and the vertical midline of the field of view (FOV), *f* = focal length, *ab* = image distance, *H* perpendicular to *AB* and lasers parallel with the optical axis. (C) The image of the present frame shows *ab* for both frames and the distance between the optical axes in the present and previous frame ($a_F a_{F-1}$). Note the difference between *ab* in F-1 and F, because of the change in *H*.

projected laser point and its position within the camera's field of view (FOV) are known and static. In using common, relatively inexpensive, materials configured in an adaptable setup, we have increased the application and usability of MiLS as well as allowed for the potential to revisit previously recorded benthic video for further analyses, which include MiLS measurable parameters.

Photogrammetric scale equations are the basis of the MiLS analysis. Each video still frame of a MiLS transect is processed, using derivatives of two scale equations, to measure the topography of a unique location. By calculating the distance traveled between successive frames and the height value for the laser dot within each frame, we generate a microtopographic profile (x- and y-axes) of the transect.

Used to calculate distance traveled between successive frames (x-axis), the photogrammetric scale equation relating the distance between two points in an image to the true distance on the ground is:

$$scale = \frac{ground\ distance}{image\ distance} \tag{1}$$

Once the scale is established, the equation can be reordered to solve for an unknown ground distance. The scale changes with distance from the camera (Eq. 2), so a calculated scale is specific to a region of a photograph.

Used to calculate the height value for the laser dot (y-axis), similar triangles relate image distance (ab) and ground distance (AB) to camera focal length (f) and camera height (H) as expressed by:

$$\frac{H}{AB} = \frac{f}{ab} \quad \text{or} \quad f = ab \cdot \frac{H}{AB} \quad \text{or} \quad H = AB \cdot \frac{f}{ab} \tag{2}$$

Focal length (f) is usually a constant value in photogrammetry given by the camera manufacturer. However, underwater, the refraction of light at the interface of water and

the housing port, and the housing port and air in the camera housing alters focal length as a function (f) of height (H):

$$f = \mathrm{f}(H) \tag{3}$$

Furthermore, water qualities such as temperature and salinity affect the index of refraction. Owing to the variation of an underwater camera's apparent focal length, a calibration of the topographic height scale equation (Eq. 2) for the specific camera and environment is required; once established, small variations encountered during a habitat specific survey should not affect results.

The MiLS field procedure consists of two parts: the calibration exercise and the video surveying along transects. For both procedures, camera zoom is at a constant setting, otherwise focal length (f) will change; we suggest minimum zoom for wide field of view.

Calibration is done over a flat bottom area within the study site by raising and lowering the platform through a range of known heights (H). This range should reflect the expected changes in microtopography at the study site, and when possible, exceed the total change. The height measurements to the camera lens (cm) are made using an onboard altimeter, depth gauge, or physical scale. We recommend at least 50 to 100 height measurements to ensure confidence in generating a relationship equation. This may require several vertical rises to generate enough measurements.

The appropriate surveying procedure for a MiLS transect will depend on the terrain and on the study's equipment and experimental design. A transect may be continuous or an assemblage of short segments, and range in length from centimeters to tens of meters. With the camera and laser(s) switched on, the platform moves forward at a constant speed and slope. The speed should reflect the desired x-axis resolution ([link] ~~fractal~~

length increases with the speed of the platform) and be slow enough that the substratum overlaps between sequential frames (easily satisfied with a standard frame rate of 30 s^{-1}). The simplest method to maintain a constant slope is to keep depth unchanging (slope of zero; aided by a depth gauge). When a change of depth is required, it is preferable to adjust vertically and then continue forward at a new constant depth (e.g., asterisked flight path in Fig. 2.1B) to avoid gaps in coverage. When a depth change during transecting is necessary (e.g., asterisked flight paths in Fig. 2.1A & C), an onboard positioning system and altimeter can supply the information to determine a constant slope. With a downward-facing camera-laser array, a vertical flight path (e.g., asterisked flight path in Fig. 2.1B), has no 'forward' movement, and cannot yield length data (x-axis). However, if the array mount can tilt forward-facing, vertical substrata (e.g., cliff or the side of a structure) can be scanned using a vertical flight path, during which the MiLS method remains the same except the transecting protocol is adjusted by 90°.

MiLS video may be collected opportunistically during other benthic sampling techniques (e.g., ROV-based habitat/species surveys, bottom plankton tows, and multibeam scans) as it requires only minor augmentation of some common protocols to execute MiLS concurrently. Video processing uses image analysis programs. We used open-source programs Kinovea Motion Tuner ver. 0.8.15 and ImageJ 1.42q, however other applications have similar capabilities (e.g., Tracker 4.62). The simplest approach to computing topographic data is to export the photogrammetric measurements from the video analysis program to a spreadsheet containing the equations (see Appendix B for a spreadsheet example).

With the video file opened in an image analysis program, we navigate to the calibration exercise and locate the still frames recorded at the 50 to 100 'known heights'. The next step is to choose the exact location within the projected laser dot to use for every image, such as the central pixel. Record all distances in the same unit, including the image distance (in our assessment studies, we use centimeters). Next, calibrate the topographic height scale equation (Eq. 2) for the variable apparent focal length (*f*, Eq. 3). For each frame, we know the height (*H*) and the ground distance between the laser dot and the vertical midline of the FOV (*AB*; in our assessment examples *AB* = 5 cm), we measure the image distance (*ab*) and solve for apparent *f* (Eq. 2; e.g., Fig. 2.2A). By plotting the apparent *f* and *H*, we generate a power equation expressing focal length as a function of height and two constant variables (*j* and *k*):

$$f = \mathrm{f}(H) = j \cdot H^{k} \tag{4}$$

We insert Eq. 4 into Eq. 2 to create the calibrated height scale equation (with the two constant variables, j and k) specific for the study's camera and environment:

$$H = AB \cdot \frac{(j \cdot H^{k})}{ab} \quad \text{or} \quad H = \sqrt[1-k]{j \cdot \frac{AB}{ab}} \tag{5}$$

With the calibration complete, Eq. 5 parameters are entered in the spreadsheet formula to begin transect analyses. Photogrammetric measurements for each video still frame's length (x-axis) and height (y-axis) values can be done simultaneously.

Length values are generated by tracking the relative movement of optical axis point (A_{F}; Fig. 2.2B) from the location in the previous frame ($A_{\mathrm{F}-1}$; Fig. 2.2A) and using Eq. 1. Again, with known AB_{F} and measured ab_{F} (Fig. 2.2B & C), we solve for scale (Eq. 1). Then, using the calculated scale, we measure the image distance between the optical axis

point in the frame and the location of the previous frame's optical axis point ($a_{\mathrm{F}}a_{\mathrm{F}-1}$; Fig. 2.2C) and solve for the distance travelled between frames ($A_{\mathrm{F}}A_{\mathrm{F}-1}$).

The first frame of a transect is set as $\mathrm{X}_1 = 0$ cm, thus length across all succeeding frames is:

$$\mathrm{X}_{\mathrm{F}} = \sum_{i=2}^{\mathrm{F}} (A_i A_{i-1}) \tag{6}$$

Height values are generated by tracking the image distance (ab) between the laser dot and the vertical midline of the FOV (Fig. 2.2C) and using Eq. 5. With the measured ab, we solve for the distance between the camera and the ground at line AB (H; Eq. 5). To convert the camera's relative H to topographic height (Y) we inverse H and standardize so $\mathrm{Y}_1 = 0$ cm:

$$\mathrm{Y}_{\mathrm{F}} = -1(H_{\mathrm{F}} - H_1) \tag{7}$$

If required, relative topography is generated by adjusting the transect's overall slope to zero, correcting each X and Y value for the transects overall slope:

$$\text{slope} = m = \frac{\mathrm{Y}_i - \mathrm{Y}_n}{\mathrm{X'}_i - \mathrm{X'}_n} \tag{8}$$

$$\mathrm{X}' = \sqrt{\mathrm{X}^2 + (\mathrm{X} \cdot m)^2} \tag{9}$$

$$\mathrm{Y}' = \mathrm{Y} + (\mathrm{X} \cdot m) \tag{10}$$

With a length and height data point calculated for each frame, we create a microtopographic profile by plotting the data points (e.g., Fig. 2.3A-C).

From the microtopographic profile, simple ~~fractal~~ trigonometry returns small-scale roughness indices, for example, rugosity. Rugosity is a dimensionless ratio between the surface contour-following distance and the linear distance between two points (Risk 1972). Similar to the parameter *tortuosity* used in terrestrial ecology, this measure encompasses and combines structural relief and roughness (Moser et al. 2007), where a

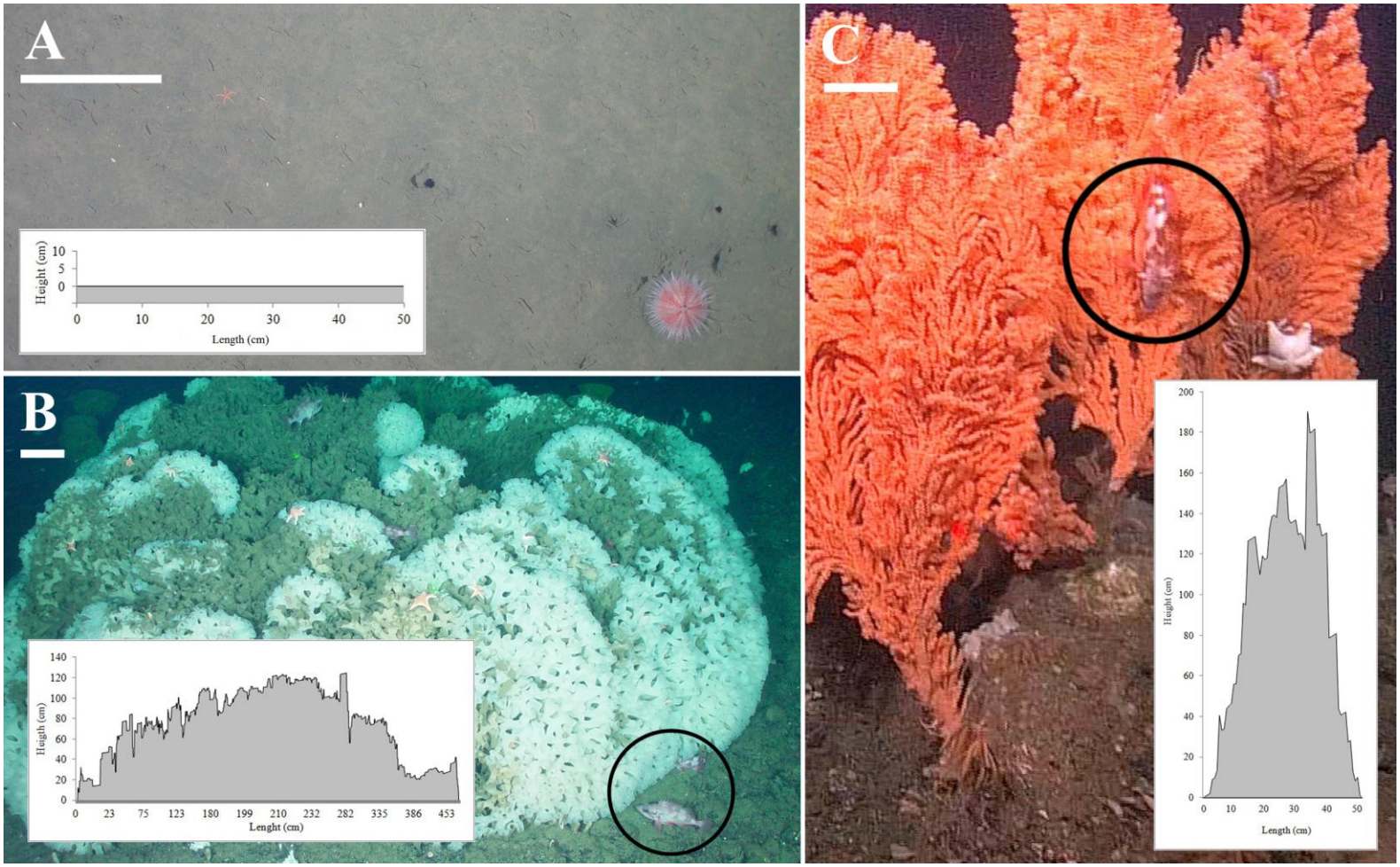

Figure 2.3. Three examples of deep seafloor microtopographic laser scanning (MiLS) transects and generated microtopographic profiles: (A) an S9 transect of a patch of sand with a rugosity of 1.00; (B) an S16 transect of a *Farrea occa occa* sponge with a rugosity of 3.59; and (C) an S7 transect of a *Primnoa pacifica* red tree coral with a rugosity of 6.78 (for locations of transects see Fig. 2.4). B and C are rockfish transects (both *Sebastes zacentrus*; circled in black). White bars are 10 cm.

flat surface has a rugosity value of one. Both distances were calculated from the profile using Pythagorean Theorem: the surface contour following distance is the summation of the hypotenuse between each successive data point and the linear distance is the hypotenuse between the transect's first and last data point:

$$rugosity = \frac{contour\ following\ distance}{linear\ distance} = \frac{\sum_{i=1}^{n}\left(\sqrt{(\mathrm{X}_{i+1}-\mathrm{X}_i)^2+(\mathrm{Y}_{i+1}-\mathrm{Y}_i)^2}\right)}{\sqrt{(\mathrm{X}_n-\mathrm{X}_i)^2+(\mathrm{Y}_n-\mathrm{Y}_i)^2}} \quad (11)$$

Characteristics of the equipment and environment that may affect the overall resolution and accuracy of MiLS include: minimum controllable platform speed; camera height, focal length, frame rate and image resolution; thickness and material of the housing portal (affecting index of refraction); resolution of the image analysis software; water visibility; bottom current; and larger scale variability in seafloor slope.

Assessment

A lab trial was conducted to assess the strengths and limitations of microtopographic laser scanning (MiLS) under controlled subaerial conditions. Our objective was to determine the accuracy and precision of MiLS by measuring dimensions and rugosity of objects with known values. A lab trial offers a detailed assessment not feasible during the field study.

The platform was a trolley with attached arm with a downward-facing camera-laser array; the arm extended the array away from the platform, perpendicular to the trolley's leading edge (Fig. 2.1D; Table 2.1). Two lasers were positioned in parallel, 5 cm on either side of the center of the camera lens in a straight line with the camera's optical axis; we selected the one on the right to be the MiLS laser.

Table 2.1. Equipment used in the lab trial and field study.

Item	Description
Lab trial	
Camera	Panasonic DMC-T25 camera (640 x 480 pixels and 29 frames sec^{-1})
Lasers	2 x green lasers
Vehicle	4-wheel trolley with mounted camera jib
Kinovea motion tuner ver. 0.8.15	video analysis program capable of measuring laser dot center measured to the nearest whole pixel
Field study	
Camera	Sony DXC-990 three CCD standard-definition video camera (720 x 480 pixels and 29 frames sec^{-1})
Lasers	2 x A.G.O. 532 nm green lasers
ROV *ROPOS*	electro-hydraulic science/work-class remotely operated vehicle (app. length of 3 m, width of 1.8 m and height of 1.7 m)
Altimeter	Kongsberg Simard 1007 altimeter
Depth gauge	Paroscientific depth gauge
Position system	IXSEA GAPS Ultra Short BaseLine (USBL) system, RDI navigator doppler and IXSEA Octans III fibre-optic gyroscope
Lights	3 x 400W HMI, 2 x 150W HID and 6 x 100W LED
CCGS *John P. Tully*	offshore oceanographic science vessel from which *ROPOS* is deployed and piloted (length of ~70 m)
ImageJ 1.42q	image analysis program capable of measuring laser dot center measured to the fraction of a pixel

In subaerial conditions, the height scale equation (Eq. 2) is solved using the camera's true focal length, but in an aquatic environment, the calibration of this equation for a variable focal length (f) is a critical component of the MiLS method so, for the purpose of this article, we included the calibration exercise in our lab trial. Using the extendable tripod, the camera-laser array was set at ~50 different heights (H), ranging from 0.7 to 1.7 m, with the resulting calibrated height scale equation (Eq. 5) constants: AB = 5.0 cm, j = 36, and k = –0.093.

Table 2.2. Summary of the true dimension (dim) and the resolution (res), accuracy (acc) and precision (pre) for the microtopographic laser scanning (MiLS) of 13 demonstration objects scanned during the lab trial. The MiLS calculated length, height and rugosity of each object analysed (n = 3) for mean MiLS [link] ~~fractal~~ length (resolution), the difference between the mean MiLS measurement and the real dimension of the structure (accuracy; 0 = highly accurate) and the standard deviation between the replicate MiLS measurements (precision).

No. and structure	Length (cm)				Height (cm)				Rugosity		
	dim	res	acc	pre	dim	res	acc	pre	dim	acc	pre
1. bedrock	50.4	0.7	-1.0	2.4	17.7	3.1	-3.1	0.0	1.5	0.0	0.0
2. bedrock	35.7	0.6	-1.0	0.8	53.5	2.2	1.2	0.0	4	-0.1	0.1
3. boulder	33.6	0.7	-1.9	1.9	34.0	2.7	0.6	0.0	3	-0.1	0.1
4. boulder	26.5	0.7	-1.1	0.2	13.5	3.1	-0.3	2.0	1.6	0.2	0.1
5. cobble	19.5	0.7	-3.1	4.5	13.5	3.1	2.6	1.8	2	0.2	0.3
6. cobble	20.0	0.7	0.0	0.0	9.5	3.1	0.9	2.0	1.7	0.1	0.1
7. pebbles*	30.0	0.6	0.9	0.7	5.5	3.2	0.9	0.0	1.3	0.6	0.2
8. sand*	44.5	0.7	-0.8	0.3	0	3.2	0.0	0.0	1	0.0	0.0
9. wood	12.5	0.7	-0.3	0.9	11	3.2	-0.4	1.9	2.2	0.2	0.1
10. coral	31.0	0.7	-0.4	0.6	60	2.1	-9.2	0.5	4.4	-0.2	0.4
11. sponge	5.7	0.8	-0.8	0.2	30.7	2.8	-2.0	2.0	11.7	-2.1	0.8
12. sponge	9.6	0.7	-0.9	0.5	10.6	3.2	0.1	1.9	3.2	-0.3	0.4
13. sponge	6.1	0.7	-1.0	0.2	22.0	3.0	-0.3	2.0	8.4	-1.5	0.4
Mean ± SE	21.7 ± 5.1	0.7 ± 0.0	-0.9 ± 0.3	1.0 ± 0.4	25.0 ± 4.0	2.9 ± 0.1	-0.7 ± 0.8	1.1 ± 0.3	3.5 ± 0.9	-0.2 ± 0.2	0.2 ± 0.1

*a patch placed on the floor

Objects scanned during the lab trial represented structures that we found at our deep-sea study site and included a patch of sand, pebbles, cobbles, boulders, bedrock, and artificial deep-sea sponges and corals (n = 13; Table 2.2). Dimensions and rugosity of each object were determined using a measuring tape and the chain-and-tape method (Risk 1972). Objects averaged 25.0 cm, 21.7 cm and 3.5 in length, height and rugosity respectively (Table 2.2). For the lab trial, the array was set at a height of 1.2 m. The target object was positioned to the side and front of the trolley platform. The trolley was pulled at an approximate speed of ~15 cm s^{-1} until the laser transited the entire structure. This procedure was replicated three times for each object to assess MiLS precision.

We determined the limiting factors in resolving both length and height (x- and y-axes; Table 2.2). The resolution of length is dependent on the speed of the platform and the video frame rate (Table 2.1); we resolved an average of 0.7 ± 0.0 cm (Table 2). The resolution of height is limited by factors relating to the resolution of the video camera, fineness of the laser dot and the lowest measurable level of the image analysis software (Table 2.1). Height resolution is also inversely related to the distance between the sensor and the scanned structure; we resolved an average of 2.9 ± 0.1 cm (Table 2.2). The resolution of the microtopographic profile [links] ~~fractals~~, which are used to calculate the rugosity, is a product of the length and height resolutions.

Resolution directly influences accuracy: long x-axis [links] ~~fractals~~ are more likely to miss edges and long y-axis [links] ~~fractals~~ have lower sensitivity to changes in topography. The

demonstration objects ranged in rugosity from 1.00 to 8.44 and MiLS calculated rugosities were, on average, accurate to –0.2 ± 0.2 (Table 2.2).

Precision between replicates is affected by each transect's start location and the platform speed; variations in either or in both has the potential to decrease the precision (Table 2.2). During video processing, precision can be affected by inconsistencies in the technician's method, for example differences in the relative location within the laser dot used.

Our lab trial demonstrates MiLS can be used to collect topographic data from an off-bottom moving platform at a centimeter-scale, generate microtopographic profiles, and calculate quantified small-scale roughness measurements. The MiLS method is accurate and precise at this centimeter-scale.

The goal of the field study was to demonstrate MiLS through a real-world application in which we measured the small-scale bottom rugosity in deep-sea sponge and coral habitat. This field study is a follow-up study to our work on *Sebastes* rockfish distributions in this habitat (Du Preez and Tunnicliffe 2011 [Chapter 4]). In our previous work, we used categorical descriptions of habitat usage and showed rockfish affiliate with boulders, sponges, and corals, but could only speculate on the reason. We suggested high roughness as the primary attractant but now, with our new MiLS method, we are able to address the research question: *Do deep-sea benthic* Sebastes *rockfish associate with high roughness seafloor?*

In July 2008, we deployed the ROV *ROPOS* (Fig. 2.1A) at Learmonth Bank, British Columbia, Canada (Fig. 2.4; 54°24′59″N, 133°05′00″W). Learmonth has a rough seafloor as a granite massif surrounded by glacial sediments and scoured by currents (Bornhold and Barrie 1991; Barrie and Conway 1999). Abundant deep-sea sponges and corals

(Ardron et al. 2007) add to the seafloor roughness. A detailed description of the study area is available in Du Preez and Tunnicliffe (2011) [Chapter 4].

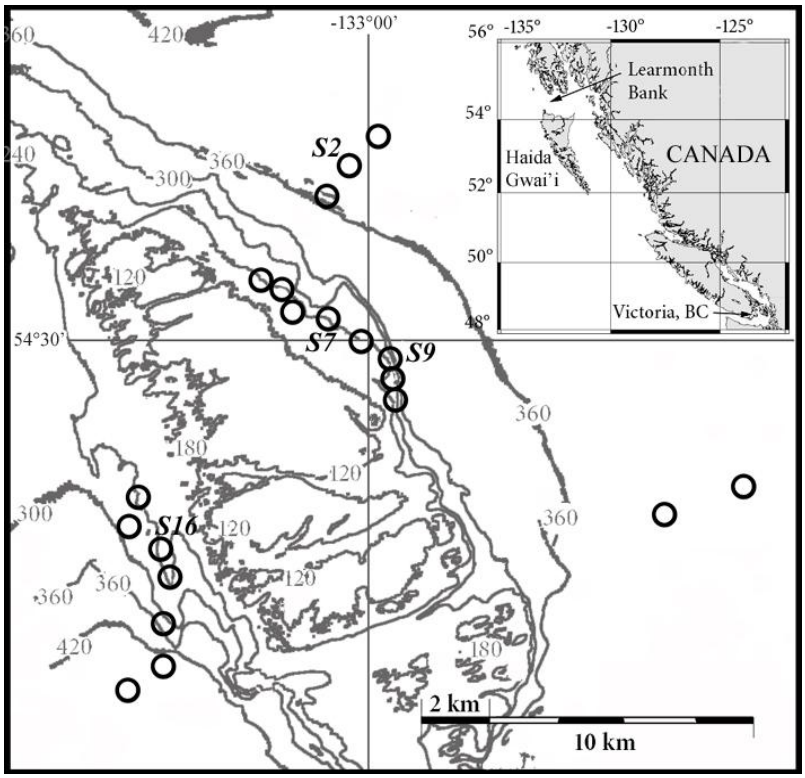

Figure 2.4. Bathymetry (m) of Learmonth Bank (54°24′59″N, 133°05′00″W) with the 20 survey sites (black circles). MiLS transects from sites *S7*, *S9*, and *S16* are used as examples of the MiLS output (Fig. 2.3) and a transect from *S2* is used in the workable spreadsheet example (Appendix B). Inset shows location of study area off the coast of British Columbia, Canada. Map is adapted from Du Preez and Tunnicliffe (2011) [Chapter 4].

The ROV program was planned within the context of examining the corals and sponges of Learmonth Bank; the MiLS video for this study was collected concurrently with ROV transects run for other primary objectives. The downward-facing lights and camera-laser array were mounted forward on the ROV, at a height of 0.9 m (Fig. 2.1A; Table 2.1). Two lasers were positioned in parallel, 5 cm on either side of the center of the camera

lens and 24 cm to the front of the camera's optical axis due to mount constraints; we selected the one on the right to be the MiLS laser.

The calibration exercise was executed over a flat, sandy area. Using the ROV's onboard altimeter (Table 2.1), ~70 different camera heights (*H*) were measured, ranging from 1.0 to 3.0 m, with the resulting calibrated height scale equation (Eq. 5) constants: AB = 5.0 cm, j = 8.0 and k = 0.33.

The MiLS transect protocol was to "fly" the ROV into the current at speeds of 25 to 50 cm s^{-1} (0.5 to 1 knots), at a constant forward slope where possible while keeping the camera within 1 to 2 m off the seafloor. ROV motions other than the forward flight (e.g., roll and pitch) were relatively slow; within the length of our transects, we considered these motions negligible. During the surveying flight path segments appropriate for MiLS analyses were up to tens of meters in length but to address our specific rockfish research question we required only small, ~50 cm, transects. From previous work, we knew that the majority of rockfish associating with the seafloor were in physical contact with it and that most structure-creating element on Learmonth's seafloor (patches of cobble, boulders, sponges and corals) were < 50 cm in length (Du Preez and Tunnicliffe 2011 [Chapter 4]). Thus we determine a 50 cm MiLS transect, starting at the rockfish, was an appropriate transect length for sampling the rugosity of adjacent seafloor.

Twenty sites at Learmonth Bank were surveyed, 8 on the bank and 12 in the surrounding area (at app. 200 m and 450 to 270 m depth respectively; Fig. 2.4). At each site, a ~1 km benthic survey was conducted for a previous study (Du Preez and Tunnicliffe 2011 [Chapter 4]) but, within the sites, two ~50 cm segments (paired transects) for the present study were used. We randomly selected two video time-codes

from each survey. The location of the laser dot at the selected time was the start of a transect. One time-code was randomly selected from the entire survey and one was randomly selected from observations of station-holding rockfish directly below the camera (queried from video annotation of Learmonth Bank 2008 *ROPOS* dives). We define station-holding rockfish as those rockfish remaining in one location for the duration of the pass, not actively or passively moving. From the start location, we executed a MiLS transect for a length of 50 cm. If the 50 cm scan captured a longer structure (e.g., large boulder, coral or sponge), it was continued to the edge of the structure; scans averaged 50.7 ± 4.2 cm in length.

For each transect, we generated a microtopographic profile, structural dimensions and a measure of rugosity (examples shown in Fig. 2.3A-C). To answer our specific field study research question, we augmented the MiLS approach with video survey imagery to annotate data on substratum type and benthic fauna. Furthermore, we also detailed the passive movement of particulates, debris, and fauna to confirm the ROV's relative heading was directly into the bottom current (relevant to the interpretation of the results).

The ~~fractal~~ resolutions for our deep-sea field study are slightly lower than in the lab trial (Table 2.2): 1.4 ± 0.1 cm for length and 4.1 ± 0.5 cm for height. Higher platform transit speed reduced the length resolution. Multiple factors affected height resolution: the refraction of light through water magnified the image, and we used a higher resolution image analysis program (Table 2.1) yielding better resolution in photogrammetric measurements, but the ROV altitude was greater than the lab trial because the structures were taller; this second factor decreased resolution.

The random transects were relatively ‘flat’, averaging only 1.22 ± 0.08 in rugosity (Fig. 2.5A) with the seafloor consisting primarily of sand or pebbles and sand (Fig. 2.5B; e.g., Fig. 2.3A). The rockfish transects were relatively ‘rough’, averaging 4.33 ± 0.77 in rugosity (Fig. 2.5A) with seafloor consisting primarily of boulder or bedrock with an attached sponge or coral (Fig. 2.5B). Rockfish were more frequently associated with these structures over the more available but less complex substratum types, such as sand and pebbles (Fig. 2.5B). Sponge structures scanned during rockfish transects ranged from 10 cm to 1 m in height and included *Farrea occa occa* (Fig. 2.3B), *Mycale bellabellensis*, *Poecillastra tenuilaminaris*, and *Heterochone calyx*; coral structures ranging from 1 to 2.5 m were *Primnoa pacifica* (red tree coral; Fig. 2.3C). The transects into the current from the rockfish were, in all 20 cases, the most rugose seafloor observed in the immediate surroundings. The rugosity of these transects was significantly higher than would be expected if rockfish were randomly distributed within their habitat (Fig. 2.5A; Wilcoxon Signed Ranks Test: $P = 0.001$).

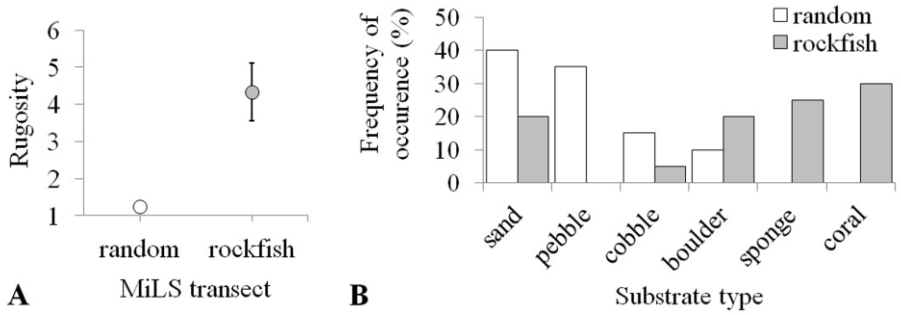

Figure 2.5. Paired microtopographic laser scanning (MiLS) transects on and around Learmonth Bank: a random transect (white) and a *Sebastes* rockfish transect (gray; $n = 20$). (A) The mean ± SE rugosity of the microtopography measured into the current from a station-holding rockfish is significantly higher than the region’s average rugosity (Wilcoxon Singed Ranks Test: $P = 0.001$) and (B) the frequency of occurrence of substratum shows rockfish associate with boulders, sponges, and corals over the more available but less complex substratum types.

Although deep-sea sponge and coral habitats have been identified as likely important to rockfish, it has proven difficult to determine the driver behind the associations. This is in part because work on the subject has used categorical descriptions of rockfish habitat usage (Krieger and Wing 2002; Freese and Wing 2003; Auster 2005, 2007; Du Preez and Tunnicliffe 2011 [Chapter 4]). Using MiLS, we have quantified small-scale seafloor rugosity and identified high roughness and relief as seafloor characteristics that attract rockfish. The location of the rugose structures, directly upstream from the station-holding rockfish, supports the hypothesis that the high relief and roughness of sponges and corals provide effective refuge from bottom current (also suggested by Auster 2007; Du Preez and Tunnicliffe 2011 [Chapter 4]).

Our 'off-bottom' platform did profile fragile deep-sea sponges and corals successfully but, with no bottom contact, it may be difficult to control camera height in some applications (as in Briggs 1989); rigorous care is required to maintain a constant slope while transecting. Controlling the flight path slope is likely the most difficult specification of the MiLS procedure, and transects that do not satisfy this requirement cannot be included in the analysis. The strong bottom current at Learmonth Bank did not present a challenge to maintaining a constant slope; rather, adjusting depth to transect over tall biostructures demanded the most care.

Our Learmonth Bank field study was a successful application of MiLS; video imagery supported annotation of multiple seafloor phenomena at the same centimeter-scale and resolved fauna distribution in relation to small-scale seafloor bottom rugosity. This deep-sea field study demonstrates MiLS usability, even in a relatively inaccessible habitat vulnerable to physical contact.

Discussion

Aquatic scientists require a standard yet versatile field method of measuring small-scale bottom roughness to address a breadth of scientific questions. Current techniques vary among habitats, largely dependent on accessibility. These techniques rarely support inter-habitat comparisons and may also be invasive. The deep sea is particularly poorly studied. Sonar, radar, and lidar are noninvasive but may be difficult to link with the small-scale phenomena of interest. As underwater image quality improves and submersible platforms diversify, the application of video transecting for small-scale measurements is promising.

Our goal was to develop and test a new technique for measuring small-scale bottom roughness using video transecting. The video transect technique of microtopographic laser scanning (MiLS) overcomes many of the challenges presented by traditional techniques. MiLS equipment is deployable on various types of platforms, hence there is potential to apply MiLS in any aquatic habitat. MiLS yields absolute measurements of bottom roughness resolved to ~1-2 cm (on the scale of visual context with the bottom) with a high degree of accuracy and precision. The off-bottom transect protocol is noninvasive, and the bottom imagery collected can be processed to generate associated data of many types of visual events.

Many fields of study may benefit from the MiLS approach. The chain-and-tape method to measure rugosity is popular on coral reefs (Hill and Wilkinson 2004); MiLS offers a relatively inexpensive off-bottom alternative to physical contact. For submarine geology, the ability to profile bedforms generated by currents and waves (Viana et al. 1998) will aid interpretation of the local hydraulic regime. A significant advantage of MiLS is

intercomparison among different habitats and studies to examine a broader generalization of roughness effects; for example, in benthic ecology, it will be possible to study the influence of organism-scale roughness on biodiversity patterns. MiLS may also support efforts in aquatic habitat restoration and conservation, particularly with respect to use of artificial substrata. It is important for the effective use of artificial substratum that we understand how small-scale roughness may enhance ecosystem development (Spieler et al. 2001; Sherman et al. 2002). Potential MiLS studies to guide the optimal design of artificial substratum include comparative studies referencing natural habitat roughness; temporal monitoring of roughness to inform on biostructure recruitment and growth; and investigating interactions of fauna from the subsequent video imagery.

Comments and recommendations

Researchers can use microtopographic laser scanning (MiLS) in any aquatic habitat accessible by a submarine platform. The sensitivity of MiLS to detect changes in microtopography is limited by the resolution of the equipment (video camera and laser) and the video analysis software, as well as the behavior of the platform in terms of speed and control. For transects with long length [links] ~~fractals~~ (x-axis) using a moving average of the present and previous frame's scale may increase length accuracy.

Our lab trial demonstrated the adapted MiLS technique for application in subaerial habitat. Unlike an aquatic system, the procedure does not require the calibration exercise. We recommend using an 'off-ground' platform, for example: a remotely control aircraft, balloon, or suspended glider on a wire system. Wetlands, forests, and the intertidal are subaerial habitats in which microtopographic roughness studies have been conducted

(e.g., Beatty 1984; Beck 1998; Moser et al. 2007). The advantages of the MiLS approach should be considered for future studies on land.

Acknowledgments

We thank the field team for data collection and advice, especially J. Boutillier (Chief Scientist), J. Rose, E. Edinger, and J. Chu. Personnel of the Canadian Scientific Submersible Facility and the Canadian Coast Guard Ship (CCGS) *John P. Tully* aided field operations. Our thanks to J. St Laurent for comments on the manuscript. Research is sponsored by the Natural Sciences and Engineering Research Council (NSERC) through the Canadian Healthy Oceans Network, a university-government partnership dedicated to biodiversity science for the sustainability of Canada's three oceans. Additional support was provided by a University of Victoria Fellowship and a NSERC postgraduate scholarship to C. Du Preez.

Literature cited

Ardron, J. A., G. S. Jamieson, and D. Hangaard. 2007. Spatial identification of closures to reduce the by-catch of corals and sponges in the groundfish trawl fishery, British Columbia, Canada. Bull. Mar. Sci. 81:157-167.

Auster, P. J. 2005. Are deep-water corals important habitats for fishes?, p. 747-760. *In* A. Freiwald and J. M. Roberts [eds.], Cold-water corals and ecosystems. Springer-Verlag. [doi:10.1007/3-540-27673-4_39].

———. 2007. Linking deep-water corals and fish populations. Bull. Mar. Sci. 81:93-99.

Barrie, J. V., and K. W. Conway. 1999. Late quaternary glaciation and postglacial stratigraphy of the Northern Pacific margin of Canada. Quart. Res. 51:113-123 [doi:10.1006/qres.1998.2021].

Beatty, S. W. 1984. Influence of microtopography and canopy species on spatial patterns of forest understory plants. Ecology 65:1406-1419 [doi:10.2307/1939121].

Beck, M. W. 1998. Comparison of the measurement and effects of habitat structure on gastropods in rocky intertidal and mangrove habitats. Mar. Ecol. Prog. Ser. 169:165-178 [doi:10.3354/meps169165].

Bornhold, B. D., and J. V. Barrie. 1991. Surficial sediments on the western Canadian continental shelf. Cont. Shelf Res. 11:685-699 [doi:10.1016/0278-4343(91)90074-G].

Boudreau, B. P., and B. B. Jørgensen. 2001. The benthic boundary layer: transport processes and biogeochemistry. Oxford Univ. Press.

Briggs, K. B. 1989. Microtopographical roughness of shallowwater continental shelves. IEEE J. Oceanic Eng. 14:360-367 [doi:10.1109/48.35986].

Caress, D. W., and others. 2008. High-resolution multibeam, sidescan, and subbottom surveys using the MBARI AUV D.

Allan B., p. 47-69. *In* J. R. Reynolds and H. G. Greene [eds.], Marine habitat mapping technology for Alaska. Alaska Sea Grant College Program, Univ. of Alaska Fairbanks [doi:10.4027/mhmta.2008.04].

Courtwright, J., and S. E. G. Findlay. 2011. Effects of microtopography on hydrology, physiochemistry, and vegatation in a tidal swamp of the Hudson River. Wetlands 31:239-249 [doi:10.1007/s13157-011-0156-9].

Du Preez, C., and V. Tunnicliffe. 2011. Shortspine thornyhead and rockfish (Scorpaenidae) distribution in response to substratum, biogenic structures and trawling. Mar. Ecol. Prog. Ser. 425:217-231 [doi:10.3354/meps09005].

Freese, J. L., and B. L. Wing. 2003. Juvenile red rockfish, *Sebastes* sp., associations with sponges in the Gulf of Alaska. Mar. Fish. Rev. 65:38-42.

Haralick, R. M., K. Shanmugam, and I. Dinstein. 1973. Textural features for image classification. IEEE Trans. Syst. Manage. Cyber. 3(6):610-621 [doi:10.1109/TSMC.1973.4309314].

Hill, J., and C. Wilkinson. 2004. Methods for ecological monitoring of coral reefs: a resource for managers. Australian Institute of Marine Science.

Krieger, K. J., and B. L. Wing. 2002. Megafauna associations with deepwater corals (*Primnoa* spp.) in the Gulf of Alaska. Hydrobiologia 47:83-90 [doi:10.1023/A:1016597119297].

Leatherman, S. P. 1987. Field measurement of microtopography. J. Coastal Res. 3(2):233-235.

Lund-Hansen, L. C., and others. 2004. A new video and digital camera system for studies of the dynamics of microtopographic features on tidal flats. Mar. Georesourc. Geotechnol. 22:115-122 [doi:10.1080/10641190490473443].

McCormick, M. I. 1994. Comparison of field methods for measuring surface topography and their associations with a tropical reef fish assemblage. Mar. Ecol. Prog. Ser. 112:87-96 [doi:10.3354/meps112087].

McCoy, E. D., S. S. Bell, and H. R. Mushinsky. 1991. Habitat structure: synthesis and perspectives, p. 427-430. *In* S. S. Bell, E. D. McCoy, and H. R. Mushinsky [eds.], Habitat structure: the physical arrangement of objects in space. Chapman and Hall.

Moser, K., C. Ahn, and G. Noe. 2007. Characterization of microtopography and its influence on vegetation patterns in created wetlands. Wetlands 27:1081-1097 [doi:10.1672/0277-5212(2007)27[1081:COMAII]2.0.CO;2].

Risk, M. J. 1972. Fish diversity on a coral reef in the Virgin Islands. Atoll Res. Bull. 193:1-6 [doi:10.5479/si.00775630.153.1].

Sanson, G. D., R. Stolk, and B. J. Downes. 1995. A new method for characterizing surface roughness and available space in biological systems. Funct. Ecol. 9:127-135 [doi:10.2307/2390100].

Sherman, R. L., D. S. Gilliam, and R. E. Spieler. 2002. Artificial reef design: void space, complexity, and attractants. ICES J. Mar. Sci. 59:S196-S200 [doi:10.1006/jmsc.2001.1163].

Shumway, C. A., H. A. Hofmann, and A. P. Dobberfuhl. 2007. Quantifying habitat complexity in aquatic ecosystems. Freshw. Biol. 52(6):1065-1076 [doi:10.1111/j.1365-2427.2007.01754.x].

Snelgrove, P. V. R., and C. R. Smith. 2002. A riot of species in an environment calm: the paradox of the species-rich deepsea floor. Oceanogr. Mar. Biol. 40:311-342.

Spieler, R. E., D. S. Gilliam, and R. L. Sherman. 2001. Artificial substrate and coral reef restoration: what do we need to know to know what we need. Bull. Mar. Sci. 69(2):1013-1030.

Thomas, T. R. 1999. Rough surfaces, 2nd ed. Impirical College Press.

Viana, A. R., J. -C. Faugères, and D. A. V. Stow. 1998. Bottom current-controlled sand deposits—a review of modern shallow-to deep-water environments. Sediment. Geol. 115:53-80 [doi:10.1016/S0037-0738(97)00087-0].

Walker, B. K., L. K. B. Jordan, and R. E. Spieler. 2009. Relationship of reef fish assemblages and topographic complexity on southeastern Florida coral reef habitats. J. Coastal Res. 53(6):39-48 [doi:10.2112/SI53-005.1].

Wright, C. W., and J. C. Brock. 2002. EAARL: a lidar for mapping shallow coral reefs and other coastal environments. Proc. Seventh International Conference on Remote Sensing for Marine and Coastal Environments, Miami.

Chapter 3: A new arc-chord ratio (ACR) rugosity index for quantifying landscape structural complexity

Preface

Chapter 3 is a methods article published in the peer-reviewed journal *Landscape Ecology*: Du Preez, C. (2014) A new arc-chord ratio (ACR) rugosity index for quantifying landscape structural complexity. *Landscape Ecology.* doi: 10.1007/s10980-014-0118-8. This is my first solo-author article although I received extremely helpful input and edits from Dr. Verena Tunnicliffe and from Dr. Rosaline Canessa (Thesis supervisor and Thesis committee member, University of Victoria).

Abstract

Introduction Rugosity is an index of surface roughness that is widely used as a measure of landscape structural complexity in studies investigating spatially explicit ecological patterns and processes. This paper identifies and demonstrates significant issues with how we presently measure rugosity and, by building on recent advances, proposes a novel rugosity index that overcomes these issues.

Methods The new arc-chord ratio (ACR) rugosity index is defined as the contoured area of the surface divided by the area of the surface orthogonally projected onto a plane of best fit (POBF), where the POBF is a function (interpolation) of the boundary data only. The ACR method is described in general, so that it may be applied to a range of rugosity analyses, and its application is detailed for three common analyses: (a) measuring the rugosity of a two-dimensional profile, (b) generating a rugosity raster from

an elevation raster (a three-dimensional analysis), and (c) measuring the rugosity of a three-dimensional surface.

Case studies and results Two case studies are used to compare the ACR rugosity index with the rugosity index most commonly used (i.e. surface ratio rugosity), demonstrating the advantages of the ACR index.

Discussion and conclusions The ACR method for quantifying rugosity is simple, accurate, extremely versatile, and consistent in its principles independent of data dimensionality (2-D or 3-D), scale and analysis software used. It overcomes significant issues presented by traditional rugosity indices (e.g. decouples rugosity from slope) and is a promising new landscape metric. To further increase ease of use I provide multiple ArcGIS® resources in the electronic supplementary materials (e.g. Du Preez 2014, Online Appendix 1: a downloadable ArcToolbox containing two ACR rugosity geoprocessing model tools).

Keywords

Rugosity · Arc-chord ratio · Slope · Structural complexity · Topographic heterogeneity · Landscape ecology · Roughness · ArcGIS

Introduction

Rugosity is an index of surface roughness that is a common measure for quantifying landscape structural complexity (i.e. topographic heterogeneity). Many scientific fields use rugosity to study the influence of structural complexity on biotic and abiotic patterns and processes, but rugosity is most often adopted in spatially explicit studies

investigating bio- or social-ecological patterns and processes e.g. environmental monitoring and assessment, Hill and Wilkinson 2004; habitat restoration, Moser et al. 2007; landscape modelling, Hoechstetter et al. 2008; ecosystem services management, Barsimantov 2010; predictive mapping, McArthur et al. 2010). The rugosity hypothesis most commonly studied is that of a positive relationship between species diversity and rugosity (Risk 1972; Levin 1974; Huston 1979; Beatty 1984; Cusson and Bourget 1997; Beck 1998; Levin et al. 2001; Gratwicke and Speight 2005; Dufour et al. 2006; Larkin et al. 2006; Moser et al. 2007; Schlacher et al. 2007; Shumway et al. 2007; Walker et al. 2009; Bridge et al. 2010). Rugosity may also indicate a specific species habitat as rugosity can be a surrogate of various environmental gradients (e.g. substrate type, Dunn and Halpin 2009; anthropogenic disturbance, Du Preez and Tunnicliffe 2011). Rugosity influences bio-ecological patterns and processes through various mechanisms (e.g. affecting the available surface for settlement, access to nutrients, protection from predation, exposure or shelter, hydrodynamics) but, as with any ecological pattern, the underlying drivers likely vary among species, habitats, and scales (Levin 1992; Chave 2013).

Although there are multiple measures of structural complexity (McCormick 1994), for over forty years many ecologists have used the rugosity index:

$$\text{Rugosity} = \frac{\text{Contoured distance}}{\text{Planar distance}} \text{ or } \frac{\text{Contoured area}}{\text{Planar area}} \qquad \text{(Eq. 1)}$$

where rugosity is a ratio of the contoured distance, or area of the surface, divided by the distance, or area of the surface, orthogonally projected onto a plane (i.e. planar distance or area; Fig. 3.1). A flat surface has a rugosity value = 1 (the minimum value possible), while a rougher surface, or a surface with more relief, has a higher rugosity value (>1).

The widespread use of rugosity is likely owing to its versatility: topographic (elevation) or bathymetric (depth) datasets can be collected using a variety of instruments and methods; rugosity can be calculated from two- or three-dimensional data at any scale; and the resulting index is a single dimensionless value—making it easy to scale up and useful in comparative studies (Stahl 1962). Despite its widespread use, there are a few significant issues with how we presently measure rugosity that require addressing.

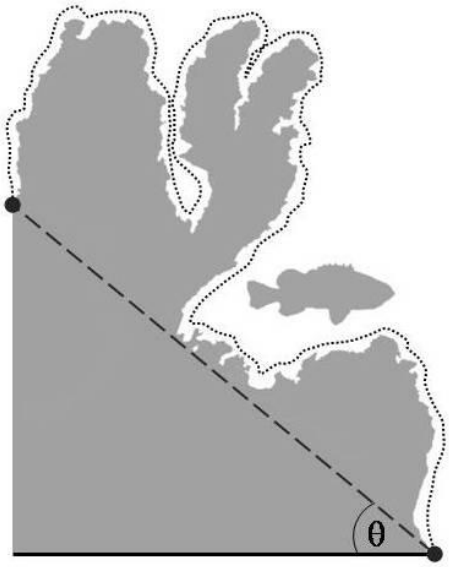

Fig. 3.1 The rugosity of a surface (e.g. grey profile of a coral reef) is the ratio between the contoured distance (*dotted line*; 11.12 m) and the planar distance (or area for three-dimensional data). The standard surface ratio (SR) method for calculating a planar distance is to project the surface onto a *horizontal plane* (solid line; 2.58 m), but this method inadvertently confounds rugosity with slope (θ) at the scale of the surface (*solid line*), whereas the arc-chord ratio (ACR) method calculates the planar distance by projecting the surface boundary onto a boundary data (*black dots*) plane of best fit (POBF; *dashed line*; 3.46 m) effectively decoupling rugosity from slope at the scale of the surface. The resulting rugosity indices for the two methods are 4.31 and 3.21 respectively

The standard surface ratio (SR) method for measuring rugosity was introduced in the early 1970s (Risk 1972; Dahl 1973). Likely owing to the modest hand-held instruments used and the limited analytical options, the denominator of the rugosity equation (Eq. 1)

was calculated by simply projecting the surface onto a horizontal plane (Lundblad et al. 2006; Wright and Heyman 2008; Friedman et al. 2012) thereby coupling rugosity with slope at the scale of the surface. Early spatial ecologists warned against using horizontal area units, specifying that the plane is misleading unless corrected for the actual surface (Dahl 1973). Using a horizontal plane to calculate rugosity puts arbitrary value on the relative orientation of the surface since distance and area (in this case the contoured distance/area; Eq. 1) increases with increasing slope (Fig. 3.2; law of cosines, where cos (θ) = adjacent side ÷ hypotenuse side). Therein lies the fundamental issue presented by the traditional methods for measuring rugosity. Despite advances in spatial data acquisition and processing, we have yet to readdress effectively how we measure rugosity without confounding and distorting the index with slope.

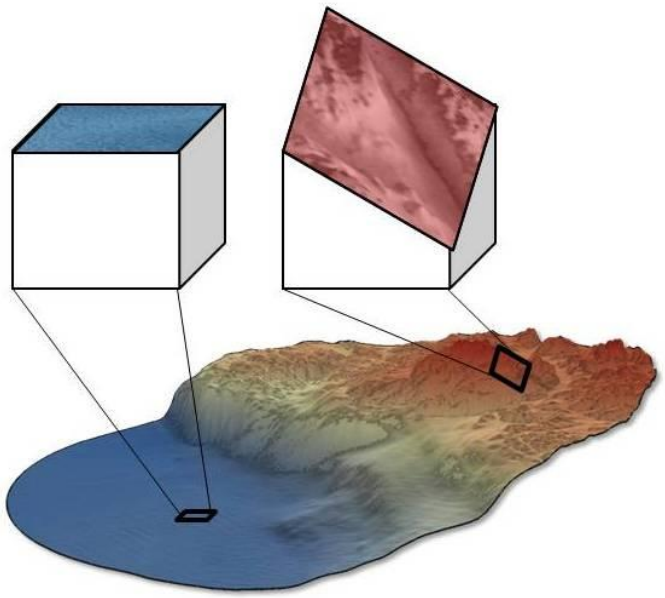

Fig. 3.2 Two windows of equal horizontal dimensions but varying slopes and areas. The area within a fixed window increases with increasing slope (law of cosines). A surface with no overall slope (0°; left window) is minimal whereas a surface with slope (>0°; right window) is larger. Slope at the scale of the surface confounds surface ratio (SR) rugosity by exaggerating the contoured area (Eq. 1). The arc–chord ratio (ACR) method decouples rugosity from slope at the scale of the surface by increasing the planar area (Eq. 1) as a function of the slope too

Coupling rugosity with slope is not a trivial oversight, as most natural surfaces have some degree of slope and slope is an independent geomorphic component of the environment known to have its own significant effects on the distribution of organisms and on ecological processes (Swanson et al. 1988). Erroneous rugosity-related findings may have significant implications, as studies that use rugosity have informed a variety of subjects, including: environmental risk assessment, species management and conservation, distribution of commercial species, and predictive mapping of vulnerable marine ecosystems (Stambaugh and Guyette 2008; Wedding et al. 2008; Galparsoro et al. 2009; Woodby et al. 2009). With the increasing number of studies that use landscape spatial analyses, it is critical to understand and enhance those metrics most commonly used (Wu 2013).

Two studies recently proposed similar methods for measuring the rugosity of a two-dimensional profile independent of slope (Du Preez and Tunnicliffe 2012; Friedman et al. 2012). Instead of projecting the surface onto a horizontal plane, the methods use a plane of best fit (POBF; Fig. 3.1). In both studies, the POBF is a function of the boundary data only (the two end points of the profile). By using the boundary data to generate the denominator, the rugosity equation (Eq. 1) is synonymous with a simple arc–chord ratio (ACR) and the resulting rugosity index is independent of slope at the scale of the surface. With the increasing availability and usage of multibeam sonar and LIDAR, there is a pressing need to adapt this two-dimensional solution for three-dimensional analyses.

Friedman et al. (2012) made a positive advance in measuring the rugosity index of a three-dimensional surface independent of slope. Using a principal component analysis of the surface dataset, they replace the horizontal plane with a POBF (Fig. 3.3). This method

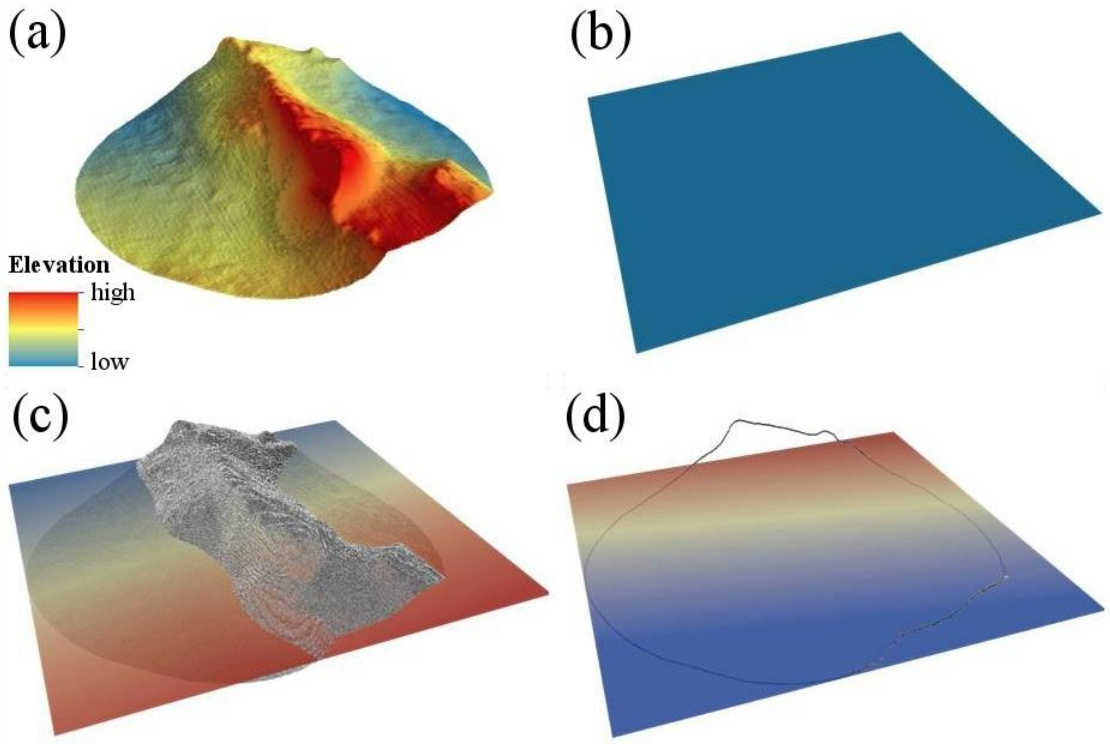

Fig. 3.3 **a** A three-dimensional surface, and **b–d** the data (*black dots*) and generated planes used by three different methods for measuring rugosity: **b** a *horizontal plane* (no data required) used in the surface ratio (SR) method, **c** the entire dataset plane of best fit (POBF) used in the principal component analysis method, and **d** the boundary data POBF used in the arc-chord ratio (ACR) method. The resulting planes of the different methods vary in slope (and aspect), which affects the planar area of the rugosity index equation (Eq. 1)

effectively decouples rugosity from slope at the scale of the surface; however, the entire dataset is used to calculate both components of the rugosity equation (Eq. 1; the denominator becomes numerator dependent). This approach is inconsistent with the widely accepted definition and method for calculating two-dimensional rugosity and problematic for the comparability of the rugosity index. For example, measuring two-dimensional rugosity along multiple transects within a sample area is a common technique used to represent three-dimensional rugosity but it assumes methodological consistency independent of data dimensionality.

Quantifying spatial patterns is a fundamental step to addressing key research questions regarding patterns of organisms, materials, energy and disturbance in relation to landscape heterogeneity and their underlying present and historic processes (Risser et al. 1984; Wu 2013). Here, I propose a novel method for measuring rugosity that (1) decouples rugosity from slope and (2) is consistently independent of data dimensionality and scale. The method builds on recent advances and utilizes modern tools but, in principle, it is a simple adaptation of an ACR. The method replaces the horizontal plane with a POBF, where the POBF is a function (interpolation) of the boundary data only (Fig. 3.3d). Thus, rugosity is decoupled from slope at the scale of the surface, while remaining consistent with two-dimensional analyses by maintaining the independence of the numerator and denominator in the rugosity equation (Eq. 1). Furthermore, the ACR method can be used in multi-scale analyses, an important attribute of a spatial analysis as ecological processes act at a variety of spatial scales (Levin 1992), and differ in effects and importance with scale (Wu 2013).

I describe the ACR method for measuring rugosity in general, so that it may be applied to a range of analyses (i.e. various types of data and software), and I detail its application for three common analyses: (a) measuring the rugosity of a two-dimensional profile, (b) generating a rugosity raster from an elevation raster (i.e. measuring the rugosity index of each raster cell; a three-dimensional analysis), and (c) measuring the rugosity of a three-dimensional surface. Using the ACR method is not limited to specific software, but to further increase ease of use I provide multiple ArcGIS® resources in the electronic supplementary materials including two geoprocessing model tools capable of batch processing (ArcToolbox available in Du Preez 2014, Online Appendix 1) and systematic

instructions on how to execute the steps manually in ArcGIS® (Du Preez 2014, Online Appendices 2, 3 [Appendices C, D]). I also include two case studies in which I use real multibeam bathymetry data to compare the standard SR method and the ACR method and demonstrate the advantages and drawbacks of this new method for measuring rugosity.

Methods

Data collection

Measuring rugosity requires two- or three-dimensional topographic (elevation) or bathymetric (depth) data. Datasets can be collected using a variety of field methods, including conventional surveying equipment, a falling-rod gauge, stereo imagery, LiDAR, and multibeam bathymetry. The number, size, and shape of the surfaces to be analysed is study specific. These variables are influenced by a combination of the purpose of the study, sampling design, the extent of the surveyed area and the data resolution. Data scale and resolution are also important factors in the comparability between studies and these metadata should be provided with study results.

Software

The arc–chord ratio (ACR) method for measuring rugosity is not limited to specific software. Options for managing and processing data include ArcGIS®, MATLAB®, R®, and Microsoft Excel®. In the present paper I focus on ArcGIS® (version 10.2; ESRI 2013), since it is one of the most widely used softwares for three-dimensional landscape analyses. I used the following extensions while working in ArcGIS®: 3D Analyst, Geostatistical Analyst, Spatial Analyst, and the DEM (Digital Elevation Model) Surface Tools extension (version 2.1, Jenness 2013).

Arc-chord ratio rugosity index

Despite its versatility, the principal steps of the arc–chord ratio (ACR) method for measuring rugosity are constant (Fig. 3.4). There are six basic steps that can be divided into two main tasks: calculating the contoured area and calculating the planar area (or distance if data is two-dimensional), where the last step it to solve for ACR rugosity using the rugosity index equation (Eq. 1).

To calculate the contoured area, first generate a continuous surface by interpolating the elevation (i.e. topographic or bathymetric) data into a triangulated network (step 1). The contoured area equals the sum of all the triangulated areas (step 2).

Similar to Friedman et al. (2012), the ACR method orthogonally projects the surface onto a plane of best fit (POBF) rather than a horizontal plane—decoupling rugosity from slope at the scale of the surface (Du Preez and Tunnicliffe 2012; Friedman et al. 2012). The innovation of the ACR method lies in the analysis used to generate the POBF: identify and isolate the boundary data (step 3), and use a linear polynomial interpolation of the boundary data to generate the POBF (step 4). The planar area equals the orthogonal projection of the surface onto the POBF (step 5). For software that is unable to interpolate the actual planar area, an alternative is to interpolate the angle of the POBF and use the cosine equation (and the horizontal planar area) to solve for the POBF planar area. To solve for the ACR rugosity index, use the contoured area, planar area, and rugosity index equation (Eq. 1; step 6).

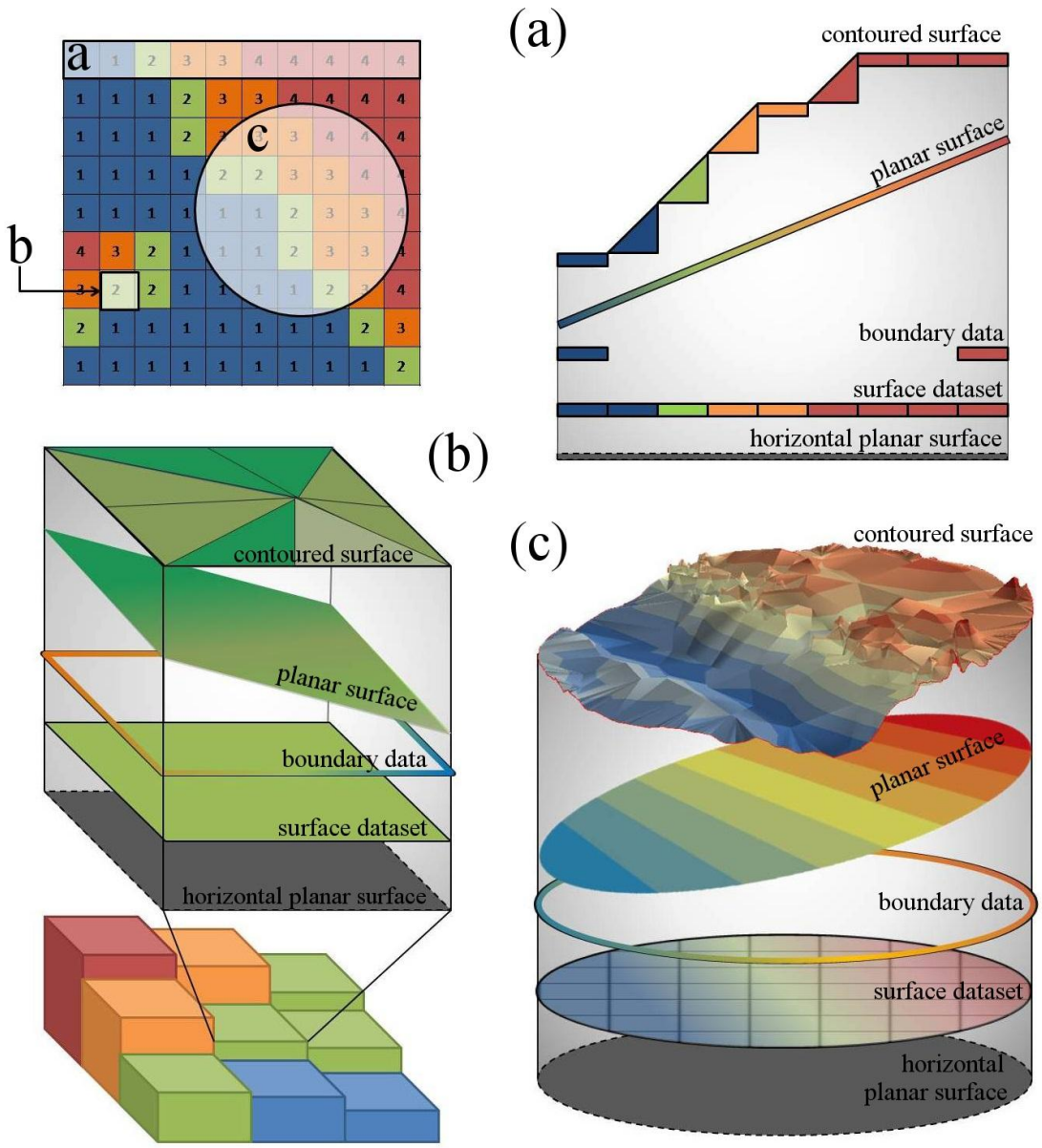

Fig. 3.4 An elevation raster dataset with overlays of the surface datasets (spatial subsets) most commonly used in rugosity analyses: **a** a two-dimensional profile, **b** individual raster cells (i.e. generating a rugosity raster from an elevation raster), and **c** a three-dimensional surface. **a–c** The arc–chord ratio (ACR) method for measuring rugosity is consistently independent of the data dimensionality. Steps include triangulating the contoured surface, generating the planar surface from the boundary data plane of best fit (POBF), and (optional) calculating slope at the scale of the surface using the law of cosines and the horizontal planar area (see Table 3.1 for details)

Table 3.1 The steps for measuring the arc-cord ratio (ACR) rugosity index of: (a) a two-dimensional profile, (b) each raster cell (i.e. generating a rugosity raster from an elevation raster), and (c) a three-dimensional surface (see Fig. 3.4 for diagrams of each analysis)

	Two-dimensional:	Three-dimensional	
	(a) Profile to ACR rugosity index[a]	(b) Elevation raster to ACR rugosity raster	(c) Surface to ACR rugosity index
Input data	Series of x/y elevation data	Elevation raster (each cell analysed individually)	Elevation raster & window feature (defining the spatial subset of the dataset to be analysed)
Output data	A single rugosity index value	A raster with an ACR rugosity attribute value for each cell	A single rugosity index value
Software program	Nonspecific (e.g. Microsoft Excel®)	For this example: ArcGIS® (version 10.2; ESRI 2013)	For this example: ArcGIS® (version 10.2; ESRI 2013)
Step 1 create a triangulated network representing the contoured distance/area	Calculate the hypotenuse between each successive data point of the profile	Use a 3-D interpretation of a moving 3 by 3 cell window to generate a network of eight triangles per cell (Surface Area extension, DEM Surface Tools for ArcGIS, Jenness 2004)	Convert the raster dataset into a triangulated irregular network (TIN; *Raster to TIN*)
Step 2 calculate the contoured distance/area	The contoured distance equals the sum of all the hypotenuse lengths	The contoured area equals the sum of the triangle areas within the cell (incorporated in the previous step)	(i) Clip the TIN using the window feature (*Edit TIN*) (ii) The contoured area equals the sum of the triangle areas within the window (*Polygon Volume*)
Step 3 identify & isolate the boundary data	The two end points of the profile	(incorporated in the next step)	The raster cells intersected by the windows perimeter (multiple tools required: *Buffer*, *Clip*, & *Raster to Point*)
Step 4 interpolate the plane of best fit (or its slope)	Use a linear interpolation between the two end points (i.e. hypotenuse between the two end points of the profile)	Calculate the slope of each cell (*Slope*; uses a moving 3 by 3 cell window)	Interpolate a linear polynomial for the boundary elevation data and convert the output polygon to a TIN (*First-Order Global Polynomial Interpolation* & *Raster to TIN*)
Step 5 calculate the planar distance/area	The planar distance equals the linear interpolation distance between the two end points	Calculate the planar area using the cosine equation, the slope, and the horizontal cell area (*Raster Calculator*) [Note: trigonometric functions require angle values to be converted into radians first, i.e. multiple degrees by 0.01745]	(i) Orthogonally project the window onto the fitted plane (*Edit TIN*) (ii) The planar area equals the sum of the triangle areas within the window (*Polygon Volume*)
Step 6 calculate the ACR rugosity	Solve for Eq. 1 using the contoured distance and planar distance	Solve for Eq. 1 using the contoured area and planar area (*Raster Calculator*)	Solve for Eq. 1 using the contoured area and planar area (*Add Field* & *Calculate Field*)
Additional step (optional)	Solve for the surface-scale slope using the cosine equation	Solve for the surface-scale (cell) aspect (*Aspect*; slope already calculated in Step 4)	Solve for the surface-scale slope & aspect (*Surface slope* & *Surface aspect*)

ArcGIS® tools are in italics.

[a] Steps adapted from Du Preez and Tunnicliffe (2012) but summarized and presented to demonstrate the methodological consistency of the ACR method and to provide a comprehensive list of how it can be applied

These six principal steps can be easily applied with methodological consistency to the three most common rugosity analyses, measuring the rugosity of: (a) a two-dimensional profile, (b) individual raster cells (i.e. generating a rugosity raster from an elevation raster; a three-dimensional analysis), and (c) a three-dimensional surface (Table 3.1). Additional planar parameters slope and aspect can also be easily calculated (Table 3.1). See Du Preez 2014, Online Appendix 1 for ArcGIS® geoprocessing model tools (in an ArcToolbox) and Online Appendices 2 and 3 [Appendices C, D] for ArcGIS® systematic instructions for the two three-dimensional rugosity analyses.

Case Studies and Results

Two case studies were conducted to assess the strengths and drawbacks of applying the arc–chord ratio (ACR) method to the two most common three-dimensional rugosity analyses: generating a rugosity raster from an elevation raster and measuring the rugosity index of a three-dimensional surface. In both case studies the standard surface ratio (SR) method is used as a comparison (which uses a horizontal planar area). The SR method is the most widely used and, as with the ACR method, the SR method is consistent in its application independent of data dimensionality.

Both case studies use an elevation raster dataset of Learmonth Bank, British Columbia (54°24'59"N, 133°05'00"W). The survey of Learmonth Bank was conducted from the Canadian Coast Guard Ship Vector using a ship-based multibeam ecosounder (Simrad® EM 1002, Kongsberg Maritime, Norway; Milner 2008). The resulting raster covers approximately 42 km × 38 km of seafloor at a resolution of 5 by 5 m (cell size).

Learmonth Bank is a submarine sill of rugged volcanic bedrock with scattered erratic boulders and unconsolidated glacial moraines, geologic features from the regions glaciated periods (Bornhold and Barrie 1991; Barrie and Conway 1999, 2002). The bank's plateau often ends abruptly as a steep ridge towering over the surrounding flat sandy basin. The bank spans much of Dixon Entrance, rising from -480 to -25 m and, likely owing to tidal rectification and density forcing, is encircled by a clockwise eddy (Crawford and Greisman 1987; Bornhold and Barrie 1991; Ballantyne et al. 1996; Barrie and Conway 1999). Learmonth Bank was primarily selected as a study site for its variability in elevation and slope but Learmonth Bank also receives a great deal of scientific interest owing to its abundance of vulnerable marine ecosystems (Du Preez and Tunnicliffe 2011; Neves et al. 2014), the high activity of commercial fisheries (Sinclair et al. 2005), its potential as a marine protected area (Ardron 2005), and the contention over an international border placement (Gray 1997).

I used ArcGIS® (version 10.2; ESRI 2013) and the ACR rugosity model tools (ArcToolbox available for download in Du Preez 20014, Online Appendix 1) for the rugosity analyses and PASW® Statistics 18 for the statistical analyses. Kolmogorov–Smirnov tests indicated non-normal distributed data (for $n < 50$), therefore correlations were performed using the non-parametric Spearman correlation (significant at $p < 0.05$).

Case study 1: comparing methods for generating a rugosity raster from an elevation raster

I derived four secondary rasters from the primary Learmonth Bank elevation raster: a slope raster (Fig. 3.5a), a standard surface ratio (SR) rugosity raster (Fig. 3.5b), an arc–chord ratio (ACR) rugosity raster (Fig. 3.5c), and a ratio of the two rugosity indices raster

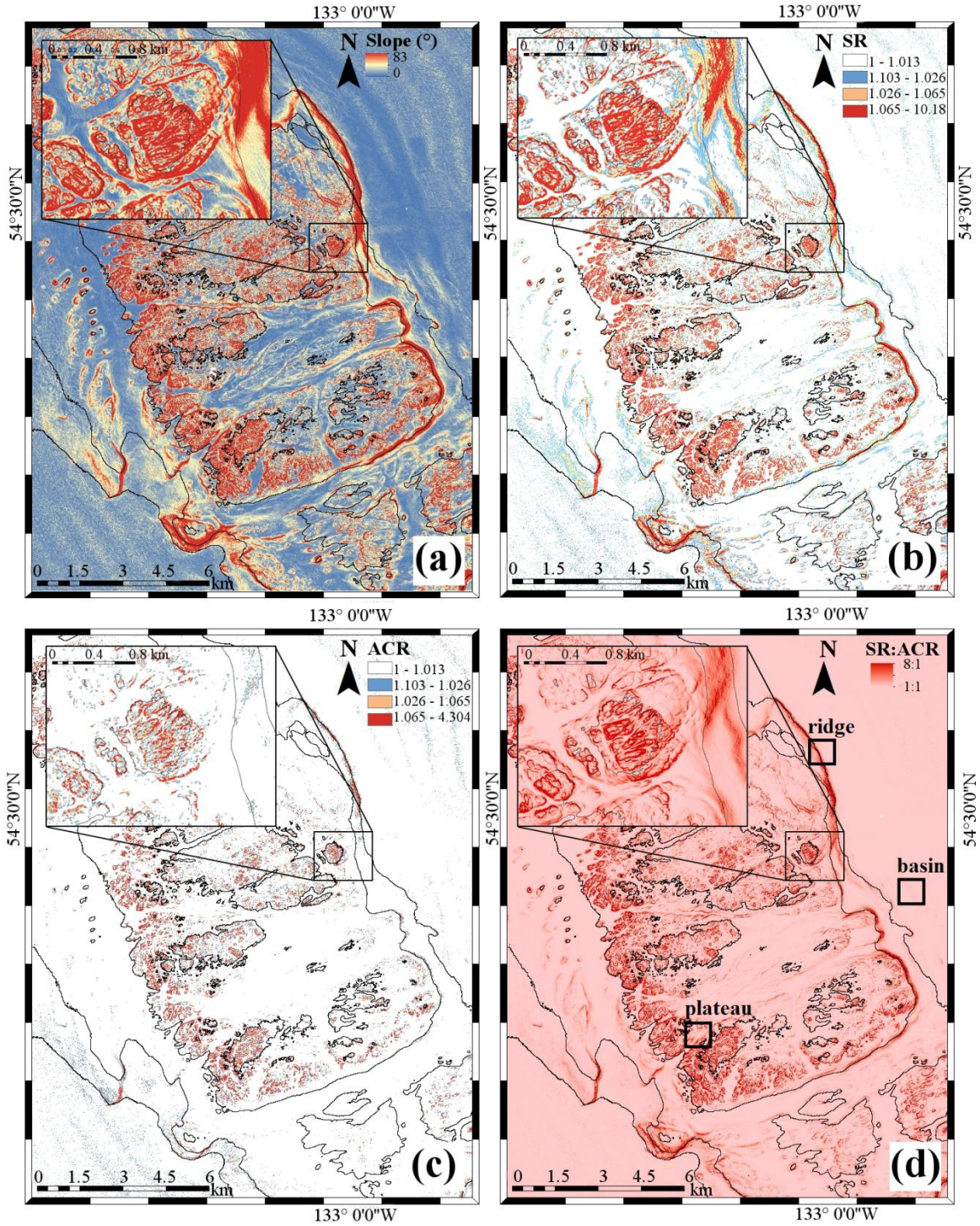

Fig. 3.5 Four raster maps of Learmonth Bank, British Columbia, Canada: **a** slope in degrees, **b** standard surface-ratio (SR) rugosity, **c** arc–chord ratio (ACR) rugosity, and **d** the ratio of SR and ACR rugosity values. Insets show a magnified example area (2 km × 1.8 km) of the bank plateau and steep eastern ridge. Bold black boxes indicate spatial subsets used in second case study: from the basin, ridge and plateau (see Fig. 3.6). Black contour lines at 100 m intervals

(SR:ACR; Fig. 3.5d). The slope raster was generated using the ArcGIS® slope function. The SR rugosity raster was generated using the Calculate Surface Ratio Raster extension tool (Jenness 2013). The ACR rugosity raster was generated using the *Elevation Raster to ACR Rugosity Raster* geoprocessing model tool (Du Preez 2014, Online Appendix 1; steps described in Table 3.1). The SR:ACR ratio raster was generated using the ArcGIS® raster calculator. Statistical analyses were performed using a random1,000 data point subsample.

The seafloor of Learmonth Bank ranges in slope from horizontal to near vertical (0°–83°; Fig. 3.5a). The steepest regions of Learmonth Bank (red areas in Fig. 3.5a) are also the most rugose regions (red areas in Fig. 3.5b, c; e.g. the ridges of the bank). Spearman correlation tests confirm a strong significant positive correlation between slope and SR rugosity ($r = 0.871$, $p < 0.001$, $n = 1{,}000$), and a weaker, but still significant, positive correlation between slope and ACR rugosity ($r = 0.517$, $p < 0.001$, $n = 1{,}000$). The difference between the two indices (i.e. the SR:ACR ratio; Fig. 3.5d) is highest in steep regions (red areas in Fig. 3.5a) and a Spearman correlation test confirms that the difference is exponentially correlated with slope ($r = 1.0$, $p < 0.001$, $n = 1{,}000$). Although it is intuitive that slope and rugosity have some correlation (because ridges and cliffs usually have a rough topography), SR rugosity is both correlated and confounded by slope at the scale of the surface (i.e. raster cell size). As a result the SR rugosity value of over 91 % of the raster cells in this case study are up to eight times greater than the rugosity values measured using the ACR method (Fig. 3.5d).

Case study 2: comparing methods for measuring the rugosity of a three-dimensional surface

The second case study considers three 1 km^2 square spatial subsets of the Learmonth Bank elevation raster: surface A is from the sandy basin, surface B is from the northeast ridge, and surface C is from the glacier-scarred plateau (Fig. 3.6). The slope (in degrees), surface ratio (SR) rugosity, and arc–chord ratio (ACR) rugosity were measured for each surface (Fig. 3.6). ACR rugosity was measured using the *Elevation Raster to ACR Rugosity Index* geoprocessing model tool (Du Preez 2014, Online Appendix 1; steps described in Table 3.1). Slope was calculated from the ACR rugosity using the cosine equation. SR rugosity was measured using the same steps as the ACR rugosity (Table 3.1), but the plane of best fit (POBF) was replaced with a horizontal plane.

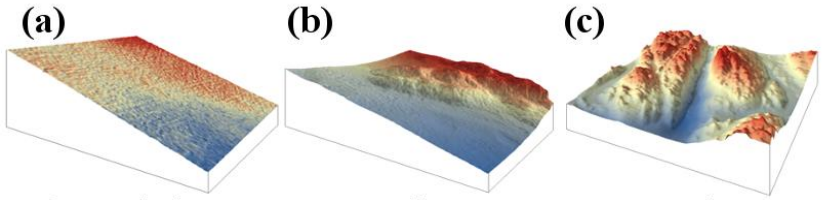

Landscape	basin	ridge	plateau
Slope	20.2°	19.0°	9.9°
SR	1.0656	1.0629	1.0355
ACR	1.0000	1.0050	1.0201

Fig. 3.6 Three-dimensional surfaces with slope (at the scale of the surface), surface ratio (SR) rugosity, and arc–chord ratio (ACR) rugosity values. Despite the visual evidence, the SR rugosity values indicate surface A is the most rugose and surface C is the least. In contrast, the ACR rugosity values indicate surface A is flat and surface C is the most rugose. Surfaces: 1 km^2 clipped spatial subsets from the **a** basin, **b** ridge, and **c** plateau of Learmonth Bank, British Columbia (see Fig. 3.5 for locations) [for display purposes surfaces have a 3-times vertical exaggeration]

The three surfaces vary in slope, SR rugosity, and ACR rugosity (Fig. 3.6). Surface A has the greatest slope and C has the smallest. Despite the visual evidence (Fig. 3.6), the

SR rugosity values indicate surface A is the most rugose and surface C is the least. In contrast, the ACR rugosity values indicate surface A is a flat plane with no rugosity and surface C is the most rugose. The three surfaces represent a rare situation where slope and structural complexity are negatively correlated. Owing to this relationship, this case study demonstrates how a SR rugosity index can be an artifact of slope and misrepresent the degree of structural complexity (by over- or under-exaggerating it).

Discussion

The new arc–chord ratio (ACR) rugosity index for quantifying landscape structural complexity was developed to overcome significant issues presented by traditional rugosity indices. In comparison to other methods for measuring rugosity, there are several advantages of the ACR rugosity index indentified and demonstrated in this paper: (1) ACR rugosity is separated from slope at the scale of the surface (potentially enabling enhanced detection of patterns and processes related solely to structural complexity), (2) the ACR rugosity principles are consistently independent of data dimensionality, (3) there is consistency in the ACR methodology (six basic steps) despite the versatility in its application, (4) the ACR method maintains independence of the numerator and denominator in the rugosity equation, (5) the ACR rugosity index is comparable between different habitats and studies (assuming equal data resolution and extent), (6) it is easy to calculate slope as a separate environmental parameter using the ACR method, and (7) it is quick and easy to execute an ACR rugosity analyses using the ArcGIS® geoprocessing model tools (ArcToolbox available for download in Du Preez 2014, Online Appendix 1). In comparison to other methods for measuring rugosity, the ACR method can be slightly

more labour intensive as it requires additional steps (i.e. identifying, isolating, and interpolating the boundary data) but using the geoprocessing model tools obviates this drawback.

The primary objective behind developing a new rugosity index was to decouple rugosity from slope (similar to terrain ruggedness, which is less correlated with slope than traditional rugosity indices; Sappington et al. 2007). In the two case studies, the standard surface ratio (SR) method (most commonly used rugosity index) yielded exaggerated rugosity measurements (Figs. 3.5d, 3.6) where amplification of the measurement was related exponentially to the slope at the scale of the surface. Most natural surfaces have some degree of slope (e.g. Figs. 3.5a, 3.6) and, if not controlled for, part or all the rugosity measurement will be an artifact of slope. Since the rugosity-slope issue is embedded in the details of the standard SR equation, many ecological studies that use or suggest the SR method do not recognize the problem (Roberts and Ormond 1987; Ierodiaconou et al. 2007; Wedding et al. 2008). Some studies inadvertently exacerbate the issue by including both SR rugosity and slope as independent environmental parameters within the same analyses (Ahsan 2010; Henry et al. 2013). The ACR rugosity index allows analysts to examine both parameters without confounding effects.

The second objective behind developing a new rugosity index was to produce a method that is consistently independent of data dimensionality and scale. The ACR rugosity index fulfills this objective and will enable future research to consider both study aspects based on other important factors; for example, linear two-dimensional data are strongly coupled to directionality and, as with any spatial heterogeneity metric, different spatial resolutions and extents will yield different rugosity values and corresponding ecological

patterns and processes (Levin 1992; Wu 2004; Chave 2013). With the increasing ease of spatial analyses, a multi-scale approach is strongly suggested for comprehensive research in the future.

Although rugosity is the most widely used index (likely owing to the simplicity of its definition), there are many other indices used for measuring landscape structural complexity, ranging from descriptive to counts of discrete structures, from categorical to quantitative, from measures of overall variability (i.e. nonspatial) to local variability (i.e. spatial). Examples of other popular metrics used in landscape ecology include: the standard deviation of elevation or slope (basic summary statistics of surface characteristics; McCormick 1994), three-dimensional vector variation metrics (e.g. the surface roughness factor, Hobson 1972; terrain ruggedness, Sappington et al. 2007), and the topographic position index (identifies relative position in relation to its local neighbourhood; Jenness 2006). The field of surface metrology (measuring microscopic features on precision surfaces) also offers a variety of metrics for quantifying surface roughness, for example: ten-point height, surface area ratio and root mean square slope (McGarigal et al. 2009; as calculated using Scanning Probe Image Processor software, SPIP). Although the ecological relevance of these metrology metrics remains largely unknown, McGarigal et al. (2009) demonstrate surface roughness metrics that are conceptually and theoretically independent are actually highly correlated and they advocate that these metrics have the potential to offer new insights into landscape pattern-process relationships. ACR rugosity is similar to the metrology surface area ratio metric (SPIP) insofar as both metrics are ratios of surface area and a planar area but, as with SR rugosity, the surface area ratio metric uses a horizontal (xy) planar area (SPIP).

Like all indices, rugosity has its own strengths and limitations in its ability to differentiate structural complexity (McCormick 1994). Since ACR metrics are a function of relief and roughness (Moser et al. 2007), a single rugosity value can be calculated from a variety of different surface profiles. Certain features, such as large abrupt depressions, would produce the same rugosity measurement as a mound with the equivalent protruding topography but the effect of a depression and a mound on environmental gradients maybe opposite (e.g. hydrodynamics; Nowell and Jumars 1982). In future work, it may be advantageous to calculate ACR rugosity in reference to the plane of best fit (similar to a position index; e.g. Jenness 2006), such that a positive value represents relief and a negative value represents a depression.

Many scientists suggest using multiple landscape metrics when studying ecological patterns and processes owing to the complexity of the systems (e.g. Wilson et al. 2007). Software packages facilitating such analyses include the ArcGIS Benthic Terrain Modeler (BTM; Wright et al. 2012) and FRAGSTATS (McGarigal et al. 2012). With the adaptability of the ACR rugosity index, future research could incorporate it as one of many metrics in a landscape analysis.

The present paper provides multiple resources to facilitate use, so the ACR method can be widely adopted and further improved (e.g. ArcGIS® geoprocessing model tools and step-by-step instructions; available in the Du Preez 2014 Online Appendices). Improving standard methods for the detection and investigation of bio- and social-ecological patterns will lead to better scientific information for generalizations, ecological theory, and management and conservation initiatives.

Acknowledgements

My thanks to V. Tunnicliffe (supervisor and mentor) for her invaluable support and advice and R. Canessa for introducing me to GIS; both provided valuable comments on the manuscript. I also thank my colleagues J. Rose, and E. Edinger for their helpful ideas. Learmonth Bank multibeam bathymetry was collected by the Canadian Hydrographic Service and personnel of the Canadian Coast Guard Ship (CCGS) Vector, and provided by J. Vaughn Barrie (Geological Survey of Canada). Research was sponsored by the Natural Sciences and Engineering Research Council (NSERC) through the Canadian Healthy Oceans Network, a university-government partnership dedicated to biodiversity science for the sustainability of Canada's three oceans. Additional support was provided by a University of Victoria Fellowship and a NSERC postgraduate scholarship.

Literature cited

Ahsan N (2010) Predictive habitat models from AUV-based multibeam and optical imagery. In: OCEANS 2010 MTS/IEEE Seattle, IEEE, Seattle

Ardron J (2005) Protecting British Columbia's coral and sponges. Living oceans society report (v. 1.0), Sointula, BC

Ballantyne VA, Foreman MGG, Crawford WR, Jacques R (1996) Three-dimensional model simulations for the north coast of British Columbia. Cont Shelf Res 16:1655–1682

Barrie JV, Conway KW (1999) Late quaternary glaciation and postglacial stratigraphy of the Northern Pacific margin of Canada. Quart Res 51:113–123. doi:10.1006/qres.1998.2021

Barrie JV, Conway KW (2002) Contrasting glacial sedimentation processes and sea-level changes in two adjacent basins on the Pacific margin of Canada. In: Dowdeswell J, O'Cofaigh C (eds) Glacier-influenced sedimentation on high-latitude continental margins. Geological Society, London 203:181–194

Barsimantov JA (2010) Vicious and virtuous cycles and the role of external non-government actors in community forestry in Oaxaca and Michoacán, Mexico. Hum Ecol 38(1):49–63

Beatty SW (1984) Influence of microtopography and canopy species on spatial patterns of forest understory plants. Ecology 65:1406–1419. doi:10.2307/1939121

Beck MW (1998) Comparison of the measurement and effects of habitat structure on gastropods in rocky intertidal and mangrove habitats. Mar Ecol Prog Ser 169:165–178

Bornhold BD, Barrie JV (1991) Surficial sediments on the western Canadian continental shelf. Cont Shelf Res 11:685–699. doi:10.1016/0278-4343(91)90074-G

Bridge TCL, Done TJ, Beaman RJ, Friedman A, Williams SB, Pizarro O, Webster JM (2010) Topography, substratum and benthic macrofaunal relationships on a tropical mesophotic shelf margin, central Great Barrier Reef, Australia. Coral Reefs 30:143–153

Chave J (2013) The problem of pattern and scale in ecology: what have we learned in 20 years? Ecol Lett. doi:10.1111/ele.12048

Crawford RW, Greisman P (1987) Investigation of permanent eddies in Dixon Entrance, British Columbia. Cont Shelf Res 7:851–870

Cusson M, Bourget E (1997) Influence of topographic heterogeneity and spatial scales on the structure of the neighbouring intertidal endobenthic macrofaunal community. Mar Ecol Prog Ser 150:181–193

Dahl AL (1973) Surface area in ecological analysis: quantification of benthic coral-reef algae. Mar Biol 23:239–249

Du Preez, C. 2014. A new arc-chord ratio rugosity index for quantifying three-dimensional landscape structural complexity. Landscape Ecology. doi: 10.1007/s10980-014-0118-8.

Du Preez C, Tunnicliffe V (2011) Shortspine thornyhead and rockfish (Scorpaenidae) distribution in response to substratum, biogenic structures and trawling. Mar Ecol Prog Ser 425:217–231

Du Preez C, Tunnicliffe V (2012) A new video survey method of microtopographic laser scanning (MiLS) to measure small scale seafloor bottom roughness. Limnol Oceanogr Method 10:899–909

Dufour A, Gadallah F, Wagner HH, Guisan A, Buttler A (2006) Plant species richness and environmental heterogeneity in a mountain landscape: effects of variability and spatial configuration. Ecography 29:573–584

Dunn DC, Halpin PN (2009) Rugosity-based regional modeling of hard-bottom habitat. Mar Ecol Prog Ser 377:1–11

ESRI (2013) ArcGIS Desktop 10.2. Environmental Systems Resource Institute, Redlands, California

Friedman A, Pizarro O, Williams SB, Johnson-Roberson M (2012) Multi-scale measures of rugosity, slope and aspect from benthic stereo image reconstructions. PLoS One 7(12):1–14

Galparsoro I, BorjaA ´ , Bald J, Liria P, Chust G (2009) Predicting suitable habitat for the European lobster (Homarus gammarus), on the Basque continental shelf (Bay of Biscay), using Ecological-Niche Factor analysis. Ecol Model 220:556–567

Gratwicke B, Speight MR (2005) The relationship between fish species richness, abundance and habitat complexity in a range of shallow tropical marine habitats. J Fish Biol 66:650–667. doi:10.1111/j.1095-8649.2005.00629.x

Gray DH (1997) Canada's unresolved maritime boundaries. Boundary Secur Bull 5(3):61–71

Henry L-A, Navas JM, Hennige SJ, Wicks LC, Vad J, Roberts JM (2013) Cold-water coral reef habitats benefit recreationally valuable sharks. Biol Conserv 161:67–70

Hill J, Wilkinson C (2004) Methods for ecological monitoring of coral reefs. Australian Institute of Marine Science, Townsville

Hobson RD (1972) Surface roughness in topography: quantitative approach. In: Chorley RJ (ed) Spatial analysis in gemorphology. Harper and Row, New York, pp 221–245

Hoechstetter S, Walz U, Dang LH, Thinh NX (2008) Effects of topography and surface roughness in analyses of landscape structure: a proposal to modify the existing set of landscape metrics. Landscape Online 3:1–14. doi:10.3097/LO.200803

Huston M (1979) A general hypothesis of species diversity. Am Nat 113(1):81–101

Ierodiaconou D, Laurenson L, Burq S, Reston M (2007) Marine benthic habitat mapping using multibeam data, georeferenced video and image classification techniques in Victoria, Australia. J Spat Sci 52(1):93–104

Jenness J (2006) Topographic position index (TPI) v. 1.2 [Electronic manual]. Jenness Enterprises, Flagstaff. http://www.jennessent.com/downloads/TPI_Documentation_online.pdf

Jenness J (2013) DEM surface tools for ArcGIS [Electronic manual]. Jenness Enterprises, Flagstaff. http://www.jennessent.com/downloads/DEM%20Surface%20Tools%20for%20ArcGIS_A4.pdf

Larkin D, Vivian-Smith G, Zedler JB (2006) Topographic heterogeneity theory and ecological restoration. In: Donald A, Falk MP, Zedler J (eds) Foundations of restoration ecology. Island Press, Washington, pp 142–152

Levin SA (1974) Dispersion and population interactions. Am Nat 108:207–228

Levin SA (1992) The problem of pattern and scale in ecology. Ecology 73:1943–1967

Levin LA, Etter RJ, Rex MA, Gooday AJ, Smith CR, Pineda J, Stuart CT, Hessler RR, Pawson D (2001) Environmental influences on regional deep-sea species diversity. Annu Rev Ecol Syst 32:51–93

Lundblad ER, Wright DJ, Miller J, Larkin EM, Rinehart R, Naar DF, Donahue BT, Anderson SM, Battista T (2006) A benthic terrain classification scheme for American Samoa. Mar Geod 29:89–111

McArthur MA, Brooke BP, Przeslawski R, Ryan DA, Lucieer VL, Nichol S, McCallum AW, Mellin C, Cresswell ID, Radke LC (2010) On the use of abiotic surrogates to describe marine benthic biodiversity. Estuar Coast Shelf Sci 88:21–32

McCormick MI (1994) Comparison of field methods for measuring surface topography and their associations with a tropical reef fish assemblage. Mar Ecol Prog Ser 112:87–96

McGarigal K, Tagil S, Cushman SA (2009) Surface metrics: an alternative to patch metrics for the quantification of landscape structure. Landscape Ecol 24:433–450

McGarigal K, Cushman SA, Ene E (2012). FRAGSTATS v4: spatial pattern analysis program for categorical and continuous maps. Computer software program produced by the authors at the University of Massachusetts, Amherst. http://www.umass.edu/landeco/research/fragstats/fragstats.html

Milner PR (2008) Final field report: CCGS Vector, North Coast and Queen Charlotte Island Surveys, July 25–September 8, 2008. Institute of Ocean Sciences, Department of Fisheries and Oceans, Sydney

Moser K, Ahn C, Noe G (2007) Characterization of microtopography and its influence on vegetation patterns in created wetlands. Wetlands 27:1081–1097

Neves BM, Du Preez C, Edinger E (2014) Mapping coral and sponge habitats on a shelf-depth environment using multibeam sonar and ROV video observations: Learmonth Bank, northern British Columbia, Canada. Deep-Sea Res Pt II 99:169–183

Nowell ARM, Jumars PA (1982) Flow environments of aquatic benthos. Annu Rev Ecol Syst 15:303–328

Risk MJ (1972) Fish diversity on a coral reef in the Virgin Islands. Atoll Res Bull 193:1–6

Risser PG, Karr JR, Forman RTT (1984) Landscape ecology: directions and approaches. Illinois Natural History Survey Special Publ. 2, Champaign

Roberts CM, Ormond RF (1987) Habitat complexity and coral reef fish diversity and abundance on Red Sea fringing reefs. Mar Ecol Prog Ser 41:1–8

Sappington JM, Longshore KM, Thompson DB (2007) Quantifying landscape ruggedness for animal habitat analysis: a case study using Bighorn Sheep in the Mojave Desert. J Wildl Manag 71:1419–1426

Schlacher TA, Schlacher-Hoenlinger MA, Williams A, Althaus F, Hooper JNA, Kloser R (2007) Richness and distribution of sponge megabenthos in continental margin canyons off southeastern Australia. Mar Ecol Prog Ser 340:73–88

Shumway CA, Hofmann HA, Dobberfuhl AP (2007) Quantifying habitat complexity in aquatic ecosystems. Freshwater Biol 52(6):1065–1076. doi:10.1111/j.1365-2427.2007.01754.x

Sinclair AF, Conway KW, Crawford WR (2005) Associations between bathymetric, geologic and oceanographic features and the distribution of the British Columbia bottom trawl fishery. ICES CM 2005/L:25:1–31

SPIPTM The scanning probe image processor. Image metrology APS, Lyngby. http://www.imagemet.com/

Stahl WR (1962) Similarity and dimensional methods in biology. Science 137:205–212

Stambaugh MC, Guyette RP (2008) Predicting spatio-temporal variability in fire return intervals using a topographic roughness index. For Ecol Manag 254(3):463–473

Swanson FJ, Kratz TK, Caine N, Woodmansee RG (1988) Landform effects on ecosystem patterns and processes. Bioscience 38:92–98

Walker BK, Jordan LKB, Spieler RE (2009) Relationship of reef fish assemblages and topographic complexity on southeastern Florida coral reef habitats. J Coast Res 53:39–48

Wedding LM, Friedlander AM, McGranaghan M, Yost RS, Monaco ME (2008) Using bathymetric lidar to define nearshore benthic habitat complexity: implications for management of reef fish assemblages in Hawaii. Remote Sens Environ 112(11):4159–4165

Wilson MFJ, O'Connell B, Brown C, Guinan HC, Grehan AJ (2007) Multiscale terrain analysis of multibeam bathymetry data for habitat mapping on the continental slope. Mar Geod 30:3–35

Woodby D, Carlile D, Hulbert L (2009) Predictive modeling of coral distribution in the Central Aleutian Islands, USA. Mar Ecol Prog Ser 397:227–240

Wright DJ, Heyman WD (2008) Introduction to the special issue: marine and coastal GIS for geomorphology, habitat mapping, and marine reserves. Mar Geod 31:223–230

Wright DJ, Pendleton M, Boulware J, Walbridge S, Gerlt B, Eslinger D, Sampson D, Huntley E (2012) ArcGIS Benthic Terrain Modeler (BTM), v. 3.0, Environmental Systems Research Institute, NOAA Coastal Services Center, Massachusetts Office of Coastal Zone Management. http://www.esriurl.com/5754

Wu J (2004) Effects of changing scale on landscape pattern analysis: scaling relations. Landscape Ecol 19:125–138

Wu J (2013) Key concepts and research topics in landscape ecology revisited: 30 years after the Allerton Park workshop. Landscape Ecol 28:1–11

Chapter 4: Shortspine thornyhead and rockfish (Scorpaenidae) distribution in response to substratum, biogenic structures, and trawling

Preface

Chapter 4 is a research article published in the peer-reviewed journal *Marine Ecology Progress Series*: Du Preez, C., and Tunnicliffe, V. (2011) Shortspine thornyhead and rockfish (Scorpaenidae) distribution in response to substratum, biogenic structures and trawling. *Marine Ecology Progress Series* **425**: 217-231. Dr. Verena Tunnicliffe (Thesis supervisor, University of Victoria) provided the resources for this work and assisted with the writing of this article. My contribution was collecting and analysing the data, and writing the article.

Abstract

Learmonth Bank in northern British Columbia sustains an active trawl fishery that returns large bycatches of deep-sea sponges and corals. To examine effects of biogenic structures on the distribution of fish, we examined nearly 30 km of high-definition imagery from a remotely operated vehicle and documented locations of 2770 scorpaenid fish. The 2 local genera have similar abundances, averaging about 1.2 individuals 100 m^{-2}, but have different spatial abundance patterns: shortspine thornyhead *Sebastolobus alascanus* are randomly distributed on featureless substrata and their abundance increases with depth. Rockfish *Sebastes* spp. associate with higher seafloor relief nonrandomly and select for sponges and corals over the inert substrata alone; 95% of the rockfish occurred on 27% of the seafloor surveyed. Sponges (Demospongiae and Hexactinellida) were abundant on the bedrock and boulders of the bank and adjacent

moraine and covered 30 to 55% of the seafloor compared with 1% of the sediment and aggregates of the surrounding basin. The majority of rockfish (80%) occurred with sponges ≥50 cm in height, and even beds of short sponges attracted 4 times as many rockfish than did substrata with no large epifauna. While over half of primnoid corals over 30 cm tall had associated rockfish, less than 2% of the seafloor had large coral, and small coral had no associated rockfish. On the adjacent seafloor with past trawling activity, *Primnoa pacifica* was 13 times less abundant, and large corals and sponges were rare. Thornyhead abundance doubled but rockfish had a 3-fold reduction in numbers. Our study indicates that degradation of biogenic structures is a long-term detriment to rockfish species and, although the driver remains unclear, our data suggest it occurs through the destruction of a habitat that is more effective for shelter than rough inert seafloor.

Keywords

Scorpaenidae · Rockfish · Shortspine thornyhead · Biogenic structure · Sponge · Coral · Trawling · Remotely operated vehicle

Introduction

Geological and biological characteristics of the seafloor can influence benthic fish assemblage composition and abundance (Richards 1986, Krieger & Wing 2002, Freese & Wing 2003); however, our understanding of the functional significance of these associations remains limited (Roberts et al. 2009). High abundances of benthic fish occur with some deep-sea sponges and corals (Krieger & Wing 2002, Freese & Wing 2003),

but it is unclear whether the associations are obligate or facultative, or whether the co-occurrence reflects similar requirements (Auster 2005, 2007). Questions regarding the ecological relevance of sponges and corals to fish populations are increasingly pertinent to fish stock management as capture fisheries grow and diversify (Morgan & Chuenpagdee 2003). Resolution of such relationships will guide conservation decisions in areas of abundant biogenic structures. Biogenic structures are highly vulnerable to physical contact with trawling gear (Heifetz et al. 2009). Their recovery from trawling activity may be so slow (Andrews et al. 2002, Risk et al. 2002) that these biogenic habitats should be viewed as a nonrenewable feature.

Because deep-water research is limited by natural conditions, studies on scorpaenid fish associations with seafloor characteristics are often descriptive (Krieger & Wing 2002) or examine only 1 or 2 features of the seafloor, for example: a generalization of the habitat (Richards 1986), large-scale terrains (Yoklavich et al. 2000), substrata (Pearcy et al. 1989), corals (Husebø et al. 2002), sponges (Freese & Wing 2003), depth and trawling activity (Hixon & Tissot 2007). Our study includes all these factors and attempts to control for their confounding interrelationships to separate the specific effects of sponges and corals on the scorpaenid fish assemblage. This approach also enabled us to follow Auster's (2005) suggestion to compare biogenic habitats with other habitats.

Benthic fish must contend with bottom currents and avoid downstream displacement from preferred habitats by station-holding (Webb 1989). Because stationholding by swimming is energetically expensive, a more effective strategy is for fish to reduce form drag by finding refuge in a location with lower flow velocity (Webb 1989). There are 2 basic morphologies of benthic fish (Bone & Marshall 1982): flattened and fusiform. A

flattened morphology facilitates stationholding by allowing the fish to hide within the boundary layer against the seafloor (Arnold & Weihs 1978); this shape is an adaptation for inhabiting featureless seafloors (Allen et al. 2006). Structures on the seafloor modulate the local flow regime and provide areas of reduced currents where fusiform fish can take refuge. Auster (2007) suggests geological and biological habitats are functionally equivalent as fish flow refuge. In the present study, we investigate fish selection for sponge and coral biogenic structures over inert abiotic structures alone.

British Columbia's Learmonth Bank area is regarded as a 'hotspot' for demersal fish trawling activity (Sinclair et al. 2005) and the 2 local scorpaenid genera are common in catches (Fisheries and Oceans Canada 2010). Reports of coral/sponge bycatch here are among the highest amounts on British Columbia's continental shelf and have led to consideration of the area for protection (Ardron et al. 2007). Ardron et al. (2007) suggest that *in situ* studies measuring the actual effects of trawling are the only true indicator of the ecological benefits of the proposed closure. It is usually difficult to examine effects of trawling because areas of similar environmental conditions and accessibility adjacent to a trawled area rarely remain untrawled (Sinclair et al. 2005). Nonetheless, such conditions still exist in Learmonth Bank as a consequence of an unresolved maritime boundary dispute between Canada and the USA (Gray 1997), providing a unique opportunity to compare very similar trawled and untrawled coral habitats.

This study uses *in situ* imagery to examine the seafloor factors that influence scorpaenid fish abundance patterns controlling for the confounding interrelationships. A major objective is to determine the nature of both a scorpaenid fish assemblage and the benthic biotopes. In addition, we examine 3 hypotheses: (1) shortspine thornyhead

Sebastolobus alascanus and rockfish *Sebastes* spp. distribution patterns are markedly different with respect to seafloor relief; (2) the abrupt vertical relief of large biogenic structures attracts rockfish in a facultative association over the relief of inert substrate alone; and (3) degradation of biogenic structures such as corals by trawling has direct consequences on rockfish abundance and distribution patterns.

Materials and methods

Study area

Learmonth Bank spans ~37 km across the opening of Dixon Entrance, north of Haida G'wai, British Columbia, Canada (54° 24' 59"N, 133° 05' 00"W; Fig. 4.1). This submerged granite massif is surrounded by glacial till largely composed of mud and sand (Bornhold & Barrie 1991, Barrie & Conway 1999). Scattered erratic boulders and the rugged topography reflect the region's glaciated periods when the sea level was 150 m lower than it is now and the bank was exposed to glacial erosion and iceberg scour (Bornhold & Barrie 1991, Barrie & Conway 1999, 2002).

Dixon Entrance opens onto the continental shelf with a high wave exposure and open ocean swells (fetch > 500 km). Strong freshwater inputs from mainland rivers drive an estuarine circulation through Dixon Entrance with a northwestward surface outflow and an eastward bottom inflow (Zacharias et al. 1998). Owing to its transverse orientation and rise from ~400 to ~50 m depth, Learmonth Bank is a submarine barrier that, through the processes of tidal rectification and density forcing, is encircled by a clockwise eddy (Crawford & Greisman 1987, Ballantyne et al. 1996). These geologic and oceanographic features could facilitate food trapping, detritus falls and vertical migration of zooplankton that may contribute to the high abundance of fish (Sinclair et al. 2005).

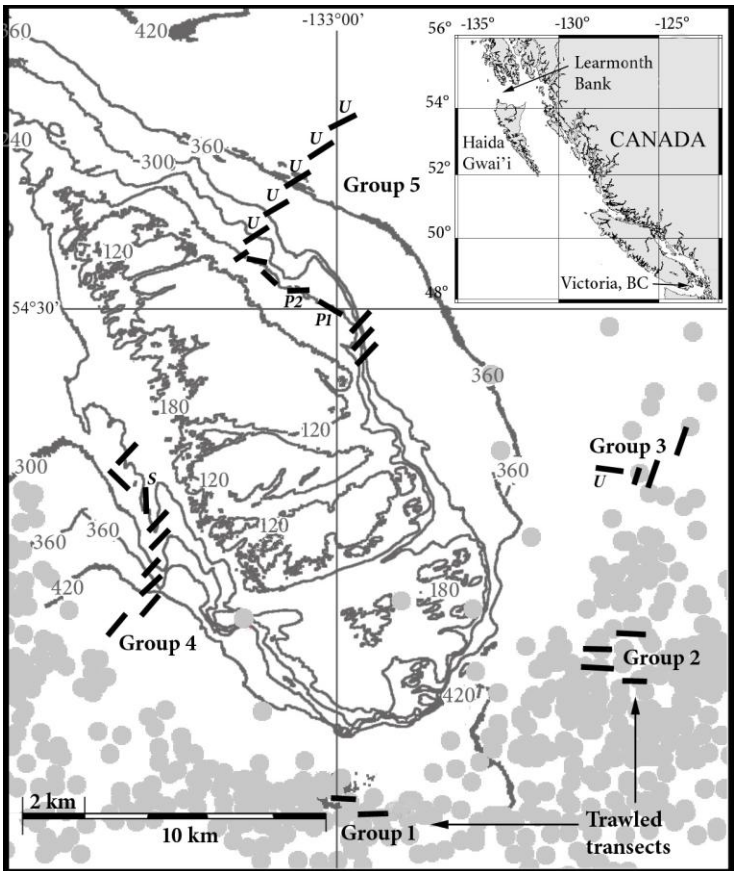

Figure 4.1. Bathymetry (m) of Learmonth Bank with locations of ROV transects (black lines, in 2008) and commercial trawl sets (grey circles, from 2002 to 2007). Inset shows location of study area off the coast of British Columbia. Six transects were made in trawled areas (Groups 1 and 2) and 26 in untrawled areas. Trawling does not occur north of 54° 30' because of an unresolved boundary dispute in this area. Labeled transects: (U) 6 untrawled transects used for comparisons (see 'Materials and methods: Data analysis'); (P1) highest and (P2) second highest abundances of Primnoa pacifica; and (S) largest patch of Tall sponge gardens (see Table 2 for definition) and highest abundance of rockfish. Map is adapted from multibeam bathymetry and Fisheries and Oceans Canada summary groundfishery records for 2002 to 2007 in Dixon Entrance (courtesy of J. V. Barrie and J. Boutillier). [Black contour lines at 60 m intervals]

Field work

In July 2008, a remotely operated vehicle (ROV 'ROPOS') executed 5 dives on and around Learmonth Bank, all above 500 m depth. The ROV flew 32 transects (Fig. 4.1, Table 4.1), ranging between 0.55 and 1.05 km long, at average speeds between 0.5 to 1

knot and 0.5 to 1 m off the seafloor. In total, we collected data from 29.2 km of transects (average swath, ~4 m wide) with imagery from high definition (HD) video recordings. The HD video camera (Zeus Plus, Insite Pacific) was mounted facing forward to provide continuous recording of a constant field of view that included 2 parallel laser points projected 10 cm apart for scale.

Dive sites were selected to sample within the 3 seascapes of Learmonth Bank (Fig. 4.1, Table 4.2): the bank itself (8 southern transects in Group 5), the western moraine (7 northern transects in Group 4) and the basin areas (remaining transects). Fisheries and Oceans Canada summary of groundfishery records for 2002–2007 in Dixon Entrance assisted in identifying areas of trawl activity around Learmonth Bank.

Table 4.1. Distribution of observations among the seascapes including occurrences of substratum types and epifauna types (see Table 2 for definitions of seascape, substratum and epifauna types).

	Trawled (in Basin)	Basin	Moraine	Bank
Number of transects	6	11	7	8
Total transect length (m)	5,600	10,250	7,050	6,300
No. of transect records	23,177	45,548	32,888	27,963
Average (±SE) depth (m)	419 ± 19	377 ± 15	278 ± 20	234 ± 20
Average (±SE) surveyed surface area (m^2)	3,578 ± 260	3,509 ± 272	4,756 ± 349	3,809 ± 453
Average % surface area (±SE) of substratum type				
Sand	18.8 ± 6.1	64.2 ± 8.7	37.5 ± 6.9	30.2 ± 8.4
Aggregates	58.3 ± 9.2	24.9 ± 7.9	27.6 ± 5.3	23.4 ± 7.9
Boulder/bedrock	22.9 ± 7.4	10.9 ± 5.3	34.9 ± 4.4	46.4 ± 4.7
Average % surface area (±SE) of epifauna cover				
Epifauna absent	81.2 ± 14.7	98.8 ± 1.0	67.5 ± 9.5	40.7 ± 8.1
Short sponge gardens	18.5 ± 14.5	0.9 ± 0.9	8.3 ± 3.6	22.5 ± 4.0
Tall sponge gardens	0.2 ± 0.2	0.2 ± 0.1	24.2 ± 7.6	32.0 ± 5.6
Coral stands	0.0 ± 0.0	0.1 ± 0.1	0.1 ± 0.1	4.8 ± 3.3

Table 4.2. Each of the 230 000 records was classified within a seascape, substratum type and epifauna cover category. The possible combinations result in 12 mutually exclusive biotopes for each seascape. Within a classification categories are listed in order of low to high relief.

Classification/ category	Description
Seascape	**Large-scale context of a record based on location with regards to geological features, depth, and topography**
Basin	Deepest seascape: generally flat and uniform
Moraine	Sinuous feature with gradual slopes composed of large-scale mounds of coarse sediment
Bank	Shallowest and most heterogeneous with seafloor orientation ranging from flat plateaus to ~300 m cliffs
Substratum type	**Substratum classification based on percent cover of surficial sediment types per record**
Sand (Snd)	Fine and unconsolidated; sediment composed of ≥90 % sand (Fig. 4.2D)
Aggregates (Agg)	Mainly aggregates (pebble and cobble); sediment composed of <90 % sand, ≤5 % boulder and no bedrock
Boulder/bedrock (Bol)	Hard substratum prevalent; >5 % boulder and/or bedrock present (Fig. 4.2C)
Epifauna cover	**Biological classification based on composition, density, and height of epifauna per record**
Epifauna absent (EA)	Bare substratum (Fig. 4.2D) or small epifaunal organisms attached with short erect sponges <3 ind. 1 m^{-2}
Epifauna present (EP)	
Sponge gardens:	Community of Demospongiae and/or Hexactinellida:
Short sponge gardens (SSG)	Dense short erect sponge cover; ≥3 ind. per 1 m^{-2}
Tall sponge gardens (TSG)	Tall erect sponge; ≥1 ind. 1 m^{-2} (Fig. 4.2B)
Coral stands (CS)	Tall *Primnoa pacifica*; ≥1 ind. per 2 m^{-2} (Fig. 4.2C)

A transect's 'trawl status' was confirmed by blind-testing for trawl evidence in the video recording without prior knowledge of trawl records. Visual evidence included trawl scars, door and roller marks, pinned nets (Fig. 4.2A) and dragged or overturned boulders. The presence or absence of trawl scars in 100 m range sonar scans, taken from the ROV every 250 m, provided further confirmation of a transect's trawl status. Six 'Trawled' transects were identified (Groups 1 and 2 in Fig. 4.1).

Video recording analysis

Position (ROV 'ROPOS' accuracy: ±1% of water depth) and imagery information was transferred to a relational database linked by time stamps. Forty-six hours of transecting was parsed into more than 230 000 records. A record represents non-overlapping seafloor observed during 1 to 2 s of transecting (averaging 1 to 2 m^2 of seafloor per record). Several thousand records in serial succession describe the length of a transect. Biological and geological features (some after Sameoto et al. 2008) were annotated for each record and included substratum (as percent cover of 6 sediment types), epifauna cover (i.e. sponges and coral; Fig. 4.2B,C), scorpaenid fish identity (Fig. 4.2B–D) and events of interest (e.g. trawl evidence; Fig. 4.2A). The distribution of substratum type and epifauna cover over the 3123 records in a single transect is illustrated in Fig. 4.3. Other information included the ROV's survey mode and the camera's field of view (Sameoto et al. 2008). Species identification from imagery can be difficult. Sponges can be particularly problematic; thus, we used a high taxonomic level in this study to identify all to the same taxonomic level. Size of fauna was estimated by using the projected laser scale as a guide.

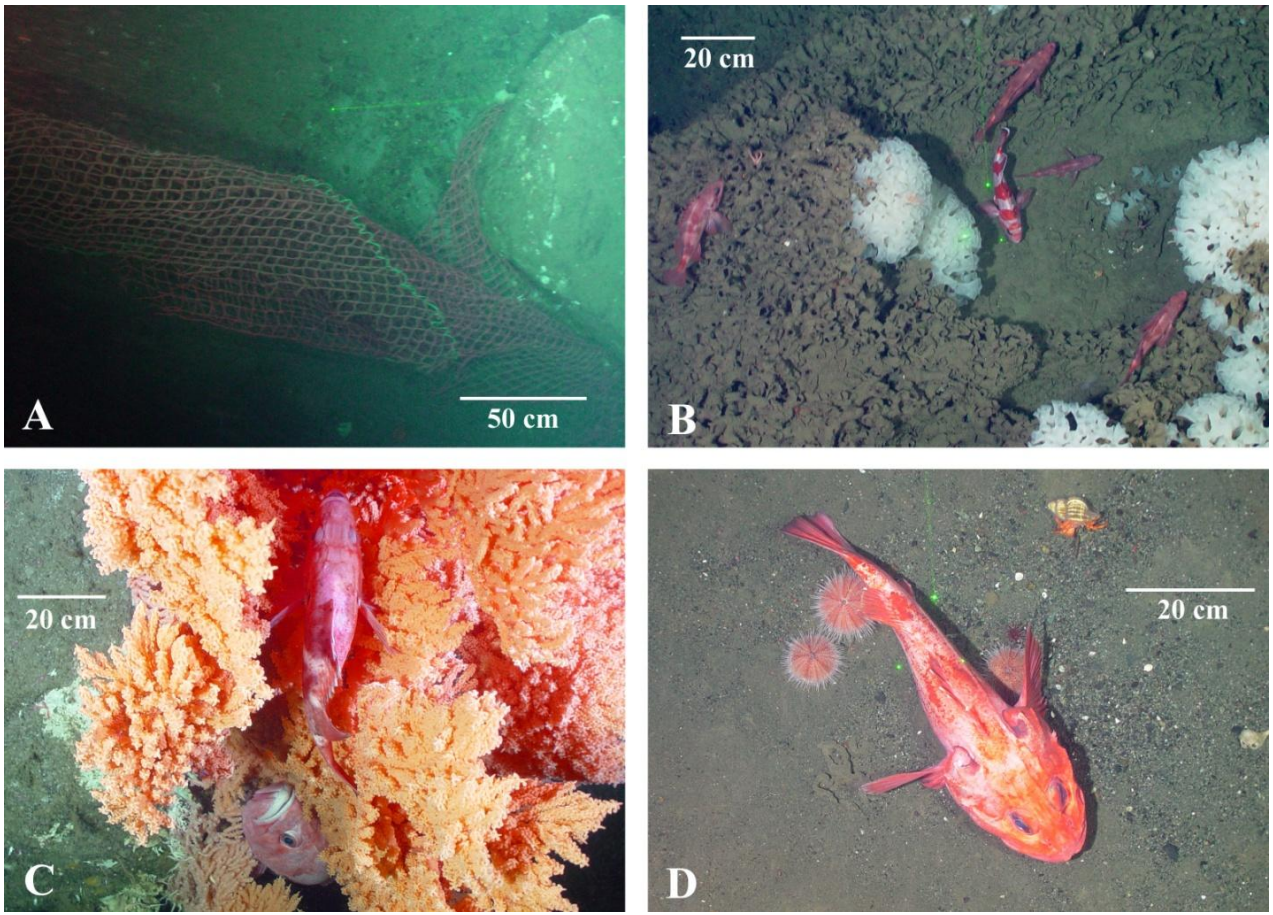

Figure 4.2. (A) A piece of bottom trawling net pinned beneath an overturned boulder showing evidence the large boulder was dragged >10 m before breaking free; such observations confirmed the trawled status of a transect. (B) Four sharpchin rockfish and a redbanded rockfish among mounds of a *Farrea occa* sponge; record type is Tall sponge garden on Boulder. (C) Two shortraker rockfish between the branches of *Primnoa pacifica*; record type is Coral stand on Boulder. (D) Large shortspine thornyhead on sand; record type is Epifauna absent on Sand. Images were taken with ROV 'ROPOS'. See Table 4.2 for definitions of record types.

We used a classification scheme to characterise the seafloor's bottom roughness for each record (Table 4.2) with 3 parameters: seascape, substratum type and epifauna cover. Each has a hierarchy of 3 to 4 mutually exclusive categories relating to bottom roughness. Vertical relief at the scale of the parameter is a proxy for bottom roughness, where topography determines 'seascape' at a scale of tens to hundreds of metres, sediment size based on the Wentworth scale determines 'substratum type' at a scale of centimetres and organism type and height determines 'epifauna cover' at a scale of centimetres. The combination of substratum type and epifauna cover produces 12 biotopes for each seascape (Table 4.2).

The epifauna cover category Epifauna absent (EA) includes bare substratum (Fig. 4.2D) and substratum with small epifaunal organisms attached, for example encrusting sponges, *Stylaster* and hydroids; we focussed only on larger epifauna. The categories Short sponge gardens (SSG) and Tall sponge gardens (TSG) are not defined by specific species (Table 4.2). The majority of short sponges (between 10 and 50 cm) were Demospongiae, while the majority of tall sponges (≥50 cm) were Hexactinellida with a few Demospongiae. Red tree coral *Primnoa pacifica* height categories are short (between 10 and 30 cm) and tall (≥30 cm). Owing to the small size and limited abundance of other coral species, only tall *P. pacifica* (Fig. 4.2C) defines the category coral stands (CS; Table 4.2). Two genera of scorpaenid fish occur at Learmonth Bank, thornyhead *Sebastolobus* and rockfish *Sebastes*. Scorpaenid fish were classified to the lowest taxonomic level possible (Table 4.3) and their physical association with bottom features was recorded. Within this study 'association' is defined as from close proximity (≤10 cm) to full contact (most observations) with the structure.

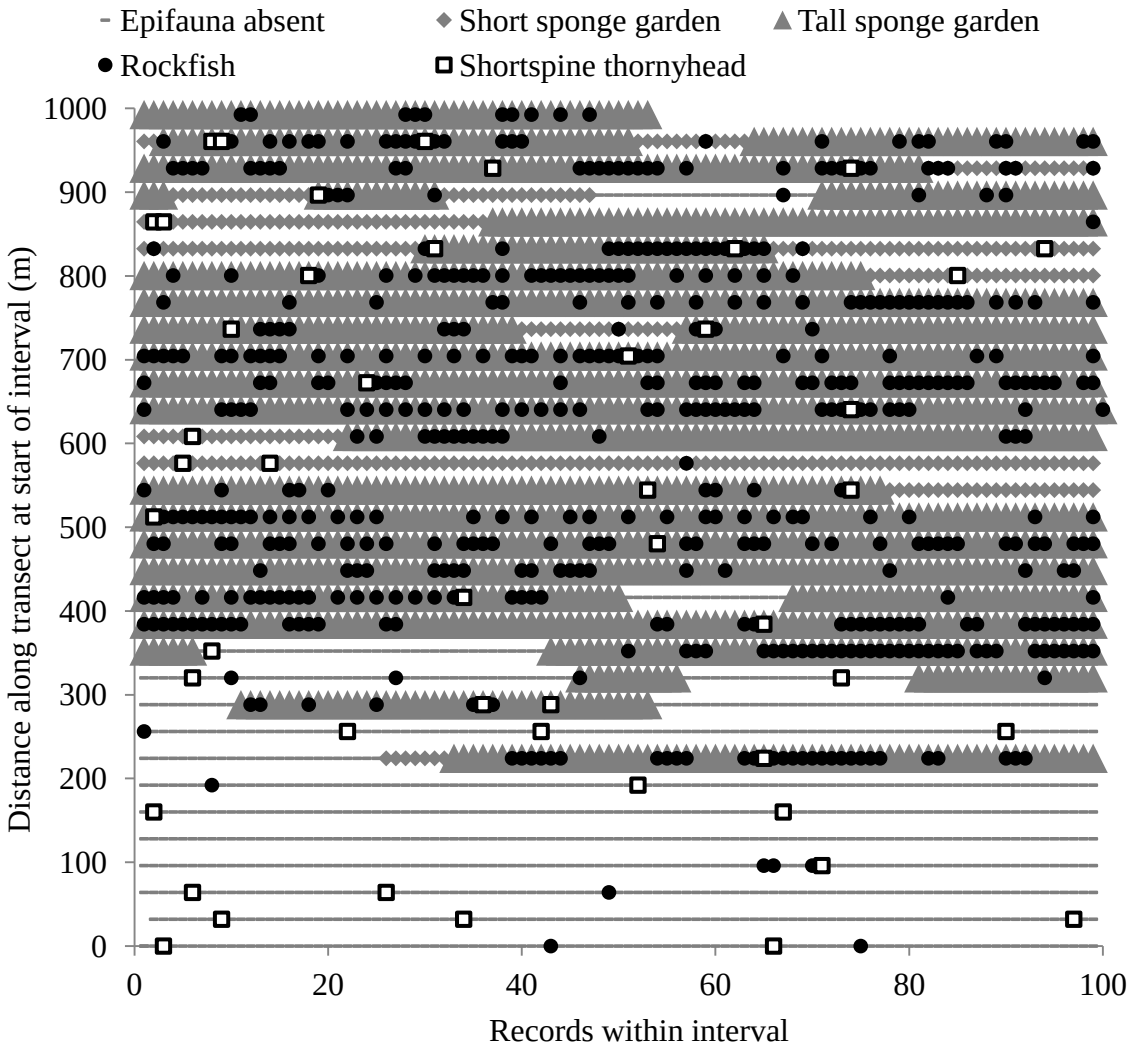

Figure 4.3. Example of observations along a 1 km transect. The 3123 non-overlapping records describe the epifauna cover and scorpaenid fish distribution for a moraine transect ('S' in Fig. 1). Transect begins at lower left of the figure and continues in a straight line although it is broken into stacked 'intervals' to display here. Each record represents ±0.33 m along the transect. The figure illustrates the random distribution of shortspine thornyheads compared with the clumped distribution of rockfish associating with 'Tall sponge gardens'.

Data analysis

All data annotated from the video analysis were entered into an ACCESS database to support subsequent queries. Using the size of the camera's footprint and the location of the record, percent coverage of record attributes and discrete counts produced estimates of seafloor surface area and density measurements. Densities were standardised to 100 m^2 or to the average surveyed area of transects, 4000 m^2. All analyses, except the comparison between Trawled (Tr) and Untrawled (UTr), excluded the 6 Tr transects and, therefore, n_{max} = 26 transects. For all analyses, transects were used as replicates and averages reported with SE. A minimum of 5 transect replicates were required to run a statistical test. CS represented only <2 % of the surveyed area resulting in low statistical power for analyses with CS biotopes.

We used PASW Statistics 18 software for our statistical analyses. The variance: mean ratio (VMR), an index of dispersal, was used to determine a species distribution pattern over the 26 untrawled transects, where VMR = 1 indicates a species has a random distribution, and VMR < 1 and VMR > 1 suggest even and clumped distributions, respectively. A Mann-Whitney *U*-test determined significance of the difference between the VMR and a value of 1. To investigate interdependence between scorpaenid fish abundances and seafloor variables, we used Pearson correlations. Within the correlation matrix, we included depth, one category to represent the substratum type, Boulder/bedrock (Bol), and one category to represent the epifauna cover, Epifauna present (EP). To resolve for independent relationships influencing thornyhead and rockfish abundance patterns, we used partial correlations (Table 4.4) and stepwise multiple regressions (Else et al. 2002). Variables for the correlation matrices were

Table 4.3. Distribution of scorpaenid fish species among the seascapes. Overall abundances and rockfish species richness include only untrawled transects (n = 26). While nearly equal numbers of the 2 genera were observed, there are differences in their distributions.

	Taxon	Trawled (in Basin)	Basin	Moraine	Bank	Total
Shortspine thornyhead	*Sebastolobus alascanus*	262	270	516	309	1357
All rockfish	*Sebastes* spp.	9	40	787	577	1413
Sharpchin	*S. zacentrus*	1	4	680	443	1128
Rosethorn	*S. helvomaculatus*	0	0	77	83	160
Rougheye	*S. aleutianus*	4	20	9	6	39
Redbanded	*S. babcocki*	1	7	8	13	29
Silvergray	*S. brevispinis*	0	0	5	13	18
Shortraker	*S. borealis*	0	3	1	3	7
Redstripe	*S. proriger*	0	0	0	7	7
Bacaccio	*S. paucispinis*	0	0	1	3	4
Yelloweye	*S. ruberrimus*	0	2	0	0	2
Unidentified		3	4	6	6	19
Unidentified scorpaenid fish		9	14	75	103	201
Average abundance (no. 100 m^{-2} ±SE):						
Thornyhead	*S. alascanus*	1.2 ± 0.2	0.7 ± 0.2	1.7 ± 0.4	1.1 ± 0.3	1.1 ± 0.2[a]
Rockfish	*Sebastes* spp.	<0.1 ± 0.0	0.1 ± 0.0	2.1 ± 1.4	2.2 ± 0.7	1.3 ± 0.5[a]
Rockfish species richness		3	5	7	8	9
No. of transects		6	11	7	8	32

[a] Trawled (in Basin) transects excluded

log(y + 1) transformed to normalize (n = 15 Moraine and Bank transects; Basin transects had too many null values for the variables to be included). To investigate the independent response of scorpaenid abundance to the presence of large sponges and corals, we controlled for substratum type in each epifauna cover category. For this analysis, all biotopes had to occur on the transect to reduce variation among transects; biotope comparisons were of patches of the seafloor located on the same transect. Thus, we can identify rockfish interactions specifically with biogenic structures rather than just

Table 4.4. Pearson pairwise correlation (lower left) and partial correlation (upper right) matrices for thornyhead and rockfish abundance (ind. per 100 m2), depth and percent surface area of Boulder/bedrock and Epifauna present (n = 15 transects). Significant correlations are in **bold** text ($p < 0.05$).

	Thorny-head	Rock-fish	Depth	Boulder/ bedrock	Epifauna present
Thornyhead		-0.03	**0.57**	-0.33	0.20
Rockfish	**-0.68**		0.07	0.14	0.49
Depth	**0.83**	**-0.79**		0.45	**-0.76**
Boulder/bedrock	**-0.63**	**0.73**	**-0.61**		0.51
Epifauna present	**-0.77**	**0.89**	**-0.92**	**0.76**	

recording fish co-occurrence with biogenic structures and their substrata. To test scorpaenid response to substratum type and epifauna cover separately, we used *t*-test, Mann-Whitney *U*-test, ANOVA and Kruskal-Wallis approaches.

To select comparable untrawled transects for the 6 trawled transects, we considered location and proximity to other seascapes, percent cover of Bol and depths (Table 4.5). Six UTr transects ('*U*' in Fig. 1) were comparable with the 6 Tr transects. All 12 transects are within the Basin. Between the Tr and UTr transects, there was no significant difference in percent surface area comprising Bol (see Results). Although there was a difference in the average depths, the depth ranges overlapped substantially and lay within ranges known for all study organisms (Love et al. 2002, Lamb & Hanby 2005).

Results

Scorpaenid fish assemblage

Three orders dominated the demersal fish of Learmonth Bank: the Scorpaeniformes (rockfishes and thornyheads) represented 78% of the fish observed, the

Table 4.5. Descriptors of the 6 Trawled and 6 comparable Untrawled transects (seascape = Basin for both) and their average abundances of *Primnoa pacifica*, thornyhead and rockfish. p-value indicates significance of difference between treatments, significant p-values are in **bold** text ($p < 0.05$). Transect locations indicated in Fig. 4.1.

	Trawled	Untrawled	p-value
Total transect length (m)	5,600	5,700	
Average (±SE) occurrence of trawl evidence	15 ± 3	0 ± 0	**<< 0.01**[a]
Average (±SE) depth (m)	419 ± 19	354 ± 22	**0.03**[a]
Depth range (m)	382 to 486	238 to 402	
Average (±SE) % surface area of Boulder/bedrock	22.9 ± 7.4	18.0 ± 9.0	0.34[a]
Abundance (no. 100 m^{-2}) of:			
Primnoa pacifica	0.03 ± 0.03	0.4 ± 0.18	**0.01**[a]
Thornyhead	1.23 ± 0.23	0.63 ± 0.15	**0.03**[b]
Rockfish	0.05 ± 0.03	0.18 ± 0.05	**0.03**[b]
% of rockfish within Coral stands	0	33	

[a] Mann-Whitney *U*-test; [b] *t*-test

Pleuronectiformes (flatfishes) 12% and the Rajiformes (skates) 5%. A total of 2963 scorpaenid fish were encountered, of which half were shortspine thornyhead (Fig. 4.2D), and the remainder were rockfish (Fig. 4.2B,C, Table 4.3). Although 9 species of rockfish were observed (Table 4.3), >80% were sharpchin rockfish *Sebastes zacentrus* (Fig. 4.2B). there was no significant difference between thornyhead and rockfish overall densities (Mann-Whitney *U*-test: $p = 0.06$, $n = 26$; Table 4.3). The 2 genera showed different distribution patterns ($n = 26$): thornyhead had a random distribution (VMR = 1.0 ± 0.1; Mann-Whitney *U*-test: $p = 0.127$), while rockfish had a clumped distribution (VMR = 149.6 ± 87.5; Mann-Whitney *U*-test: $p << 0.01$).

Thornyhead and rockfish displayed distinctly different behaviours. Thornyhead usually adopted a stationary position in full contact with flat seafloor (Fig. 4.2D). Rockfish were usually quiescent beside or within erect structures (Fig. 4.2B,C), but over flat seafloor they were swimming or moved passively with the current. No schooling behaviour

occurred among the scorpaenids although several rockfish could aggregate around the same structure.

Seafloor effects on scorpaenid distribution

The correlation matrix indicated that variances of both thornyhead and rockfish abundances were interrelated with all the seafloor variables listed in Table 4.4, including the other scorpaenid species abundance; however, the partial correlation matrix indicated only a couple of pairings of variables had significant independent relationships (Table 4.4).

Seascapes

Within the study area of Learmonth Bank, there were 3 distinct terrains, or seascapes (Table 4.2). The Basin was largely flat and sandy with sparsely scattered erratic boulders. The seafloor slope and sediment size increased near the Bank and gave way to deeply incised walls that rose ~300 m. At ~200 m depth, the Bank plateaued and bedrock was scattered with boulders and pockets of sediment. Below the southwestern flank of the Bank lay a sinuous Moraine, a glacial feature of mixed sediments, about ~5 km long with relief of tens of metres. The 3 seascapes showed distinct characteristics with significantly different average seafloor depths (Kruskal-Wallis test: $p << 0.01$; all significantly different; Table 4.1) and average percent surface area comprising Bol (Kruskal-Wallis test: $p << 0.01$; all significantly different; Table 4.1). Thornyhead density was lowest in the Basin, but still nearly 7 times higher than that of rockfish, and highest on the Moraine (Mann-Whitney *U*-test: $p = 0.01$; Table 4.3). Rockfish density was an order of magnitude higher on the Moraine and Bank compared with the Basin (Mann-Whitney *U*-test: both $p << 0.01$; Table 4.3) and rockfish species diversity was lowest in the Basin (Table 4.3).

Substratum

Within the surveyed area, Sand (Snd) was the most abundant substratum type and averaged 41.4 ± 5.0% of each transect's surface area (overall, ~50 330 m^2), while Aggregates (Agg) and Bol averaged 31.1 ± 4.2% (mean ± SE) and 27.5 ± 3.5%, respectively (Fig. 4.4). Bedrock made up the majority of the hard substratum of the Bank, whereas boulders were the only hard substratum in the Basin and on the Moraine. Boulders (~0.25 to 1.50 m in diameter) tended to be dispersed rather than aggregated and added marked large-scale roughness to the seafloor, over both sediment and bedrock.

Overall, thornyhead abundance did not vary with substratum type: 0.8 ± 0.1, 1.3 ± 0.3 and 1.6 ± 0.4 ind. 100 m^{-2} on Snd, Agg and Bol, respectively (Kruskal-Wallis test: p =

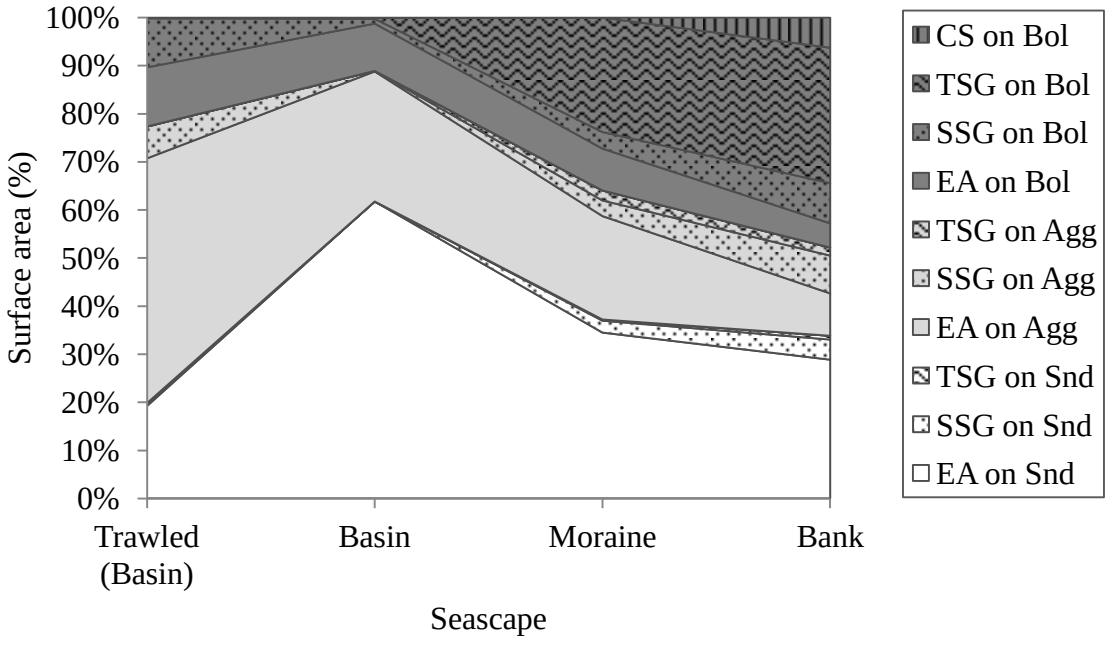

Figure. 4.4. Distribution of biotopes along transects of Learmonth Bank seascapes. CS: Coral stands, TSG: Tall sponge gardens, SSG: Short sponge gardens, EA: Epifauna absent; Bol: Boulder/bedrock, Agg: Aggregates, Snd: Sand (see Tables 4.1 & 4.2). Epifauna absent on Sand was the most abundant biotope at ~48 200 m^2 over 32 transects. Coral stands on both Sand and Aggregates occurred only in the Basin (proportions too low to show here).

0.61, n = 26). The partial correlation matrix indicated that their abundance primarily had a positive correlation with seafloor depth (Table 4.4). Rockfish abundance increased significantly with higher substratum relief: 0.2 ± 0.1, 0.5 ± 0.2 and 3.7 ± 0.9 ind. 100 m^{-2} on Snd, Agg and Bol, respectively (Kruskal-Wallis test $p << 0.01$, n = 26; significant difference between Snd & Bol and Agg & Bol). While rockfish abundance had a strong positive correlation with the percent area comprising Bol, the partial correlation matrix suggested this was due to covariance with other variables (Table 4.4). The biotope analyses (Fig. 4.5), when we controlled for the epifauna cover on each substratum type, supported the observed trends with higher substratum relief: thornyhead abundance did not show a consistent response while rockfish abundance increased.

Epifauna effects on scorpaenid distribution

Epifauna cover

Of the ~122 000 m^2 of surveyed seafloor, ~30% was bare of epifauna and ~43% contained small epifaunal organisms; combined, these observations form our EA category at ~73%. Of the remainder with EP, ~11% was covered in SSG, ~15% in TSG and <2% in CS (Table 4.2, Fig. 4.4). The abundances of sponge gardens and CS were lowest in the Basin and highest on the Bank (Table 4.1, Fig. 4.4). EP coverage had a strong negative partial correlation with depth and a strong positive correlation with the percent surface area comprising Bol, although the partial correlation indicated this was not a significant independent relationship (Table 4.4). Although the proportions varied among seascapes, each contained all 3 substratum types and all 4 epifauna cover categories (Table 4.1, Fig. 4.4). Some biotopes were rare: CS on Snd and on Agg only occurred in the Basin.

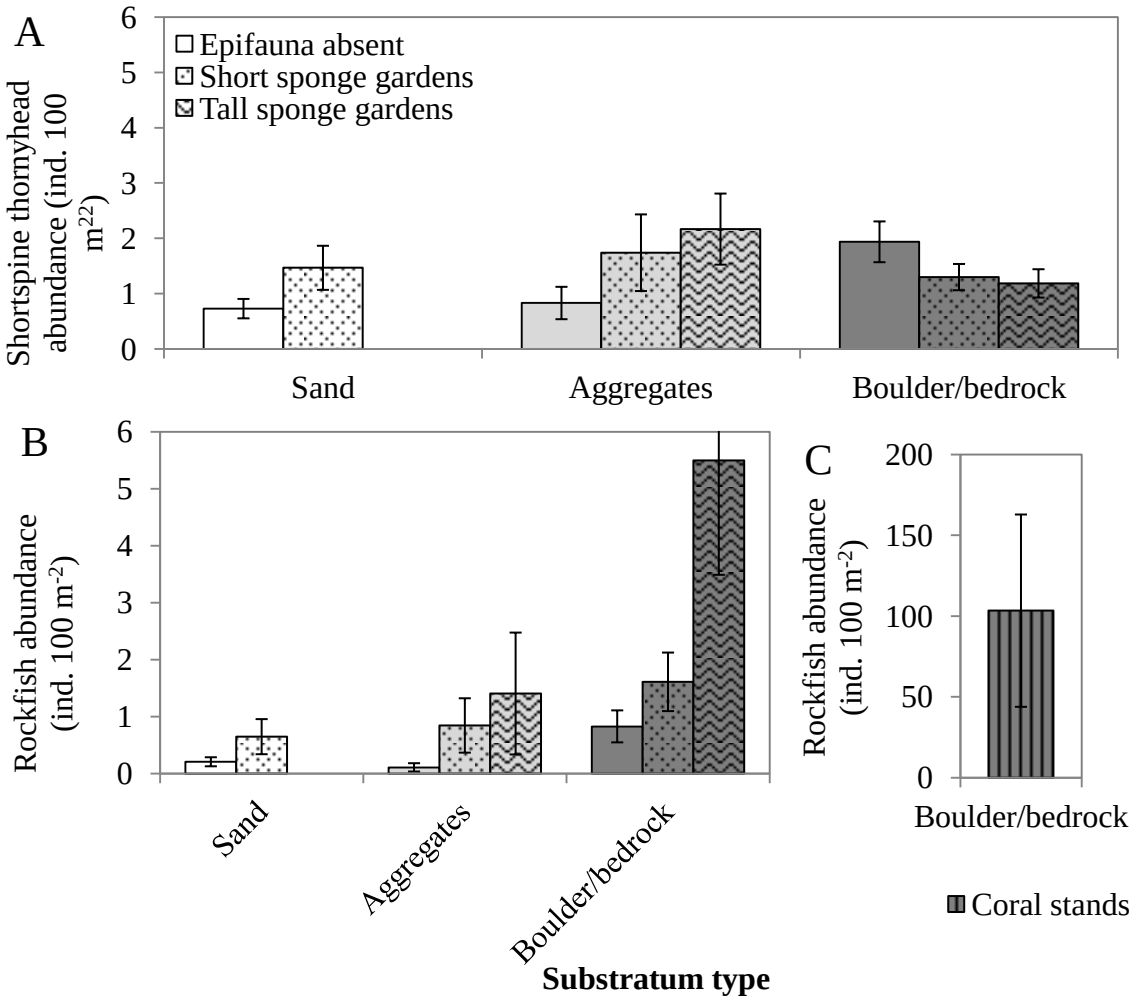

Figure 4.5. Scorpaenid fish abundances in Learmonth Bank biotopes. (A) Thornyhead: abundances did not show consistent differences as substratum or epifauna relief increased. (B & C) Rockfish: abundances were higher with higher substratum and epifauna relief, with a 2 order of magnitude increase in Coral stands on Boulder/bedrock.

Thornyhead abundance varied slightly with epifauna cover: 0.9 ± 0.2 ind. 100 m^{-2} on EA seafloor, 1.4 ± 0.3 and 1.3 ± 0.2 ind. 100 m^{-2} in SSG and TSG, respectively (Kruskal-Wallis test: $p = 0.01$; significant difference between EA & SSG and EA & TSG). The correlation matrix indicated a strong negative relationship between thornyhead abundance and EP coverage; however, the partial correlation suggests this is probably due in part to covariance with depth (Table 4.4). In general, thornyhead distribution

reflected distribution of epifauna cover: 25% of these fish (339) occurred on bare substratum that represented 30% of the seafloor while 43% occurred on substratum that contained small epifaunal organisms, which was also 43% of our seafloor. In contrast, only 5% of all rockfish occurred on bare/ small epifauna while 95% occurred on EP substrata, which only represented 27% of the surveyed seafloor (Fig. 4.4). See Fig. 4.3 for an example of such distributions along one transect. Rockfish abundance varied significantly with epifauna cover: 0.1 ± 0.0 ind. 100 m^{-2} on EA seafloor, 1.0 ± 0.2, 4.1 ± 1.1 and 103.2 ± 59.5 ind. 100 m^{-2} in SSG, TSG and CS, respectively (Kruskal-Wallis test: $p << 0.01$; all significantly different). Note that the majority of CS patches surveyed were much smaller than 100 m^2 in size. The correlation matrix suggested a strong positive relation between rockfish abundance and EP coverage although significance is reduced in the partial correlation matrix (Table 4.4).

Stepwise multiple regressions for thornyhead and rockfish abundances, including all variables listed in Table 4.4, resulted in models that attributed the best covariance to linear relationships with single variables in both cases. The regression models were:

$$T = 2.13 \cdot D - 3.42, \quad r^2 = 0.69$$

$$R = 0.762 + 5.61 \cdot \mathrm{EP}, \quad r^2 = 0.77$$

where T is thornyhead abundance, D is depth (m), R is rockfish abundance (ind. 100 m^{-2}) and EP is Epifauna present (%). Thornyhead abundance increased with depth and rockfish abundance increased with higher percent coverage of EP (SSG, TSG and CS). No interaction between the 2 fish groups emerged.

The only substratum type with all 4 epifauna cover categories in substantial abundances was Bol. Rockfish species richness was significantly higher in EP categories

on Bol in comparison with EA on Bol (Kruskal-Wallis test: $p << 0.01$, $n = 9$). Species richness, expressed as fish density, averaged 0.9 ± 0.0 ind. 100 m^{-2} on EA seafloor, 1.6 ± 0.1, 2.3 ± 0.1 and 2.0 ± 0.2 ind. 100 m^{-2} in SSG, TSG and CS, respectively. All scorpaenid species occurred at least once in sponge gardens in which sharpchin rockfish and rosethorn rockfish *Sebastes helvomaculatus* were the most frequent. All species, except bocaccio *S. paucispinis*, also occurred at least once in CS. A greater proportion of the larger rockfish species (rougheye rockfish *S. aleutianus* and shortraker rockfish *S. borealis)* were associated with CS compared with sponge gardens.

EP substrata had noticeably denser aggregations of benthic macrofauna in comparison with surrounding EA substrata. Macrofauna observed on EP substrata, other than scorpaenid fish, included crinoids *Florometra* sp., basket stars *Gorgonocephalus eucnemis*, octopus *Octopus rubescens*, hagfish *Eptatretus stoutii*, brittle stars, shrimps, crabs, squat lobsters, and hydroids. Macrofauna associated with *Primnoa pacifica*, but not sponges, included sea stars *Hippasteria heathi*, nudibranchs *Tritonia diomedea*, barnacles, anemones, skate eggs, sculpins, and a single golden king crab *Lithodes aquaspina*. These organisms did not appear to be obligate associates of sponges or corals and occurred elsewhere.

Sponges

The most abundant short sponge was *Auletta* sp. (new species, Demospongiae; H. M. Reiswig pers. comm.) and the most abundant tall sponges were *Acanthascus* spp. *(A. dawsoni*, *A. dowlingi*, *A. cactus* and *A. platei*; Hexactinellida) and *Aphrocallistes vastus* (Hexactinellida). Other sponge species identified include 2 Hexactinellida, *Farrea occa* (Fig. 4.2B) and *Heterochone calyx*, and 2 Demospongiae, *Mycale bellabellensis* and *Poecillastra tenuilaminaris*. SSG occurred on 13 of the 26 untrawled transects, while

TSG occurred on 16. When present on a transect, sponge gardens averaged 42.2 ± 6.5% of the seafloor coverage. The majority of observed patches were ~200 m in length, and the largest nearly continuous patch of sponge gardens stretched >700 m along Transect *S* (Figs. 4.1 & 4.3); over one-third of all rockfish (573) observed were on this Moraine transect.

With the biotope comparative analyses (Fig. 4.5), we controlled for substratum type and quantified the independent effect of epifauna cover on scorpaenid abundance. Thornyhead abundance did not change consistently from EA seafloor to SSG and TSG. For the 3 substratum types, thornyhead abundance was significantly higher in SSG compared with EA on Snd (*t*-test: $p = 0.03$, $n = 8$), but did not differ among the 3 epifauna categories on Agg (Kruskal-Wallis test: $p = 0.4$, $n = 9$) or on Bol (ANOVA: $p = 0.17$, $n = 9$) (Fig. 4.5A).

Rockfish showed preference for TSG; 80% of rockfish observations were in the 14.6% of the seafloor covered in TSG. Within the biotope comparative analyses, rockfish abundance consistently increased with higher epifauna relief created by sponge gardens, independent of substratum type. From EA seafloor, the average rockfish abundance increased 4.2 times in SSG and 9.7 times in TSG. The differences among all 3 epifauna cover categories were significant on Bol (ANOVA: $p < 0.03$, $n = 8$) although not on Snd (Mann-Whitney *U*-test: $p = 0.74$, $n = 8$) or Agg (Kruskal-Wallis test: $p = 0.07$, $n = 9$) (Fig. 4.5B).

Coral

Eight taxa of corals were present: *Primnoa pacifica* (Fig. 4.2C), *Stylaster* spp., *Swiftia pacifica*, *Paragorgia* sp., Pennatulacea, Scleractinia, and 2 unidentified soft corals.

Stylaster spp. were the most abundant but they grow to only a few centimetres in height. Observations of the other corals were few, except for 750 encounters with *P. pacifica*.

Primnoa pacifica occurred exclusively anchored to hard substratum; both were most abundant on the Bank where the number of *P. pacifica* was positively correlated with the percent surface area comprising Bol (Spearman r = 0.80, p = 0.02, n = 8). We encountered two-thirds of the *P. pacifica* on 2 Bank transects, *P1* and *P2*, where the surveys were ~50% Bol; 365 corals occurred on the 850 m long *P1* transect alone (Fig. 4.1). The CS category, at 1.6%, was rare (Fig. 4.4) and scattered along 16 of the 26 transects with only a single occurrence on a trawled transect. Tall corals (≥30 cm in height) tended to occur in groups and the largest groupings were ~2 m in height and ~4 m in width on boulders of Basin transects. The largest patch of clustered CS stretched ~200 m along a Bank transect (‘*P1*’ in Fig. 4.1), but most often patches were sparse and only a few metres in length. Over 50% of CS (at least 1 coral ≥30 cm height) had at least one rockfish associated with their structure, while no rockfish were associated with short corals (between 10 and 30 cm height).

Bottom trawling effects on scorpaenid distribution

Six Tr (Groups 1 and 2 in Fig. 4.1) and 6 UTr transects (‘*U*’ in Fig. 4.1) of similar characteristics were compared (Table 4.5). Trawl evidence ranged between 5 and 22 events per Tr transect and averaged 15 ± 3 events, while no trawl evidence occurred on any UTr transect (Table 4.5). No *Primnoa pacifica* was observed on boulders that had visual evidence of trawling and there was ~13 times less coral in the Tr transects than in the UTr, which was a significant difference (Table 4.5). Of the few corals within the Tr transects, ~90% were short (between 10 and 30 cm in height), whereas within the UTr only ~20% were this small size. Thornyhead abundance on the UTr transects was the

same as on the Moraine, the seascape with the highest abundance of thornyhead (Mann-Whitney *U*-test: p = 0.09, n = 7 and 6; Tables 4.3 & 4.4), whereas thornyhead abundance on the Tr transects was significantly higher (Table 4.5). Rockfish abundance was significantly lower on Tr transects, by 4-fold (Table 4.5). No Tr transect rockfish occurred within CS while 33% of UTr transect rockfish were within CS (Table 4.5).

Discussion

Scorpaenids of Learmonth Bank

Shortspine thornyhead and rockfish represented 78% of demersal fishes observed at Learmonth Bank; this assemblage is the most common commercial fish captured in similar habitats of Alaska (Heifetz 2002). The 2 scorpaenid genera have similar life history characteristics (Love et al. 2002) and there was no difference in their overall abundances, a similarity that made subsequent comparisons of the genera more robust. The overall thornyhead abundance of 1.1 ± 0.2 ind. 100 m^{-2} is comparable with abundances in the Gulf of Alaska over a similar depth range (Else et al. 2002). The distribution of thornyhead over Learmonth Bank was random with relatively little variability among transects or among seascapes. Sightings were mostly of solitary individuals; the drivers for this behaviour might include reduction of intraspecific interaction in a species known to be cannibalistic (Love et al. 2002) or reduction of intraspecifc competition for resources. In contrast, rockfish distribution was clumped and abundances were higher on the Bank and Moraine where substratum was rougher. Learmonth Bank's rockfish assemblage comprised 9 species, a regional assemblage richness not uncommon on the northeast Pacific coast where there are nearly 100 known species of rockfish (Love et al. 2002).

Benthic biotopes and scorpaenid associations

Glaciation has created a diversity of seafloor habitats on and around Learmonth Bank. The seascapes surveyed varied from sandy plains of glacial till (majority), to a moraine of aggregated mixed sediments, to deeply incised bedrock. Scattered boulders added marked relief and were often colonised by large biogenic structures especially in the flat, sandy Basin, where *Primnoa pacifica* on boulders was the only large-scale relief. While each seascape had different degrees of representation by biotopes, most transects were a mosaic of all 12 biotopes. The patchiness of biotopes over a small scale (metres) facilitated observation of habitat use by scorpaenid fish.

Ocean waters off British Columbia generally support an abundance of sponges including glass sponges (Hexactinellida), possibly because of high dissolved silicate levels (Leys et al. 2004, Whitney et al. 2005). Learmonth Bank's sponge aggregations were encrusting on hard substrata where aggregations could be so dense they completely covered the seafloor; however, they did not form sponge reefs (sensu Cook et al. 2008). Similar sponge gardens occur along the British Columbia coast (Marliave et al. 2009). Sponges were observed on large cobbles while *Primnoa pacifica* exclusively anchored to boulders and bedrock. Large biogenic structures require sturdy, immobile substratum to persist, otherwise current forces can destabilize the entire structure (Tunnicliffe & Syvitski 1983).

Overall, thornyhead were no more abundant when sponges were present than on the same substratum type with bare surfaces or those covered with small epifauna. Occurrence with *Primnoa pacifica* was too low to test for a difference, but numbers and observations suggest no apparent association. There is a likely relationship of thornyhead abundance with depth as seen in the Gulf of Alaska (Else et al. 2002). Else et al. (2002)

also report a positive relationship between thornyhead and hard substratum, unlike Stein et al. (1992), Love et al. (2002), and the present study. The discrepancy may stem from inclusion of cobbles as hard substratum by Else et al. (2002). Thornyhead abundance patterns may also respond to prey distribution (authors' pers. obs.) and density-dependent negative feedback (Love et al. 2002). [Although no interaction between thornyhead and rockfish emerged within this study, there was a negative pairwise correlation between the two groups and each responded differently to depth. Thornyhead abundance increased with depth and ,although this study limit was just over 400 m, their range extents to approximately 1500 m depth (Love et al. 2002). The increase in thornyhead abundance with depth and a range beyond the lower limits of most rockfish species (Else et al. 2002; Love et al. 2002; present study) suggests thornyhead distribution may be influenced by competition with rockfish.]

Rockfish abundance was strongly related to the presence of sponge garden and CS coverage and rockfish were consistently more abundant on substrata covered in higher-relief epifauna. This rockfish study is the first to investigate abundance responses to both sponges and corals. Large sponges are emerging as major components of benthic habitat, from Washington State to Alaska (Campbell & Simms 2009) yet their role as fish habitat is poorly studied, although 2 recent studies in British Columbia demonstrate higher rockfish abundances on large reefs of glass sponges (Cook et al. 2008, Marliave et al. 2009). Our work, however, records the important role of scattered sponges on hard substratum—a habitat much more abundant in coastal and shelf waters. Even dense stands of smaller sponges (10 to 50 cm in height) harbour an order of magnitude greater density of rockfish than do bare surfaces. Average rockfish species richness was double

in sponge and coral biotopes, and similar to the higher diversity seen in undamaged versus trawled sponge reefs in Hecate Strait (Cook et al. 2008).

There is much attention paid to the role of corals like *Primnoa pacifica* in providing shelter for fish (e.g. Roberts et al. 2009). However, important fish habitats are those that support a significant percentage of the population at comparatively high densities (Auster 2005). Although rockfish density in coral biotopes was much higher than in sponge biotopes, *P. pacifica* was not abundant throughout the study area. TSG covered 10 times more surface area than CS and contained over 13 times the number of rockfish, i.e. ~80% of all observed rockfish. Similarly in the Gulf of Alaska, *P. pacifica* occurred on only 1% of boulders (Krieger & Wing 2002). The limited cover by the coral biotopes reduced statistical power in our analyses of rockfish distributions. Compared with the Bank and Moraine, the apparent importance of corals in the Basin was higher; one-third of Basin rockfish were associated with *P. pacifica*, which only covered 0.1% of the surveyed Basin. Corals a couple metres high provided relief in the otherwise flat and uniform Basin. The Basin is where trawling has its greatest impact and these large gorgonian corals are the main bycatch of Learmonth Bank's trawl fishery (Ardron et al. 2007).

Role of seafloor relief

Proposed causes of rockfish attraction to biogenic structures from previous work include enhanced prey availability, shelter for predator avoidance and juvenile nursery areas (Fosså et al. 2000, Krieger & Wing 2002, Auster 2007). These factors may be secondary effects of high relief and not unique to sponges and corals. For example, scorpaenid prey species (Love et al. 2002) observed on sponges and corals also occur throughout the surrounding area (Krieger & Wing 2002, the present study). Through stomach content analyses, Husebø et al. (2002) found rockfish are not linked to coral sites

through feeding habits and suggest the physical structure of corals attracts rockfish, rather than some biological attribute.

We used height in our classification scheme to determine the role of relief rather than just the identity of the biogenic structure. Over 50% of *Primnoa pacifica* taller than 30 cm had at least one associated rockfish and often several while, in comparison, not one rockfish was observed with *P. pacifica* under 30 cm in height. The same trend occurred with sponges: rockfish abundances were 4 times greater among tall (over 50 cm) than short sponges. When we controlled for the presence of biogenic structures, increasing substratum relief (Snd to Agg to Bol) resulted in a similar increase in rockfish abundance. Likewise, a submersible study off the coast of Washington concluded that rockfish were 3 times more abundant in higher than in lower bottom relief habitat (Jagielo et al. 2003).

Learmonth Bank's scorpaenids have different morphologies and behaviour. Thornyhead feed on a wide variety of benthic prey, including shrimps, amphipods, zooplankton and small fish, and usually settle motionless on the seafloor (Else et al. 2002, Love et al. 2002) as we observed in nearly all our sightings; not once did a thornyhead occur within a sponge or coral. Dense aggregations of biogenic structures, as occurred on boulders and bedrock, may reduce available space for thornyhead. The thornyhead body has a flattened ventral surface, broad head, broad pectoral fins and a narrowed anterior, features that assist the fish to maintain position in bottom currents (Hoerner 1965, Webb 1989), while a low, flattened body form maintains the animal within the boundary layer (Arnold & Weihs 1978). Unlike rockfish, the thornyhead has no swim bladder, an adaptation for buoyancy control in midwater; instead, the benthic position reduces energy expenditure (Fänge 1966). We suggest the morphology and

behaviour of thornyhead allows it an energy efficient means to hold its station or position (stationhold) on the current-swept seafloor of Learmonth Bank independently of seeking the shelter created by seafloor structures, such as sponges and corals.

The rockfish of Learmonth Bank feed on similar prey items as the thornyhead but displayed a different behaviour: most were stationary against or within erect structures. Nearly all rockfish were associated with either sponge or coral biotopes that comprised only 27% of the surveyed seafloor. Other studies also record rockfish against or within sponges, corals and boulders (Krieger & Ito 1999, Fosså as reported in Husebø et al. 2002, Krieger & Wing 2002, Freese & Wing 2003). Associating with tall biogenic structures might provide proximate flow refuge while feeding on advecting zooplankton above the substratum. Most rockfish over flat seafloor were passively moving with the current or actively swimming, which suggests these rockfish cannot station-hold on the current swept seafloor of Learmonth Bank without seeking out shelter created by seafloor structures, such as sponges and corals.

The bottom currents on Learmonth Bank that maintain the sediment-free bare substrata preferred by sponges and corals also challenge rockfish to hold station. We suggest that, while rough bottom provides shelter to rockfish, the abrupt vertical relief created by tall sponges and corals is effective as refuge from currents; Auster (2007) also proposes this role for corals. Further work that incorporates current measurements, quantifies relief and observations of scorpaenid behaviour should provide further tests of these ideas.

Effects of trawling

A consequence of the natural distribution of substratum types on the seascapes is a fishing ground bias, as illustrated by the distribution of commercial trawl sets (Fig. 4.1). Nearly all the trawl sets are located in Snd biotopes of Learmonth Bank's Basin. Ground-

contact trawlers avoid rough and rocky seafloors, like those on the Bank and Moraine, to reduce net ensnarement and gear damage (Sinclair et al. 2005). While we observed numerous trawling events, we have little evidence for frequency or timing of the observed incidence. Bottom currents and organism activity redistribute sediment and, over time, visual evidence of trawling activity fades, so our study may reflect relatively recent trawling activity on our transects. The distribution of the 2002 to 2007 commercial trawl sets (Fig. 4.1) illustrates the relative intensity of trawling around Learmonth Bank but only as the trawl start points. For the depth range of Learmonth Bank, the median length of a bottom trawl in British Columbia extends 10 km from the start point (Ardron et al. 2007) suggesting the affected area at Learmonth Bank is more extensive than we can demonstrate.

All scorpaenid species observed at Learmonth Bank are British Columbia commercial demersal fish. The shortspine thornyhead fishery is large and rapidly expanding (Love et al. 2002), and 95% of British Columbia's total allowable shortspine thornyhead catch is allocated to the demersal fish trawling sector (Fisheries and Oceans Canada 2010). Thornyhead were the single most abundant scorpaenid species at Learmonth Bank and, within the trawlable habitat of the basin, their abundance was 7 times that of all rockfish species combined. Its abundance was also higher on the Tr than on UTr transects. Hixon and Tissot (2007) report a similar observation on Oregon's continental shelf and suggest that mobile scavengers may aggregate along trawl-door tracks where high-intensity trawling can increase preferred prey (Engel & Kvitek 1998). Unlike Hixon & Tissot (2007), our study compared adjacent regions of similar depth and, thus, we have greater confidence that abundance differences were not confounded by depth effects.

The presence and abundance of short sponges and corals on Tr transects may relate to several factors. First, the Agg category was more abundant and small sponges colonised cobbles. Second, smaller epifauna may escape destruction by trawling. Third, damage may reduce the size of these structures: *Primnoa pacifica* can lose most of their branches after a single trawl tow (Krieger 2001) and both corals and sponges show damage in high-intensity trawled areas (Heifetz et al. 2009). A fourth possibility is recent recolonisation, as observed in the Gulf of Alaska for *P. pacifica* (Krieger 2001). Whatever the cause, these smaller biogenic structures attracted few rockfish, probably because size is an important factor. *P. pacifica* was exclusively anchored to hard substratum, but despite the similar availability of suitable substratum, UTr transects had 12 times the numbers of *P. pacifica* than did Tr transects. Thus, even if a trawled area has begun to recover, rockfish are unlikely to repopulate until biogenic structures reach a substantial size. Rockfish were found substantially less often on Tr transects, which is attributable to lack of appropriate sponges or corals. Thus, as in Norway (Husebø et al. 2002), rockfish catch sizes will remain low in trawled areas.

Auster (2005) suggests the resilience of rockfish populations to disturbance may be reduced in the absence of biogenic structures. Given their longevity and low reproductive rates rockfish species are particularly susceptible to population crashes (COSEWIC 2007, 2008). Over half the rockfish on the UTr Basin transects were rougheye rockfish and yelloweye rockfish *Sebastes ruberrimus*, 2 of the largest and slowest growing rockfish species (up to 205 and 120 yr, respectively); both species have ‘special concern’ status with fishing as an identified threat (COSEWIC 2007, 2008). Their presence in the

Learmonth Bank area is probably because the untrawled basin area is under jurisdictional dispute.

By using high definition quality video from an ROV, we could detail spatial relationships of benthic species at a scale not ordinarily achieved; normally survey data are equivalent to the length of an entire transect. Scientific trawling is destructive and, although a basic technique in deep-sea biology (Roberts 2002), it is limited in sampling as it cannot tow on rough substratum (Sinclair et al. 2005). Such habitat bias reduces the validity of rockfish stock estimates and supports the need for visual surveys to conduct population studies (Jagielo et al. 2003). Learmonth Bank is a proposed coral–sponge protection area and this study implies there are ecological benefits of such closure. There are marked differences in distribution patterns and associations of 2 scorpaenid groups. The shortspine thornyhead would not be adversely affected by losses in biogenic structures such as sponges and corals and could even concentrate in areas of localized trawling or areas of low biogenic structure density. However, the consequence to rockfish of extensive sponge and coral loss, especially near the bank, would be reduced numbers for sustained periods.

Acknowledgements

We thank the field team for data collection and advice, especially J. Boutillier (Chief Scientist), J. Rose, E. Edinger and J. Chu. Personnel of the Canadian Scientific Submersible Facility and the CCGS ‘John P. Tully’ aided field operations. S. Leys and J. V. Barrie provided additional insight. Research is sponsored by the Natural Sciences and Engineering Research Council Canadian Healthy Oceans Network, a university–

government partnership dedicated to biodiversity science for the sustainability of Canada's 3 oceans. Additional support was provided by a University of Victoria Fellowship to C. Du Preez and by Fisheries and Oceans Canada.

Literature cited

Allen LG, Pondella DJ II, Horn MH (eds) (2006) The ecology of marine fishes: California and adjacent waters. University of California Press, Los Angeles, CA

Andrews AH, Cordes EE, Mahoney MM, Munk K, Coale KH, Cailliet GM, Heifetz J (2002) Age, growth and radiometric age validation of a deep-sea, habitat-forming gorgonian (*Primnoa resedaeformis*) from the Gulf of Alaska. Hydrobiologia 471:101–110

Ardron JA, Jamieson GS, Hangaard D (2007) Spatial identification of closures to reduce the by-catch of corals and sponges in the groundfish trawl fishery, British Columbia, Canada. Bull Mar Sci 81:157–167

Arnold GP, Weihs D (1978) The hydrodynamics of rheotaxis in the plaice (*Pleuronectes platessa*). J Exp Biol 75:147–169

Auster PJ (2005) Are deep-water corals important habitats for fishes? In: Freiwald A, Roberts JM (eds) Cold-water corals and ecosystems. Springer-Verlag, Berlin, p 747–760

Auster PJ (2007) Linking deepwater corals and fish populations. In: George RY, Cairns SD (eds) Conservation and adaptive management of seamount and deep-sea coral ecosystems. Rosensteil School of Marine and Atmospheric Science, Miami, FL, p 93–99

Ballantyne VA, Foreman MGG, Crawford WR, Jacques R (1996) Three-dimensional model simulations for the north coast of British Columbia. Cont Shelf Res 16:1655–1682

Barrie JV, Conway KW (1999) Late quaternary glaciation and postglacial stratigraphy of the Northern Pacific margin of Canada. Quat Res 51:113–123

Barrie JV, Conway KW (2002) Contrasting glacial sedimentation processes and sea-level changes in two adjacent basins on the Pacific margin of Canada. In: Dowdeswell J, O'Cofaigh C (eds) Glacier-influenced sedimentation on high-latitude continental margins. Geol Soc Lond Spec Publ 203:181–194

Bone Q, Marshall NB (1982) Biology of fishes. Blackie, London

Bornhold BD, Barrie JV (1991) Surficial sediments on the western Canadian continental shelf. Cont Shelf Res 11: 685–699

Campbell JS, Simms JM (2009) Status report on coral and sponge conservation in Canada. Fisheries and Oceans Canada, Ottawa. Available at: www.dfo-mpo.gc.ca/oceans/publications/cs-ce-2009-eng.pdf

Cook SE, Conway KW, Burd B (2008) Status of the glass sponge reefs in the Georgia Basin. Mar Environ Res 66: S80–S86

COSEWIC (Committee on the Status of Endangered Wildlife in Canada) (2007) COSEWIC assessment and status report on the Rougheye Rockfish *Sebastes* sp. type I and *Sebastes* sp. type II in Canada. COSEWIC, Ottawa. Available at: http://dsp-psd.pwgsc.gc.ca/collection_2007/ec/CW69-14-526-2007E.pdf

COSEWIC (Committee on the Status of Endangered Wildlife in Canada (2008) COSEWIC assessment and status report on the Yelloweye Rockfish *Sebastes ruberrimus*, Pacific Ocean inside water population and Pacific Ocean outside waters population, in Canada. COSEWIC, Ottawa. Available at: http://www.sararegistry.gc.ca/virtual_sara/files/cosewic/sr_yelloweye_rockfish_0809_e.pdf

Crawford RW, Greisman P (1987) Investigation of permanent eddies in Dixon Entrance, British Columbia. Cont Shelf Res 7:851–870

Else P, Haldorson L, Krieger K (2002) Shortspine thornyhead (*Sebastolobus alascanus*) abundance and habitat associations in the Gulf of Alaska. Fish Bull 100:193–199

Engel J, Kvitek R (1998) Effects of otter trawling on a benthic community in Monterey Bay National Marine Sanctuary. Conserv Biol 12:1204–1214

Fänge R (1966) Physiology of the swimbladder. Physiol Rev 46:299–322

Fisheries and Oceans Canada (2010) Pacific region integrated fisheries management plan: groundfish. Available at: http://www-ops2.pac.dfo-mpo.gc.ca/xnet/content/MPLANS/plans11/2011%20Groundfish%20IFMP_Final_Complete.pdf

Fosså JH, Mortensen PB, Furevik DM (2000) *Lophelia* korallrev langs norskekysten forekomst og tilstand. Prosjektrapp Havforskningsinst, Bergen

Freese JL, Wing BL (2003) Juvenile red rockfish, *Sebastes* sp., associations with sponges in the Gulf of Alaska. Mar Fish Rev 65:38–42

Gray DH (1997) Canada's unresolved maritime boundaries. IBRU Boundary Security Bull Autumn 1997, p 61–71

Heifetz J (2002) Coral in Alaska: distribution, abundance, and species associations. Hydrobiologia 471:19–28

Heifetz J, Stone RP, Shotwell SK (2009) Damage and disturbance to coral and sponge habitat of the Aleutian Archipelago. Mar Ecol Prog Ser 397:295–303

Hixon MA, Tissot BN (2007) Comparison of trawled vs. untrawled mud seafloor assemblages of fishes and macroinvertebrates at Coquille Bank, Oregon. J Exp Mar Biol Ecol 344:23–34

Hoerner SF (1965) Fluid-dynamic drag. Hoerner Fluid Dynamics, Brick Town, NJ

Husebø A, Nøttestad L, Fosså JH, Furevik DM, Jørgensen SB (2002) Distribution and abundance of fish in deep-sea coral habitats. Hydrobiologia 471:91–99

Jagielo T, Hoffmann A, Tagart J, Zimmermann M (2003) Demersal groundfish densities in trawlable and untrawlable habitats off Washington: implications for the estimation of habitat bias in trawl surveys. Fish Bull 101: 545–565

Krieger KJ (2001) Coral (*Primnoa*) impacted by fishing gear in the Gulf of Alaska. In: Willison JHM, Hall J, Gass SE, Kenchington ELR, Butler M, Doherty P (eds) Proceedings of the 1st international symposium on deep-sea corals, Halifax, Nova Scotia, 30 July–2 August 2000. Ecology Action Centre, Dalhousie University and Nova Scotia Museum, Halifax, p 106–116

Krieger KJ, Ito DH (1999) Distribution and abundance of shortraker rockfish, *Sebastes borealis*, and rougheye rockfish, *S. aleutianus*, determined from a manned submersible. Fish Bull 97:264–272

Krieger KJ, Wing BL (2002) Megafauna associations with deepwater corals (*Primnoa* spp.) in the Gulf of Alaska. Hydrobiologia 471:83–90

Lamb A, Hanby BP (2005) Marine life of the Pacific Northwest: a photographic encyclopedia of invertebrates, seaweeds and selected fishes. Harbour Publishing, Madeira Park

Leys SP, Wilson K, Holeton C, Reiswig HM, Austin WC, Tunnicliffe V (2004) Patterns of glass sponge (Porifera, Hexactinellida) distribution in coastal waters of British Columbia, Canada. Mar Ecol Prog Ser 283:133–149

Love MS, Yoklavich M, Thorsteinson L (2002) The rockfishes of the Northeast Pacific. University of California Press, Los Angeles, CA

Marliave JB, Conway KW, Gibbs DM, Lamb A, Gibbs C (2009) Biodiversity and rockfish recruitment in sponge gardens and bioherms of southern British Columbia, Canada. Mar Biol 156:2247–2254

Morgan LE, Chuenpagdee R (2003) Shifting gears: addressing the collateral impacts of fishing methods in U.S. waters. Pew Science Series, Island Press Publication Services, Washington, DC

Pearcy WG, Stein DL, Hixon MA, Pikitch EK, Barss WH, Starr RM (1989) Submersible observations of deep-reef fishes of Heceta Bank, Oregon. Fish Bull 87:955–965

Richards LJ (1986) Depth and habitat distribution of three species of rockfish (*Sebastes*) in British Columbia: observations from the submersible PISCES IV. Environ Biol Fishes 17:13–21

Risk MJ, Heikoop JM, Snow MG, Beukens R (2002) Lifespans and growth patterns of two deep-sea corals: *Primnoa resedaeformis* and *Desmophyllum cristagalli.* Hydrobiologia 471:125–131

Roberts CM (2002) Deep impact: the rising toll of fishing in the deep sea. Trends Ecol Evol 17:242–245

Roberts JM, Wheeler A, Freiwald A, Cairns S (2009) Coldwater corals: the biology and geology of deep-sea coral habitats. Cambridge University Press, Leiden

Sameoto JA, Lawton P, Strong MB (2008) An approach to the development of a relational database and GIS applicable scheme for the analysis of video-based surveys of benthic habitats. Can Tech Rep Fish Aquat Sci 2818

Sinclair AF, Conway KW, Crawford WR (2005) Associations between bathymetric, geologic and oceanographic features and the distribution of the British Columbia bottom trawl fishery. ICES CM 2005/L:25 Available at: www.ices.dk/products/CMdocs/2005/L/L2505.pdf

Stein DL, Tissot BN, Hixon MA, Barss W (1992) Fish–habitat associations on a deep reef at the edge of the Oregon continental shelf. Fish Bull 90:540–551

Tunnicliffe V, Syvitski JPM (1983) An unusual mechanism of sediment transport. Limnol Oceanogr 28:564–568

Webb PW (1989) Station-holding by three species of benthic fishes. J Exp Biol 145:303–320

Whitney F, Conway K, Thomson R, Barrie V, Krautter M, Mungov G (2005) Oceanographic habitat of sponge reefs on the Western Canadian continental shelf. Cont Shelf Res 25:211–226

Yoklavich MM, Greene HG, Sullivan DE, Lea RN, Love MS (2000) Habitat associations of deep-water rockfishes in a submarine canyon: an example of a natural refuge. Fish Bull 98:625–641

Zacharias MA, Howes DE, Harper JR, Wainwright P (1998) The British Columbia marine ecosystem classification: rationale, development and verification. Coast Manag 26:105–124

Chapter 5: Influence of multiple scales of topographic heterogeneity on localized benthic diversity

Preface

This chapter is a first draft of a manuscript to be modified for submission.

Introduction

Deep-sea habitats harbour a tremendous amount of biological diversity and contribute extensively to the $ 8.3 trillion worth of ecosystem services that the open ocean provides each year (Costanza et al., 1997). Yet despite intrinsic and economic value, deep-sea habitats are among the poorest known and least studied on Earth. With present and anticipated anthropogenic impacts (e.g., overfishing, climate change and ocean acidification) there is increasing urgency in the need to establish baseline information. Diversity is the single most assessed biological component of marine ecosystems (Corrigan and Kershaw, 2008) partially owing to its positive linkages with ecosystem services, functions, stability and recovery potential (Worm et al., 2006). Seafloor characteristics are often used to assess bottom habitat and predict biological parameters in data limited areas (McAuthur et al., 2010).

The hypothesis that diversity relates positively with topographic heterogeneity (i.e., variation in elevation) is well supported in many terrestrial and aquatic habitats. Marine studies on the hypothesis are largely based in relatively accessible habitats, such as the intertidal and shallow subtidal (Risk, 1972; Cusson and Bourget, 1997; Beck, 1998; Guichard and Bourget, 1998; Guichard et al., 2001; Barros et al., 2004; Brock et al., 2004; Gratwicke and Speight, 2005; Purkis et al., 2008; Walker et al., 2009). Suspected

drivers behind the relationship include increased niche availability, shelter from predation or environmental hazards, increased food accessibility, modified recruitment processes and increased surface area. Although there is a general consensus among these studies that benthic diversity positively relates with topographic heterogeneity, wider application needs study. Diversity patterns and drivers vary among habitats, species assemblages, and scales (Chave, 2013). Resolving this diversity pattern in deep-sea habitats has application for both ocean conservation and management as well as for ecological theory.

There are a variety of metrics to measure topographic heterogeneity but the most widely used is rugosity (McCormick, 1994). Rugosity is a simple ratio of the contoured distance of a surface and the planar distance (or area for 3-D analyses). I use the new arc-chord ratio (ACR) rugosity index, which has merits over traditional indices that were important to this study (Du Preez and Tunnicliffe, 2012; Du Preez, 2014 [Chapter 2 and 3]). I include slope in analyses as a separate seafloor variable and, unlike most other rugosity indices, ACR rugosity is decoupled from slope. I investigate rugosity at multiple scales (resolution and extent) using both two- and three-dimensional data and, unlike many rugosity indices, ACR rugosity application is independent of the data dimensionality and scale. Qualifying small-scale rugosity in remote habitats is challenging, hence most studies occurring in easily accessible shallow-water habitats. Here I use the new microtopographic laser scanning method (MiLS; Du Preez and Tunnicliffe, 2012 [Chapter 2]) to remotely measure deep-sea substratum rugosity at a centimetre scale.

This study uses remotely operated vehicle imagery and multibeam sonar to investigate the relationship between deep-sea local epibenthic diversity and topographic

heterogeneity (measured as rugosity). Studying an ecological question across multiple spatial scales is critical for establishing a pattern and its underlying drivers (Chave, 2013). The resolution and extent (scales) of a study often depend on arbitrary sampling method limitations with little to no ecological relevance (Chave, 2013). Single-scale analyses also tend to inadequately characterize environmental heterogeneity (e.g., a slope at small scale may be an element of rugosity at a larger scale; Wu 2004). This study examines diversity responses to multiple scales of local and regional topographic heterogeneity (two resolutions: centimetre-scale and 5 m^2; extent range: 10 to 250,000 m^2). Replicating research is critical for detecting and establishing patterns of diversity and in this work I replicated the same natural experiment at study sites located on six different deep-sea bathymetric features in three geographically distant regions on the Canadian Pacific and Atlantic continental shelf. I examine three hypotheses: (1) local epibenthic diversity correlates positively with local microtopographic heterogeneity, (2) local epibenthic diversity correlates positively with multiple scales of regional topographic heterogeneity, and (3) bottom flow hydrodynamics is an important underlying driver of these relationships.

Methods and Materials

Field work

Study sites

The hypotheses were tested by studying epibenthic communities at six study sites located on different deep-sea bathymetric features on the Canadian Pacific and Atlantic continental shelves (Fig. 5.1; Table 5.1). Three sites were in the region of Learmonth Bank, located off the Pacific coast in an exposed east-west strait (Dixon Entrance)

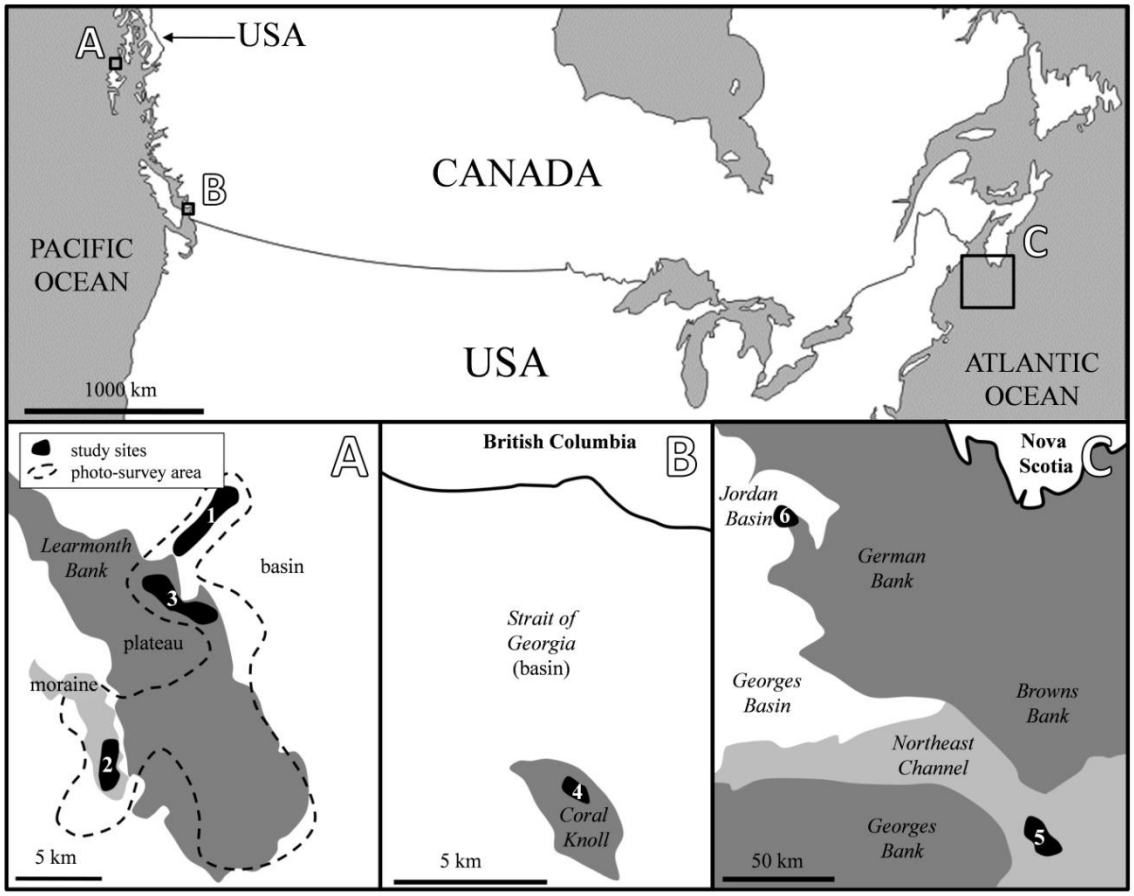

Figure 5.1.The six study sites on the Canadian continental shelf. At each site we flew 16 video transects 10 m in length to analyse the relationship between epibenthic diversity and microtopographic heterogeneity. Photographic quadrats at (A) Learmonth Bank (n = 137 quadrats; where each quadrat = 0.25 m^2) were analysed for the relationship between epibenthic diversity and multiple large scales of topographic heterogeneity. (A-C) Grey shading differentiates the bathymetric features of each region: basin (white), bank (dark grey), and other (light grey). See Table 5.1 for site details and coordinates.

between the Haida Gwaii islands (Canada) and the Alexander Archipelago (USA; Fig. 5.1). Within this high-energy environment I surveyed a basin, a moraine, and atop a plateau (sites 1 to 3; Fig. 5.1A; Table 5.1). The fourth site lay in the sheltered Strait of Georgia east of Vancouver Island (Fig. 5.1) where I surveyed the summit of the steep seamount-shaped Coral Knoll (site 4; Fig. 5.1B; Table 5.1). The two Atlantic sites were located within the Gulf of Maine, a semi-enclosed sea bounded by the mainland and

submarine banks (Fig. 5.1). Surveys were done on one flank of the Northeast Channel at the edge of the gulf and at the "Rock Garden" pinnacles of Jordan Basin within the gulf (sites 5 and 6; Fig. 5.1C; Table 5.1). For detailed descriptions of each site, see: Greisman, 1986 (Learmonth Bank); Barrie and Conway, 1999 (Learmonth Bank); Conway et al. 2007 (Coral Knoll); Kenchington and Vickers, 2007 (Jordan Basin and Northeast Channel); and Kelly et al. (2010; Northeast Channel).

Although the Pacific basin and the Atlantic channel sites (sites 1 and 5) are good deep-sea environments for bottom-contact fishing activities, both sites are within protected areas. The Pacific basin site is in an unresolved maritime boundary disputed area (between Canada and the USA; Gray, 1997) and the Atlantic channel site is in the Northeast Channel Coral Conservation Area (Brock et al., 2009). The complex bathymetry of the other sites (2, 3, 4, and 6; Table 5.1) is a natural deterrent to bottom-contact fishing (e.g. bottom trawling; Sinclair et al., 2005).

Table 5.1. Location features of study sites surveyed using benthic video transects in the region of Learmonth Bank (LB), in the Strait of Georgia (SoG), and in the Gulf of Marine (GoM). Depth is mean (standard error) and distance indicates the maximum spacing between transects within the site.

Study site	1	2	3	4	5	6
Region	LB	LB	LB	SoG	GoM	GoM
Feature	basin	moraine	plateau	knoll	channel	pinnacles
Latitude (N)	54°35'	54°26'	54°29'	49°22'	41°59'	43°19'
Longitude (W)	132°59'	133°08'	133°00'	123°53'	65°38'	67°03'
Depth (m)	373 ±6	304 ±14	196 ±3	183 ±4	182 ±6	156 ±4
Distance (km)	5	7	7.5	0.5	4.5	4

Multibeam sonar survey

The Learmonth Bank multibeam sonar survey was conducted by Natural Resources Canada in August 2008 (Milner, 2008) using a Kongsberg Simrad EM 1002 (95 kHz) Multibeam Echo Sounder. Processed bathymetry (depth) and backscatter (signal intensity) raster datasets were mapped using a grid cell 5 by 5 m spatial resolution (25 m^2) and georeferenced with an accuracy of 1 % of water depth (w.d.) for latitude and longitude and 0.3 % w.d. for depth (per comm J. V. Barrie and K. Picard, Geological Survey of Canada).

Although I had access to Coral Knoll (site 4) multibeam sonar, the area I was able to survey using the remotely operated vehicle (ROV) was only 0.5 km in length, which ruled out conducting any large-scale spatial analysis. Multibeam sonar of the Gulf of Maine (sites 5 and 6) was not available.

Remotely operated vehicle (ROV) benthic surveys

Between July 2008 and February 2012 I conducted benthic video surveys of the six study sites using three remotely operated vehicles (ROVs) during four expeditions (Table 5.2). It is common practice to collaborate with other scientists when using ROVs and so ours was not always the primary objective of a survey cruise or dive. The benthic survey design at each study site was therefore the result of a collaboration of scientific objectives. For this study an optimal site survey involved strictly following preplanned transects and not deviating to investigate events of interest. The video survey of each site was either conducted during a single dive (sites 1 to 4), or during multiple dives over a two to three day period (sites 5 and 6).

Table 5.2. Summary of remotely operated vehicle (ROV) cruises, surveys, and equipment.

Survey period	July 2008	June 2009	July/Aug 2010	Feb 2012
Study site	Learmonth & 1, 2, 3	Learmonth	5, 6	4
ROV	ROPOS	Phantom HD2+2	ROPOS	Oceanic Explorer
Survey type	video transects, bottom flow (video), & photographic quadrats	bottom flow (video) & photographic quadrats	video transects	video transects
Survey camera(s)	Sony DXC-990 3-CCD standard definition video camera; Sony Cybershot digital still camera	Sony EVI 330 standard definition video camera; C-MAP Systems Cyclops digital still camera	Insite Pacific Mini Zeus high definition video camera	Insite Pacific Mini Zeus high definition video camera

To collect the seafloor video imagery the ROVs were equipped with downward-facing cameras (Table 5.2), lights, and a set of parallel lasers to project a scale onto the seafloor. The laser projections were also used to measure small-scale rugosity using the microtopographic laser scanning method (MiLS; Du Preez and Tunnicliffe, 2012 [Chapter 2]). Video transects were conducted at an average speed of 0.5 to 1 knots, between 0.5 to 2 m off the seafloor, following the MiLS protocol (Du Preez and Tunnicliffe, 2012 [Chapter 2]) and video was recorded continuously. During the 2008 video surveys of sites 1, 2, and 3 I simultaneously conducted a photographic survey of the Learmonth Bank region and in 2009 a second ROV accessed the shallow regions of Learmonth Bank (Fig. 5.1A; Table 5.2). Both video and photographic imagery was georeferenced with x,y,z coordinates (latitude, longitude, and depth) from the ROV

navigational data with an accuracy of approximately 1 % of w.d. (per comm Ian Murdock, ROV ROPOS technician).

Video transect analysis

Benthic video transects were analysed to characterize and quantify epibenthos and microtopographic heterogeneity at a scale of 10 m^2. The length of the benthic video surveys at each site ranged between 0.5 to 7.5 km (Table 5.1). To standardize sampling, 16 non-overlapping video transects 10 m in length (± 3 seconds of video) were randomly selected for each site (for example video transect see Fig. 5.2A). In preliminary analyses using species accumulation curves, 10 m was found to be a sufficient length to sample the benthic fauna at these sites while meeting the requirements of the MiLS protocol (Du Preez and Tunnicliffe, 2012 [Chapter 2]).

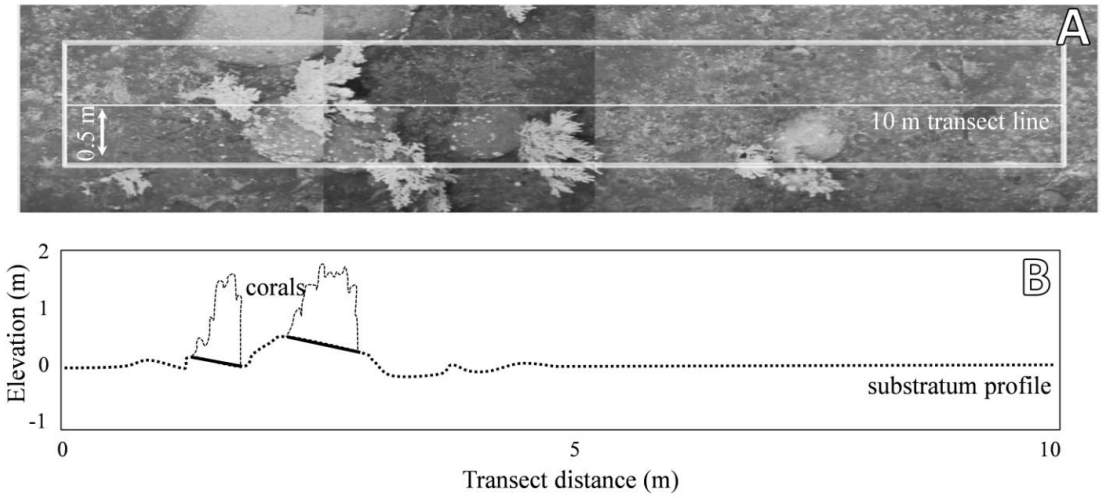

Figure 5.2. Video transect methods. (A) An example video transect from site 2. Discrete counts of epibenthic fauna within 0.5 m of the 10 m transect line (10 m^2 sample area) and percent coverage of sediment along the transect line were annotated. (B) From the video recording of a projected laser I used the microtopographic laser scanning (MiLS) method to profile the seafloor along the transect line and calculate linear (2-D) rugosity (as a measure of microtopographic heterogeneity). To avoid confounding diversity and rugosity I replaced profile sections over biogenic structures (e.g. coral) with a straight line conservative estimate of the obstructed substratum.

I used the video processing software Kinovea Motion Tuner (version 0.8.15) to annotate seafloor and epibenthic fauna data from the video transects. I used the MiLS photogrammetry analysis of tracking the relative motion of the projected laser to generate centimetre-scale seafloor profiles for each 10 m video transect (Du Preez and Tunnicliffe, 2012 [Chapter 2]; Fig. 5.2B). To avoid confounding the measure of microtopographic heterogeneity with the community variables I replaced sections of the profile where biogenic structures were present (e.g. corals and sponges) with a straight line; the conservative assumption is that the obscured substratum was flat. The resulting seafloor profile is therefore a function of the substratum structure only. I used the substratum profiles and the arc-chord ratio (ACR) rugosity index to calculate the linear rugosity of each 10 m transect as a measure of microtopographic heterogeneity (resolved at a centimeter scale; Du Preez and Tunnicliffe, 2012 [Chapter 2]; Du Preez, 2014 [Chapter 3]). While executing the MiLS analysis I simultaneously recorded the frequency of fine-grained sediment under the laser projection for the length of each transect (i.e., clastic substrata < cobble size.)

Using the parallel laser scales I superimposed a 1 m horizontal midline across the video and recorded epibenthic fauna that crossed over it during the 10 m transect (Fig. 5.2A). Fauna were identified to the lowest taxonomic level possible with confidence and counted. If identification to species-level was not possible I used the lowest taxonomic level possible and assigned an OTU (Operational Taxonomic Unit) designation based on morphology (e.g. *Sebastes* sp.1). Differences in equipment (Table 5.2) and survey conditions yielded variation in the quality of video imagery among sites. To mitigate biases in the annotation of fauna owing to image quality I standardized by recording only

fauna > 5 cm in size (in preliminary analyses of the video, 5 cm was the finest resolution attainable from all six sites). Individual organisms and colonies of small organisms (e.g. corals and sponges; where individuals could not be resolved but the colony was > 5cm) were treated as discrete occurrences. Fish in physical association with the seafloor (substratum or biogenic structures) were considered epibenthic and recorded.

Photographic quadrats analysis

Benthic photographic quadrats were analysed to quantify epibenthos at a scale of 0.25 m^2. From the hundreds of seafloor photographs taken at Learmonth Bank during the 2008 and 2009 cruises (Table 5.2) a subset of 137 photographs was selected haphazardly with the constraint of a minimum 250 m interval between photographs (the maximum distance between two photographs was 24.2 km). I used the image processing software ImageJ (version 1.42q) to analyse the photographs. Using the parallel laser scales I superimposed a 50 by 50 cm quadrat (0. 25 m^2) on each photograph (in preliminary analyses of photographs, 0.25 m^2 was the maximum quadrat size consistently attainable; for example photographic quadrat see Fig. 5.3A). Similar to the video analysis, epibenthic fauna were identified to the lowest taxonomic level possible with confidence. If identification to species-level was not possible I used the lowest taxonomic level possible and assigned an OTU (Operational Taxonomic Unit) designation based on morphology. The photographs were resolvable to the fine-scale of 0.5 cm. At this scale the majority of epibenthic fauna were colonial encrusting organisms; therefore, instead of discrete counts I recorded fauna as percent coverage. Solitary and colonial organisms were treated the same. To measure percent coverage I superimposed 5 by 5 cm square cell grid and counted the number of cells each taxon covered. Percent coverage was recorded at a resolution of 1 % (5 by 5 cm) unless an organism covered < 1 %, in which case I recorded it as 0.5 %.

Community variables

From the transect and photograph epibenthos datasets I calculated three community variables: abundance, richness, and diversity. Abundance (*N*) is the sum of discrete counts of organisms along transects and as the sum of the percent coverage of organisms within quadrats. By treating solitary and colonial organisms the same within a survey type (i.e., transects or quadrats) I was able to calculate single diversity index that

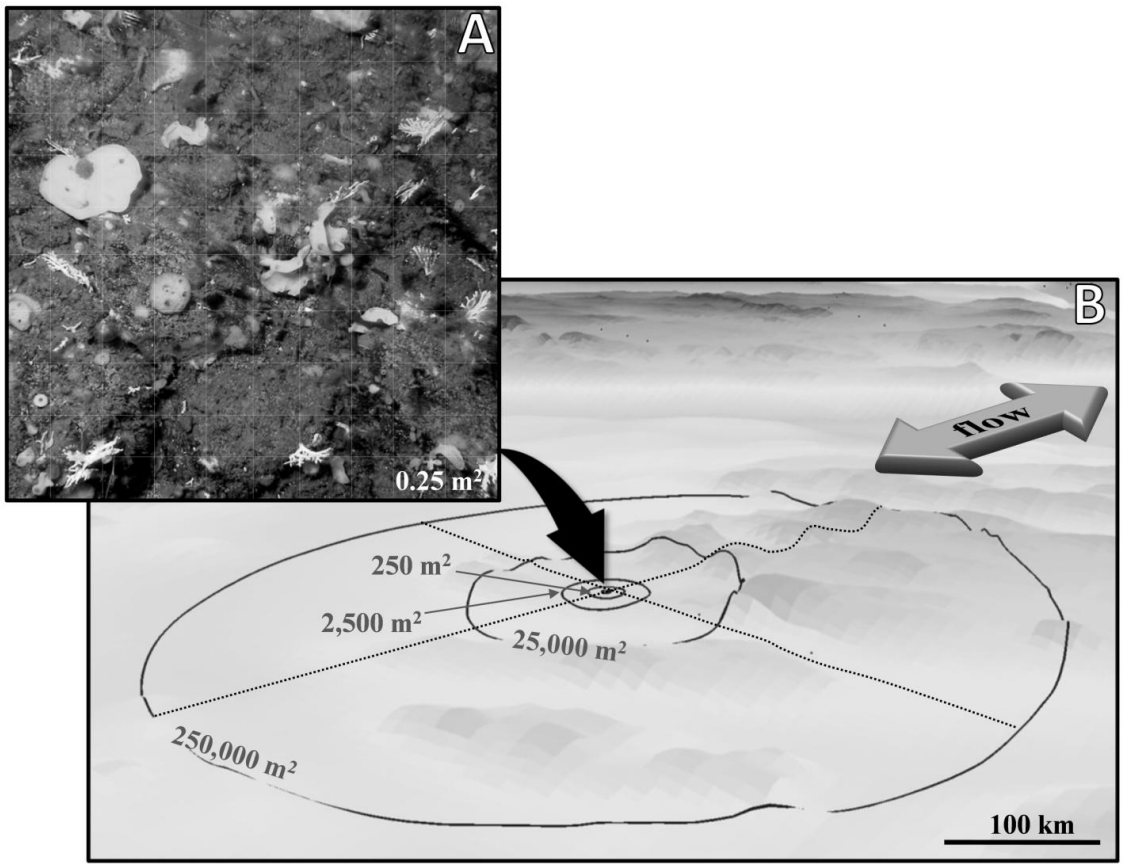

Figure 5.3. (A) An example photographic quadrat from the Learmonth Bank. Epibenthic animals within the 50 by 50 cm quadrat (0.25 m^2) were annotated as percent coverage. (B) From the multibeam sonar data we measured backscatter (a proxy for hard substratum), slope, depth, and areal (3-D) rugosity at each quadrat location (finest resolution possible, 25 m^2). We also measured areal and linear (2-D) rugosity at four larger spatial scales surrounding each quadrat (scales between 250 and 250,000 m^2). Linear rugosity was measured twice at each spatial scale: once parallel (aligned) and once perpendicular (across) the major axis of the Learmonth Bank bottom flow direction.

represented all fauna. Richness (S) is the total number of taxa. I calculated diversity as the Shannon index: $H' = \sum_{i=1}^{S} p_i \ln p_i$ where p_i is the proportion of taxon i. The Shannon index (also known as the Shannon-Weaver index, the Shannon-Wiener index, the Shannon's diversity index, and Shannon entropy) ranges from 0 and higher, where a value of 0 represents no uncertainty in predicting the identification in a randomly selected individual and values >> 0 represent a higher diversity. I calculated alpha diversity (α-diversity) as the mean diversity in a site and beta diversity (β-diversity; turnover) as the extent to which diversity of the entire site (gamma diversity; γ-diversity) is greater than the diversity of an average transect (Magurran, 2004): $\beta\text{-diversity} = \gamma - \overline{\alpha}$. Within this paper I use the term "diversity" to refer to the overall general pattern considering all the aforementioned community variables.

Because I collected abundance data differently in the two surveys (count and percent coverage), diversity indices from transects and quadrats are not mixed and are analysed separately. I distinguished mobile epibenthic fauna from sessile fauna and calculated the community variables for these groups separately. Mobile fauna were defined as any taxon that had potential to relocate actively outside of the transect swath/quadrat while sessile fauna could not.

Video analysis of bottom flow direction

To investigate hydrodynamics as an underlying driver of the potential relationship between epibenthic diversity and topographic heterogeneity I first needed to characterize the bottom flow direction over Learmonth Bank. I did this by examining all Learmonth Bank 2008 and 2009 benthic video (Table 5.2) when the ROV was stationary on the seafloor; downward-looking video captured the movement of suspended particulates

passing in front of the camera. The number of potential bottom flow direction measurements was limited by the number of times the ROV landed (to take a photograph or investigate an event or onboard instrument). The analysis yielded approximately one measurement every half hour for 72 hours of benthic video recording (58 hours from 2008; 7 hours from 2009; Table 5.2) for a total of 118 bottom flow direction measurements. The largest distance between sample was approximately 26 km. To measure the bottom flow direction only downward-facing imagery was analysed (both camera systems were <1 m above the seafloor when the ROV was set down).

Using Kinovea Motion Tuner (version 0.8.15) I tracked the path and angle of suspended particulates transiting the field of view and calculated the direction of the bottom flow relative to the ROV. Three haphazardly selected particulates with straight trajectories were tracked in series and the three angles averaged to produce one measurement. The bottom flow direction data were aligned with North to give a compass heading using the ROV heading in the navigational data. This was done after the video annotation to mitigate bias owing to *a priori* knowledge of the local surface tidal currents.

Preliminary analyses of the bottom flow direction data strongly supported the reversing (rectilinear) bottom flow model at a semidiurnal tidal cycle (Cummins and Oey, 1996). There was an abrupt 180° change in flow direction every six hours synchronized with the local high and low tides for nearby Langara Island, British Columbia; 54°15'N, 133°03'W; DFO, 2008, 2009). Twenty flow measurements were excluded from the analysis owing to little to zero measurements (no water movement or erratic particulate movement with no straight trajectories). The remaining 98 measurements were grouped

according to time in the tidal cycle (flooding or ebbing) the measurement was made. To calculate the major axis of the bottom flow direction, the two groups were then standardized to a scale of 0° to 180° and combined.

Multibeam bathymetry analysis

Multibeam sonar datasets were analysed to characterize the seafloor at large regional scales. I analysed the Learmonth Bank raster datasets using ArcGIS® version 10.2 (ESRI, 2013) and at each photographic quadrat location I measured the large-scale seafloor variables: backscatter (in decibels, db), slope (in degrees, °), depth (in meters, m), and multiple scales of areal (3-D) rugosity and linear (2-D) rugosity as measures of topographic heterogeneity. Acoustic backscatter was measured directly from the backscatter raster and used to infer substratum hardness (Dartnell and Gardner, 2004; Kloser et al., 2010) where a backscatter value of 0 db indicates hard substratum (e.g., bedrock or boulders) and a values << 0 db indicates fine-grained substrata (e.g., sand). In preliminary analyses I used data collected from the photographic quadrats for quality control of this inference. The analysis confirmed an inverse correlation between the percent coverage of sediment and backscatter (Spearman correlation $p < 0.001$, $r = -0.579$, $n = 137$). Depth was measured directly from the bathymetry raster while the remaining variables were derived using ArcGIS® tools and published automated models: I derived slope using the *Slope* function in *3D Analyst Tools*, and areal and linear rugosity using the arc-chord ratio (ACR) method and automated models (Du Preez, 2014 [Chapter 3]).

All areal seafloor variables were at the lowest spatial scale extent possible (25 m^2). Areal and linear rugosity were then measured at four larger scales using circular windows around each photograph location at 250 m^2, 2,500 m^2, 25,000 m^2, and 250,000 m^2 (for

example illustration, see Fig. 5.3B). The windows were created using the *Buffer* function in the *Proximity toolset*. Circular windows were used to avoid confounding areal rugosity measurements with directionality. These scales were determined to be the most efficient means to include a breadth of scales within the scope of this study; the lower limit for scale was limited by raster resolution and the upper limit by distance between samples. At the larger scales, because windows overlapped, areal rugosity samples were removed from analyses to avoid pseudoreplication causing a decrease in sample size.

Linear rugosity was measured along two transects within each circular window (for example see Fig. 5.3B). Transects were equal to the diameter of the window (i.e., 18 m, 56 m, 178 m, and 564 m) and orientated according to the calculated major axis of the bottom flow direction as calculated for that vicinity (above). One transect was aligned parallel and the other was perpendicular the dominant path of flow (major axis). These transect orientations at 90° were selected to explore bottom flow hydrodynamics as an underlying driver of the potential relationship between epibenthic diversity and topographic heterogeneity. Explicitly, does local diversity have a stronger relationship with large-scale rugosity aligned with the path of dominant flow? The multi-scale transects were created using the *Bearing distance to line* function in *Data management tools*.

Data analysis

To test hypotheses about the influence of multiple scales of topographic heterogeneity on local epibenthic diversity, data were analysed using multiple univariate and multivariate statistical tests in PASW Statistics 18 for significance at p-value < 0.05. Descriptive statistics of a variable included mean (μ), standard error (σ), total, maximum

(max.), minimum (min.), and Shapiro-Wilk ($n < 50$) or Kolmogorov-Smirnov ($n > 50$) test of normality.

I tested for differences between the six study sites using a Kruskal-Wallis test and I used a two step cluster analysis of ordinal level abundance variables to compare epibenthic community structure among sites (a two step cluster analysis generates clusters, assigns membership to sample, and ranks variables in order of importance). Analysis at the order rank was selected to enable comparability between the Pacific and Atlantic study sites and examine the relative composition of the benthic communities at a high level.

Throughout this study I test the hypothesis of a positive relationship between communities variables and rugosity using the Spearman correlation test. To investigate the combined strength of multiple seafloor variables I use stepwise multiple regression. The Spearman correlation test was also used to investigate interrelationships among seafloor variables. To control for a potential sampling bias between cruises and test for differences in datasets to be pooled (i.e., 2008/9 Learmonth Bank photographic quadrats and bottom flow video; Table 5.2), I tested for differences between datasets using Kruskal-Wallis tests and Mann-Whitney *U*-tests.

To examine seafloor hydrodynamics as a potential driver of the diversity-rugosity relationship, a subset of photographic quadrats ($n = 65$) was selected to control for other seafloor characteristics and environmental conditions. Photographic quadrats within the subset were all located atop the Learmonth Bank plateau, on bedrock, between 100 and 300 m depth, and within 18.5 km of each other. To test for differences in linear (2-D)

rugosity owing to orientation major axis of the bottom flow, I used a non-parametric paired *t*-test Wilcoxon.

Modelling

To test the strength of using large-scale topographic heterogeneity as a surrogate for local epibenthic diversity I created predictive models for the epibenthic abundance (*N*), richness (*S*), and α-diversity (*H'*) on a scale of 0.25 m^2 (scale of quadrats). The models were built using the analyses of Learmonth Bank photographic quadrats and areal (3-D) rugosity, the Learmonth Bank bathymetry raster dataset, and ArcGIS® version 10.2 (ESRI, 2013; ArcGIS® tools and functions in *italics*).

I generated 1,000 random spatial data points (*Create Random Points* in *Data Management* tools) and processed the set using the automated arc-chord ratio (ACR) rugosity model (Du Preez, 2014 [Chapter 3]). I interpolated the 1,000 rugosity data points into a raster (using the *3D Analyst* function of *Kriging*). The model was built in *Raster calculator* (in *Spatial Analyst*) using rugosity raster and the relationship equations from the diversity-rugosity statistical analyses. A subset of quadrats (n = 109) not included in the relationship analyses was used to test the model. Predicted values for the quadrat locations were extracted from the model (using the *Add Surface Information* in *3D Analyst*) and compared to the quadrat variables to test the accuracy (strength) of the model using the non-parametric paired *t*-test Wilcoxon and Spearman correlation tests (in PASW Statistics 18).

Results

The six study sites

The seafloor

The fine-scale seafloor characteristics varied among the six study sites. The substratum ranged from predominately fine sediment at the majority of sites, to ~50 % coverage at site 3, and almost no sediment on the bedrock pinnacles at site 6 (Fig. 5.4; differences significant at $p < 0.05$, Kruskal-Wallis test). The substratum rugosity ranged from relatively flat at sites 1, 2 and 5 to highly rugose at sites 3, 4 and 6 (Fig. 5.4; differences significant at $p < 0.05$, Kruskal-Wallis test). Generally transects over sediments yielded lower rugosity measurements while transects over bedrock and boulders yielded higher rugosity measurements. At sites 1, 2, and 3 there were strong negative correlations between the rugosity and percent coverage of sediment (site 1: Spearman $p < 0.001$, $r = -0.821$, $n = 16$; site 2: Spearman $p < 0.001$, $r = -0.888$, $n = 16$; site 3: Spearman $p = 0.001$, $r = -0.767$, $n = 16$).

The epibenthic community

Despite the variation in seafloor variables, the most conspicuous difference observed in the video transects from each site was the dominant taxa (based on counts; Fig. 5.5). Site 1 was dominated by small *Stylaster parageus* coral (Class Hydrozoa), *Ophiura sarsii* brittle stars (Class Ophiuroidea), and encrusting sponges (Class Demospongiae). Site 2 was dominated by small *Auletta* sp. sponges (Class Demospongiae), *Stylaster parageus* coral, and encrusting sponges. Site 3 was dominated by *Auletta* sp. and *Mycale bellabellensis* sponges (Class Demospongiae), *Stylaster parageus* coral, and *Florometra serratissima* crinoids (Class Crinoidea). Site 4 was dominated by *Munida quadrispina* squat lobsters (Class Malacostraca), *Acanthascus dawsoni* sponges (Class

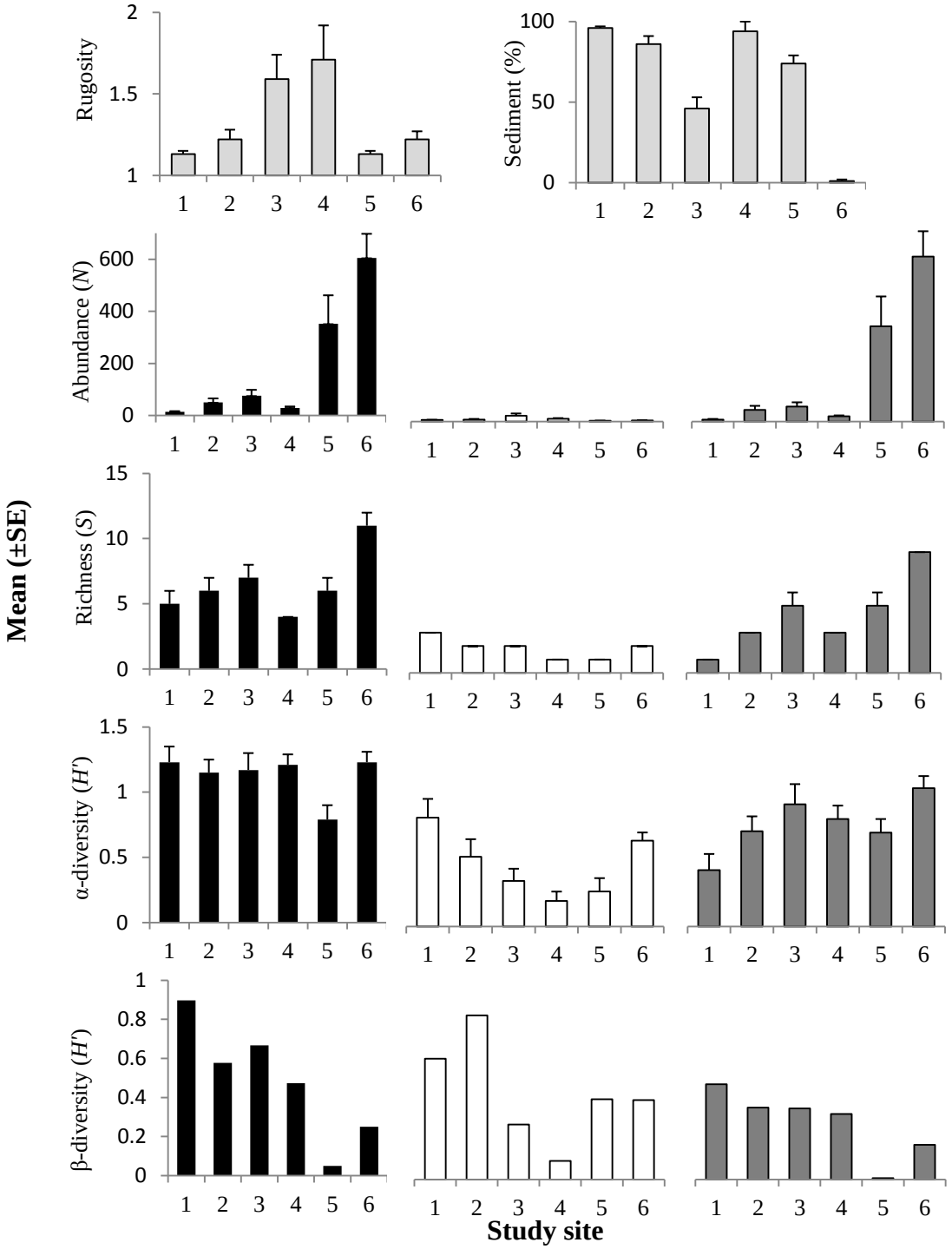

Figure 5.4. Seafloor and epibenthic community variables of the video transects at each site (mean with standard error; n = 16 each for total transect length of 160 m). Sediment refers to fine-grained clastics. Linear (2-D) rugosity is the measure of microtopographic heterogeneity. Community variables are computed from a total of 17,930 epibenthic animals. Community variables are reported three times: all fauna combined (black), mobile fauna only (fauna that can actively move; white), and sessile fauna only (fauna that cannot actively move; grey).

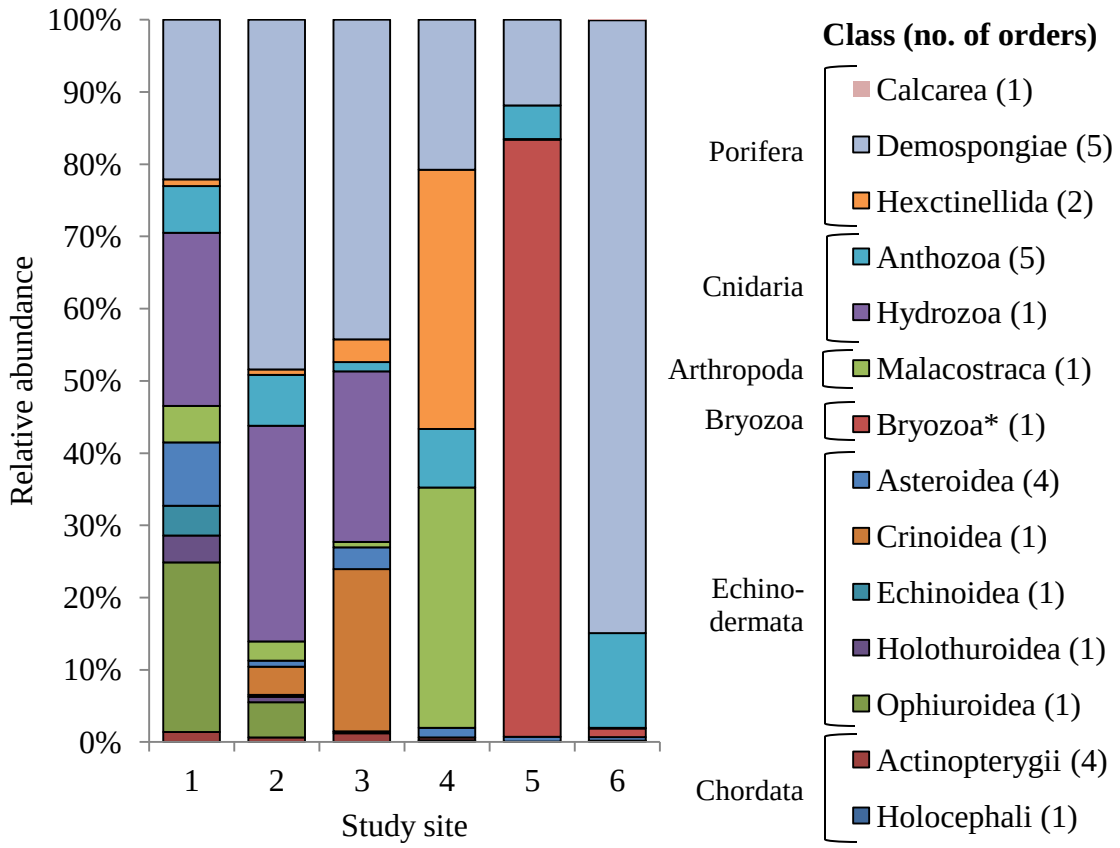

Figure 5.5. Relative abundance of classes at each site (n = 16 video transects each). Data represent a total of 17,930 epibenthic animal records from 960 m^2 of transect surveys. Classes are grouped by phylum. Number of representative orders provided in brackets. *Bryozoans were not identifiable to class.

Hexactinellida), and *Poecillastra tenuilaminaris* sponges (Class Demospongiae). Site 5 was dominated by an unidentified white encrusting Bryozoa, encrusting sponges (Class Demospongiae), and large *Primnoa resedaeformis* coral (Class Anthozoa). Site 5 also had scattered patches of dense *Ophiacantha abyssicola* brittle stars (Class Ophiuroidea) but this taxon was not included in the present study as individuals were too small to resolve and count (< 5 cm). Site 6 was dominated by multiple taxa of encrusting sponges, *Urticina* spp. and *Stomphia* spp. anemones (Class Anthozoa), and *Sebastes marinus* rockfish (Class Actinopterygii). Site 6 also had dense patches of colonial Zoantharia

(Class Anthozoa) but, although the coverage of some patches was extensive, this taxon is colonial and a patch was only counted as one (i.e. not a dominant taxon based on counts).

The 96 video transects (total area of 960 m^2) yielded 17,930 individual organisms from 80 epibenthic species or operational taxonomic units (OTUs) from 29 orders, 14 classes, and 9 phyla (Fig. 5.5). Most taxa were scattered and patchy in distribution but at sites 5 and 6 a few taxa were observed in relatively high densities, for example encrusting Bryozoa on several transects at site 5, and anemones (Class Anthozoa) and *Epizoathus papillosus* zoanthids (Class Anthozoa) at site 6.

The majority of dominant taxa were sessile animals from phyla Porifera and Cnidaria (Fig. 5.5). Mobile animals were less abundant than sessile animals but were still represented at all sites (Fig. 5.5) mostly as Echinodermata and Arthropoda. Of the small proportion of mobile animals from phylum Chordata, the majority were *Sebastes* spp. rockfish. The highest abundance of fishes was recorded at site 3.

The ordinal level community structure varied among some of the study sites. A two step cluster analysis of the 96 transects using the abundances of 29 orders generated 3 distinct clusters with reasonable cluster cohesion and separation (Fig. 5.6). In total 53 % of transects are in cluster 1, 21 % in cluster 2, and 26 % in cluster 3 (Fig. 5.6). The majority of transects from sites 1, 2, 3, and 5 grouped together in cluster 1 .Site 1 transects were the most frequent within cluster 1 while site 5 transects were the closest to an even split between two clusters (clusters 1 and 3). The majority of transects from site 4 grouped alone in cluster 2 while the majority of transects from site 6 grouped alone cluster 3 (Fig. 5.6). The high abundances of *Acanthascus* spp. sponges (order Lyssacinosida), *Poecillastra tenuilaminaris* sponges (order Astrophorida), and *Munida quadrispina* squat

lobsters (order Decapoda) at site 4 were most important in generating cluster 2 (importance values = 1.00, 0.95, and 0.80 respectively). The high abundances of multiple Poecilosclerida encrusting demosponges and *Epizoanthus* spp. (order Zoantharia) were important in generating cluster 3 (importance values = 0.65 and 0.63 respectively). Orders of fish were collectively the least important variables in creating the clusters (cumulative important values << 0.01).

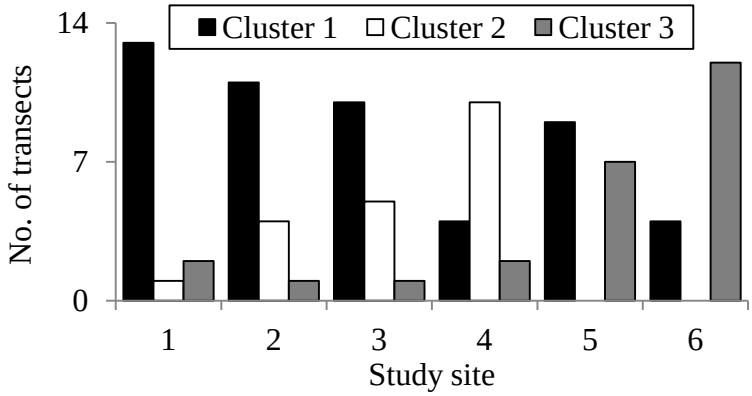

Figure 5.6. Frequency of transects from each site assigned to the three clusters generated by the two step cluster analysis of the ordinal level community structure (29 order-level abundance variables). The majority of transects from sites 1, 2, 3, and 5 are grouped together in cluster 1 (black bar) while the majority of transects from sites 4 and 6 are outliers in clusters 2 (white bar) and 3 (grey bar) respectively.

The differences in community structure among sites are also reflected in the variation of the three variables: average abundance (*N*) of the transects at each site ranged from 10s to 100s of individuals, average richness (*S*) ranged from 4 to 11 taxa, average α-diversity (*H'*) ranged from 0.79 to 1.23, and average β-diversity (*H'*) ranged from 0.05 to 0.90 (Fig. 5.4). Mean community variables of site 5 and 6 were frequently outliers in comparison with the other sites (Fig. 5.4). Among other differences, abundance was higher and β-diversity was lower at sites 5 and 6 and richness was higher at site 6 (Fig. 5.4; differences significant at $p < 0.05$, Kruskal-Wallis test).

Epibenthic diversity and microtopographic heterogeneity

At most study sites there were strong significant correlations between at least one of the community variables and small-scale seafloor variables (Fig. 5.7). When significant, community variables were negatively correlated with sediment cover (Fig. 5.7). Significant correlations between community variables and linear (2-D) rugosity were more frequent and stronger than with sediment (Fig. 5.7). Site 6 was the only site where none of the community variables correlated with rugosity (Fig. 5.7). In general, abundance and richness correlations were stronger than the α-diversity correlations but all significant correlations accounted for > 50 % of variance at each site (Fig. 5.7).

Separate analysis of mobile and sessile fauna indicates that the correlations were largely driven by sessile fauna; however, analyses that included all fauna (both mobile and sessile) yielded stronger correlations than those that only included sessile fauna (Fig. 5.7). Site 3 had the highest abundance of mobile fauna and yielded strong positive correlations between all mobile fauna community variables and rugosity (Fig. 5.7).

Learmonth Bank

The seafloor

The seafloor of the Learmonth Bank region surveyed using the photographic quadrats was highly variable: depth ranged from 74 to 445 m, substrata ranged from fine-grain to hard substrata (inferred from backscattered data and groundtruthed using the photographs), incline ranged from horizontal (0°) to steep (57°), and areal (3-D) rugosity ranged from flat (1.000) to high measures depending on scale and quadrat location (Table 5.3).

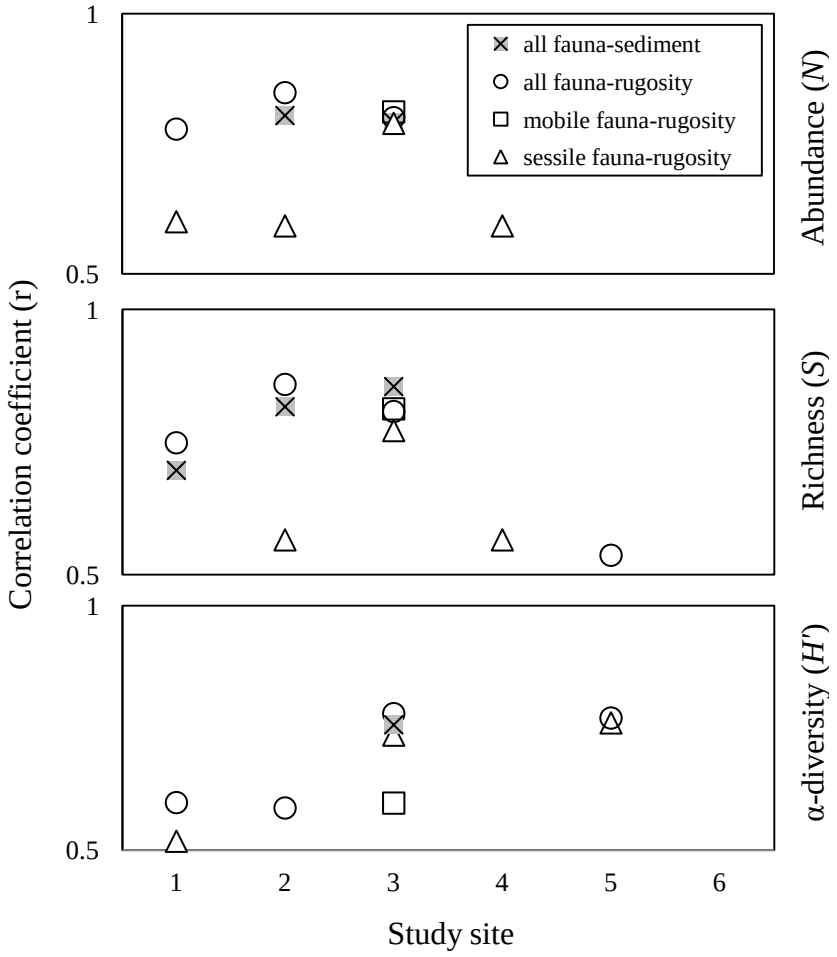

Figure 5.7. Absolute values of the significant correlation coefficients (r) for epibenthic community variables with sediment cover and rugosity. Each site includes 16 transects in which all animals over 5 cm were recorded in video imagery. Correlations significant at Spearman $p < 0.05$ ($n = 16$); negative in grey. Missing data points indicate non-significant correlations ($p > 0.05$) including site 6 where no relationship was significant.

At the smallest scale (25 m^2) seafloor variables were weakly correlated with each other: areal rugosity was positively correlated with backscatter (Spearman $p < 0.001$, $r = 0.302$, $n = 137$) and slope (Spearman $p < 0.001$, $r = 0.346$, $n = 137$), and negatively correlated with depth (Spearman $p = 0.002$, $r = 0.263$, $n = 137$). The four larger scale areal (3-D)

Table 5.3. Large-scale seafloor data from multibeam sonar data at the Learmonth Bank photographic quadrat locations (n ≤ 137). Backscatter is reported as a proxy for substratum hardness (0 = hard, << 0 soft). See Fig. # for linear rugosity data.

	Backscatter (db)	Slope (°)	Depth (m)	Areal (3-D) rugosity				
Scale (m^2)	25	25	25	25	250	2,500	25,000	250,000
n	137	137	137	137	137	137	133	28
max.	-6	57.3	445	1.187	2.784	1.454	1.183	1.079
min.	-69	0.2	74	1.000	1.000	1.000	1.000	1.000

rugosity variables (> 25 m^2) were positively correlated with backscatter (Spearman p = 0.005, 0.001, 0.001, & 0.008; r = 0.246, 0.309, 0.311, & 0.490; n = 137, 137, 133, & 28) and all positively inter-correlated with each other (Spearman correlations between all four scales $p < 0.001$, $n \leq 137$).

The epibenthic community

Analysis of the137 quadrats yielded 789 animal records and recognized 79 species or operational taxonomic units (OTUs) from 29 different orders, 17 classes, and 9 phyla. Of these, 40 % and 9 % could be identified to species or genus only, respectively. The epibenthos composition was highly variable among quadrats, ranging from sparse organisms of a single taxon to dense mats of multiple taxa (Table 5.4). Sessile fauna dominated in abundance, richness, and α-diversity (Table 5.4). The majority of sessile fauna were encrusting sponges and hydroids, anemones, and corals. The majority of mobile fauna were *Pandalus* spp. shrimp, various species of sea stars and *Sebastes* spp. rockfish.

Table 5.4. Summary of epibenthic community data for the Learmonth Bank photographic quadrat survey (n = 137) for all fauna combined (789 records in total), mobile fauna only (203 records), and sessile fauna only (586 records). Each quadrat was 50 by 50 cm with < 1 cm image resolution (for a total area of 34.25 m^2).

	All fauna	Mobile fauna	Sessile fauna
Abundance (% cover)			
max.	71.0	15.0	70.0
min.	0.0	0.0	0.0
$\mu \pm \sigma$	13.2 ±1.4	2.8 ±0.2	10.4 ±1.4
Richness (*S*)			
total	79	28	51
$\mu \pm \sigma$	6 ±0	1 ±0	4 ±0
α-diversity (*H'*)			
$\mu \pm \sigma$	1.22 ±0.06	0.41 ±0.04	1.02 ±0.08

Epibenthic diversity and regional scale topographic heterogeneity

The majority of correlations between quadrat scale community variables and large-scale seafloor variables at all five scales yielded strong significant results (for example see Fig. 5.8). Abundance, richness, and α-diversity were positively correlated with backscatter, slope, and rugosity, and negatively correlated with depth (Fig. 5.9).

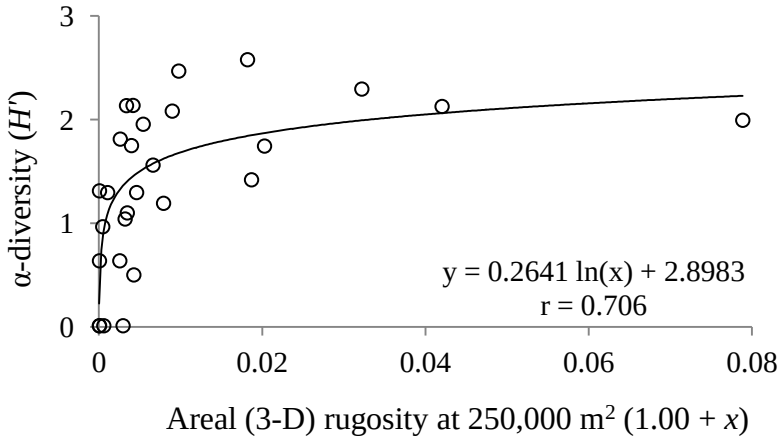

Figure 5.8. The positive correlation between epibenthic α-diversity (*H'*) from the quadrats and seafloor areal (3-D) rugosity measured from multibeam sonar at a scale of 250,000 m^2. The correlation is significant and the line of best-fit is logarithmic (Spearman $p < 0.001$, $r = 0.706$, $n = 28$). The r correlation is data point "1" in Fig. 5.9.

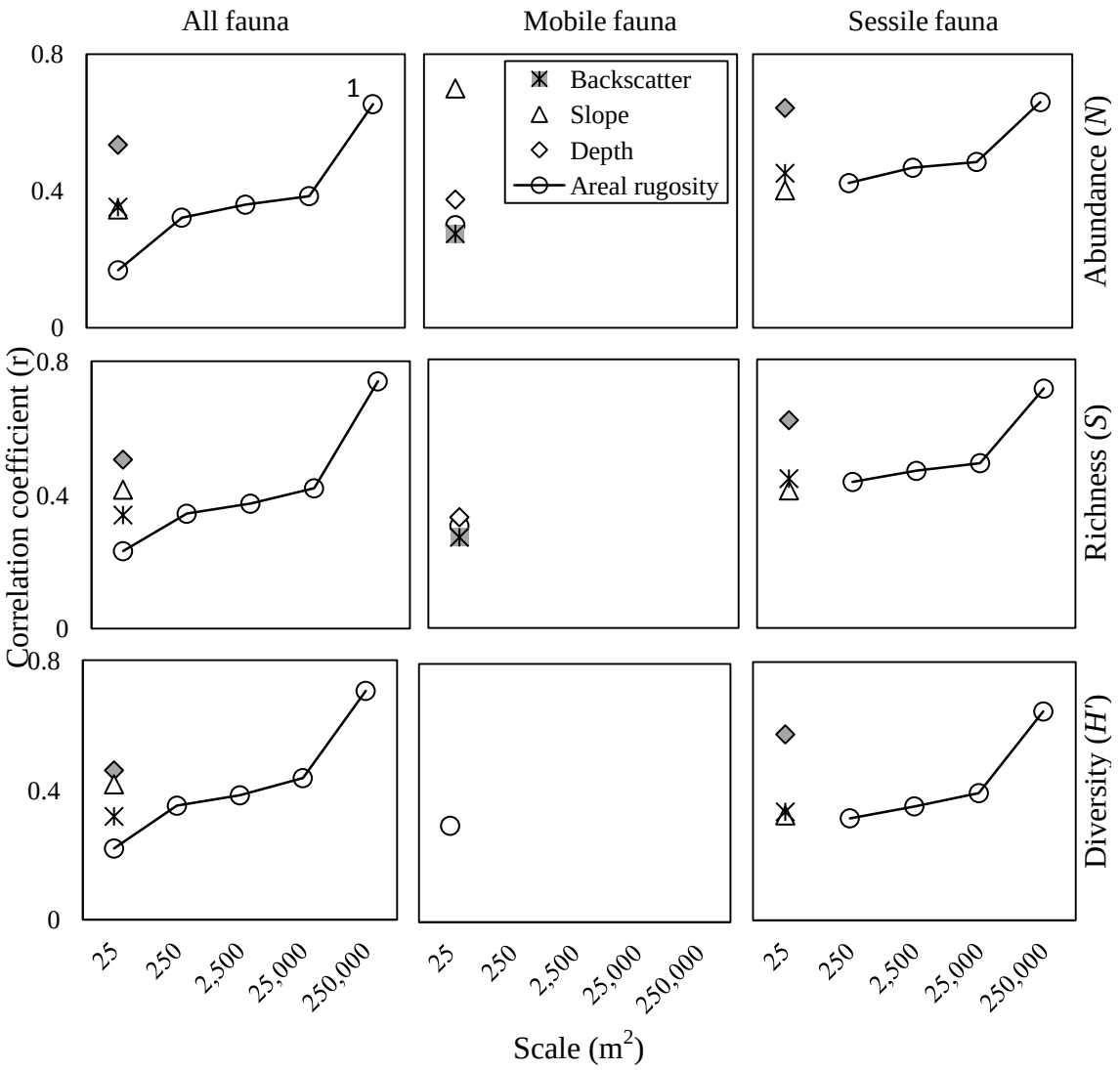

Figure 5.9. Absolute values of the significant correlation coefficients (r) between epibenthic community variables and the seafloor variables backscatter (proxy for hard substrate), slope, depth, and areal (3-D) rugosity. Each scale includes ≤ 137 quadrats (in which all animals > 1 cm were recorded) and seafloor variables (sample size decreased with increasing scale; n = 137, 137, 137, 133, and 28 respectively). Only rugosity was measured at the four larger scales. Correlations significant at Spearman $p < 0.05$; positive for rugosity and slope relationships, negative (shaded grey) for some backscatter and depth relationships. Missing data points indicate non-significant correlations ($p > 0.05$) including the mobile fauna community variables at the four larger scales where no relationship was significant. (in first panel) [1]The correlation coefficient (r) from Fig. 5.8.

In the separate analyses of mobile and sessile fauna, correlations of community variables with both backscatter and depth were opposite for mobile and sessile animal (e.g., the diversity-depth correlations were positive for mobile fauna but negative for sessile fauna; Fig. 5.9). Rugosity was the only large-scale seafloor variable for which correlations for all fauna, mobile fauna animals, and sessile fauna community variables were consistently positive. At the smallest scale (25 m^2) sessile fauna diversity-rugosity correlations were non-significant while at the four larger scales mobile fauna diversity-rugosity correlations were non-significant.

The strength of the diversity-rugosity correlations all increased with increasing scale (Fig. 5.9). The coefficients at any given scale were similar and the increments between scales were nearly the same. The majority of the rugosity correlations were stronger than any of the other large-scale seafloor variable correlations, and at the largest scale (250,000 m^2) rugosity accounted for the most variability (Fig. 5.9). The largest scale rugosity accounted for more variability in the three community variables than combination analyses of all the bathymetric metrics (including the smaller scale rugosity metrics; Stepwise multiple regression tests). The line of best-fit for all diversity-rugosity correlations was logarithmic (for example α-diversity-rugosity dataset see Fig. 5.9).

The direction of bottom flow over Learmonth Bank

The abrupt 180° change in bottom flow direction every six hours strongly suggests there is a reversing (rectilinear) bottom flow around Learmonth Bank driven by the local semidiurnal tidal cycle (Fig. 5.10). From the video analysis of the bottom flow I calculate the major axis of the bidirectional bottom flow over Learmonth Bank is 122° ±5.3° flooding and 302°±5.3° ebbing (mean ± SE; n = 98 measurement; Fig. 5.10).

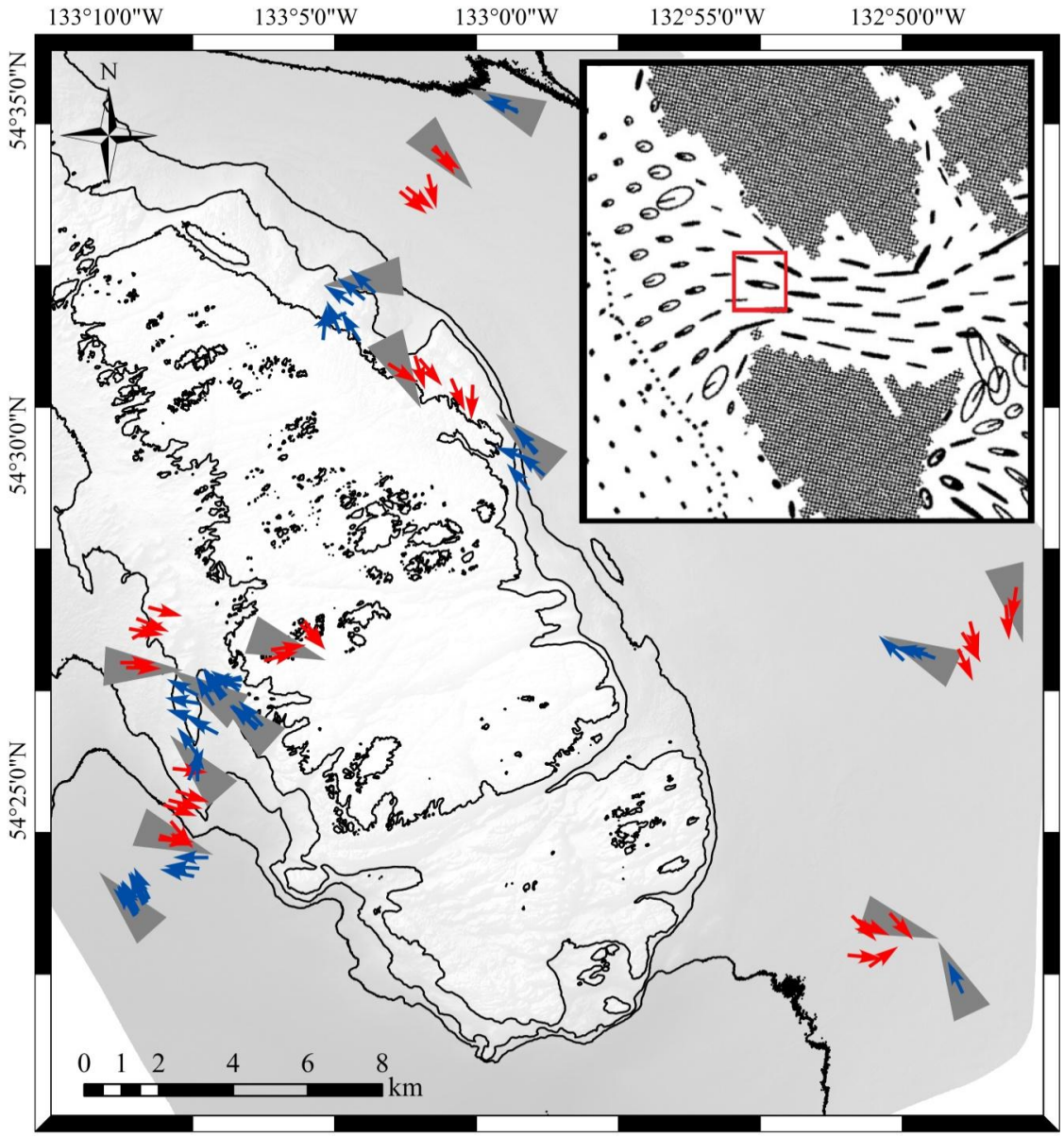

Figure 5.10. The heading and location of the 98 bottom flow direction measurements (small arrows) at Learmonth Bank (from 2008/9 benthic video; Table 5.2). Grey arrows represent the average direction for a 6 hour flood (red arrows) or ebb (blue arrows) period (observations at a site did not extend over the full tidal cycle). Findings support a reversing (rectilinear) bottom flow model with a major axis = 122° (flood) and 302° (ebb). Inset is of depth-average M_2 barotropic current ellipses modelled for Dixon Entrance (map adapted from Cummins and Oey, 1996). Ellipses over Learmonth Bank (red square) predict reversing tidal currents with a major axis of east-southeast to west-northwest (similar to this study).

There was no significant difference in the direction of bottom flows among different regions of the bank: northern, south-western, and south-eastern (Fig. 5.10; Kruskal-Wallis test p = 0.559). There was also no significant difference in the direction of bottom flow measurements among cruises (July 3rd to 6th, 2008; and June 11th, 2009; Mann-Whitney *U*-test p = 0.767).

During the hour leading to a reverse in flow direction ("slack water"; when tidal current velocity is minimal and for a short period is still) the direction of flow would begin to deviate from the major axis. Although the flow was often too weak to measure direction with certainty during this period, it was evident the deviation was not characteristic of a rotary current (tidal influenced) as the flow direction did not consistently move through the compass clockwise or anticlockwise. Rather, it appeared to only move through northern headings on the western side of Learmonth Bank and southern headings of the eastern side.

Epibenthic diversity, hydrodynamics, and topographic heterogeneity

The analysis of bottom flow hydrodynamics as an underlying driver of the diversity-rugosity relationship is based on the premise that the major direction of the bottom flow over Learmonth Bank is 122° (or reciprocal). I assume that at any given location this axis represents the alternating (every 6 hours) direction of the upstream and downstream seafloor rugosity over which the bottom water flows. I further assume that perpendicular to the major axis (32°) represents the most infrequent directions of the upstream and downstream rugosity over which bottom water flows.

There is no significant difference in the linear (2-D) rugosity measurements along parallel and perpendicular transects at any of the four scales (Wilcoxon paired *t*-test p = 0.971, 0.736, 0.376, 0.161; n = 65; Fig. 5.11). Unlike areal (3-D) rugosity, there is no

significant correlation between any linear rugosity measurements and the backscatter variable at the photographic quadrat (multiple Spearman correlation tests $p > 0.05$, $n = 137$).

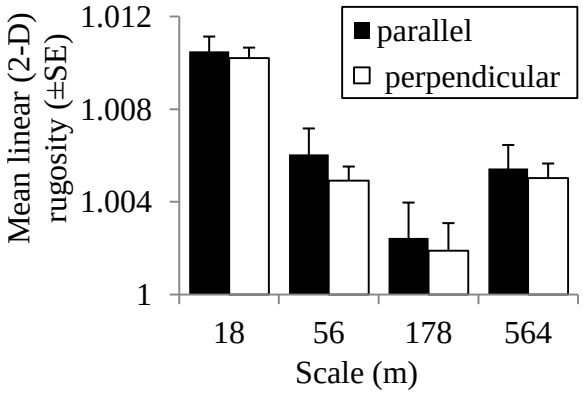

Figure 5.11. Seafloor linear (2-D) rugosity measurements along four scales of transects at each of the Learmonth Bank photographic quadrat (n = 65). Scales were measured twice per quadrat: once parallel (aligned; black bars) and once perpendicular (across; white bars) the major axis of the Learmonth Bank bottom flow direction (122°). There is no significant difference between the paired rugosity measurements at any scale (Wilcoxon paired *t*-test p = 0.971, 0.736, 0.376, 0.161; n = 65).

The coefficients of the parallel diversity-rugosity correlations were more often significant and consistently stronger than the perpendicular diversity-rugosity correlations (Fig. 5.12). This trend was consistent for all fauna, mobile fauna, and sessile fauna community variables (Fig. 5.12). Similar to the correlations with areal (3-D) rugosity (Table 5.8), the strength of the correlations between diversity and linear (2-D) rugosity all increased with increasing scale (Fig. 5.12). Parallel linear rugosity correlations consistently yielded stronger coefficients at all scales than areal rugosity; they were also significantly correlated with mobile fauna variables when areal rugosity was not (Fig. 5.9 and 5.12).

Diversity-rugosity models

I generated predictive models for abundance , richness , and α-diversity at Learmonth Bank (Fig. 5.13) using the relationship equations from correlations between quadrat community variables and the largest scale of areal (3-D) rugosity (250,000 m^2; n = 28; e.g., see Fig. 5.9). The models were tested using the 109 photographic quadrats that were not included in analyses at that scale. The standard deviations between predicted values

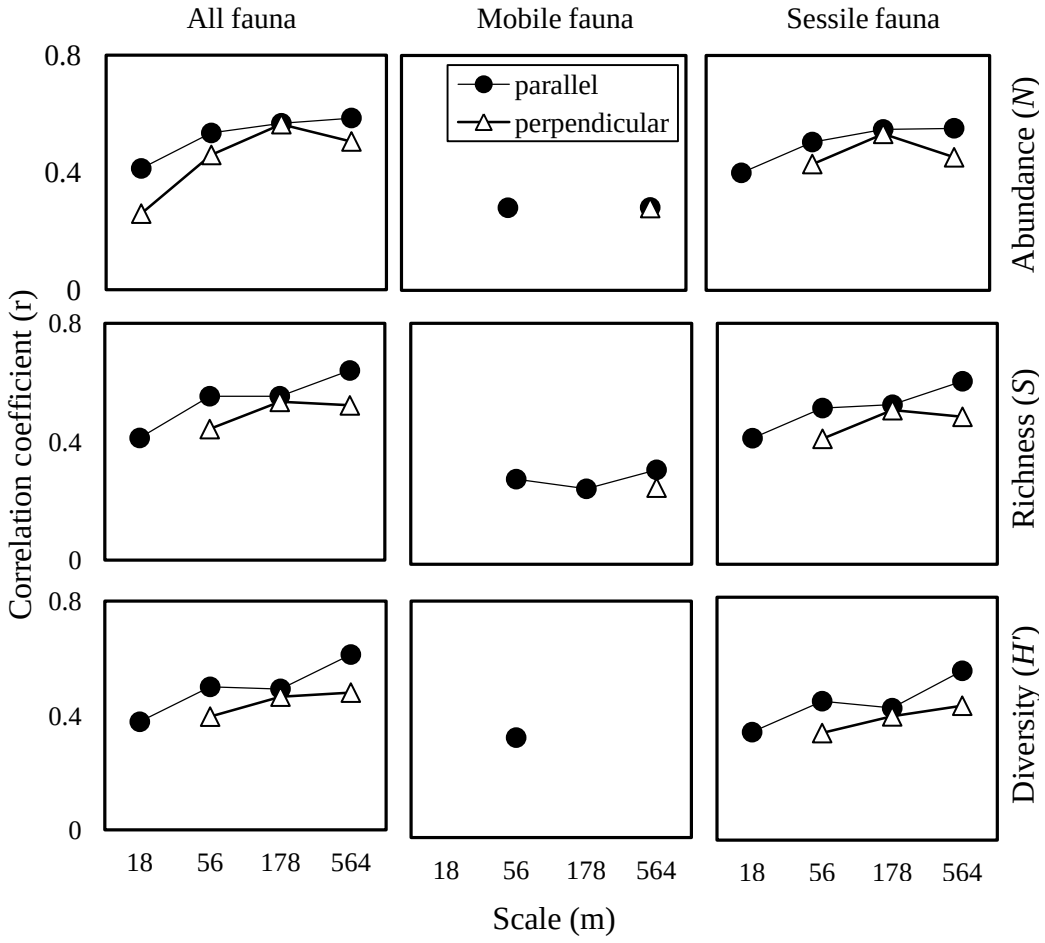

Figure 5.12. Absolute values of the significant correlation coefficients (r) between epibenthic community variables and seafloor linear (2-D) rugosity at four spatial scales (n = 65 quadrats in which all animals ≥ 1 cm were recorded). Scales were measured twice per quadrat: once parallel (aligned; black dots) and once perpendicular (across; white dots) the major axis of the Learmonth Bank bottom flow direction. Correlations significant at Spearman $p < 0.05$ (n = 65); all positive relationships. Missing data points indicate non-significant correlations ($p > 0.05$).

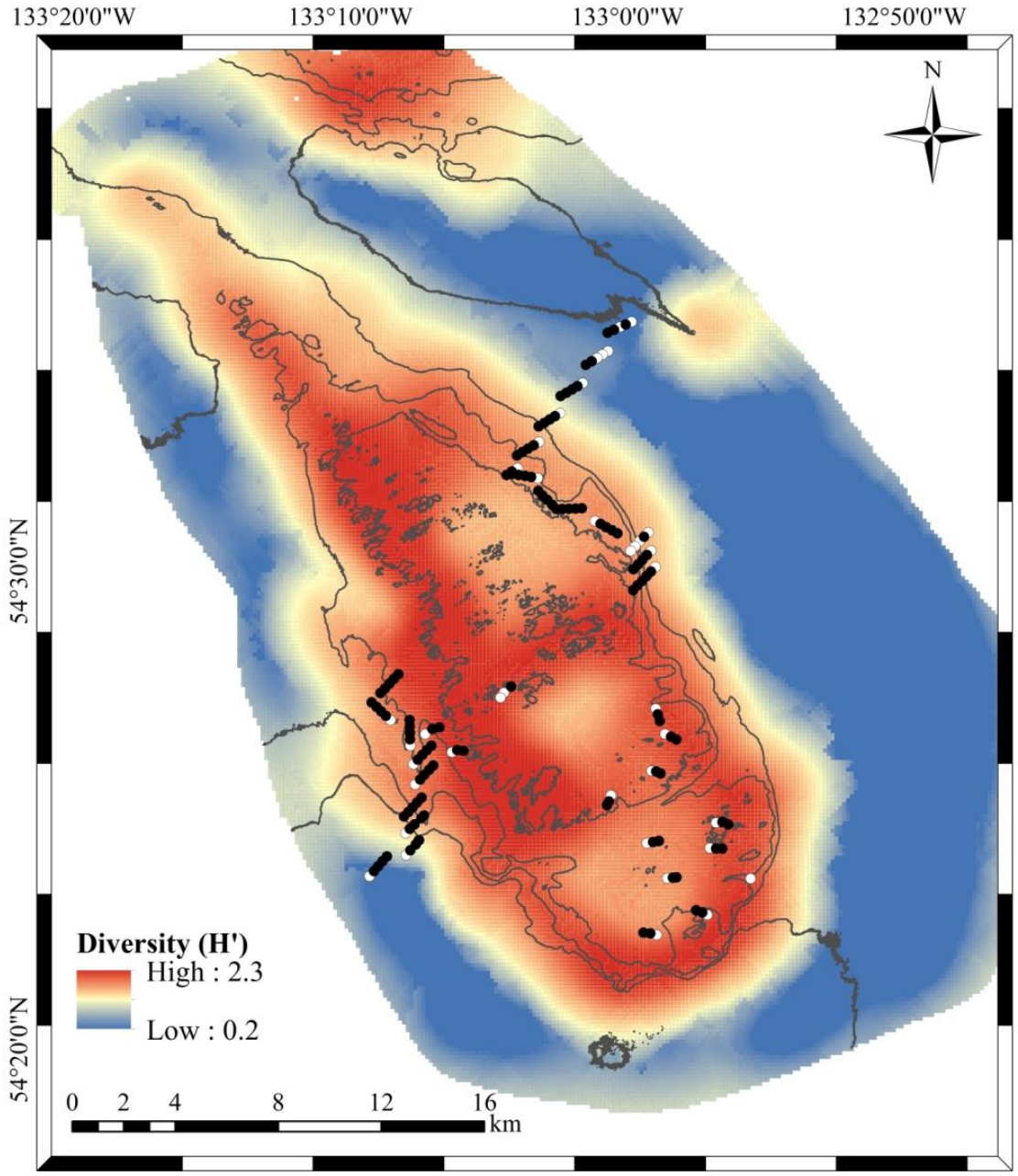

Figure 5.13. Predictive model of epibenthic α-diversity (*H'*) on a scale of 0.25 m^2 at Learmonth Bank. The model was generated using the relationship equations from correlations between quadrat α-diversity measurements from photographic quadrats (white dots) and the largest scale of areal (3-D) rugosity from multibeam sonar (n = 28; Fig. 9). The model was tested using the excluded 109 quadrats (black dots) and there was no significant difference between predicted values and quadrat measurements (Wilcoxon paired *t*-test p =0.064). Models for epibenthic abundance (*N*) and richness (*S*) were also generated. See text for model details and Table 1 for site information.

and quadrat measurements are: ± 8.7 % cover for abundance, 2.6 taxa for richness, and 0.4 for α-diversity. All predicted values are positively correlated with the quadrat community variables (Spearman $p = 0.383$, 0.475, & 0.409; $r < 0.001$ for all three; $n = 109$ for all three respectively). There is a difference between the predicted values and the quadrat measurements for abundance and richness (Wilcoxon $p < 0.001$) but there is no significant difference between the predicted values and the quadrat measurements of α-diversity (Wilcoxon $p = 0.064$; Fig. 5.13).

Discussion

Local benthic diversity and microtopographic heterogeneity

The epibenthic community of each study site varied in taxon composition, abundance, richness, and α- and β-diversity. Yet despite the differences in model systems, the majority of sites yielded similar results for a number of lines of inquiry. At the majority of study sites, epibenthic community variables abundance, richness, and alpha diversity (α-diversity) correlated positively with substratum linear (2-D) rugosity at a local scale of 10 m^2 thereby supporting the hypothesis that local diversity positively relates with microtopographic heterogeneity (Fig. 5.14). Abundance- and richness-rugosity correlations were similar in strength whereas alpha diversity-rugosity correlations were slightly weaker, indicating diversity evenness has a weak or no correlation with rugosity.

In one of the deeper studies on this diversity pattern, Bridge et al. (2010) found substratum rugosity and substratum type to be important factors influencing shelf margin epibenthic macrofauna (< 145 m depth). Although the present study yielded diversity-sediment correlations too, these correlations were weaker and less frequent than the diversity-rugosity correlations and only occurred at the three sites where sediment and rugosity were also

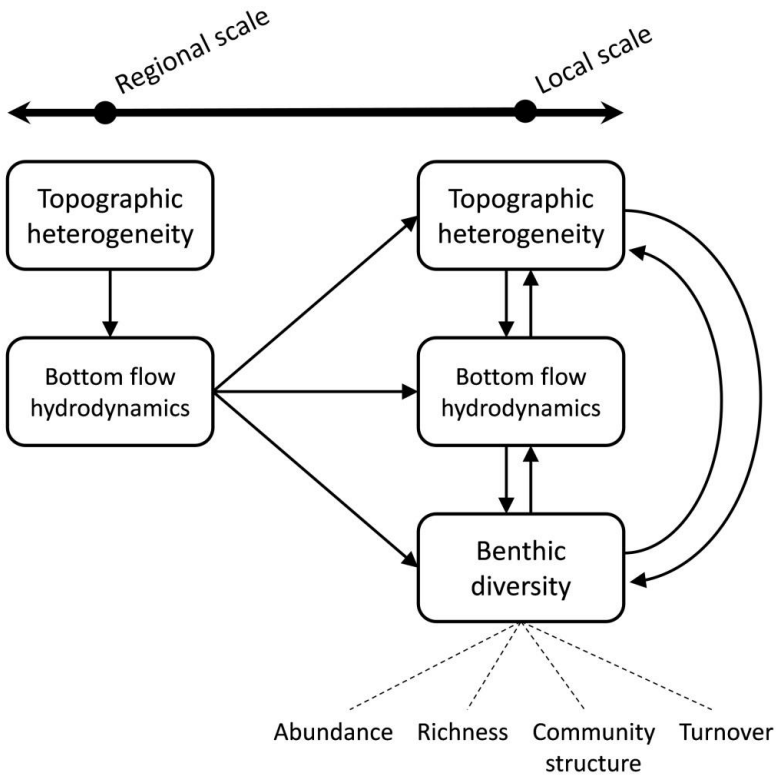

Figure 5.14. Conceptual model of the direct and indirect relationships (black lines) linking local benthic diversity and regional and local scale topographic heterogeneity. Community variables that influence benthic diversity listed (dashed lines).

correlated (sites 1, 2 and 3). This suggests the diversity-sediment correlations were mediated by the same driver as the diversity-rugosity correlations (or are in some way interconnected). Small changes in microtopography close to the seafloor can greatly influence hydrodynamic heterogeneity (owing to the steep flow velocity gradient of the boundary layer), influencing sediment dynamics and local benthic community features (Nowell and Jumars, 1984; Fig. 5.14). Resulting epibenthic patterns may be more detectable in communities dominated by sessile fauna (such as in sites 1, 2 and 3) over those dominated by mobile fauna as sessile fauna are more reliant on bottom hydrodynamics for biological functions. These results suggest the relationship between

local benthic diversity and microtopographic heterogeneity involves hydrodynamic heterogeneity (Fig. 5.14).

Independent analysis of epibenthic mobile and sessile fauna community variables and rugosity identifies sessile fauna as the driver behind the overall correlations at the study sites but two lines of evidence suggest mobile fauna share a similar, albeit weaker, relationship with rugosity. First, correlations with rugosity that included all fauna (mobile and sessile) were stronger than those that only included sessile fauna. Second, the site with the highest mobile fauna abundance (site 3) did yield significant correlations between all mobile variables and rugosity.

Site 6 (pinnacles) and, to a lesser extent, site 4 (a knoll) are the two outlier sites where few or no correlations between community variables and rugosity were observed. Comparing among sites, site 6 has the lowest mean sediment cover and the highest mean abundance and richness. Site 4 is less conspicuous but still differs from site 6 and the other sites with its high mean rugosity and low mean abundance and richness. A clear distinction of these two sites is apparent in the ordinal level community structure analysis, which generated 3 clusters grouping site 6 and site 4 alone. At site 6, a few sessile taxa were extremely dominant and carpeted much of the seafloor. This could be evidence that space was a limiting resource at site 6 and that competitive exclusion by dominant taxa may be influencing local diversity. But this is also true in tropical coral reef habitats (Aronson and Precht, 1995) where the positive relationship between diversity and microtopographic heterogeneity is well established (Fuad, 2010). The "Rock Garden" in Jordan Basin is an abrupt topographic feature in a high energy tidal environment encircled by a cyclonic gyre (Pettigrew et al., 1998). The lack of surficial

sediment and abundance of low-profile taxa are also indicative of a high energy flow environment (further supported by field observations of strong bottom currents). I submit that the regional scale high energy flow regime, combined with the relatively low levels of small-scale rugosity (no local refuge), causes a high frequency of ecological disturbance, which reduces local epibenthic diversity according to the intermediate disturbance hypothesis (Townsend and Scarsbrook, 1997). This theory is consistent with the community structure of a few dominant species and a low beta diversity.

Although not included in the survey, imagery from the cliff base at site 6 depicts a drastically different, much slower, flow regime with higher epibenthic diversity than observed elsewhere at the site: dominant species reduced, more bare substratum, higher taxon richness, and large mobile species and erect biogenic structures. Levin and Sibuet (2012) note that the abrupt topography of canyon cliffs also affects the particulate organic carbon gradient through flow dynamics, which indirectly affects the adjacent benthic diversity (based on studies by McClain and Barry, 2010). These findings and anecdotal observations suggest regional scale topographic heterogeneity and flow regimes effect, and at times may overshadow, the local scale relationship between diversity and microtopographic heterogeneity. This emphasizes the importance of considering multi-scale spatial resolutions when investigating ecological patterns and processes.

The decision to delete sections of the profile where biogenic structures were scanned (to avoid confounding substratum rugosity with the community variables) may explain the weaker relationships at site 4. Biological structures are a source of habitat heterogeneity in deep-sea habitats (Buhl-Mortensen et al., 2010) which my study design did not control for. *Munida quadrispina* squat lobsters and *Acanthascus dawsoni* sponges

were the two most common species at site 4 contributing largely to the site 4 cluster grouping. Squat lobsters associate with erect biogenic structures, such as *A. dawsoni* and many of the other sponge taxa that made up ~60 % of the organisms at site 4 (Cook, 1999; Chu and Leys, 2010). These biogenic structures provided almost all of the relief on the seafloor at site 4, which likely weakens the relationship between epibenthic diversity and substratum specific topographic heterogeneity. It does, however, support the importance of biogenic structures in providing niche diversity.

Local diversity and regional scale topographic heterogeneity

The positive correlations between community variables abundance, richness, and alpha diversity and areal (3-D) rugosity at Learmonth Bank at all scales from 25 to 250,000 m^2 support the hypothesis that regional scale topographic heterogeneity influences local diversity. Results also demonstrate that these community variables increase with greater bottom hardness and slope, and decrease with increasing depth although relationships were weaker and less consistent than relationships with rugosity. Owing to the practicality and efficiency of using large-scale abiotic surrogates to describe marine benthic diversity, many studies have investigated the strength of relationships between multibeam or LiDAR bathymetric derived variables and benthic diversity (reviewed in McArthur et al., 2010). The majority of these studies yield similar results: benthic diversity correlates with multiple bathymetric variables (e.g., substratum hardness, slope, depth and rugosity) and that these bathymetric variables correlate with each other. For example, similar to this study, De Leo et al. (2014) found backscatter (a proxy for substratum hardness) and slope are good predictors of benthic diversity in deep-sea canyons. Schlacher et al. (2007) reported a decline of sponge species richness with depth which is mirrored in the present results of a decline in taxon richness. Walker et al.

(2009) reported fish abundance and species richness appeared to increase with increasing areal rugosity.

Studies that include areal rugosity metrics at scales equal to the bathymetric map resolution are the most common (e.g., Bridge et al., 2011). It is rare for studies to include larger scales. In this study, all three community variable correlations exhibit a similar positive pattern related to an increasing scale of topographic heterogeneity and at the largest scale rugosity was stronger than any other single bathymetric variable or combination of variables. Of the regional scales tested, this identifies 250,000 m^2 (or 0.25 km^2) as the most ecologically relevant to local diversity at a scale of 0.25 m^2.

I identify two changes in the diversity-rugosity correlation among scales tested, thus illustrating the importance of studying ecological questions across multiple scales (Chave, 2013). First, at the smallest scale (25 m^2) mobile fauna appear to drive the correlations while at larger scales (250 to 250,000 m^2) sessile fauna appear to drive the correlations. High rugosity substratum in aquatic environments is said to influence fish and other mobile fauna by providing enhanced feeding opportunities and protection for both juveniles and adults (Yoklavich et al., 2000; Krieger and Wing, 2002; Freese and Wing, 2003; Walker et al., 2009). These findings suggest, within small spatial scales that may reflect a species' home range, mobile fauna actively locate to most suitable habitat. Complex seafloor may function as a natural aggregating device for structure-orientated species (as suggested by Yoklavich et al., 2000). Second, the increasing correlation strength between diversity and rugosity with increasing scale suggests, in combination with the aforementioned change, that the driver behind these correlations operates at or beyond the largest scale tested in this study (> 250,000 m^2) and that it more strongly

influences sessile fauna than mobile fauna. Large-scale bathymetric structure has previously been identified to affect distant sedentary communities indirectly through topographically controlled large-scale flow regimes (Netto et al., 1999; Barros et al., 2004). These scale-dependent findings emphasize the importance of considering multi-scale spatial extents when investigating ecological patterns and processes.

The direction of bottom flow over Learmonth Bank

The data indicate the direction of bottom flow over Learmonth Bank reverses about every six hours in synchrony with the local semidiurnal high and low tides for nearby Langara Island, British Columbia (54°15'N, 133°03'W; DFO, 2008, 2009). This reversal is consistent with rectilinear tidal flow patterns through relatively restricted passages or channels, such as Dixon Entrance (DFO, 2014). Although the bottom flow direction dataset was limited to a few days one year apart, the results of a east-southeast and west-northwest reversing bottom flow are corroborated by current models for the region where current ellipses over Learmonth Bank predict a reversing tidal current with a similar major axis (Greisman, 1986; Crawford and Greisman, 1987; Cummins and Oey, 1997).

A secondary non-tidal current influences the direction of bottom flow over Learmonth Bank during slack water. The pattern of bottom flow direction deviating north on the western side of Learmonth Bank and south on the eastern side is consistent with the permanent anti-cyclonic surface eddy described by Greisman (1986) and Crawford and Greisman (1987). These results suggest the Learmonth Bank eddy extends through the water column to the seafloor and, when the rectilinear tidal current is minimal or zero, drives the direction of bottom flow clockwise around Learmonth Bank.

Bottom flow hydrodynamics as an underlying driver

There was no significant difference between the rugosity measurements parallel to bottom flow and perpendicular to bottom flow, yet correlations between epibenthic community variables and parallel rugosity were stronger at every scale in comparison with perpendicular rugosity. These results strongly indicate bottom flow hydrodynamics as an important link between local epibenthic diversity and regional large-scale topographic heterogeneity (Fig. 5.14). This is the first study to provide multi-scale evidence of the relationship between topography, bottom flow, and benthic communities at regional scales and in a deep-sea habitat. Other evidence of derives mostly from small scale studies in easily accessible habitats (Butman, 1987; Wheatcroft, 1994; Cusson and Bourget, 1997; Guichard and Bourget, 1998; Cardinale et al., 2001; Guichard et al., 2001; Barros et al., 2004) with sparse mention of the relationship at larger scales or in deeper habitats (although examples include, Netto et al., 1999; Bianchi et al., 2011; De Leo et al., 2014).

A featureless bottom experiences lower shear stress and turbulence while bottom flow over and around abrupt protruding features increases shear stress and turbulence in a thinner boundary layer (Nowell and Jumars, 1984). The latter creates differentiated hydrodynamic features such as eddies, recirculation, reduced flow, and apparent randomness (increasing hydrodynamic heterogeneity). In ecology, these hydraulic events are usually considered as small-scale isolated events around sediment or biogenic structures (most commonly in the study of larval recruitment; Nowell and Jumars, 1984). Bottom flow over large-scale topographic features creates similar hydraulic events, but on a much larger scale, that affect bottom flow hydrodynamics downstream thereby establishing environmental gradients and the local flow regimes for extensive distances

before bottom flow returns to an equilibrium (Fig. 5.14; Baumert et al., 2005). Although it is difficult to model and predict flow around irregular objects on the bottom (Nowell and Jumars, 1984), one study of tidal generated flow over a sill detected turbulence more than 6 km away from the topographic feature (Klymak et al., 2004). Environmental gradients that can influence local communities downstream include changes in pressure, dissolved gases, shear stress (suspension and deposition), particulate load, entrained organisms and larvae, and water stratification (Nowell and Jumars, 1984; Baumert et al., 2005). Changes in the local bottom flow regime (including changes to flow velocity, energy, and directionality) affect epibenthic community diversity through larval delivery and recruitment, delivery of oxygen and nutrients (i.e., particulate organic matter flux and bacterial production), feeding opportunities, removal of waste, the passive collection or dispersal of organisms, suspension and deposition of sediment (i.e., available substratum and turbidity), scouring and erosion of sediment and of organisms, and levels of biotic and abiotic disturbance (Fig. 5.14; Butman, 1987; Levin et al., 2001; McArthur et al., 2010; Bianchi et al., 2011; Palardy and Witman, 2011; Elahi et al., 2014). In addition, the synergistic effects caused by interactions between factors may further affect diversity in a system (Levin et al., 2001; McArthur et al., 2010). Considering the general differences in mobile and sessile fauna life histories, bottom flow hydrodynamics as a driver of the diversity-rugosity relationship would likely influence sessile fauna more than mobile fauna, a pattern I consistently observed at all of the scales investigated (25 to 250,000 m^2).

The large-scale turbulence created by bottom water flowing over bathymetric features for a fetch $\geq$ 260 m (half the length of the longest transect tested) appears to have the

largest influence on epibenthic diversity at Learmonth Bank than any of the regional seafloor variables measured. Since turbulence is a function of fluid velocity and surface roughness among other factors (Vogel, 1981), the most ecologically relevant spatial scale for the relationship will likely vary among habitats and communities. Learmonth Bank plateau is a good initial study site for this research as it covers a large area with a narrow range of depth and substratum types, it has relatively high large-scale topographic heterogeneity (erosion and iceberg scour from the region's glaciated periods; Bornhold and Barrie, 1991) and is a high-energy environment. Learmonth Bank experiences tidal rectification, high wave exposure (fetch > 500 km), a freshwater input driven estuarine circulation, and a strong regional wind regime (Crawford and Greisman, 1987; Ballantyne et al., 1996; Zacharias et al., 1998) that generate the fast, reversing flows that we experienced on the bottom.

Topographic heterogeneity as a surrogate from marine benthic diversity

My model using the diversity-rugosity relationship at the largest scale accurately predicted local epibenthic diversity. Although topographic heterogeneity has been suggested as an important factor of marine diversity (Levin et al., 2001) and a potential surrogate for marine benthic diversity (McArthur et al., 2010) this is the first time it has been modeled. There was no significant difference in the alpha diversity predicted by the model using arc-chord ratio (ACR) rugosity spatial analysis of multibeam sonar and the visual measurement annotated from the remotely operated vehicle (ROV) benthic survey. Where management strategies rely on surrogate measures in data-poor areas, mapping benthic diversity using ACR rugosity at large scales should provide good representation.

Recommendations for future work

This paper treats all sessile animals the same and all mobile animals the same but species composition likely affects the community response to topographic heterogeneity. Studies on individual species or more defined groups (e.g., feeding guilds) would provide further tests of specific responses. However, the importance of fluid motion to aquatic organisms is ubiquitous (Vogel, 1981; Nowell and Jumar, 1984) and if hydrodynamics is the indirect link by which topographic heterogeneity influences benthic diversity these patterns detected in this study may prove consistent throughout aquatic benthic communities.

Despite the strong ecological relationships established with the arc-chord ratio (ACR) rugosity index, the correlations are not perfect and including a wider range of environmental metrics (e.g., local primary productivity, temperature, oxygen concentration) would likely enhance the detection of ecological patterns (as demonstrated in Wilson et al., 2007). The inclusion of more topographic heterogeneity metrics alone may be promising. The surface ratio (SR) rugosity index has functioned well in many coral reef studies but on occasion was found to have a relative weak or no relationship with biological variables (McCormick, 1994; Alexander et al., 2009). Rugosity is limited in its ability to differentiate topographic heterogeneity (McCormick, 1994) and, since rugosity is a function of relief and roughness, a single rugosity value can be calculated from a variety of different surface profiles. Certain seafloor features, such as large abrupt depressions, would produce the same rugosity measurement as a mound with the equivalent protruding topography. The effect of a depression and a mound on bottom flow are opposite (i.e., a mound increases both flow velocity and turbulence levels whereas a depression decreases both; Nowell and Jumars, 1984). In work related to flow

hydrodynamics it may be advantageous to calculate ACR rugosity in reference to the plane of the flow (rather than a plane of best fit), such that a positive value represents relief and a negative value represents a depression.

The issue with deleting sections of the seafloor microtopographic profile where biogenic structures were scanned was evident in the weaker relationships at site 4. Examining diversity patterns in response to microtopographic heterogeneity of substratum and biogenic structures would provide a more complete story. Studies may benefit by creating artificial structures with the same topography as biogenic structures (to control for any biological qualities that may influence faunal associations).

It is likely that the diversity pattern related to topographic heterogeneity and hydrodynamics is only positive to a certain threshold, after which it may follow a unimodal relationship. Certain seafloor patterns, such as dense aggregations of abrupt structures, have a high measure of rugosity but both flow velocity and turbulence levels among the features decreases as flow passes above instead of through (Nowell and Jumars, 1984). Although this threshold of feature density may not be common in the deepsea (I detected logarithmic relationships), in shallow aquatic habitats, such as coral reefs and kelp forest, it may be important to consider.

Summary

This study has application for both ecological theory and ocean management. It examined the influence of multiple scales of topographic heterogeneity on local benthic diversity. Findings demonstrate a strong positive relationship across all scales tested. Epibenthic community variables abundance, richness, and alpha diversity positively correlated with both the local microtopographic heterogeneity on a scale of 10 m^2 and with the surrounding regional large-scale topographic heterogeneity on scales of 25 to

250,000 m^2. These results support the hypotheses that at the scale of the organisms high topographic heterogeneity provides more niches and ways of exploiting environmental resources while at regional scales high topographic heterogeneity indirectly influences local diversity through bottom flow hydrodynamics. As such, multi-scale topographic heterogeneity should be included in future developments of diversity theory and conservation and management strategy.

Acknowledgements

I gratefully acknowledge Verena Tunnicliffe for her support, invaluable expertise, and funding. My thanks to colleagues J. Rose and J. Chu for their helpful input. Cruises and remotely operated vehicle (ROV) operations were organized by Jim Boutilier, Peter Lawton, Anna Metaxas, and Paul Macoun and funded by Fisheries and Oceans Canada (DFO), the Canadian Healthy Oceans Network (CHONe), and VENUS subsea observatory. Personnel of the Canadian Scientific Submersible Facility, Pacific Biological Station, ITB Subsea, and the CCGS *John P. Tully*, Vector, and *Hudson* aided field operations. Learmonth Bank multibeam sonar data were collected by the Canadian Hydrographic Service and provided by J. Vaughn Barrie (Geological Survey of Canada). Access to Gulf of Maine video transects was collected by the Discovery Corridor Program and provided by P. Lawton. Research was sponsored by the Natural Sciences and Engineering Research Council (NSERC) through the Canadian Healthy Oceans Network, a university-government partnership dedicated to biodiversity science for the sustainability of Canada's three oceans. Additional support was provided by a University of Victoria Fellowship and a NSERC postgraduate scholarship.

Literature Cited

Alexander, T.J., Barrett, N., Haddon, M., and Edgar, G. 2009. Relationships between mobile macroinvertebrates and reef structure in a temperate marine reserve. Marine Ecology Progress Series **389**: 31-44.

Aronson, R.B., and Precht, W.F. 1995. Landscape patterns of reef coral diversity: a test of the intermediate disturbance hypothesis. Journal of Experimental Marine Biology and Ecology **192**: 1-14.

Ballantyne, V.A., Foreman, M.G.G., Crawford, W.R., Jacques, R. 1996. Three-dimensional model simulations for the north coast of British Columbia. Continental Shelf Research **16**: 1655–1682.

Barrie, J.V., and Conway, K.W. 1999. Late quaternary glaciation and postglacial stratigraphy of the Northern Pacific margin of Canada. Quaternary Research **51**:113–123

Barros, F., Underwood, A.J., and Archambault, P. 2004. The influence of troughs and crests of ripple marks on the structure of subtidal benthic assemblages around rocky reefs. Estuarine, Coastal and Shelf Science **60**: 781-790.

Baumert, H.Z., Simpson, J., and Sündermann, J. 2005. Marine turbulence: theories, observations, and models. Volume 1. Cambridge University Press, Cambridge, U.K.

Beck, M.W. 1998. Comparison of the measurement and effects of habitat structure on gastropods in rocky intertidal and mangrove habitats. Marine Ecology Progress Series **169**: 165-178.

Bianchi, C.N., Dando, P.R. and Morri, C. 2011. Increased diversity of sessile epibenthos at subtidal hydrothermal vents: seven hypotheses based on observations at Milos Island, Aegean Sea. Advances in Oceanography and Limnology **2**: 1-31.

Bornhold, B.D., and Barrie, J.V. 1991. Surficial sediments on the western Canadian continental shelf. Continental Shelf Research **11**: 685-699. doi:10.1016/0278-4343(91)90074-G.

Bridge, T. C. L., Done, T. J., Beaman, R. J., Friedman, A., Williams, S. B., Pizarro, O., and Webster, J.M. 2010. Topography, substratum and benthic macrofaunal relationships on a tropical mesophotic shelf margin, central Great Barrier Reef, Australia. Coral Reefs **30**: 143-153.

Brock, J.C., Wright, C.W., Clayton, T.D., and Nayegandhi, A. 2004. LIDAR optical rugosity of coral reefs in Biscayne National Park, Florida. Coral Reefs **23**: 48-59.

Brock, R., English, E., Kenchington, E., and Tasker, M. 2009. The alphabet soup that protects cold-water corals in the North Atlantic. Marine Ecology Progress Series **397**: 355-360.

Buhl-Mortensen, L., Vanreusel, A., Gooday, A.J., Levin, L.A., Priede, I.G., Buhl-Mortensen, P., Gheerardyn, H., King, N.J., and Raes, M. 2010. Biological structures as a source of habitat heterogeneity and biodiversity on the deep ocean margins. Marine Ecology **31**: 21-50.

Butman, C.A. 1987. Larval settlement of soft-sediment invertebrates - the spatial scales of pattern explained by active habitat selection and the emerging role of hydrodynamical processes. Oceanography and Marine Biology **25**: 113-165.

Cardinale, B.J., Palmer, M.A., and Collins, S.L. 2002. Species diversity enhances ecosystem functioning through interspecific facilitation. Nature **415**: 426-429.

Chave, J. 2013. The problem of pattern and scale in ecology: what have we learned in 20 years? Ecology Letters. doi:10.1111/ele.12048.

Chu, J.W.F., and Leys, S.P. 2010. High resolution mapping of community structure in three glass sponge reefs (Porifera, Hexactinellida). Marine Ecology Progress Series **417**: 97-113.

Conway, K.W., Barrie, J.V., Hill, P.R., Austin, W.C., and Picard, K. 2007. Mapping sensitive benthic habitats in the Strait of Georgia, coastal British Columbia: deep-water sponge and coral reefs. Geological Survey of Canada, Current Research 2007-A2, 6 p.

Cook, S.E. 1999. Ecology of the Hexactinellid sponge reefs on the western Canadian continental shelf. M.Sc. thesis. Department of Biology, University of Victoria, Victoria, B.C.

Corrigan, C., and Kershaw, F. 2008. Working toward high seas marine protected areas: an assessment of progress made and recommendations for collaboration. UNEP-WCMC, Cambridge, UK.

Costanza, R., d'Arge, R., de Groot, R., Farber, S., Grasso, M., Hannon, B., Limburg, K., Naeem, S., O'Neill, R.V., Paruelo, J., Raskin, R.G., Sutton, P., and van den Belt, M. 1997. The value of the world's ecosystem services and natural capital. Nature **387**: 253-260.

Crawford, R. W., and Greisman, P. 1987. Investigation of permanent eddies in Dixon Entrance, British Columbia. Continental Shelf Research **7**: 851-870.

Cummins, P. F., and Oey, L.-Y. 1997. Simulation of barotropic and baroclinic tides off Northern British Columbia. Journal of Physical Oceanography **27**: 762-781.

Cusson, M., and Bourget, E. 1997. Influence of topographic heterogeneity and spatial scales on the structure of the neighbouring intertidal endobenthic macrofaunal community. Marine Ecology Progress Series **150**: 181-193.

Dartnell, P., and Gardner, J. V. 2004. Predicted seafloor facies from multibeam bathymetry and acoustic backscatter data. Photogrammetric Engineering and Remote Sensing **70**(9): 1081-1091.

De Leo, F. C., Vetter, E. W., Smith, C. R., Rowden, A. A., and McGranaghan, M. 2014. Spatial scale-dependent habitat heterogeneity influences submarine canyon macrofaunal abundance and diversity off the Mainand Northwest Hawaiian Islands. Deep Sea Research II **104**: 267-290.

DFO. 2008. Canadian tide and current tables, 2008. Canadian hydrographic service, Hydrographic chart distribution office, Sidney, B.C.

DFO. 2009. Canadian tide and current tables, 2009. Canadian hydrographic service, Hydrographic chart distribution office, Sidney, B.C.

DFO. 2014. Tides, currents, and water levels [online]. Available from http://www.waterlevels.gc.ca/eng [accessed 11 September 2014].

Du Preez, C. 2014. A new arc-chord ratio rugosity index for quantifying three-dimensional landscape structural complexity. Landscape Ecology. doi: 10.1007/s10980-014-0118-8.

_____, and Tunnicliffe, V. 2012. A new video survey method of microtopographic laser scanning (MiLS) to measure small-scale seafloor bottom roughness. Limnology and Oceanography: Methods **10**: 899-909.

Elahi, R., Dwyer, T.R., and Sebens, K.P. 2014. Mesoscale variability in oceanographic retention sets the abiotic stage for subtidal benthic diversity. Marine Ecology Progress Series **498**: 117-132.

ESRI. 2013. ArcGIS Desktop 10.2. Redlands, California: Environmental Systems Resource Institute.

Freese, J.L., and Wing, B.L. 2003. Juvenile red rockfish, *Sebastes* sp., associations with sponges in the Gulf of Alaska. Marine Fisheries Review **65**(3): 38-42.

Fuad, M.A.Z. 2010. Coral reef rugosity and coral biodiversity. M.Sc. thesis, Department of Geo-information Science and Earth Observation, International Institute for Geo-information Science and Earth Observation, Enshede, the Netherlands.

Gratwicke, B., and Speight, M. R. 2005. The relationship between fish species richness, abundance and habitat complexity in a range of shallow tropical marine habitats. Journal of Fish Biology **66**: 650-667.

Gray, D.H. 1997. Canada's unresolved maritime boundaries. Boundary and Security Bulletin **5**(3): 61-71.

Greisman, P. 1986. Surface circulation in Dixon Entrance: results from Lagrangian and Eulerian measurements. Institute of Ocean Science, Sidney, B,C.

Guichard, F., and Bourget, E. 1998. Topographic heterogeneity, hydrodynamics and benthic community structure: a scale-dependent cascade. Marine Ecology Progress Series **171**: 59-70.

_____, _____, and Robert, J.-L. 2001. Scaling the influence of topographic heterogeneity on intertidal benthic communities: alternate trajectories mediated by hydrodynamics and shading. Marine Ecology Progress Series **217**: 27-41.

Kelly, N.E., Shea, E.K., Metaxas, A., Haedrich, R.L., and Auster, P.J. 2010 Biodiversity of the deep-sea continental margin bordering the Gulf of Maine (NW Atlantic): Relationships among sub-regions and to shelf systems. PLOS ONE **5**(11): e13832.

Kenchington, E.L., and Vickers, J. 2007. Benthic communities in the discovery corridor-Preliminary results from the 2005 Discovery cruise. *In* Challenges in environmental management in the Bay of Fundy-Gulf of Maine. Proceedings of the 7th Bay of Fundy Science Workshop, St. Andrews, N.B., 24-27 October 2006. *Edited by* G.W. Pohle, P.G. Wells, and S.J. Rolston. Bay of Fundy Ecosystem Partnership Technical Report No. 3. Bay of Fundy Ecosystem Partnership, Wolfville, N.S. pp. 30-31.

Kloser, R. J., Penrose, J. D., and Butler, A. J. 2010. Multi-beam backscatter measurements used to infer seabed habitats. Continental Shelf Research **30**(16): 1772-1782.

Klymak, J.M., and Gregg, M.C. 2004. Tidally generated turbulence over the Knight Inlet Sill. American Meteorological Society **34**: 1135-1151.

Krieger, K. J., and B. L. Wing. 2002. Megafauna associations with deepwater corals (*Primnoa* spp.) in the Gulf of Alaska. Hydrobiologia 47:83-90 [doi:10.1023/A:1016597119297].

_____, Etter, R.J., Rex, M.A., Gooday, A.J., Smith, C.R., Pineda, J., Stuart, C.T., Hessler, R.R., and Pawson, D. 2001. Environmental influences on regional deep-sea species diversity. Annual Review of Ecology and Systematics **32**: 51-93.

_____, and Sibuet, M. 2012. Understanding continental margin biodiversity: a new imperative. Annual Review of Marine Science **4**: 79-112.

Magurran, A.E. 2004. Measuring biological diversity. Blackwell Science Ltd., Oxford.

McArthur, M.A., Brooke, B.P., Przeslawski, R., Ryan, D.A., Lucieer, V.L., Nichol, S., McCallum, A.W., Mellin, C., Cresswell, I.D., and Radke, L.C. 2010. On the use of abiotic surrogates to describe marine benthic biodiversity. Estuarine, Coastal and Shelf Science **88**: 21-32.

McClain, C.R., and Barry, J.P. 2010. Habitat heterogeneity, disturbance, and productivity work in concert to regulate biodiversity in deep submarine canyons. Ecology **91**: 964–76.

McCormick, M.I. 1994. Comparison of field methods for measuring surface topography and their associations with a tropical reef fish assemblage. Marine Ecology Progress Series **112**: 87-96.

Milner, P. R. 2008. Final field report, CCGS Vector, North Coast and Queen Charlotte Island Surveys, July 25 – September 8, 2008. Institute of Ocean Sciences, Sidney, B.C.

Netto, S.A., Attrill, M.J., and Warwick, R.M. 1999. Sublittoral meiofauna and macrofauna of Rocas Atoll (NE Brazil): indirect evidence of a topographically controlled front. Marine Ecology Progress Series. **179**: 175-186.

Nowell, A.R.M., and Jumars, P.A. 1982. Flow environments of aquatic benthos. Annual Review of Ecology and Systematics **15**: 303-328.

Palardy, J.E., and Witman, J.D. 2011. Water flow drives biodiversity by mediating rarity in marine benthic communities. Ecology Letters **14**: 63-68. doi: 10.1111/j.1461-0248.2010.01555.x.

Pettigrew, N., Townsend, D., Xue, H., Wallinga, J., Brickley, P., and Hetland, R. 1998. Observations of the Eastern Maine Coastal Current and its offshore extensions in 1994. Journal of Geophysical Research **103**: 623-639.

Purkis, S.J., Graham, N.A.J., and Riegl, B.M. 2008. Predictability of reef fish diversity and abundance using remote sensing data in Diego Garcia (Chagos Archipelgao). Coral Reefs **27**: 167-178. doi 10.1007/s00338-007-0306-y.

Risk, M.J. 1972. Fish diversity on a coral reef in the Virgin Islands. Atoll Research Bulletin **193**: 1-6.

Schlacher, T. A., Schlacher-Hoenlinger, M. A., Williams, A., Althaus, F., Hooper, J. N. A., and Kloser, R. 2007. Richness and distribution of sponge megabenthos in continental margin canyons off southeastern Australia. Marine Ecology Progress Series **340**: 73-88.

Sinclair, A.F., Conway, K.W., and Crawford, W.R. 2005. Associations between bathymetric, geologic and oceanographic features and the distribution of the British Columbia bottom trawl fishery. ICES CM 2005/L:25: 1-31.

Townsend, C.R., and Scarsbrook, M.R. 1997. The intermediate disturbance hypothesis, refugia, and biodiversity in streams. Limnology and Oceanography **42**(5): 938-949.

Vogel, S. 1981. Life in moving fluids: the physical biology of flow. Willard Grant Press, Boston, Massachusetts.

Walker, B.K., Jordan, L.K.B., and Spieler, R.E. 2009. Relationship of reef fish assemblages and topographic complexity on southeastern Florida coral reef habitats. Journal of Coastal Research **53**: 39-48.

Wheatcroft, R. A. 1994. Temporal variation in bed configuration and one-dimensional bottom roughness at the mid-shelf STRESS site. Continental Shelf Research **14**(10/11): 1167-1190.

Wilson, M. F. J., O'Connell, B., Brown, C., Guinan, H. C., and Grehan, A. J. 2007. Multiscale terrain analysis of multibeam bathymetry data for habitat mapping on the continental slope. Marine Geodesy **30**: 3-35.

Worm, B., Barbier, E.B., Beaumont, N., Duffy, J.E., Folke, C., Halpern, B.S., Jackson, J.B.C., Lotze, H.K., Micheli, F., Palumbi, S.R., Sala, E., Selkoe, K.A., Stachowicz, J.J., and Watson, R. 2006. Impacts of biodiversity loss on ocean ecosystem services. Science **314**: 787-790.

Wu, J. 2004. Effects of changing scale on landscape pattern analysis: scaling relations. Landscape Ecology **19**:125-138.

Yoklavich, M.M., Greene, H.G., Sullivan, D.E., Lea, R.N., and Love, M.S. 2000. Habitat associations of deep-water rockfishes in a submarine canyon: an example of a natural refuge. Fishery Bulletin **98**: 625–641

Zacharias, M.A., Howes, D.E., Harper, J.R., Wainwright, P. 1998. The British Columbia marine ecosystem classification: rationale, development and verification. Coastal Management **26**: 105–124

Chapter 6: Conclusion

Introduction

As anthropogenic activities continue to impact our oceans, establishing robust ecological patterns related to marine diversity is becoming increasingly valuable to conservation and management efforts, especially in data-limited environments such as the deepsea. Resolving diversity patterns and their underlying drivers also has application for ecological theory. My thesis focused on the hypothesis of a positive relationship between deep-sea benthic diversity and topographic heterogeneity. Using new methods I developed, I addressed this relationship in several different deep-sea settings (e.g. a basin, a bank, pinnacles), with different assemblages of benthic animals (Scorpaenidae fishes and different size classes of epibenthic assemblages e.g., fauna > 0.5 cm and fauna > 5 cm), and different sources and scales of topographic heterogeneity (biogenic and sediment; centimeter- to kilometer-scale). See Fig. 6.1 for summary illustration of my thesis chapters.

Major outcomes

1. As presented in Chapter 2, my new microtopographic laser scanning (MiLS) method can profile the deep seafloor at a resolution of ~1-2 cm with high accuracy and precision (Fig. 6.1). Used in combination with the rugosity model (Appendix B), MiLS can measure the topographic heterogeneity of fragile and deep-sea habitats in a way that permits comparisons with different habitats. Additional advantages of MiLS over current methods include: i) the additional equipment required is minimal

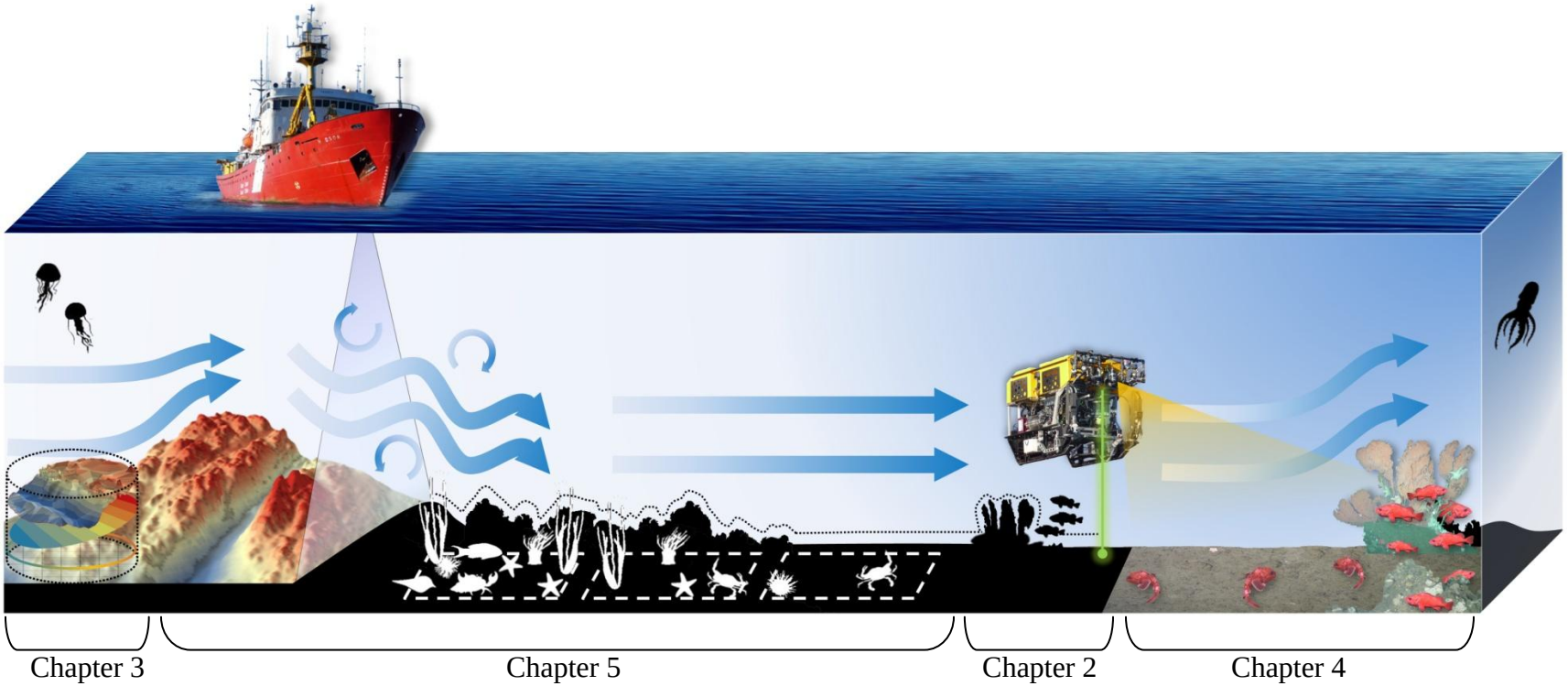

Figure 6.1. Summary illustration of my thesis on deep-sea benthic diversity and multi-scale topographic heterogeneity. I developed a new method (MiLS) to profile microtopography while surveying the benthos using a remotely operated vehicle (Chapter 2) and a new method to measure 3-D topographic heterogeneity (as rugosity) from ship-based multibeam bathymetry (Chapter 3). Using these methods I resolved positive relationships between Scorpaenidae fish diversity and deep-sea corals and sponges (Chapter 2 and 4), and local epibenthic diversity and multiple scales of substratum topographic heterogeneity (Chapter 5). I also demonstrated substratum characteristics (e.g., rugosity and composition) to be useful surrogates for epibenthic diversity (Chapter 5) and deep-sea coral and sponge habitats (Appendix F). Studies consistently identified bottom flow hydrodynamics (arrows) as an important underlying driver of these relationships.

(a video camera and optical laser), ii) the video recording captures imagery that can be annotated and used to relate visual small-scale phenomena with microtopography (e.g., substratum composition or fauna distribution), iii) MiLS is adaptable for submarine and subaerial use, iv) the protocol is off-bottom and noninvasive , and v) to facilitate use there is a working rugosity model available for download. MiLS was a major outcome of my thesis and enabled my research presented in Chapter 5.

2. As presented in Chapter 3, I developed a new arc-chord ratio (ACR) rugosity index as a measure of three-dimensional topographic heterogeneity (Fig. 6.1). The ACR rugosity index is simple, accurate, extremely versatile yet consistent, and, likely its most important feature, it decouples rugosity from slope at the scale of the surface. To facilitate use I describe the ACR method in general, I detail the three most common analyses, and I provide multiple ArcGIS® resources in supplementary material including automated geoprocessing model tools (Appendix C and D). In my major research chapter (Chapter 5) I successfully detect ecological patterns related to topographic heterogeneity using ACR rugosity.
3. Studies reported in Chapter 2 and 4 provide new information on the ecological relevance of deep-sea corals and sponges. Rockfish *Sebastes* spp. abundance and richness have positive relationships with the abundance of *Primnoa pacifica* corals and tall sponges. Rockfish species associate with higher seafloor rugosity non-randomly and select for deep-sea corals and sponges over inert substrata alone (Fig. 6.1). Data from both studies suggest this occurs because the abrupt topographic relief of tall biogenic structures alters the bottom flow regime providing refuge and an energy-efficient means for rockfish *Sebastes* spp. to hold station; Auster (2007) also

proposes this role for corals. This work provides new evidence of the ecological relevance of deep-sea corals and indicates that degradation of biogenic structures is a long-term detriment to benthic rockfishes, information pertinent to the management of fish stocks and these vulnerable marine ecosystems (DFO, 2010b).

4. Chapter 4 also documents the distribution of commercial shortspine thornyhead *Sebastolobus alascanus* and commercial and species at risk rockfish *Sebastes* spp. (COSEWIC, 2007, 2008; DFO, 2010a) and it provides new evidence of the negative impacts of trawling on red tree coral *P. pacifica* populations and associated species (Fig. 6.1).
5. In Appendix F we (Neves, Edinger, and I) test the application of a classification mapping method that uses multibeam sonar and ROV observations to map biotopes and we determined substratum type to be a good surrogate for coral- and sponge-dominated habitats (Fig. 6.1). The habitat map produced provides new information on the distribution of corals and sponges at Learmonth Bank, which can be used to guide management of vulnerable marine ecosystems at this location.
6. In my largest research chapter (Chapter 5), I provide strong support for the ecological hypothesis that diversity increases with increasing topographic heterogeneity (Fig. 6.1). I demonstrate positive relationships between local epibenthic diversity and multiple scales of substratum topographic heterogeneity (10 to 250,000 m^2) in several distinctly different deep-sea environments (Fig. 6.1). While the work affirms that local diversity correlates well with local topographic heterogeneity, perhaps most importantly the work shows that local diversity may be more strongly influenced by surrounding landscape-scale topography than by organism-scale microtopography.

Using the largest scale relationship analysis I generated a model that accurately predicted local epibenthic diversity and in doing so demonstrated topographic heterogeneity (measured as ACR rugosity) to be a useful surrogate for marine benthic diversity. The study data strongly suggests bottom flow hydrodynamics is an important underlying driver of the diversity pattern. At small scales, high topographic heterogeneity likely increases diversity by increasing the number of available niches (including hydrodynamic gradients) while at large scales, high topographic heterogeneity increases local diversity less directly through distant hydraulic events that alter bottom flow hydrodynamics. This work has application for ocean conservation, management, as well as for general ecological theory; it also emphasizes the importance of considering multi-scale spatial resolutions (grain sizes) and extents (areas) when investigating ecological patterns and processes.

Summary

Work on different model systems in several geographically distant deep-sea environments strongly supports the ecological hypothesis of a positive relationship between diversity and topographic heterogeneity at local scales. This diversity pattern is evident in the various benthic assemblages examined, which include Scorpaenidae fish, corals, sponges, and other mobile and sessile epibenthic animals. Findings on Learmonth Bank indicate that local epibenthic diversity is also positively related to the surrounding regional topographic heterogeneity on scales of 25 to 250,000 m^2.

Independent of the model system, there is evidence of a scale hierarchy, where larger scales of topographic features have a stronger influence than smaller scales. This was

exhibited among local scales (e.g., the influence of tall biogenic structures was greater than small biogenic structures) and regional scales (e.g., correlation strength between diversity and topographic heterogeneity increases with increasing scale). Bottom flow hydrodynamics is consistently implicated as an important underlying driver of the relationship. This hypothesis is corroborated by multiple lines of evidence including results that sessile fauna diversity are more strongly influenced by topographic heterogeneity than mobile fauna diversity (as sessile fauna tend to be more reliant on hydrodynamic conditions).

This work has application for ocean conservation identifying important features that enhance diversity (e.g., deep-sea corals and sponges at local scales and complex bathymetric features at regional scales). Where management strategies rely on surrogate measures in data-poor areas, mapping benthic diversity using arc-chord ratio rugosity will provide good representation. Restoration projects can benefit by optimizing multi-scale topographic heterogeneity to promote diversity.

Recommendations for future work

The microtopographic laser scanning (MiLS) and arc-chord ratio (ACR) rugosity methods I developed address problems of current methods and permit comparison among ecosystems. If used in future work for the detection and investigation of ecological patterns, they will support establishing broader generalizations that can lead to better scientific information for conservation and management initiatives.

Investigating diversity patterns in relation to large-scale topographic-influenced hydrodynamics presents an interesting area for new research. Research that incorporates

spatial analyses of local epibenthic communities in relation to large-scale seafloor topographic features and large-scale bottom hydrodynamics (e.g., models of boundary layer thickness and turbulence) would provide further testing of the how local diversity relates to surrounding large-scale topographic heterogeneity.

Another avenue of research would be to manipulate seafloor topographic heterogeneity using abiotic structures, similar to Guichard et al. (2001), but design the structure to mimic the topographic heterogeneity of biogenic structures (e.g., corals or sponges). This work would provide further tests for the characteristics of biogenic structures with which fauna associate (e.g., abiotic or biotic qualities). This has application in protection of vulnerable biogenic structures (DFO, 2010b) as well as artificial reef optimization (Spieler et al., 2001; Sherman et al., 2002).

ACR rugosity is a good surrogate for epibenthic diversity at Learmonth Bank. Replicate studies assessing its application in a variety of environments would further validate using ACR rugosity as a tool to estimate baseline information in data-poor areas.

Literature cited

Auster, P.J. 2007. Linking deepwater corals and fish populations. *In* Conservation and adaptive management of seamount and deep-sea coral ecosystems. *Edited by* R.Y. George, and S.D. Cairns. Rosensteil School of Marine and Atmospheric Science, Miami, FL, p 93–99

COSEWIC (Committee on the Status of Endangered Wildlife in Canada). 2007. COSEWIC assessment and status report on the Rougheye Rockfish *Sebastes* sp. type I and *Sebastes* sp. type II in Canada. COSEWIC, Ottawa. Available at: http://dsp-psd.pwgsc.gc.ca/collection_2007/ec/CW69-14-526-2007E.pdf

COSEWIC (Committee on the Status of Endangered Wildlife in Canada). 2008. COSEWIC assessment and status report on the Yelloweye Rockfish *Sebastes ruberrimus*, Pacific Ocean inside water population and Pacific Ocean outside waters population, in Canada. COSEWIC, Ottawa. Available at: http://www.sararegistry.gc.ca/virtual_sara/files/cosewic/sr_yelloweye_rockfish_0809_e.pdf

DFO (Fisheries and Oceans Canada). 2010a. Pacific region integrated fisheries management plan: groundfish. Available at: http://www-ops2.pac.dfo-mpo.gc.ca/xnet/content/MPLANS/plans11/2011%20 Groundfish%20IFMP_ Final_Complete.pdf

DFO (Fisheries and Oceans Canada). 2010b. National Science Advisory Process concerning corals, sponges, and hydrothermal vents in Canadian waters; March 9–12, 2010. DFO Canadian Science Advisory Secretariat Proceedings Series 2010/027.

Guichard, F., Bourget, E., and Robert, J.-L. 2001. Scaling the influence of topographic heterogeneity on intertidal benthic communities: alternate trajectories mediated by hydrodynamics and shading. Marine Ecology Progress Series **217**: 27-41.

Sherman, R.L., Gilliam, D.S., and Spieler, R.E. 2002. Artificial reef design: void space, complexity, and attractants. ICES Journal of Marine Science **59**: S196-S200.

Spieler, R.E., Gilliam, D.S., and Sherman, R.L. 2001. Artificial substrate and coral reef restoration: what do we need to know to know what we need. Bulletin of Marine Science **69**(2): 1013-1030.

Appendix A: List of additional publications

The following are additional publications I co-authored while in my PhD programme (Table A.1). All three have been submitted as either a chapter of or as an entire *Department of Fisheries and Oceans Technical Report*.

Table A.1. Additional publications not included in my PhD dissertation.

Publications
Du Preez, C., Davies, S.C., Clarke, E., Fruh, E.L, and Curtis, J. *In review.* Cobb Seamount species inventory. Canadian Technical Report of Fisheries and Aquatic Sciences 2960: XX + XX p.
Edinger, E., **Du Preez**, **C.**, Leys, S., Chu, J.W.F., and Lacharitè, M. *In review.* Cold-water corals and sponges and their habitats in Canadian waters. *In* Recent research studies on seabed structure & benthic biodiversity relationships in Canadian Marine habitats. *Edited by* P. Lawton and E. Edinger. Canadian Technical Report of Fisheries and Aquatic Sciences XXXX: XX + XX p.
Tunnicliffe, V., and **Du Preez, C.** *In review.* Notable offshore environments: hydrothermal vents & seamounts. *In* Recent research studies on seabed structure & benthic biodiversity relationships in Canadian Marine habitats. *Edited by* P. Lawton and E. Edinger. Canadian Technical Report of Fisheries and Aquatic Sciences XXXX: XX + XX p.

The first publication is a comprehensive (>120 pages) species inventory for Cobb Seamount (seamount within international waters of the Northeast Pacific Ocean). In 2012, I was aboard and assisting with a Fisheries and Oceans Canada (DFO) led an expedition (DFO Science Cruise Number PAC 2012-43) with the National Oceanic and Atmospheric Administration (NOAA) to survey the benthic communities of Cobb Seamount. The main objectives were to identify the type and location of vulnerable marine ecosystem (VME) components and document evidence of fishery interactions, to inform international fishing agreements. In this report we summarise observations of species occurrences made from the seafloor imagery collected during the 2012 cruise.

The report was a collaborative effort coordinated by Dr. Janelle Curtis at the DFO Pacific Biological Station (PBS). My contribution to this publication included field work, video and still imagery analyses, and lead author in writing.

The second and third publications are both chapters in the technical report: Recent research studies on seabed structure and benthic biodiversity relationships in Canadian Marine habitats. The report is a Canadian Health Oceans Network (CHONe) and DFO initiative coordinated by the report editors Dr. Evan Edinger and Dr. Peter Lawton. The contribution led by Dr. Evan Edinger describes and maps the location of cold-water corals and sponges and their habitats in Canadian waters. The contribution led by Dr. Verena Tunnicliffe identifies and describes hydrothermal vents and seamounts in Canadian waters. My contribution to both publications was assistance with writing and mapping.

Appendix B: Supplementary figure for Chapter 2

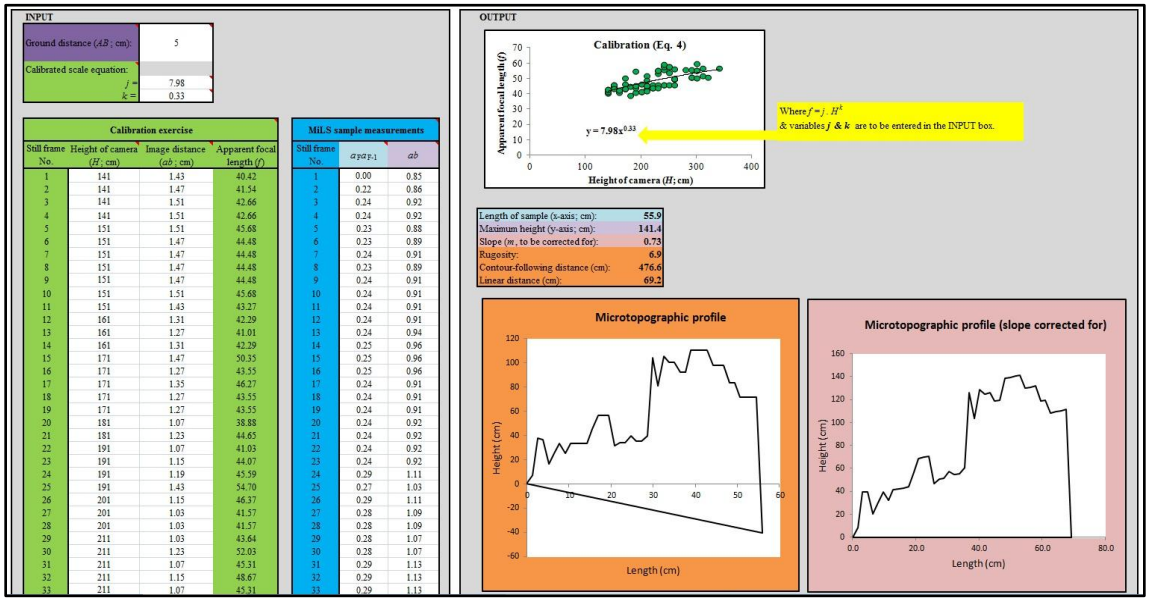

Figure. B.1. An example of the *Input & Output* spreadsheet in the microtopographic laser scanning (MiLS) workbook provided as Web Appendix I for Du Preez and Tunnicliffe (2012). To download the Excel workbook see doi:10.4319/lom.2012.10.899.

Appendix C: Supplementary material for Chapter 3

Appendix C provides ArcGIS® systematic instructions of how to generate an arc-chord ratio (ACR) rugosity raster from an elevation raster. I have developed an ArcGIS® geoprocessing model tool that automates these steps into one for quick and easy execution. This model will be available for download as an ArcGIS® tool pending the article publication (Du Preez, 2014 [Chapter 3]).

Note: Step numbers correspond to workflow illustrated in Fig. C.1.

1) Download the DEM (Digital Elevation Model) Surface Tools (version 2.1) extension for ArcGIS® <www.jennessent.com>
2) Open ArcGIS® ArcMap™ (instructions written for version 10.2).
3) Activate the necessary extensions. To do this navigate to: Customize/Extensions. Check the boxes beside 3D Analyst and Spatial Analyst.
4) Import the elevation (or bathymetric) raster using Add data.
5) To start the analysis and derive contoured area raster, navigate to: DEM Surface Tools/Surface area and ratio.
6) In the "Surface Area Analysis Parameters" dialog box, check and insert the references for the following parameters:
    a. Select Elevation Raster: insert the name of the elevation raster.
    b. Check the box beside Calculate Surface Area Raster. Below, name and specify the location to store the surface area raster.
    c. Leave the other parameters blank or at the default settings.
    d. Click Okay. The new contoured area raster will appear in the Table of Contents.
7) To derive a slope raster, navigate to: ArcToolbox/3D Analyst Tools/Raster Surface/Slope
8) In the "Slope" dialog box, insert the references for the following parameters:
    a. Input Raster: insert the name of the elevation raster.
    b. Output Raster: name and specify the location to store the resulting slope raster.
    c. Leave the other parameters blank or at the default settings.
    a. Click Okay. The new slope raster will appear in the Table of Contents.

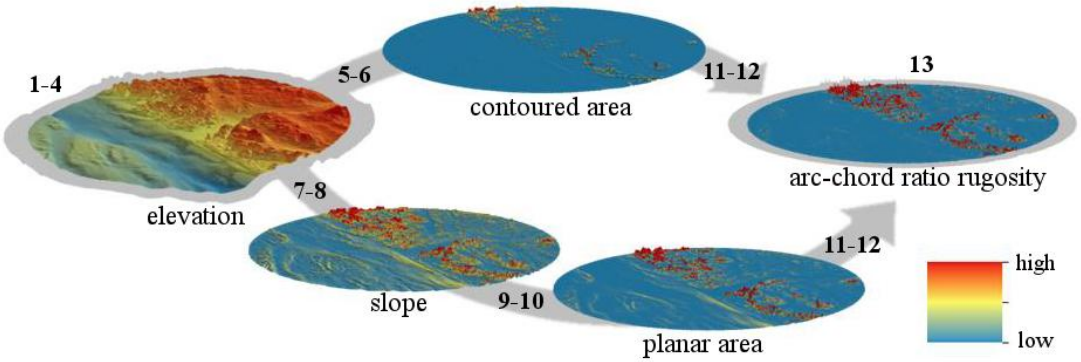

Figure C.1. The derived rasters and workflow (grey arrows) of the arc-chord ratio (ACR) method for generating a rugosity raster from an elevation raster. The example is a 2 km radius surface from the plateau at Learmonth Bank, British Columbia.

9) To derive a planar area raster, navigate to: ArcToolbox/Spatial Analyst Tools/Map Algebra/Raster Calculator.

10) In the "Raster Calculator" dialog box, write the equation and insert the references into the space provided:
    a. Note: the input values for trigonometric functions are interpreted to be radians. To use degrees as inputs, convert to radians by multiplying the input values by pi/180 or approximately 0.01745.
    b. The raster cell area is required for this calculation (in square meters; information available in metadata).
    c. Use the following adapted cosine law equation to solve for the planar area of each cell:
    $$\text{planar area} = \frac{\text{horizontal area}}{\cos\theta}$$
    The text should be entered in the space provided as:
    [insert cell area]/(Cos("[insert slope raster file name]" * 0.01745))
    or for example: 25/(Cos("slope_raster" * 0.01745))
    d. Click Okay. The new planar area raster will appear in the Table of Contents.

11) To generate the arc-chord ratio (ACR) rugosity raster, navigate to the Raster Calculator again (see step 9).

12) In the "Raster Calculator" dialog box, write the rugosity equation and insert your references into the space provided:
    a. Use the rugosity equation to solve for the ACR rugosity value of each cell (Equation 1 in paper):
    $$\text{rugosity} = \frac{\text{contoured area}}{\text{planar area}}$$
    The text should be entered in the space provided as:
    " [insert contoured area raster] "/" [insert planar area raster] "

b. Click Okay. The new ACR rugosity raster will appear in the Table of Contents.

13) To view the ACR rugosity raster check the box beside the file name in the Table of Contents. The raster imagine will appear in the Data View window.

Appendix D: Supplementary material for Chapter 3

Appendix D provides ArcGIS® systematic instructions of how to measure the arc-chord ratio (ACR) rugosity index of a three-dimensional surface. I have developed an ArcGIS® geoprocessing model tool that automates these steps into one for quick and easy execution. This model will be available for download as an ArcGIS® tool pending the article publication (Du Preez, 2014 [Chapter 3]).

Note: Step numbers correspond to workflow illustrated in Fig. D.1.

1) Open ArcGIS® ArcMap™ (instructions written for version 10.2).
2) Activate the necessary extensions. To do this, navigate to: Customize/Extensions. Check the boxes beside 3D Analyst, Geostatistical Analyst, and Spatial Analyst.
3) Import the elevation (or bathymetric) raster and the surface feature/s (defined spatial subset/s to be analysed) using Add data. Note: if you intend on analysing the entire raster (and not a subset) use the Raster Domain tool (ArcToolbox 3D Analyst Tools/ Conversion/From Raster/Raster Domain) to create a boundary (polygon) with the same dimensions as the raster.
4) Multiple features within a single feature class can be analysed simultaneously.
5) Start by calculating the contoured area (numerator of rugosity equation). To convert the raster into a triangular irregular network (TIN), navigate to: ArcToolbox/3D Analyst Tools/Conversion/From Raster/Raster to TIN.
6) In the "Raster to TIN" dialog box, insert your references for the following parameters:
    a. In Raster: insert the name of the elevation raster.
    b. Output TIN: name and specify the location to store the resulting TIN.
    c. Leave the other parameters blank or at the default settings (optional).
    d. Click Okay. The new elevation TIN will appear in the Table of Contents.
7) To clip a TIN surface, navigate to: ArcToolbox/3D Analyst Tools/Data Management Tools/TIN/Edit TIN.
8) In the "Edit TIN" dialog box, insert your references for the following parameters:
    a. Input TIN: insert the name of the elevation TIN.
    b. Input Feature Class: from the dropdown menu select the surface feature to be clipped. The selected feature will appear in the table below.
    c. In the table change: the "Height Field" to "<None>" and change the "SF Type" to "Hard_Clip".
    d. Leave the other parameters blank or at the default settings.

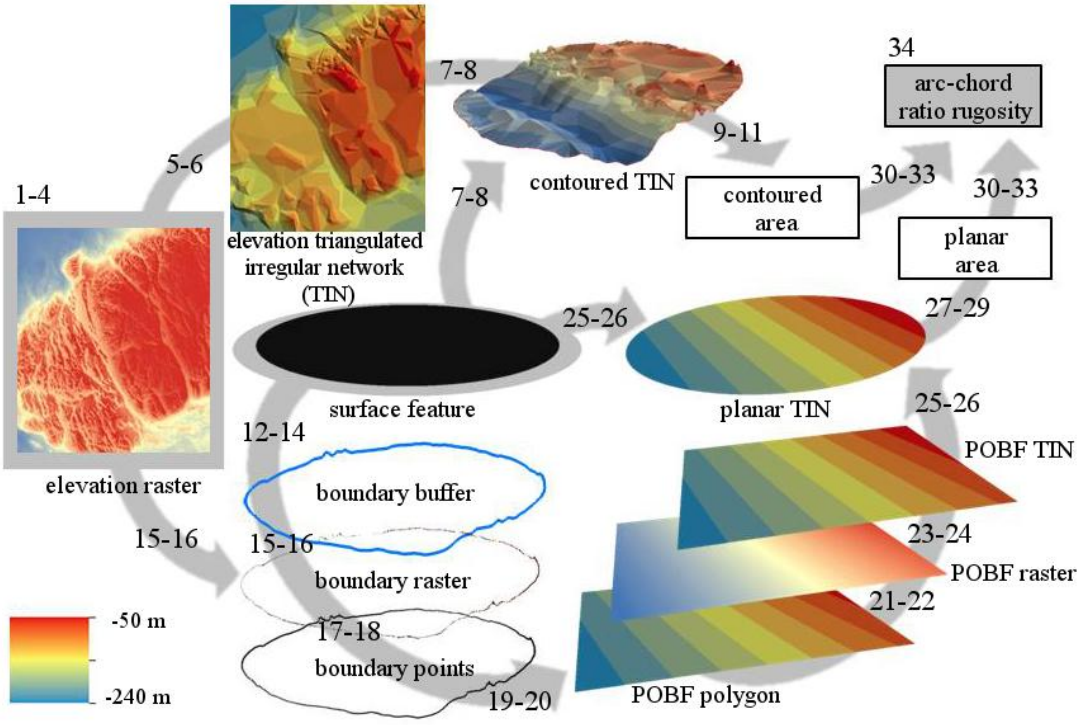

Figure D.1. The derived surfaces and workflow (grey arrows) of arc-chord ratio (ACR) method for calculating rugosity of a three-dimensional surface (elevation raster). The example is a 2 km radius surface from the plateau at Learmonth Bank, British Columbia.

e. Click Okay. This tool edits the original TIN so it will be listed under the same name and in the same location in the Table of Contents.

9) To calculate the contoured area, navigate to: ArcToolbox/3D Analyst Tools/Triangulated Surface/Polygon Volume.

10) In the "Polygon Volume" dialog box, inset your references for the following parameters:
    a. Input Surface: insert the name of your (contoured) elevation TIN.
    b. Input Feature Class: insert the name of your surface feature.
    c. Height Field: from the dropdown menu select <None>.
    d. Surface Area Field: insert the name of the new table field that will store the contoured area value (suggestion: "contoured").
    e. Leave the other parameters blank or at the default settings.
    f. Click Okay. The contoured area value will appear in the Attribute Table of the surface feature.

11) To view the contoured area value: in the Table of Contents right click the original surface feature file, select Open Attribute Table, and scroll to the end of the table.

12) To calculate the planar area, we first need to identify and then isolate the boundary data.

13) To define the boundary, navigate to: ArcToolbox/Analysis Tools/Proximity/Buffer.

14) In the "Buffer" dialog box, inset your references for the following parameters:
    a. Input Feature: insert the name of your surface feature.
    b. Output Feature Class: name and specify the location to store the resulting buffer polygon.
    c. Linear unit: enter the cell length (cell size available from raster metadata; units are in meters by default).
    d. Side Type (optional): change to OUTSIDE_ONLY.
    e. Leave the other parameters at the default settings.
    f. Click Okay. The boundary buffer polygon file will appear in the Table of Contents.

15) To isolate the boundary data use the clip tool, navigate to: ArcToolbox/Data Management Tools/Raster/Raster Processing/Clip.

16) In the "Clip" dialog box, insert your references for the following parameters:
    a. In Raster: insert the name of your elevation raster.
    b. Output Extent: insert the name of the buffer (from step 14).
    c. Check the box beside Use Input Features for Clipping Geometry.
    d. Output Raster Dataset: name and specify the location to store the resulting boundary raster.
    e. Leave the other parameters blank or at the default settings.
    f. Click Okay. The new boundary raster will appear in the Table of Contents.

17) To covert the raster to point data, navigate to: ArcToolbox/Conversion Tools/From Raster/Raster to Point.

18) In the "Raster to Point" dialog box, insert your references for the following parameters:
    a. Input raster: insert the name of the boundary raster (from step 16).
    b. Leave the other parameters at the default settings.
    c. Output point features: name and specify the location to store the resulting boundary point features.
    d. Click Okay. The new boundary point features will appear in the Table of Contents.

19) To interpolate the plane of best fit (POBF), open the Geostatistical Wizard in Geostatistical Analyst.

20) In the "Geostatistical Wizard" dialog box, insert your references for the following parameters:
    a. Methods: select Global Polynomial Interpolation
    b. Input Data, Source Dataset: insert the name of the boundary point features (from step 18).
    c. Input Data, Data Field: change to "GRID_CODE".
    d. Click Next.

e. Leave the other parameters at the default settings. Check that Order of polynomial: 1.
f. Click Finish.
g. Note the name and stored location of the resulting Global Polynomial Interpolation POBF polygon.
h. Click OK. The new planar polygon file will appear in the Table of Contents.

21) In the Table of Contents, right click the Global Polynomial Interpolation POBF polygon file, select Data, and then select Export to Raster.

22) In the "GA Layer to Grid" dialog box, insert your references for the following parameters:
    a. Input geostaticical layer: insert the name of the Global Polynomial Interpolation file (POBF polygon).
    b. Output Raster Dataset: name and specify the location to store the resulting POBF raster.
    c. Output cell size (optional): change to the cell size of the original raster.
    d. Leave the other parameters at the default settings.
    e. Click Okay. The new planar raster will appear in the Table of Contents.

23) To convert the raster into a triangular irregular network (TIN), navigate to to Raster to TIN again (see step 5).

24) In the "Raster to TIN" dialog box, insert your references for the following parameters:
    a. In Raster: insert the name of the POBF raster (from step 22).
    b. Output TIN: name and specify the location to store the resulting TIN.
    c. Leave the other parameters blank or at the default settings (optional).
    d. Click Okay. The new POBF TIN will appear in the Table of Contents.

25) Note the POBF polygon is an enveloping polygon, and therefore so is the POBF raster and TIN. To clip the POBF TIN to the appropriate surface dimensions, navigate back to Edit TIN (see step 7).

26) In the "Edit TIN" dialog box, insert your references for the following parameters:
    a. Input TIN: insert the name of the POBF TIN.
    b. Input Feature Class: from the dropdown menu select the surface feature to be clipped. The selected feature will appear in the table below.
    c. In the table change: the "Height Field" to "<None>" and change the "SF Type" to "Hard_Clip".
    d. Leave the other parameters blank or at the default settings.
    e. Click Okay. This tool edits the original POBF TIN so it will be listed under the same name and in the same location in the Table of Contents.

27) To calculate the planar area, navigate to the Polygon Volume tool again (see step 9).

28) In the "Polygon Volume" dialog box, inset your references for the following parameters:
    a. Input Surface: insert the name of your POBF TIN.

b. Input Feature Class: insert the name of your surface feature.
c. Height Field: from the dropdown menu select <None>.
d. Surface Area Field: insert the name of the new table field that will store the minimal area value (suggestion: "planar").
e. Leave the other parameters blank or at the default settings.
f. Click Okay. The planar area value will appear in the Attribute Table of the surface feature.

29) To view the planar area value: in the Table of Contents right click the original surface feature file, select Open Attribute Table, and scroll to the end of the table.

30) Before calculating the arc-chord ratio (ACR) rugosity index navigate to: ArcToolbox/Data Management Tools/Fields/Add Field.

31) In the "Add Field" dialog box, write the equation and insert the references into the space provided:
    a. Input Table: insert the name of your surface feature.
    b. Field Name: insert the name of the new table field that will store the ACR rugosity value (suggestion: "rugosity").
    c. Field Type: from the dropdown menu select DOUBLE.
    d. Leave the other parameters blank or at the default settings.
    e. Click Okay. The new field will appear in the Attribute Table of the surface feature.

32) To calculate the ACR rugosity index, navigate to: ArcToolbox/Data Management Tools/Fields/Calculate Field.

33) In the "Calculate Field" dialog box, write the rugosity equation and insert the references into the space provided:
    a. Input Table: insert the name of your surface feature.
    b. Field Name: insert the name of your ACR rugosity field.
    c. Expression: click on the calculator symbol.
    d. In the "Field Calculator" dialog box, insert the references into the space provided and solve for the ACR rugosity index using the rugosity equation (Equation 1 in paper):

$$\text{rugosity} = \frac{\text{contoured area}}{\text{planar area}}$$

    The text should be entered in the space provided as:
    [contoured area value]/([planar area value]
    or for example: [contour] / [planar]
    e. Click Okay. The ACR rugosity index value will appear in the rugosity field in the Attribute Table of the surface feature.

34) To view the ACR rugosity value: in the Table of Contents right click the original surface feature file, select Open Attribute Table, and scroll to the end of the table.

Appendix E: A scientist's guide to using remotely operated vehicles (ROVs) for benthic imagery surveys

Preface

Appendix E is a methods article submitted as a chapter in a Canadian Technical Report of Fisheries and Aquatic Sciences: Du Preez, C., Chu, J.W.F., and Rose, J. (*in review*) A scientist's guide to using remotely operated vehicles (ROVs) for benthic imagery surveys. *In* Recent research studies on seabed structure & benthic biodiversity relationships in Canadian Marine habitats. Edited by P. Lawton and E. Edinger. Canadian Technical Report of Fisheries and Aquatic Sciences XXXX: XX + XX p.

Jackson Chu (CHONe PhD student, University of Victoria) and Jonathan Rose (Research Associate, Dr. Verena Tunnicliffe laboratory, University of Victoria) contributed to this article by assisting with the writing. I contributed to this article as lead author.

Abstract

Benthic imagery surveys performed using remotely operated vehicles (ROVs) can resolve high-resolution spatial patterns. Imagery can be processed using different methods to produce multiple biotic and abiotic datasets. These datasets are relevant for ecological studies that address species distributions, produce habitat maps, document animal behaviour, and monitor ecosystem health. Independent of researcher experience, ROV and ship time is expensive and logistically challenging. Based on our combined experiences with several ROVs owned and operated in Canada, we have developed best

practices, workflow steps, and suggestions for optimizing the research potential when performing benthic imagery surveys with ROVs.

Introduction

The Canadian Exclusive Economic Zone (EEZ) expands into the Pacific, Atlantic, and Arctic oceans and is one of the largest in the world. The Canadian Healthy Ocean Network (CHONe), a five year (2009-2013) nationwide scientific initiative, addressed the biodiversity and sustainability in Canada's three oceans. One of the main tools CHONe scientists used to fill this knowledge gap were benthic imagery surveys using remotely operated vehicles (ROVs). With national and international commitments to ocean health, scientists from Canada are world leaders in the applied field of subsea technology and have extensive experience with conducting benthic imagery surveys using ROVs.

A benthic imagery survey is a spatial sampling technique where by the surface of the seafloor is non-invasively documented with video or still images. Benthic imagery surveys performed using ROVs can resolve high-resolution spatial patterns. Imagery can be processed using different methods to produce multiple biotic and abiotic datasets. These datasets are relevant for ecological studies that address species distributions, produce habitat maps, document animal behaviour, and monitor ecosystem health. Historically benthic surveying required invasive sampling methods (e.g. trawling and grabs) but an imagery survey requires little to no contact with the surveyed surface, thus such surveys are highly sought after by management and conservation groups.

ROVs are classically considered to be unmanned, ship-tethered submersibles (Fig. E.1). However, with the advent of subsea cable observatories, benthic crawlers are now

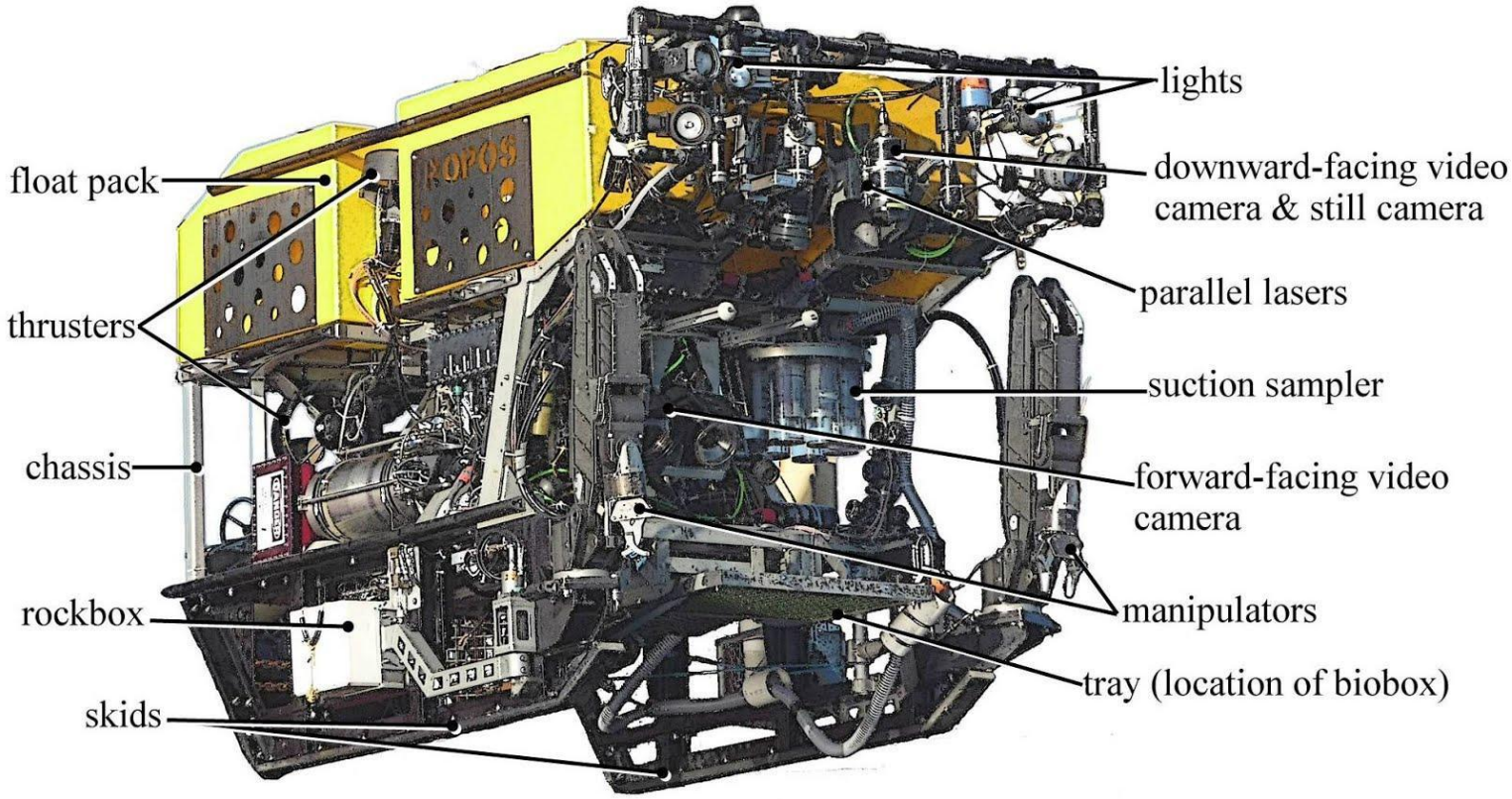

Figure E.1. The Remotely Operated Platform for Ocean Sciences (ROPOS) is a science/work-class remotely operated vehicle (ROV) developed and operated by the Canadian Scientific Submersible Facility (CSSF; dimensions: 3.1 x 1.6 x 2.2 m, 3,393 kg). Systems for benthic imagery surveys include: a primary forward-facing high-definition (HD) video camera (Insite Pacific Zeus-Plus; the pilot video camera) mounted on a pan and tilt; a secondary HD video camera (Insite Pacific Mini-Zeus) mounted on a tilt; a high-resolution digital still camera (12.1 megapixel Nikon D700) on a tilt; and over 3,700 watts of lighting (http://www.ropos.com).

considered a subcategory of ROV (e.g. NEPTUNE's Wally, an ROV tethered to the observatory). For the purpose of this paper, we focus only on ship-tethered ROVs. For imagery surveys of the benthos, ROVs have several advantages over manned submersibles or other methods such as drop cams, towed cameras, autonomous underwater vehicles (AUVs), or cabled observatories. There is near unlimited bottom time with real-time data transmission to the ship (via the umbilical tether) as compared to manned submersibles. Precision navigation, changes in flight-pattern in real-time, as well as the high powered capabilities currently enable more sophisticated imagery systems and lighting relative to AUVs. Remote operation enables higher precision in the collection of imagery and the option of deviating from the preplanned flight path compared to towed cameras. Simple drop cameras and cameras connected to cabled observatories can capture temporal data at high frequency, but only at fixed positions whereas ROV surveys capture high-resolution spatial data. Using strategic and precision sampling with ROVs can also supplement the patterns resolved by distribution mapping as opposed to the indiscrete and often destructive method of scientific trawling. Canadian ROVs have been particularly successful in this regard (e.g. Chu et al. 2011; Forget et al. 2010; Chu and Leys, 2012; Aranha et al. 2014; Tunnicliffe et al. in press).

Independent of researcher experience, ROV and ship time is expensive and logistically challenging. Based on our combined experiences with several ROVs owned and operated in Canada (Fig. E.2), we have developed several best practices, workflow steps, and suggestions for optimizing the research potential when performing benthic imagery surveys with ROVs. The remotely operated platform for ocean science

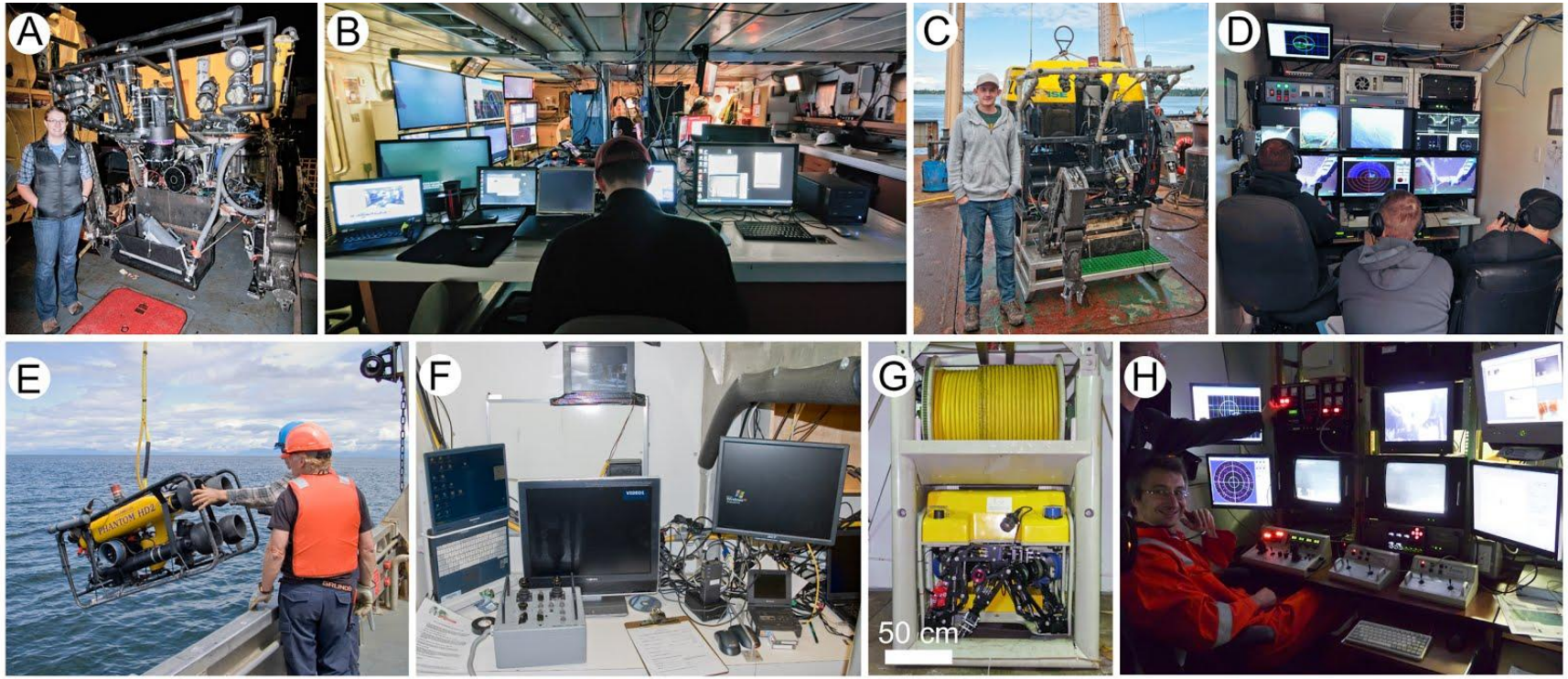

Figure E.2. Examples of Canadian remotely operated vehicles (ROVs) and their respective shipboard control stations. (A, B) ROPOS operates out of Sidney, British Columbia (BC) and has a maximum operating depth (MOD) of 5000 m. (C,D) The Oceanic Explorer operates out of Vancouver, BC, and has a MOD of 1000 m. (E,F) A Phantom HD2 operating out of the Pacific Biological Station in Naniamo, BC, with a MOD of 300 m. The Phantom is a common model and owned by several other institutions (e.g. Bamfield Marine Sciences Centre in Bamfield, BC). (G,H) A Super Mohawk owned and operated off the Canadian Coast Guard Ship Amundsen (registry port: Ottawa, Ontario) with a MOD of 1600 m. Photo credits: (A-C, E-F) J.W.F. Chu, (D) A.O.V. Bui, (G-H) C. Du Preez. An example of the control station and operating layout of ROPOS can be viewed at: https://vimeo.com/47740690.

(ROPOS, Fig. E.1) is considered a leading science ROV operating in Canada and thus we will often refer to ROPOS' systems throughout this paper. However, our general suggestions can be applied with any ROV platform given the presence or absence of certain systems. The majority of the studies cited throughout this paper were performed under the CHONe biodiversity theme. Our report will focus on pre-cruise planning, onboard operations, and *in situ* survey protocols to optimize raw imagery (data) acquisition. For post-cruise methods on data extraction and analyses, see Sameoto et al. (2008).

Methodological approach

Common systems of an ROV

In this section, we summarize common ROV systems that are relevant for benthic imagery surveys. A remotely operated vehicle (ROV) is the sum of multiple systems (Fig. E.1). Primary systems are essential for basic ROV operations and include the umbilical, thrusters, and a video camera for piloting. Secondary systems can greatly enhance the capabilities and science potential of an ROV and include additional cameras, manipulator arms, and sampling instruments. Depending on the focus and budget of the operating company, the standard configuration of an ROV may include many secondary systems with additional systems readily available upon request. Scientists can also design their own additional scientific equipment, modified to operate in conjunction with the ROV platform, to meet their specific research objectives (Yahel et al. 2007). The most effective scientific ROVs are built as adaptable robotic platforms, where systems can be added, removed, exchanged, and updated as required.

Primary ROV Systems

Chassis and float Pack: ROV systems are mounted onto the chassis. The float pack provides buoyancy (influences upper and lower depth limits). Together, they make up most of the size and weight of an ROV.

Locomotion: The number and orientation of thrusters determines the speed and maneuverability of the ROV.

Pilot video camera: ROVs have at least one forward-facing video camera which functions as the primary field of view (FOV) for the pilot.

Floodlights: Provides artificial light to illuminate the FOV in the pilot video camera. Ambient light is minimal when at depth.

Navigation: Provides real-time geospatial information such as latitude, longitude, and depth of the ROV. Accurate navigation is needed to georeference imagery and samples collected from a cruise. Accuracy of navigation is dependent on equipment and calibration (e.g. ROPOS: ±1 % water depth, Ian Murdock pers. comm.).

Umbilical: Supplies power to the ROV and enables data exchange and remote operation between the ROV and the shipboard control station. Umbilical length may limit the maximum operating depth.

Control station: The shipboard station where the remote operations occur. Pilots and scientists share this space. It includes all the components that function in controlling the ROV. Several monitors will display real time information on the ROV systems, navigation, and position relative to the ship. The size and complexity depends on the ROV operations and the ship (Fig. E.2).

Secondary ROV Systems

Additional video cameras: Video cameras used for alternative viewing angles and for recording scientific imagery. Cameras may be mounted on pan/tilt heads and have zoom lenses with manual focus capabilities. High-definition (HD) cameras are becoming more readily available and are considered upgrades to the primary cameras found on stock ROVs which may still be operating in standard-definition (SD; e.g. Super Mohawk, Fig. E.2G).

Digital still camera (DSC): DSCs capture high resolution photographs (ROPOS has a 12 megapixel, MP, DSC) which is far superior than the low resolution of frame grabs from HD video (< 2 MP). DSC functions can be manually controlled by a scientist or automated (taking images at preset intervals) and may include a strobe light (e.g. Pacific Biological Station's Phantom HD2, Fig. E.2E).

Additional lights: Additional lights may be required to illuminate the FOV of additional cameras. Video cameras require floodlights while still cameras can function with floodlights or strobes. Due to high particulates in parts of the water column, the orientation of the lights may require calibration to maximize the clarity in the FOV.

Parallel lasers: Provides a scale reference. It is common practice to attach a set of parallel lasers to the camera housing (or camera mount) to project a known scale within the FOV of the camera. More advanced image-scaling options can be provided by multi-laser configurations and associated software (e.g. Laser Measure(C) developed by MBARI, Barker et al. 2001).

Imagery recording devices: Video imagery is relayed in real-time from the ROV, via the umbilical, to a recording device at the control station. Still imagery can also be relayed in real-time or stored in-camera and downloaded upon recovery of the ROV.

Data-logging system: Software for real-time data annotation which is used by scientists during dives. It can contain useful information such as real-time user annotations, dive information, data, and events (with or without images) in a centralized, searchable, and easy to navigate interface. For example, the Canadian Scientific Submersible Facility (CSSF), which operates ROPOS, provides their Integrated Real-time Logging System (IRLS) for scientists. Fisheries and Oceans Canada developed Video Miner and ClassAct Mapper.

Manipulators: Manipulator arms are controlled by an operator and can be used to collect voucher specimens during surveys. More technical manipulators have some form of operator feedback to allow the operator to perform delicate manoeuvres. Manipulators can be used to directly collect specimens (Aranha et al. 2014) or can be used to operate collection devices such as a suction sampler or Ekman grab (Chu and Leys 2010, 2012; Chu et al. 2011). Voucher specimens are usually stored in a biobox, rockbox, or sampler containers mounted on the ROV.

Other systems: Examples of other common systems include an altimeter, CTD (conductivity, temperature, and depth sensors), oxygen sensors, sediment corers, plankton nets, Imagenex sonar, SIP water samplers (Yahel et al. 2007; Chu et al. 2011), and temperature probes (Tunnicliffe et al. in press).

Pre-cruise planning

Prior to the ROV cruise, establishing realistic survey objectives and methodology is mandatory. The best practice approach is to have multiple contingency plans that

accommodate for the potential dive time lost to technical problems, poor weather, or other unpredictable events. The end-products of a survey will highly depend on the capabilities of not only the ROV but also the experience of the ROV pilots. If possible, the cruise plan should be discussed with the ROV operation during the planning stage.

Considerations when planning

ROV capabilities: ROV options for benthic imagery surveys include a variety of vehicles, from micro-class to work-class. Smaller ROVs are generally easier and less expensive to operate. Larger ROVs maybe better suited for gathering large amounts of scientific imagery for a couple reasons: 1) larger ROVs have increased stability and handling, especially under adverse flow conditions, and 2) larger ROVs can support, and thus are equipped with, superior imaging systems and are likely to have a more precise navigation system for georeferencing the imagery. When developing realistic research objectives, the ROV systems, configuration, limitations, and the experience of the pilots are all important factors to consider. Most science ROV operations will have a detailed website to assist scientists in familiarizing themselves with the ROV's capabilities.

Collaboration among scientists: Collaborations are typical of ROV expeditions. Dive time is often split among multiple research programs within a cruise. It is imperative to have a clear plan on how time, resources, and dive products will be divided among scientists.

Multipurpose dives: Certain ROV system configurations may interfere with a benthic imagery survey. For example, mounting a front biobox may partially block the field of view (FOV) of downward camera angles. Once submerged, the refraction of light through the water-lens interface will cause objects to appear magnified (Christ and Wernli 2014). Many ROV cameras are set to autofocus and a large obstruction in the foreground can

cause the rest of the image to blur. This is particularly important to consider when using a camera set to automatic image capture or auto presets.

Dive conditions: Bathymetry, tides and currents, seasonal weather/ocean conditions, hazards, and water quality will influence a benthic survey. For example, high turbid water (found in harbours and deltas) will affect the quality of imagery. Dissolved organic matter increases light absorption and suspended matter increases light scattering, which affects the ability to capture clear images (Christ and Wernli 2014). Certain lighting configurations can mitigate these problems, but this needs to be addressed prior to the dive because the position of the lights is fixed once the ROV is launched. A priori awareness of these conditions will maximize the efficiency of a cruise.

Metadata: Adding accurate metadata to the video can be challenging. Common approaches include adding an overlay of the information onto the video or encoding it as a closed caption channel. The direct overlay usually has a negative impact on the video quality. Another option is to encode the information as an audio stream which will require dedicated hardware to decode after the cruise. A data-logging system (e.g. IRLS) is another means of recording metadata. If the ROV operation does not supply a data-logging system, the scientist will have to find or create one to suit their research needs.

Recording imagery: Standard-definition (SD) recording is relatively simple and inexpensive with viable options including digital video (DV) tapes, digital video disks (DVDs), and digital video recorders (DVRs). High-definition (HD) video streams require recording systems to compress the raw video-source into manageable file-sizes. These recording systems are more complex, costly, and require technical expertise to operate. ROPOS uses a Digital Rapids StreamZ system to record HD-video but there are other

options such as a Matrox MXO2 or a Panasonic P2 system. Some of these devices record to flash, which can then be copied to a hard drive or directly to hard disk.

The selection of a coder-decoder (codec) is another important consideration when recording HD-videos. By default, ROPOS uses a 50Mbps MPEG2 broadcast quality stream which results in a high quality, easy playback, and broad compatibility. Alternative codec options include h.264 or AVC-intra which may fit alternative editing or image quality needs. Depending on the level of video compression, HD video can require substantially more data storage space than SD video. For example, a HD video source encoded with a 50 Mbps MPEG2 stream requires 4 GB of hard drive space for every 10-11 mins of footage. Hard drives are inexpensive relative to the total expense of an ROV expedition, thus having redundant hard drives should be factored into the cruise budget.

Voucher specimen collections: Voucher specimens assist in species identification and can supplement the patterns resolved from benthic imagery survey (Chu et al. 2011, Chu and Leys 2012). Specimen collections require collection permits, planning for appropriate sample sizes and locations to collect during each dive, and preparation (fixatives and transporting of specimens) well in advance of the cruise. Sampling capabilities and sample-storage compartments on the ROV will limit the maximum number of samples in a dive.

Cruise plan: Each lead scientist is required to submit a cruise plan to the chief scientist, who then provides a copy to the ROV operation as well as the ship's captain. The cruise plan for benthic imagery survey dives should include (1) approximate launch and recovery target times, (2) dive objectives, (3) site waypoints (latitude, longitude, depth), (4) the survey protocol (detailed in the section below), and (5) maps with relevant figures

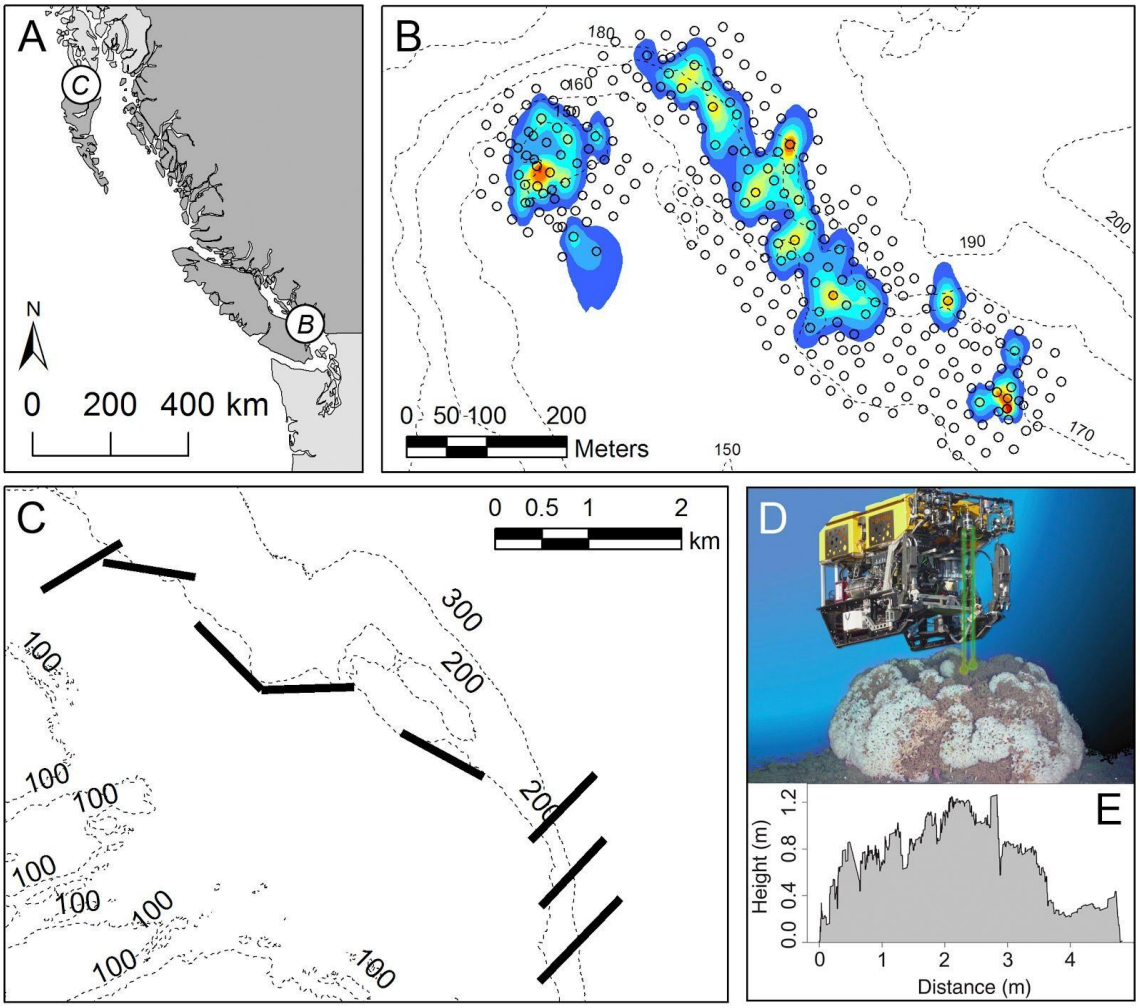

Figure E.3. Remotely operated vehicle (ROV) survey designs for benthic imagery surveys. (A) Locations of example surveys done off the Pacific coast of Canada using the ROV ROPOS (where italicized letters refer to the subsequent panels). (B) A simple stratified sampling grid of points (open circles) where photographs were taken with the downward-facing digital still camera. Live sponge cover was delineated from the images and sponge distribution maps generated post cruise (colored contours). (C) Preplanned 1 km linear video transects (black lines) for (D) a benthic video survey using the downward-facing video camera and microtopographic laser scanning (MiLS) survey protocol to measure and (E) profile cm-scale seafloor roughness (rugosity). Modified from (B) Chu & Leys (2010); and (C-E) Du Preez & Tunnicliffe (2011, 2012).

for adequate time before the cruise (or before specific dives) to configure the ROV to suit the dive objectives. Considering that most biologically relevant data extracted from imagery are in units of area (Sameoto et al. 2008), calibrating the scaling lasers mounted

to clarify any complexity in the dive plan (e.g. Fig. E.3B,C). The plan should also include the specific systems required for the survey. This will allow the ROV technicians to plan on the camera systems is paramount. Time permitting, it would be ideal to have the lasers recalibrated prior to every dive.

Survey protocols

A clear and concise survey protocol should be provided as part of the cruise plan. Prior to a dive, feasibility of the survey protocol should be discussed with the ROV operators and ship captain to anticipate potential problems and dive time constraints.

Considerations for optimizing the survey

Survey design: Due to cost and time constraints, ROV survey designs are usually based on transects or grids (Fig. E.3B,C). Both survey designs benefit from prior knowledge of the bathymetry at the dive site, the planned route for the ROV and thus the ship, and distances between specific waypoints.

Deviations from the survey design: Freedom to deviate from the survey design allows for exploration and close-up investigation of the benthos (Fig. E.4A). However, it can reduce the time allotted for completion of the original survey objectives. Accurate estimates of the time required to complete each dive objective would determine if deviations are acceptable during the dive. Deviations may be in the form of leaving the transect or grid, changing the camera settings (e.g. focus, tilt, zoom), or turning off the lasers. If deviations from the planned transect or grid is not permitted, an alternative would be to ask the ROV navigator to create a waypoint and return to the site after completion of the survey.

Number of survey sites: Surveying at one site continuously yields more imagery but limits the spatial coverage of the study. Transiting between multiple survey sites extends

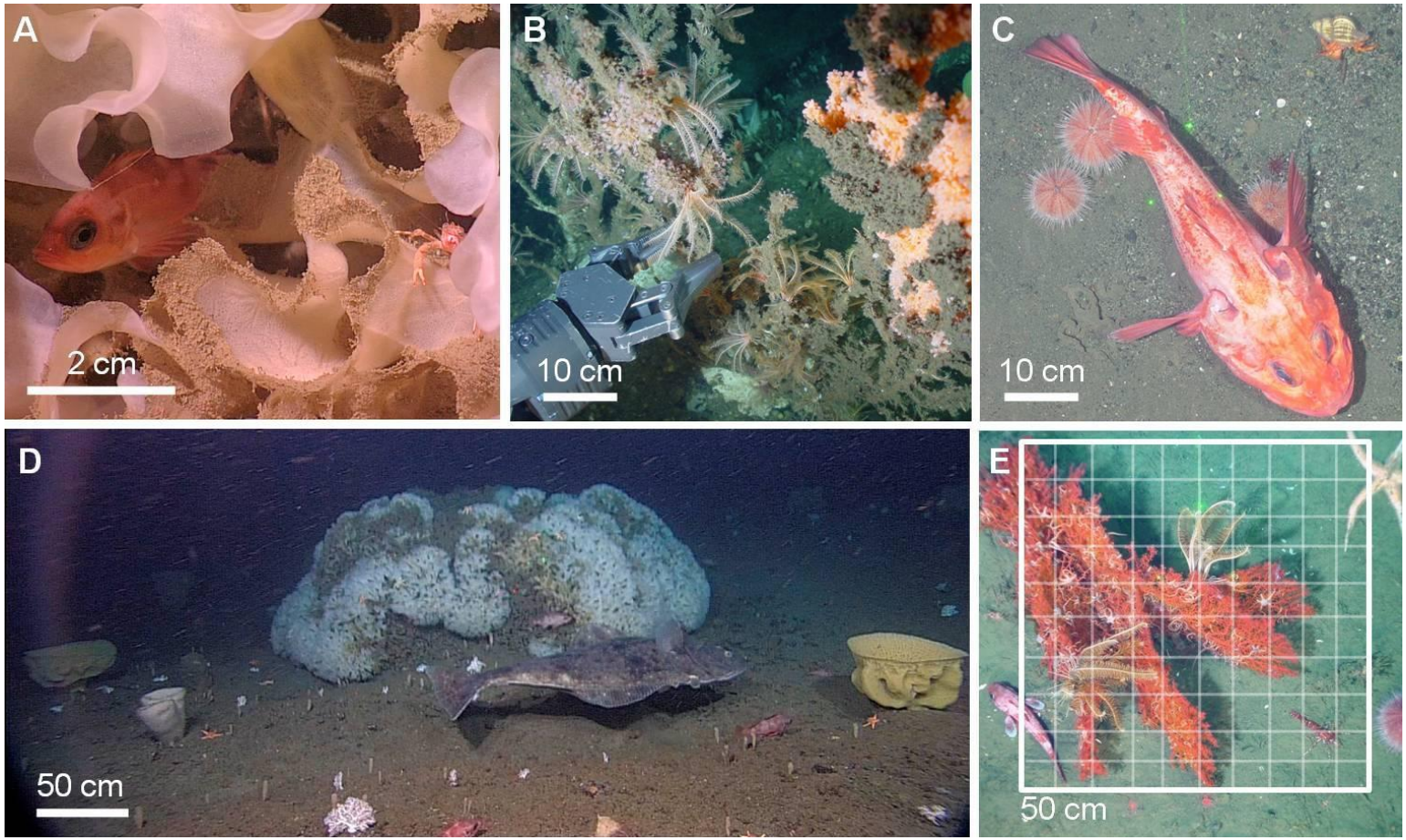

Figure E.4. Example imagery from a benthic survey using the ROV ROPOS. (A) A close-up (full zoom) using the forward-facing video camera. (B) Collection of dead coral branch adjacent to living coral using manipulator arm. (C) The narrow field of view (FOV) of the downward-facing video camera with lasers (horizontal lasers are 10 cm scale). (D) The wide FOV of the forward-facing video camera. (E) A high-resolution digital still image (DSC) with a digital quadrat grid overlay (horizontal lasers are 10 cm scale; quadrat is 50 cm x 50 cm). Imagery is from a 2008 survey at Learmonth Bank, British Columbia (Du Preez and Tunnicliffe 2011; Aranha et al. 2014; Neves et al. 2014).

the spatial coverage but reduces the time allotted to a single site and may include the need to recover and relaunch the ROV. For ROPOS, the average descent rate is approximately 45-60 mins for every 1,000 m of water column depth and the average ROV velocity at depth when transiting between sites is ~1 m s^{-1}. Decisions to remain at depth or recover the ROV should factor in the distance and time required to transit between sites.

Voucher specimen collection: A sampling protocol (including a description of the specimen, when and where it can be expected, and how it should be collected) is required to ensure accuracy and efficiency in the collection, with minimal impact to the surrounding environment (Fig. E.4B).

Considerations for optimizing imagery

Most benthic imagery surveys target the megafauna assemblage (sizes class >5 cm), thus our suggestions are for optimizing the ROV parameters for surveys of this type. High resolution still photos may resolve smaller sizes (1-2 cm) and capture the morphological characteristics required for species-level taxonomy.

ROV movement: During a survey, the ROV speed, height above the bottom, and orientation is dependent on the research objectives and methods (e.g. the MiLS survey protocol, Du Preez and Tunnicliffe 2012). General rules of thumb for ROV movement during a benthic imagery surveys are velocities no faster than 0.5 to 1 knots and keeping the ROV height above bottom to ≤ 1 m. Increasing ROV speed introduces the potential for blurred imagery yet may allow for more area to be covered. The higher the ROV altitude, the larger the field of view (FOV) with the trade-off of decreased pixel density to resolve fine scale features. Depending on the environment, the operational ROV height above bottom may need to factor in the avoidance of fragile structures (e.g. hydrothermal

vent chimneys, corals, sponges). The relative orientation of the ROV can affect the image quality. The best practice is to keep a stable plane parallel to the bottom. This will usually be horizontal, but in the case of a sloped bottom, it is recommended to survey up a slope. Cameras are normally mounted on forward brow of ROVs, thus moving upslope ideally minimizes the vertical distance between seafloor and camera. When moving down a slope, the seafloor to camera distance is larger and reduces the amount of lighting reaching the benthos. When moving down a slope over very steep terrain, the seafloor may not be visible at all. Depending on the position of the camera on the ROV and whether it has a tilt function, it may be possible to tilt the camera and survey a vertical wall (Yahel et al., 2007), however, the altimeter may not read bottom depth if hovering above the seafloor above a certain depth (25 m for ROPOS).

Setting down or on the fly: When taking digital still images, there are tradeoffs between landing the ROV or taking the images while in motion. Setting down may bias observations, allowing time for mobile animals to avoid or to be attracted to the ROV (Stoner et al. 2008). Fragile environments such as coral and sponge habitat, fast water currents, or equipment limitations can prevent the ROV from remaining stationary in the water column. When setting down is not an option, extra demand is placed on the user of the DSC system and supplementary lighting. Sensors in newer camera models have excellent low light imaging capabilities and make it possible to take sharp images while the ROV is in motion (e.g. ROPOS). A supplemental strobe (flash) may improve the quality of the still images but may affect the quality of the video. In scenarios where the ROV is in motion and the still camera lacks a strobe, the camera operator may be able to

compensate with manual exposure settings (increasing shutter speed/ISO) but this requires an understanding of exposure.

Camera orientation: A camera facing downward has a narrower FOV when compared to a forward-facing camera at a slightly oblique angle (Fig. E.4B,C). A downward-facing camera provides a more accurate estimate of area coverage, which is important for calculating density and distribution of animals. However, a forward-facing camera increases the probability of capturing mobile animals in the FOV (Stoner et al. 2008).

Camera setting: Cameras on ROVs will default to automatic settings. Auto settings are designed for ease of use yet may yield poor images under varying conditions such as fast ROV movement or high levels of suspended material in the water column. User input may help with the consistency of image capture and decrease the frequency of poor images. However, manual control settings require knowledge of photography and exposure to maximize the potential of capturing quality imagery under different water conditions. When detailed or demanding images are required in challenging conditions, scientists have hired professional photographers/videographers to operate the cameras.

Manual or automated timer: Both options are usually available on an ROV digital still camera (DSC) system. The manual setting allows for adaptation during a dive, but requires diligence. The automated timer is restrictive and may function poorly in waters with low visibility, but it removes sampling bias and some user errors.

Quadrats: Quadrats can be used to increase the precision of area measurements in imagery. A physical quadrat can be used in the FOV or calibrated scaling lasers can be used to overlay a digital quadrat grid during image processing (Fig. E.4E).

Scientist roles during the dive

Most ROV controls stations will be space limited. The chief scientist (or dive lead scientist) will usually have a seat at the ROV control station (Fig. E.2B, D, F, H) and have several key roles including providing information to the ROV operator regarding the dive plan and survey protocol, factoring in alternative scenarios when the unexpected occurs, and facilitating communications between the ROV operations with the rest of the scientific crew.

Additional tasks for the science crew may include: (1) assisting in the communication between scientists, the ROV operator, the ROV deck crew, and the ship crew; (2) monitoring the imagery recording and ensuring the video is being recorded once the ROV is at the bottom; (3) managing the data by ensuring raw video is recorded as manageable file sizes; (4) real-time data-logging and annotation and recording of audio in the control room; (5) requesting for sampling of voucher specimens at opportune moments (Fig. E.4B) and recording the proper metadata (time, site, ROV sample container); (6) operating the digital still camera (DSC); and (7) assisting the ROV technicians on deck during the descent and ascent of the ROV.

Cruise Checklist

Addressing metadata issues prior to the end of the cruise facilitates post-cruise data extraction and analysis. An example checklist of several items is noted below. Some of these items need only be checked once during a cruise while others may require multiple checks if the configuration of the ROV systems changes between dives.

- ❏ Record the specifications of the ROV equipment (camera make and model, type of lasers, navigation system, etc.).
- ❏ For every set of parallel lasers, measure the distance for scale.

- ❏ Measure the location of the cameras on the ROV relative to instruments of interest (e.g. altimeter, CTD, oxygen probes) and the height above the bottom of the ROV (skids).
- ❏ Determine if there is a delay between the navigation and the imagery data.
- ❏ Determine if and how the imagery is georeferenced, and what the means are to decode the embedded data (e.g. GPS data encoded in the audio signal of the video requires a decoder). If post-cruise georeferencing of files is required, collect the navigation files and the required information to georeference the imagery yourself.
- ❏ Determine the accuracy of the ROV navigation (usually expressed as a function of water depth).
- ❏ Determine the imagery format (video and still images) and whether they are proprietary files. Proprietary imagery files require specific software to view and edit.
- ❏ Download a copy of all the data (e.g. imagery, navigation files, and data-logging) collected for your survey (e.g. hard drives, CDs, DVDs). If this is not possible before the end of the cruise, have a clear plan organized between the chief scientist and ROV technicians for post-cruise handling and delivering of imagery and data.
- ❏ Record the names and the contact information of the chief scientist, lead scientists, other science personnel involved in the ROV operations, and the ROV technicians.
- ❏ Determine the ownership of the imagery and metadata. This is important when using imagery for publications and outreach.

Applications

The science of CHONe focused on biodiversity for the sustainability of Canada's three oceans. Of CHONe's 35 collaborative research projects conducted by over 150 researchers, many used remotely operated vehicles (ROVs) to conduct benthic imagery surveys. CHONe researchers successfully surveyed the benthos of many vulnerable deep-sea marine ecosystems using five different ROVs (Chu and Leys 2010; Forget et al. 2010; Chu et al. 2011; Du Preez and Tunnicliffe 2011; St. Germain 2011; Piepenburg et

al. 2011; Forget and Juniper 2013; Lacharitè and Metaxas 2013; Neves et al. 2014; Du Preez et al. in press; Tunnicliffe et al. in press). Maps produced from these benthic imagery surveys are commonly used when addressing issues pertaining to management and conservation. Specific CHONe examples include measuring seafloor bathymetry and rugosity at a cm-scale without disturbing the seafloor (Fig. E.3D,E); the area-coverage mapping of live sponges over the km-scale in the glass sponge reefs of British Columbia (Fig. E.3B); and ground-truthing of remote sensing data used to create sponge and coral habitat maps over the scale of 10's of km (Neves et al. 2014). In addition, novel techniques were developed to efficiently and efficiently utilize the benthic imagery collected (Gobi 2010; Du Preez and Tunnicliffe 2012). Combined, ROV benthic imagery surveys have been a central research tool in the three interrelated CHONe research themes of marine biodiversity, population connectivity, and ecosystem function in the Atlantic, Pacific, and Arctic ocean waters of Canada (http://chone.marinebiodiversity.ca/publications).

Summary and Recommendations

Although the vast majority of the deep sea (depths > 200 m) remains poorly documented, ocean exploration is rapidly advancing with the current pace of technological innovation. High resolution time-series are now streaming from advanced subsea cabled observatories like VENUS and NEPTUNE and can supplement the spatial patterns resolved by ROV mapping (Matabos et al. 2011, 2012; Robert and Juniper 2012; Robert et al. 2012). With the volumes of imagery data that is now typical of deep-sea ecological research, the motto of "garbage in, garbage out" can easily be applied to the

data collected from benthic imagery surveys performed by ROVs. It is imperative that the deep-sea community develop standardized and efficient workflows to maximize the acquisition of quality information from the deluge of raw data. To this effect, our suggested protocols and workflow can be interpreted as guidelines that were developed and successfully applied in the field under the CHONe project.

Acknowledgements

We gratefully acknowledge Verena Tunnicliffe and Sally Leys for their support, funding, and invaluable expertise in Remotely Operated Vehicle (ROV) operations. We thank personnel of the ROVs for all their assistance: Ian Murdock and CSSF-ROPOS; Wolfgang Carolsfeld, James Pegg and the Pacific Biological Station; the Super Mohawk ROV team on the Canadian Coast Guard Ship (CCGS) Amundsen, ITB Subsea, and the Simon Fraser University (SFU) ROV team. We also thank the crew of the CCGS John P. Tully, Vector, Hudson, and Amundsen, R/V Thompson; and the personnel at VENUS and NEPTUNE. Research is sponsored by the Natural Sciences and Engineering Research Council (NSERC) through the Canadian Healthy Oceans Network (CHONe). Additional support was provided by an University of Victoria Fellowship and a NSERC postgraduate scholarships to C. Du Preez and J.W.F. Chu.

Literature cited

Aranha, R. Edinger, E., Layne, G., and Piercey, G. 2014. Growth rate variation and potential paleoceanographic proxies in *Primnoa pacifica*: Insights from high-resolution trace element microanalysis. Deep-Sea Res. P.t. II 99: 213-226. doi: 10.1016/j.dsr2.2013.07.001.

Barker, B.A.J., Davis, D.L., and Smith, G.P. 2001. The calibration of laser-referenced underwater cameras for quantitative assessment of marine resources. *In* Proceedings of OCEANS 2001, MTS/IEEE Conference and Exhibition, vol. 3. Honolulu, HI, USA, 5–8 November 2001. pp. 1854-1859. doi: 10.1109/OCEANS.2001.968128.

Chu, J.W.F., and Leys, S.P. 2010. High resolution mapping of community structure in three glass sponge reefs (Porifera, Hexactinellida). Mar. Ecol. Progr. Ser. 417: 97-113. doi:10.3354/meps08794.

———. 2012. The dorid nudibranchs *Peltodoris lentiginosa* and *Archidoris odhneri* as predators of glass sponges. Invertebr. Biol. 131(2): 75-81. doi: 10.1111/j.1744-7410.2012.00262.x.

Chu, J.W.F, Maldonado, M., Yahel, G., and Leys, S. 2011. Glass sponge reefs as a silicon sink. Mar. Ecol. Progr. Ser. 441: 1-14. doi: 10.3354/meps09381.

Christ, R.D., and Wernli, R.L., Sr. 2014. Video. *In* The ROV manual: a user guide for remotely operated vehicles. Second Edition. Butterworth-Heinemann, Amsterdam. pp. 249-283.

Du Preez, C., and Tunnicliffe, V. 2011. Shortspine thornyhead and rockfish (Scorpaenidae) distribution in response to substratum, biogenic structures and trawling. Mar. Ecol. Progr. Ser. 425: 217-231. doi:10.3354/meps09005.

———. 2012. A new video survey method of microtopographic laser scanning (MiLS) to measure small-scale seafloor bottom roughness. Limnol. Oceanogr. Methods 10: 899-909. doi: 10.4319/lom.2012.10.899.

Du Preez, C., Davies, S.C., Clarke, E., Fruh, E., and Curtis, J.M.R. 2014. Cobb Seamount species inventory. Can. Tech. Rep. Fish. Aquat. Sci. In press.

Forget, N.L., and Juniper, S.K. 2013. Free-living bacterial communities associated with aggregations of *Ridgeia piscesae* undergoing different environmental conditions at Main Endeavour Vent field, Juan de Fuca Ridge. Microbiologyopen 2(2):1–17. doi: 10.1002/mbo3.70.

Forget, N.L., Murdock, S.A., and Juniper, S.K. 2010. Bacterial diversity in Fe-rich hydrothermal sediments at two South Tonga Arc submarine volcanoes. Geobiology 8: 417–32. doi: 10.1111/j.1472-4669.2010.00247.x.

Gobi, A.F. 2010. Towards Generalized Benthic Species Recognition and Quantification Using Computer Vision. *In*: Proceedings of OCEANS 2010 Conference, Sydney, Australia, 24-27 May 2010. pp. 94–100. doi: 10.1109/OCEANSSYD.2010.5603995.

Lacharitè, M., and Metaxas, A. 2013. Early life history of deep-water gorgonian corals may limit their abundance. PLoS One 8: e65394. doi: 10.1371/journal.pone.0065394.

Matabos, M., Tunnicliffe, V., Juniper, S.K., and Dean, C. 2012. A year in hypoxia: epibenthic community responses to severe oxygen deficit at a subsea observatory in a coastel inlet. PLoS One 7: e45626. doi: 10.1371/journal.pone.0045626.

Matabos, M., Aguzzi, J., Robert, K., Costa, C., Menesatti, P., Company, J.B., and Juniper, S.K. 2011. Multi-parametric study of behavioural modulation in demersal decapods at the VENUS cabled observatory in Saanich Inlet, British Columbia, Canada. J. Exp. Mar. Bio. Ecol. 401: 89–96. doi: 10.1016/j.jembe.2011.02.041.

Neves, B.M., Du Preez, C., and Edinger, E. 2014. Mapping coral and sponge habitats on a shelf-depth environment using multibeam sonar and ROV video observations: Learmonth Bank, Northern British Columbia, Canada. Deep-Sea Res. P.t. II 99: 169–183. doi: 10.1016/j.dsr2.2013.05.026.

Piepenburg, D., Archambault, P., Ambrose, W.G., Blanchard, A.L., Bluhm, B.A., Carroll, M.L., Conlan, K.E., Cusson, M., Feder, H.M., Grebmeier, J.M., Jewett, S.C., Lévesque, M., Petryashev, V.V., Sejr, M.K., Sirenko, B.I., and Włodarska-Kowalczuk, M. 2010. Towards a pan-Arctic inventory of the species diversity of the macro- and megabenthic fauna of the Arctic shelf seas. Mar. Biodivers. 41: 51–70. doi: 10.1007/s12526-010-0059-7.

Robert, K., and Juniper, S. 2012. Surface-sediment bioturbation quantified with cameras on the NEPTUNE Canada cabled observatory. Mar. Ecol. Prog. Ser. 453: 137–149. doi:10.3354/meps09623.

Robert, K., Onthank, K.L., Juniper, S.K., and Lee, R.W. 2012. Small-scale thermal responses of hydrothermal vent polynoid polychaetes: Preliminary *in situ* experiments and methodological development. J. Exp. Mar. Bio. Ecol. 420-421: 69–76. doi: 10.1016/j.jembe.2012.03.019.

Sameoto, J.A., Lawton, P., and Strong, M.B. 2008. An approach to the development of a relational database and GIS applicable scheme for the analysis of video-based surveys of benthic habitats. Can. Tech. Rep. Fish. Aquat. Sci. 2818: 40 p.

St. Germain, C. 2011. Reproductive and physiological condition and juvenile recruitment in the hydrothermal vent tubeworm Ridgeia piscesae Jones (Polychaeta: Siboglinidae) in the context of a highly variable habitat on Juan de Fuca Ridge. MSc Thesis. University of Victoria, Victoria, BC, Canada.

Stoner, A.W., Ryer, C.H., Parker, S.J., Auster, P.J., and Wakefield, W.W. 2008. Evaluating the role of fish behavior in surveys conducted with underwater vehicles. Can. J. Fish. Aquat. Sci. 65(6): 1230-1243.

Tunnicliffe, V., St. Germain, C., and HilÃ¡rio, A. 2014. Phenotypic variation and fitness in a metapopulation of tubeworms (Ridgeia piscesae Jones) at hydrothermal vents. PLoS One. In press.

Yahel, G., Whitney, F., Reiswig, H.M., Eerkes-Medrano, D.I., and Leys, S.P. 2007. *In situ* feeding and metabolism of glass sponges (Hexactinellida, Porifera) studied in a deep temperatre fjord with a remotely operated submersible. Limnol. Oceanogr. 52: 428-440.

Appendix F: Mapping coral and sponge habitats on a shelf-depth environment using multibeam sonar and ROV video observations: Learmonth Bank, northern British Columbia, Canada

Preface

Appendix F is a research article published in the peer-review journal *Deep-Sea Research II*: Neves, B.M., Du Preez, C., and Edinger, E. (2014) Mapping coral and sponge habitats on a shelf-depth environment using multibeam sonar and ROV video observations: Learmonth Bank, northern British Columbia, Canada. *Deep-Sea Research II* 99: 169-183.

Bárbara Neves (CHONe MSc student, Memorial University) contributed to this article by analysing the multibeam sonar data, producing the supervised classifications and maps, and assisting with the writing. Dr. Evan Edinger (professor and CHONe primary investigator, Memorial University) oversaw this work and assisted with the writing of this article. I contributed to this article by collecting and analysing the video data, investigating the biotope-substrate associations, and assisting with the writing.

Abstract

Efforts to locate and map deep-water coral and sponge habitats are essential for the effective management and conservation of these vulnerable marine ecosystems. Here we test the applicability of a simple multibeam sonar classification method developed for fjord environments to map the distribution of shelf-depth substrates and gorgonian coral- and sponge-dominated biotopes. The studied area is a shelf-depth feature Learmonth

Bank, northern British Columbia, Canada and the method was applied aiming to map primarily non-reef forming coral and sponge biotopes. Aside from producing high-resolution maps ($5m^2$ raster grid), biotope-substrate associations were also investigated. A multibeam sonar survey yielded bathymetry, acoustic backscatter strength and slope. From benthic video transects recorded by remotely operated vehicles (ROVs) six primary substrate types and twelve biotope categories were identified, defined by the primary sediment and dominant biological structure, respectively. Substrate and biotope maps were produced using a supervised classification mostly based on the inter-quartile range of the acoustic variables for each substrate type and biotope. Twenty-five percent of the video observations were randomly reserved for testing the classification accuracy. The dominant biotope-defining corals were red tree coral *Primnoa pacifica* and small styasterids, of which *Stylaster parageus* was common. Demosponges and hexactinellid sponges were frequently observed but no sponge reefs were observed. The substrate classification readily distinguished fine sediment, Sand and Bedrock from the other substrate types, but had greater difficulty distinguishing Bedrock from Boulders and Cobble. The biotope classification accurately identified Gardens (dense aggregations of sponges and corals) and *Primnoa*-dominated biotopes (67%accuracy), but most other biotopes had lower accuracies. There was a significant correspondence between Learmonth's biotopes and substrate types, with many biotopes strongly associated with only a single substrate type. This strong correspondence allowed substrate types to function as a surrogate for helping to map biotope distributions. Our results add new information on the distribution of corals and sponges at Learmonth Bank, which can be used to guide management at this location.

Keywords

Habitat mapping · Deep-sea coral · Biotopes · Substrate · Remote sensing · Supervised classification · Northeast Pacific

1. Introduction

Deep-water coral and sponge habitats have received more attention in recent decades as their vulnerability to human activities has been recognized. The fragility and importance of these organisms have been made evident: they are highly vulnerable to physical contact (Heifetz et al., 2009), some species have great longevity and extremely slow growth rates in the scale of millimeters per year (e.g. Andrews et al., 2002, Fallon et al., 2010, Roark et al., 2009 and Sherwood and Edinger, 2009), many provide habitat for other species (Auster, 2005, Costello et al., 2005, Du Preez and Tunnicliffe, 2011 and Hogg et al., 2010), they can act as paleoceanographic monitors (Aranha et al., 2014, Sherwood et al., 2005 and Sherwood et al., 2011) and some are promising in the biotechnological industry (Ehrlich, 2010, Hogg et al., 2010 and Sundar et al., 2003). Of the numerous anthropogenic impacts affecting these habitats, commercial fisheries (e.g. bottom trawling) stand out as creating long-lasting impacts that have the potential to be irreversible (Althaus et al., 2009, Hall–Spencer et al., 2002, Jones, 1992 and Wassenberg et al., 2002). The loss of coral and sponge habitat is comparable to terrestrial deforestation (Watling and Norse, 1998), with potential consequences for biodiversity and fisheries (Danovaro et al., 2008).

The recognition that vulnerable marine habitats have been destroyed faster than we are able to discover them has been raising world concerns. With its advent and continued

improvement, marine habitat mapping has quickly become an essential instrument in marine conservation (Brown et al., 2011, Cogan et al., 2009,Copeland et al., 2011, Gonzalez-Mirelis and Lindegarth, 2012 and Pickrill and Todd, 2003). Sonar technologies together with photography and video have proven to be particularly useful data sampling tools in the context of deep-water habitat mapping (Brown et al., 2011, Kenny et al., 2003 and Kostylev et al., 2001). Multibeam echosounders (MBES) generate continuous swaths of bathymetry and backscatter (acoustic return strength) data simultaneously (e.g. Courtney and Shaw, 2000) providing information on both seafloor topography and substrate type (Harris and Baker, 2012). Because surficial geology is an important determinant of the distribution of benthic organisms, especially deep-sea corals and sponges (Leys et al., 2004, Edinger et al., 2011 and Baker et al., 2012), MBES plays an important role in this context (e.g. Whitmire et al., 2007;Wilson et al., 2007).

Benthic habitat maps have been produced through the use of environmental variables as proxies for habitats, which in general can be oceanographic and/or geomorphologic (Brown et al., 2011). While successfully applied in global (Davies and Guinotte, 2011, Tittensor et al., 2009 and Yesson et al., 2012) and regional contexts (e.g. Bryan and Metaxas, 2007, Gonzalez-Mirelis and Lindegarth, 2012, Guinan et al., 2009, Buhl-Mortensen et al., 2009, Ross and Howell, 2012, Tong et al., 2012 and Tracey et al., 2011) variation in oceanographic variables is more difficult to measure at local scales (Brown et al., 2011 and Dolan et al., 2008). Some studies have included only terrain variables as proxies for biotope or taxa distribution (e.g. Anderson et al., 2011, Conway et al., 2005, Dolan et al., 2008 and Huang et al., 2011). Copeland et al. (2011) presented a method for supervised classification of multibeam to map substrates and habitats in a

fjord environment (Gilbert Bay, Eastern Canada) based on the inter-quartile ranges (IQR) of bathymetry, backscatter and slope values, ground-truthed with underwater video and bottom sediment samples. Those authors were able to distinguish eight substrates and five statistically distinct habitats.

Here, we test the applicability of the IQR method to map substrate types and coral- and sponge-dominated biotopes on a shelf-depth feature, Learmonth Bank (Dixon Entrance, British Columbia, Canada). Learmonth Bank has abundant corals and sponges, based on reports of high by-catch density in this location (Ardron et al., 2007). Between the years 1996 and 2002, observed bottom trawls (representing 2.62% of all bottom trawling activity in British Columbia) recovered, approximately 2400 kg of gorgonian corals in by-catch at Learmonth Bank (Ardron et al., 2007). Detailed data on coral and sponge by-catch at this location are not available for publication (pers. comm. Greg Workman). Learmonth Bank is considered a hotspot for demersal fish trawling activity (Sinclair et al., 2005), but due to an unresolved maritime boundary dispute between Canada and the USA (Gray, 1997), the area under dispute receives almost no fishing pressure. The entire area under dispute in Dixon Entrance is 2764 km^2 (806 M^2) (Gray, 1997), 21% (approximately 216 km^2) of the bank receives almost no fishing pressure. Du Preez and Tunnicliffe (2011) found corals and sponges to be significantly more abundant in untrawled than in trawled areas of the bank, and Ardron et al. (2007) suggested the entire bank should be a coral–sponge protected area. No formal protection measures have yet been implemented for Learmonth Bank, or Dixon Entrance.

In this study we used backscatter, bathymetry and slope, ground-truthed with video data, to map substrates and coral- and sponge-dominated biotopes on Learmonth Bank.

Four specific objectives were recognized: (1) to investigate the applicability of a simple supervised classification method described for fjords in a continental shelf setting; (2) to determine the degree of association between biotopes and substrate types and to assess substrate as a surrogate for biotope using video data; (3) to investigate the applicability of using backscatter, bathymetry and slope to determine signatures for non-reef-forming coral and sponge biotopes; (4) to use the resultant map to investigate the distribution of corals and sponges at Learmonth Bank.

2. Material and methods

2.1. Study area

Learmonth Bank (hereafter referred to as Learmonth) is a large granite massif located at the western end of Dixon Entrance, a broad trough (~150 km by ~55–65 km; Ballantyne et al., 1996) which lies between northern British Columbia, Canada, and southernmost Alaska, USA (Fig. F.1; 54° 24′ 59″N, 133° 05′ 00″W). It is considered a rugged, dissected granitic bank with depths that range from roughly 500 to less than 30 m (Barrie and Conway, 1999). It is approximately 45 km long and about 27 km wide with an area of ~1022 km^2 (present study).

Dixon Entrance is approximately 150 km in length, and about 55–65 km in width (Ballantyne et al., 1996). This region was glaciated during the Pleistocene and as a consequence it is characterized by the occurrence of several bedrock ridges and sediments of glacial origin (Barrie and Conway, 1999). The geology of Dixon Entrance includes a suite of volcanic rocks exposed at the seafloor (Barrie and Conway, 1999)

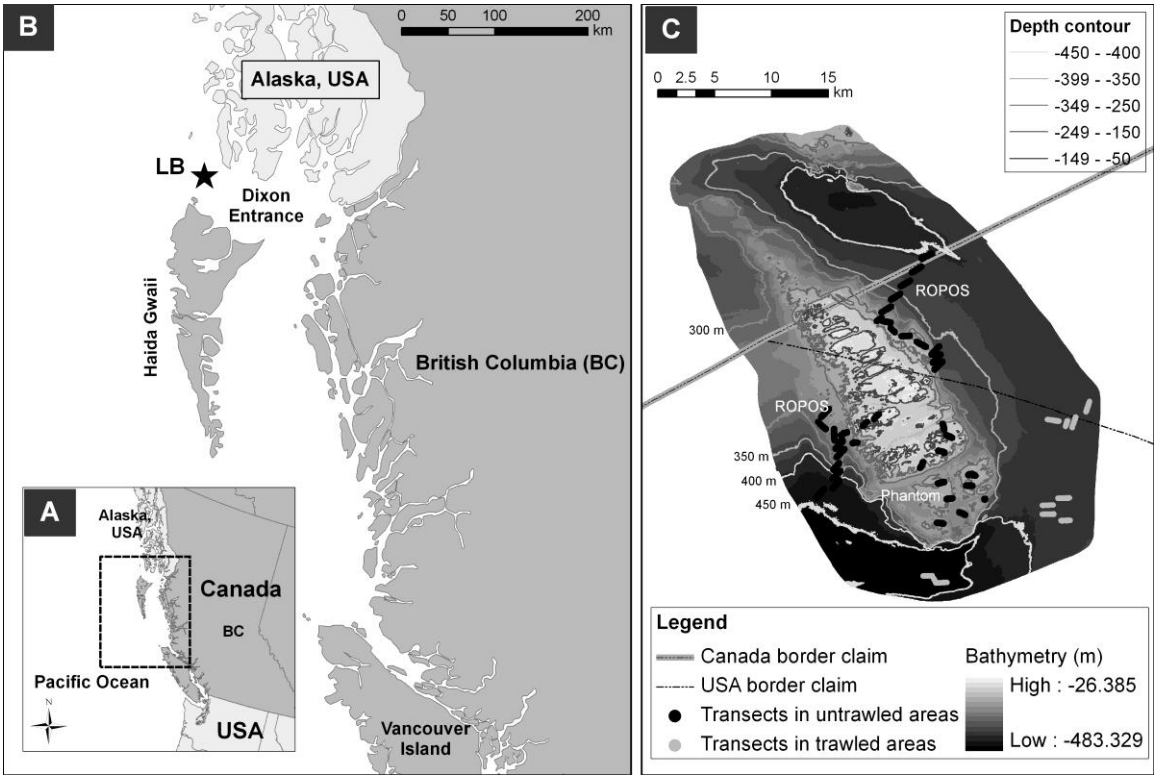

Figure F.1. Location of Learmonth Bank (LB) (A–B). (C) Bathymetry of Learmonth Bank showing transects and boundaries as claimed by Canada and the USA. Canadian boundary layer from GeoBase (www.geobase.ca) and USA boundary layer from NOAA's Office of Coast Survey (http://www.nauticalcharts.noaa.gov/csdl/mbound.htm#data).

and Learmonth itself is surrounded by glacial deposits largely composed of mud and sand (Barrie et al., 1991). During the Late Pleistocene deglaciation the sea level in this region was 150 m lower than the actual, leaving Learmonth briefly exposed (Hetherington et al., 2004).

The present mean tidal range in the region varies from east to west from 5 to 3.5 m (Barrie and Conway, 1999) resulting in strong bottom currents that can reach more than 90 cm s^{-1} (Crawford and Thomson, 1991). Dixon Entrance receives the influence of the Nass and Skeena rivers, which is most strongly felt in late spring and summer. The average sea surface temperatures in the northern shelf region of British Columbia vary

from 6 °C in April to 14 °C in August and prevailing winds are from the west (Thomson, 1981).

2.2. Data collection

2.2.1. Multibeam sonar data collection

Multibeam sonar survey was conducted by the Geological Survey of Canada (GSC) in 2008 (courtesy of J.V. Barrie). The MBES Simrad EM 1002 (95 kHz frequency) was used and the bathymetric data were processed by CHS with CARIS Hydrographic Information Processing Software (HIPS®). Bathymetry (meters) and backscatter (digital numbers) were gridded to 5 m spatial resolution, which we received from the GSC. Slope (degrees) was calculated from the bathymetry raster. Average swath width was ~1200 m in deep water areas (>400 m w.d.).

2.2.2. Video data collection

The video sampling was carried out on the Canadian Coast Guard Ship (CCGS) *John P. Tully* using the remotely operated vehicle (ROV) ROPOS in 2008 and the CCGS *Vector* using Fisheries and Oceans Canada Phantom ROV in 2009 (Table F.1). The 2008 video was filmed using a high definition HD video camera (Zeus Plus, Insite Pacific) while the 2009 video was filmed using a SD camera (Sony EVI 330). Both camera systems included two parallel lasers that projected 10 cm apart for scale within the camera's field of view. The vehicle average speeds were between 0.5 and 1 knot, flying at 0.5 to 1 m off the bottom. Transects for the ROPOS dives were designed for another study comparing trawled and untrawled areas (Du Preez and Tunnicliffe, 2011) and aimed to include the three main regions of the bank (basin, moraine and bank itself). ROPOS dives covered 32 one-km transects in five dives (Fig. F.1C), however

Table F.1. Specifications of data sampling at Learmonth Bank per ROV. ROPOS all stands for all dives (untrawled and trawled areas).

Specifications	**ROV**		
	ROPOS all	**ROPOS untrawled**	**Phantom**
Year	2008	2008	2009
Camera	HD	HD	SD
Number of transects	32	22	15
Minimum depth (m)	165	165	68
Maximum depth (m)	482	445	272
Average depth (m)	330	241	166
Vehicle average speed (knots)	0.5–1	0.5–1	0.5–1
Distance from the bottom (m)	0.5–1	0.5–1	~1

Only ROPOS untrawled and Phantom transects were used in this study.

because Du Preez and Tunnicliffe (2011) found trawled and untrawled areas at Learmonth Bank to be significantly different, we excluded transects in the trawled areas from the analysis. Therefore, 22 ROPOS transects were kept within the bathymetric range of 165–445 m (Fig. F.1C). Transects for the Phantom ROV were designed to cover the shallower areas of the bank itself and covered approximately 10 km of transects from 68 to 272 m depth.

2.3. Data analysis

2.3.1. Video annotation

A detailed description of the video annotation method is reported in Du Preez and Tunnicliffe (2011). Briefly, the video from the 2008–9 ROV transects was parsed into more than 45,000 records, where a record represents 1–2 m^2 of non-overlapping seafloor. For each record the correspondent substrate and biotope category was annotated (Table F2; some after Sameoto et al. (2008)). The substrate types were defined as the primary

Table F.2. Description of primary substrate categories and biotopes found at Learmonth Bank (based on Sameoto et al., 2008 and Du Preez and Tunnicliffe, 2011).

Category	Description
Substrate	Primary sediment as measured by percent surface area coverage
Fine sediment	Primary sediment <63 µm in size
Sand	Primary sediment is within the 63 µm to 2 mm size range
Pebble	Primary sediment is within the 2–6 cm size range
Cobble	Primary sediment is within the 6–26 cm size range
Boulder	Primary sediment is >26 cm in size
Bedrock	Primarily unbroken solid rock
Biotope	Dominant biological structure as measured by a combination of the size and density of epifauna present
No epifauna	No biological structures
Worms	High density of tube worms (>20 m^{-2})
Ophiuroids	Dense mat of brittle stars (>25% of seafloor covered)
Stylaster	Hydrocoral *Stylaster* spp. corals (>3 m^{-2}), usually with associated brittle stars (a filter feeding complex may be present at a lesser density)
Filter-feeding	A complex composed of a variety of small (<10 cm in height) filter-feeding organisms (e.g. hydroids, *Stylaster* spp., encrusting sponges, etc.; >3 per m^{-2})
Tubes	High density of *Auletta* sp. tubular sponges (>3 per m^{-2}; a complex may be present at a lesser density)
Small sponges	High density of small sponges (10–50 cm in height; 5–40 m^{-2}), majority Demospongiae
Calcigorgia	Dense *Calcigorgia spiculifera* gorgonian seafan coral (>4 m^{-2}), where these corals are the tallest biological structures present
Large sponges	High density of large sponges (>50 cm in height; ≥0.5 per m^2), majority glass sponges (Hexactinellida) with a few Demospongiae
Garden	A dense garden of large and small sponges and *Stylaster* spp. (>4 m^{-2})
Primnoa	High density aggregations of gorgonian corals consisting mainly of red tree coral *Primnoa pacifica* (with sparse occurrence of bubblegum coral *Paragorgia* sp.; ≥0.5 m^{-2})
Dead sponges	Dead sponge debris that formed piles meters high

substrate as measured by the percent surface area using the Wentworth scale of sediment sizes (Wentworth, 1922), adapted from Sameoto et al. (2008) to include bedrock and fine grained sediment. Biotope categories are hierarchical biogenic roughness categories and

were visually defined by the dominant biological structure as measured by a combination of the size and density of biogenic structures present (Table F.2). Both biotope and substrate type names are capitalized to emphasize that they represent the classes determined in this study, rather than individual taxa of corals or sponges. Biological structures ranged from small (~5 cm; resolution of video) tube worms, ophiuroids and sponges to large aggregations of corals and sponges (living and dead; Table F.2). A Microsoft Access 2007 database was used to store, query and relate the annotated video data.

Twelve biotopes (Fig. F.2) and six primary substrate classes were identified from the video analysis (Table F.2). The most common substrate observed was Sand, followed by Bedrock, with the other substrate types representing 23% of the surveyed area (Table F.3). Garden was the most frequent biotope followed by Worms, and epifauna was not observed in ca. 17% of the video data (Table F.3). Corals and sponges (represented by six biotopes) were observed in ~55% of video data (Table F.3). The most common corals were the gorgonian *Primnoa pacifica* (Fig. F.2K), and the hydrocoral *Stylaster* sp. (Fig. F.2D). Sea pens (Pennatulacea) and other corals were also observed but not considered a biotope due to their sparse frequency as observed in the videos. Demosponges and hexactinellid sponges were observed and although reef-forming species were present (e.g. *Heterochone calyx, Mycale bellabellensis*), no sponge reefs were observed. The two categories produce 72 possible combinations of variables, however, only 50 were observed to occur. Each biotope was observed on nearly all substrate types, except for Worms which was only observed on Fine sediment, and Ophiuroids and Dead sponges,

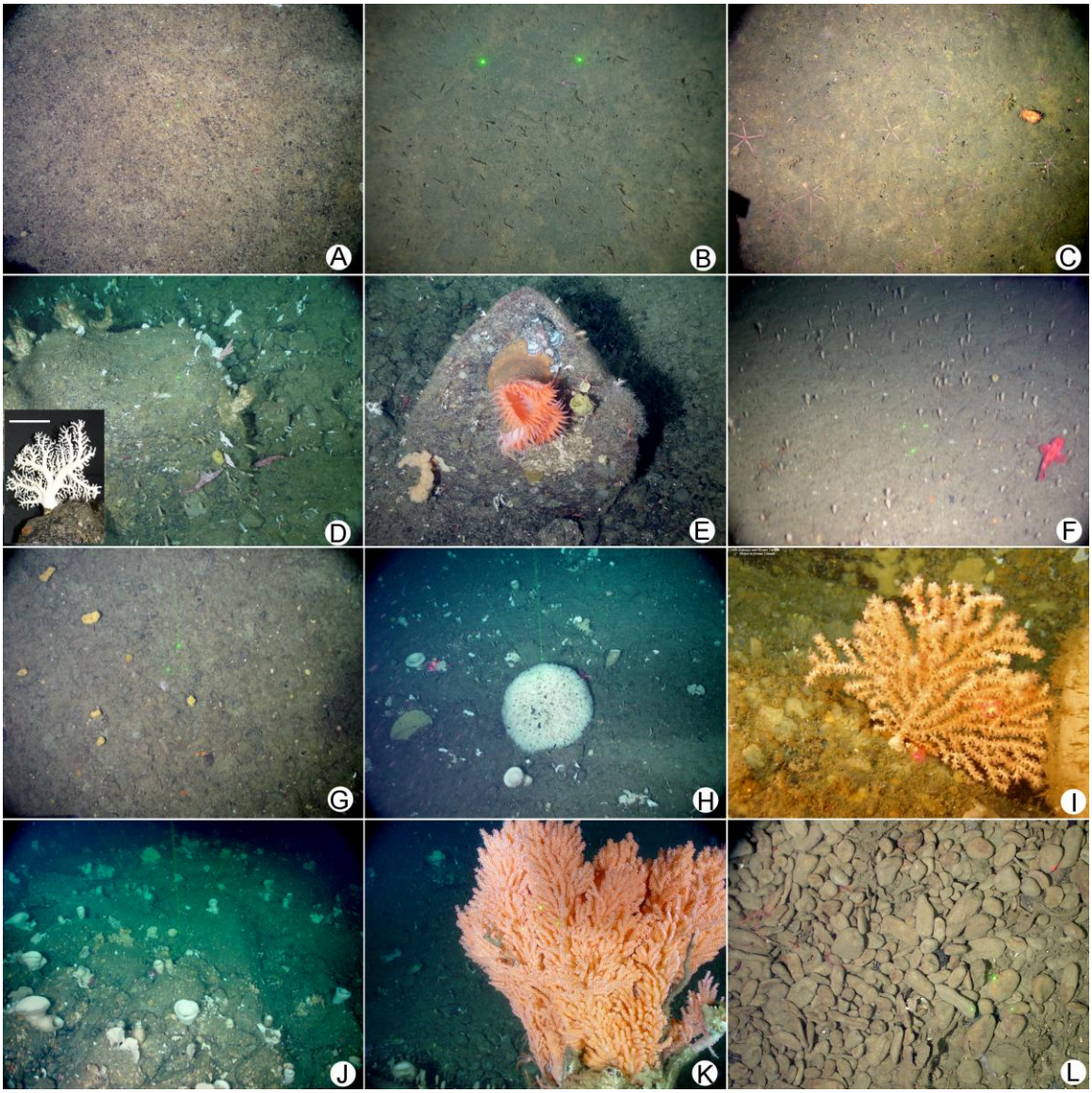

Figure F.2. Photo plate of the 12 biotopes identified from the video transects at Learmonth Bank. Refer to Table F.2 for biotope descriptions. (A) No epifauna; (B) Worms; (C) Ophiuroids; (D) *Stylaster*; (E) Filter-feeding; (F) Tubes; (G) Small sponges; (H) Large sponges; (I) *Calcigorgia*, (J) Garden; (K) *Primnoa*; (L) Dead sponges. Distance between green laser points is 10 cm. Scale in D is 5 cm.

Table F.3. Frequency of substrate types and biotopes at Learmonth Bank observed in the video transects. Refer to Table F.2 for biotope descriptions.

Substrates	**Counts**	**%**	**Biotopes**	**Counts**	**%**	**Biotopes**	**Counts**	**%**
Bedrock	15,267	30.65	No epifauna	7859	17.15	Sm. sponges	1990	4.03
Boulder	2612	5.24	Worms	9023	19.69	Lrg. sponges	5142	10.40
Cobble	4100	8.23	Ophiuroids	56	0.12	*Calci-gorgia*	1487	3.01
Pebble	4283	8.60	*Stylaster*	832	1.68	Garden	14,500	29.33
Sand	22,964	46.11	Filter-feeding	3049	6.65	*Primnoa*	1148	2.32
Fine	581	1.17	Tubes	657	1.43	Dead sponges	80	0.17
Totals	49,807	100					45,823	100

which were only observed on Sand (Table F.3). Dense accumulations of dead sponges occasionally forming piles over the seafloor were observed (Fig. F.2L). Due to their brownish color they were initially thought to be rocks, but when the ROV made a tentative to collect a sample the sponge was crushed, exposing the spicules.

2.3.2. Supervised classification of multibeam data

Slope values for each pixel covered by each substrate type and biotope observed in the video surveys were extracted from the bathymetry raster grid for the entire dataset using the GIS software ESRI® ArcMap™ 9.3. A supervised classification of the multibeam data was performed using exploratory data analysis (EDA) through IBM© SPSS® 20.0. A total of 25% of the points were randomly excluded and were used later for testing the accuracy of the adopted classification criteria (see section 2.3.5). Box-plots were produced to visualize the acoustic characteristics of the substrate types and biotopes observed in the videos. The inter-quartile ranges of bathymetry, backscatter, and slope for each class identified in the video analysis were calculated to generate the first iteration of

classification rules therefore used to produce the maps (after Copeland et al. (2011)). The first map produced had many unclassified areas; therefore the classification criteria of at least one acoustic variable for most of the classes were extended beyond the inter-quartile range. The criteria for choosing theses limits was based on (1) giving priority for corals and sponges and extending their ranges over other biotopes; (2) extending ranges based on values on cells that remained unclassified after using the inter-quartile range. These classification rules determined the range of depth, backscatter and slope values corresponding to a given class.

Using the MBES interval values designated through the classification criteria, individual map layers were created for each biotope and substrate class using ArcMap *raster calculator* tool. These individual layers were then overlapped to produce two single maps (one for biotopes and the other for substrates). In this study corals and sponges were prioritized over the other biotopes, meaning that where the depth, backscatter, and slope values for a pixel met the classification criteria for more than one biotope, the individual layers of coral and sponge biotopes were placed over the layers of the other biotopes. Similarly, rare biotopes and substrate classes were placed over the others.

The number of unclassified cells was determined using ArcMap tool *combine*, which by combining all the individual layers generated a single map containing all classes and combination of overlapped classes. From the attribute table created with this new map it was possible to determine how many cells remained unclassified.

2.3.3. Correspondence between physical substrate types and biotopes

A contingency table was constructed using the twelve biotopes (rows) and six primary substrate classes (columns; Table F.4) and input the frequency of occurrence using the 45,823 records. The correspondence analysis was performed using Smart Correspondence Analysis for a two-way frequency table (MYSTAT version 12). A Chi-square test was used to test for an association between the two factors. As a post-hoc test, the degree of association between each biotope and substrate class was quantified by calculating the distance between the variables using the correspondence analysis coordinates. After calculating the distance ("association") for each biotope–sediment pairing this value was standardized on a scale of 0.0 to 100.0; where 0.0 represents the largest distance between a pairing (i.e. the weakest association) and 100.0 represents an exact overlap (i.e. an exclusive association). From the quantified degree of association

Table F.4. Contingency table of the frequencies of biotopes and substrate types observed in the video transects at Learmonth Bank.

Biotope/ Substrate	**Bedrock**	**Boulder**	**Cobble**	**Pebble**	**Sand**	**Fine**	**Totals**
No epifauna	113	49	192	1542	5963	0	7859
Worms	0	0	3	55	8384	581	9023
Ophiuroids	0	0	0	0	56	0	56
Stylaster	9	26	76	27	694	0	832
Filter-feeding	180	66	50	37	2716	0	3049
Tubes	239	30	36	30	322	0	657
Sm. sponges	92	56	487	516	839	0	1990
Calcigorgia	524	221	718	0	24	0	1487
Lrg. sponges	2809	284	1038	549	462	0	5142
Garden	10,531	1682	1415	142	730	0	14,500
Primnoa	715	193	28	0	212	0	1148
Dead sponges	0	0	0	0	80	0	80
Totals	15,212	2607	4043	2898	20,482	581	45,823

Refer to Table F.2 for biotope descriptions.
χ^2=45,245, df=55.

finer details of the associations could be teased out, for instance: the stronger association when variables appeared equidistant in the correspondence plot.

The results from the correspondence analysis were used to produce a single map of biotopes based on both MBES data and substrate types. In ArcMap each individual biotope layer was combined to the two substrate types (1st and 2nd) that showed the strongest association with each biotope using the *combine* Spatial Analyst tool. For each biotope–substrates pairing a new individual map layer was generated, which were overlapped and a single biotope map produced, where both MBES and substrate types were used to define biotope distributions.

2.3.4. Quality assessment

Both ROV's navigational data were recorded every ±1 s interval. These databases were temporally related to the video annotation databases, and so provided the georeferencing for biotope and substrate data. The navigational data accuracy is determined by the summation of the ROV's navigational data accuracy (±1% of water depth, w.d) and the delay between the video and the navigational data collection (1–2 s delay or ±1.5 m; preliminary work and personal communication Ian Murdock, ROV technician), giving us an accuracy of ±2.2–6.5 m at the depths sampled (70–500 m).

The multibeam bathymetry latitudinal and longitudinal data is accurate to 1% of w.d. and its depth data accuracy is 0.3% of w.d. (per comm Vaughn Barrie and Kim Picard, Geological Survey of Canada). The resulting multibeam bathymetry data accuracy at the depths sampled is ±0.7–5 m for latitude and longitude and ±0.2–1.5 m for depth.

2.3.5. Accuracy and ambiguity analysis

A total of 25% of the points were excluded from the training dataset to test the accuracy of the classification criteria. From this dataset the number of points plotted in the appropriate cell in the final map was determined using Arc Map tool *select by attributes* and the number of points plotted in unclassified cells was determined using ArcMap tool *extract values to points*. The uniqueness of the classes was determined by calculating how many cells were classified as one, two or more classes simultaneously using Arc Map tool *combine* (described in Section 2.3.3); the binary attribute table generated from this procedure indicated the number of unique cells and cells simultaneously classified as more than one class.

2.3.6. Overall data accuracy assessment

In this study the confidence that the video data is georeferenced within the correct multibeam 5 m×5 m cell increases with decreasing depth. At this study's shallowest depths the summed accuracy is ±2.5 m and at the deepest it is ±10 m. The deeper samples are within the basin surrounding Learmonth where the bathymetry is quite homogenous. Within the basin, where the lowest accuracy could place the video data incorrectly into a neighboring cell, it is most probable neighboring cells have the similar, if not the same, bathymetric, backscatter, and slope characteristics, and should not affect the analysis.

Although the MBES survey was not conducted simultaneously to the video data, there is no literature to suggest major geological changes at Learmonth within the small temporal period between data collection. We therefore assume that the bathymetry of the Learmonth was not drastically altered during the time frame. Similarly, spatial position of

biotopes composed of sedentary organisms in the 5 m×5 m multibeam cells should not show much variation in this temporal lapse.

3. Results

3.1. Supervised classification of the multibeam data

The distribution of the acoustic data for the substrate classes showed some overlap, with slope being the variable that showed most overlap among the classes (Fig. F.3). Backscatter was the variable that best distinguished the substrate classes. Fine sediment and Sand were the classes showing the most distinct backscatter and bathymetry values, respectively (Fig. F.3). The distribution of bathymetry, backscatter and slope values for biotopes showed little variation among the classes, with bathymetry values showing the least overlap (Fig. F.4). Worms showed the highest ranges of backscatter, Filter-feeding of bathymetry and Garden of slope values (Fig. F.4).

From the analysis of box-plots and percentiles the classification rules for substrate types and biotopes were determined (Table F.5). Bathymetry values for the substrate class Fine sediment were not included in its classification rules because the bathymetric range over which this substrate was observed to occur as the primary substrate was too narrow (441.14 to 445.21 m; Fig. F.3); therefore its distribution was determined based on its characteristic low backscatter and slope values only.

3.2. Correspondence analysis

More than 45,000 records from the 2008–9 ROV surveys of Learmonth were included in the contingency table used for the correspondence analysis (Table F.4). The result

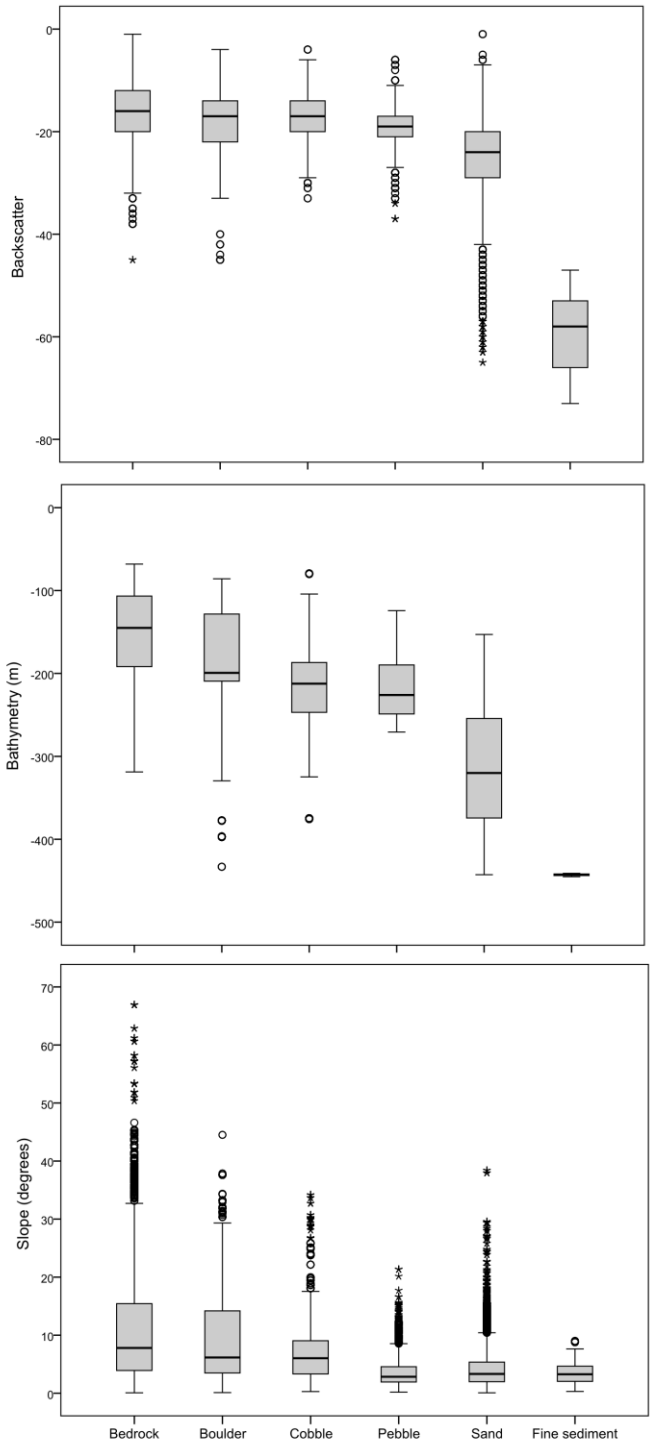

Figure F.3. Box-plots showing the distribution of backscatter, bathymetry and slope values for the six substrate types identified in the video transects at Learmonth Bank. The boxes represent the inter-quartile interval; circles represent outliers; stars represent extreme (far) outliers and horizontal lines in the box represent the median.

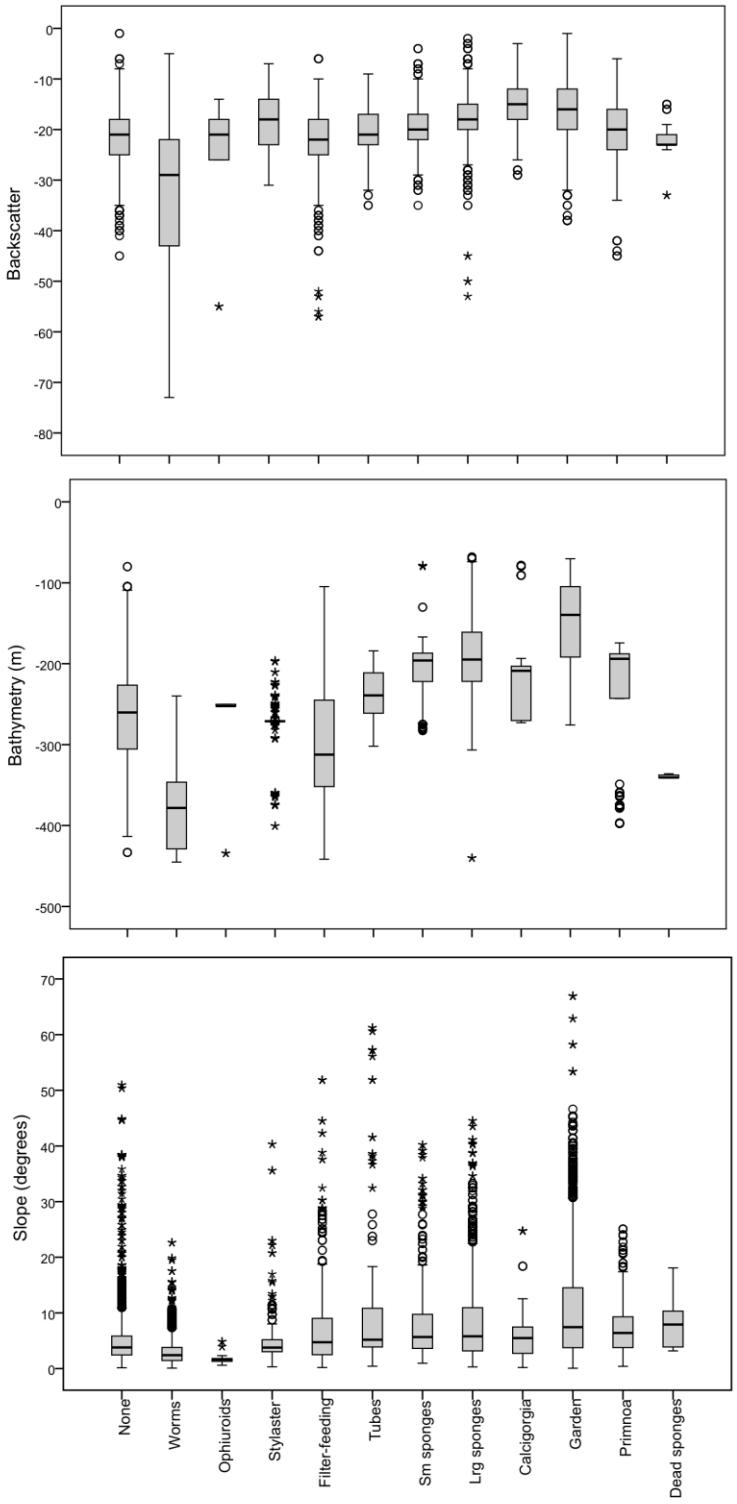

Figure F.4. Box-plots showing the distribution of backscatter, bathymetry and slope values for the twelve biotopes identified in the video transects at Learmonth Bank. The boxes represent the inter-quartile interval; circles represent outliers; stars represent extreme (far) outliers and horizontal lines in the box represent the median.

Table F.5. Classification criteria for substrates and biotopes at Learmonth Bank based on multibeam echosounder (MBES) and video data.

Category	Backscatter	Bathymetry (m)	Slope (degrees)
Substrates			
Bedrock	≥−20.00	≥ −226.49	≥1.40
Boulder	−26 to −10	−274.00 to −97.40	1.41 to 26.57
Cobble	−23 to −14	−272.87 to −176.3	1.83 to 13.57
Pebble	−25 to −15	−268.87 to −131.96	1.07 to 4.59
Sand	≤−16.00	−420.97 to −214.89	0.75 to 11.23
Fine sediment	≤ −49	any value	0.83 to 6.43
Biotopes			
No epifauna	−18 to −45	−198 to −384	2.44 to 5.84*
Worms	−22 to −57	≤ −300.02	0.49 to 3.8
Ophiuroids	−14 to −26	−250.15 to −252.55*	0.605 to 4.84
Stylaster	−10 to −23	−270.59 to −374.37	1.08 to 5.19
Filter−feeding	−18 to −25*	−121.9 to −419.54	1.24 to 9.01
Tubes	−13 to −23	−200.53 to −283.37	3.87 to 51.88
Sm. sponges	−13 to −22	−176.38 to −248.41	1.90 to 23.26
Calcigorgia	−7 to −18	−202.17 to −272.87	1.20 to 10.63
Lrg. sponges	−12 to −20	−106.48 to −246.41	1.28−10.96
Garden	−7 to −20	≥ −222.84	≥ 1.29
Primnoa	−8 to −29	−183.31 to −242.7	1.44–18.20
Dead sponges	−20.5 to −23*	−335.97 to −341.3	3.88–18.1

*Inter-quartile values. Refer to Table F.2 for biotope descriptions.

from the Chi square analysis showed a highly significant non-random association between the biotopes and substrate types (χ^2=45,245 and df=55, P<0.001; Table F.4). From the coordinate positions in the correspondence plot (Fig. F.5), it can be seen that the *Primnoa* biotope was associated with seafloor composed primarily of Bedrock and Boulder, Garden was associated with Bedrock, Large sponges were associated with Cobble and Boulder, *Calcigorgia* was associated with Cobble, Small sponges were associated with Pebble, and the remaining biotopes (Tubes, Filter-feeding, *Stylaster*,

Ophiuroids, Worms, None and Dead sponges) were associated with Sand. No biotope was closely associated with Fine sediments.

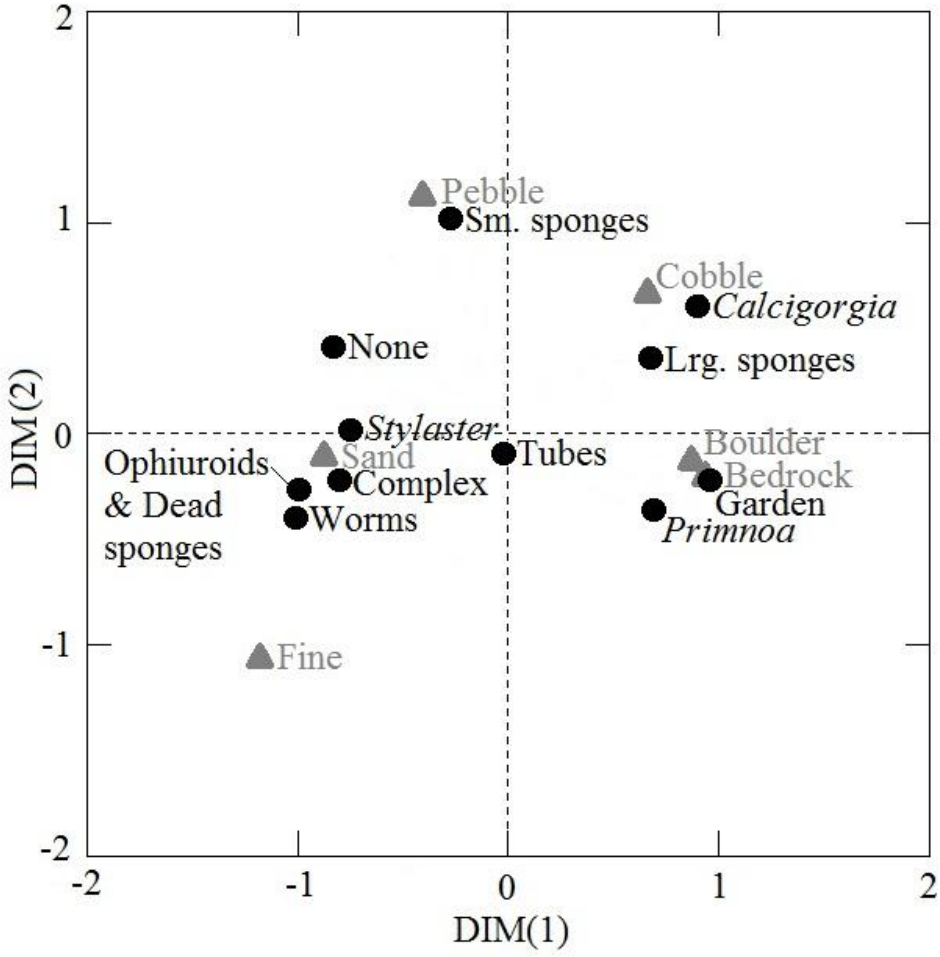

Figure F.5. Correspondence plot of the six substrate types (gray triangles) and 12 biotopes (black dots) observed in the video transects at Learmonth Bank.

From the quantified degree of association (Table F.6) the associations between the biotopes and substrate classes can be detailed: *Primnoa* was slightly more associated with seafloor composed primarily of Boulder than Bedrock, Large sponges were more associated with Cobble than Boulder, and the order of association of biotopes with Sand was as follows (most to least): Filter-feeding>*Stylaster*>Ophiuroids=Dead

sponges>Worms>None>Tubes. Of all the biotopes Worms were the most associated with Fine sediment.

Table F.6. Degree of association between each biotope and substrate class observed at Learmonth Bank; the scale ranges from 0.0 to 100.0, where 0.0 is least associated and 100.0 is an exclusive association.

Biotope/Substrate	**Bedrock**	**Boulder**	**Cobble**	**Pebble**	**Sand**	**Fine**
No epifauna	34.4	38.7	40.2	74.0	94.1	55.1
Worms	31.2	34.4	28.2	56.3	87.8	73.1
Ophiuroids	32.1	35.7	32.2	62.6	93.8	66.6
Stylaster	34.7	38.5	36.1	66.4	97.9	63.0
Filter-feeding	35.8	40.5	45.3	81.1	87.4	48.3
Tubes	42.1	45.8	41.4	66.5	92.4	62.4
Sm. sponges	38.7	44.4	65.4	87.1	57.1	18.9
Lrg. sponges	78.3	83.7	83.8	53.5	43.8	18.5
Calcigorgia	62.8	67.0	91.2	47.4	29.2	0.0
Garden	99.4	94.1	62.7	35.7	35.4	20.6
Primnoa	88.9	88.1	58.2	39.1	43.3	31.0
Dead sponge	32.1	35.7	32.2	62.6	93.8	66.6

Refer to Table F.2 for biotope descriptions.

3.3. Accuracy and ambiguity analysis

The accuracy analysis for the substrate types showed a good agreement between the multibeam data in the testing dataset and the classified data, with a total of 60% of the points correctly classified. Bedrock, Boulder and Fine sediment had the highest agreements (Table F.7; Fig. F.6). The general accuracy of the classification for the biotopes was weaker than that of the substrates, with 54% of the points correctly classified (Table F.7; Fig. F.7). It must be noticed that this high accuracy is mostly driven by *Primnoa* and Garden, which showed an accuracy of ~67% each. The biotope Filter-feeding had the lowest accuracy, with only 38% of the points correctly classified (Table F.7). No classes had more misclassified than correctly classified points (Table F.7).

Table F.7. Accuracy (%) of the classification criteria used for and substrates based biotopes on testing dataset containing 25% of the points. Refer to Table F.2 for biotopes descriptions.

	Correct	**Incorrect**	**Unclassified**
Substrate			
Bedrock	73.22	13.32	13.46
Boulder	64.59	26.12	9.29
Cobble	48.14	37.06	14.80
Pebble	52.09	40.80	7.12
Sand	53.10	22.69	24.21
Fine sediment	93.88	0.00	6.12
Biotope			
Ophiuroids	85.00	5.00	10.00
Calcigorgia	63.01	25.00	11.99
Dead sponges	55.56	0.00	50.00
Filter-feeding	38.34	28.33	33.33
Garden	67.33	12.79	19.88
No epifauna	45.38	37.76	16.86
Primnoa	67.82	27.34	4.84
Lrg. sponges	45.48	43.61	10.90
Sm. sponges	58.41	35.91	5.68
Stylaster	49.74	44.56	5.70
Tubes	43.31	38.22	18.47
Worms	49.27	24.04	26.69

Regarding the classification ambiguity for the substrates, 50.18% of the points were uniquely classified, with Sand being the major contributor for this result (41.68%) (Table F.8). A total of 15.89% of the points were simultaneously classified in two substrate classes and 27.21% of the points remained unclassified (Table F.8). The biotopes had a higher ambiguity than the substrate classes with up to eight classes simultaneously classified in the same cell, although only 12% of the points were classified in three or more classes (Table F.8). The class Worms had the strongest influence in the uniqueness of biotopes (Table F.8).

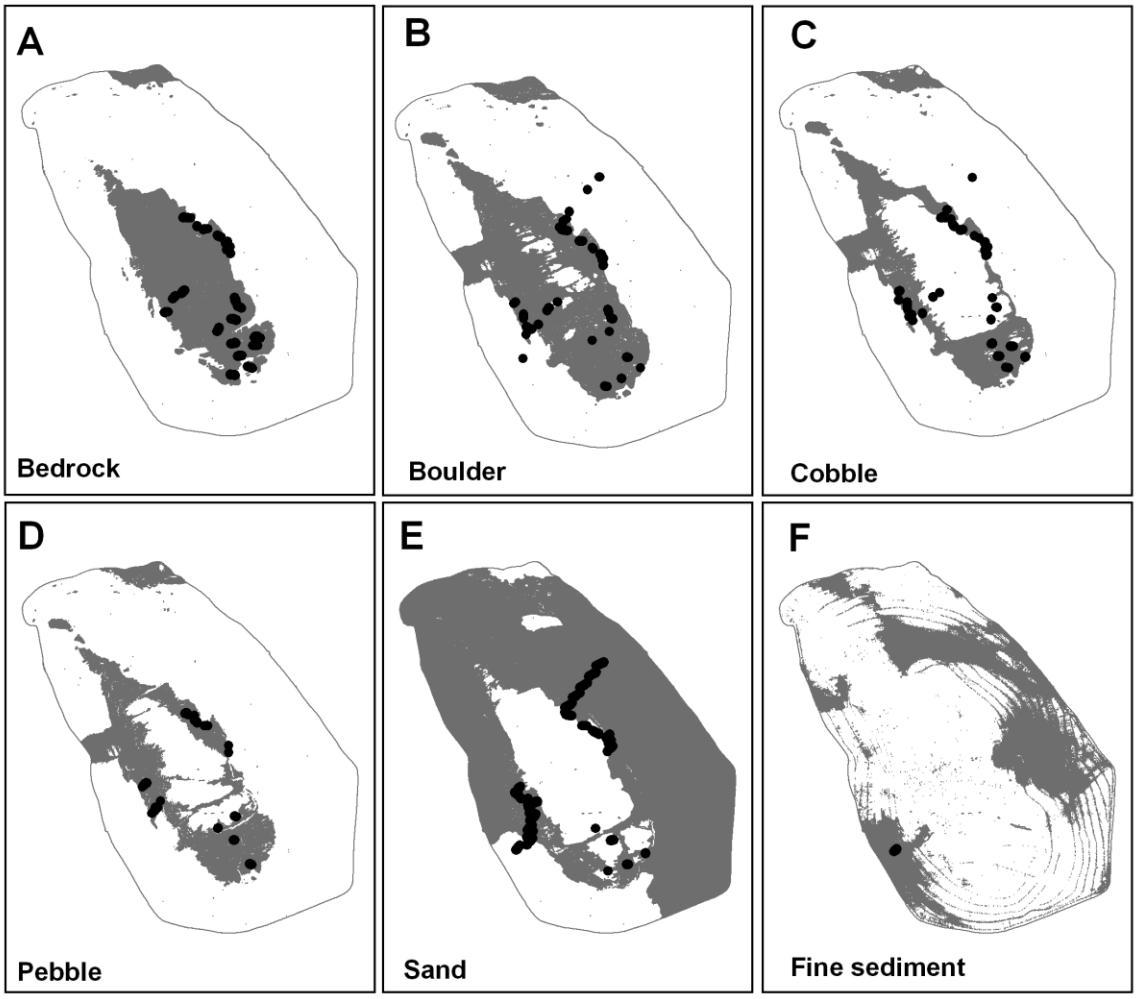

Figure F.6. Predicted individual distribution of substrate types at Learmonth Bank using bathymetry, backscatter and slope as proxies. Black dots in each map represent the corresponding substrate class as observed in the video transects using 25% of the data.

3.4. Predicted distribution of biotopes and substrate types within the multibeam surveyed area

The substrates map suggests Sand as the most frequent substrate type at Learmonth, occupying an area of 520 km^2, which can represent more than 50% of Learmonth area (Table F.9). The map shows Bedrock and Cobble distributed on the center of Learmonth with Cobble extrapolating to deeper areas. Pebble does not show a very clear pattern, being found in intermediate regions between hard and soft substrate types

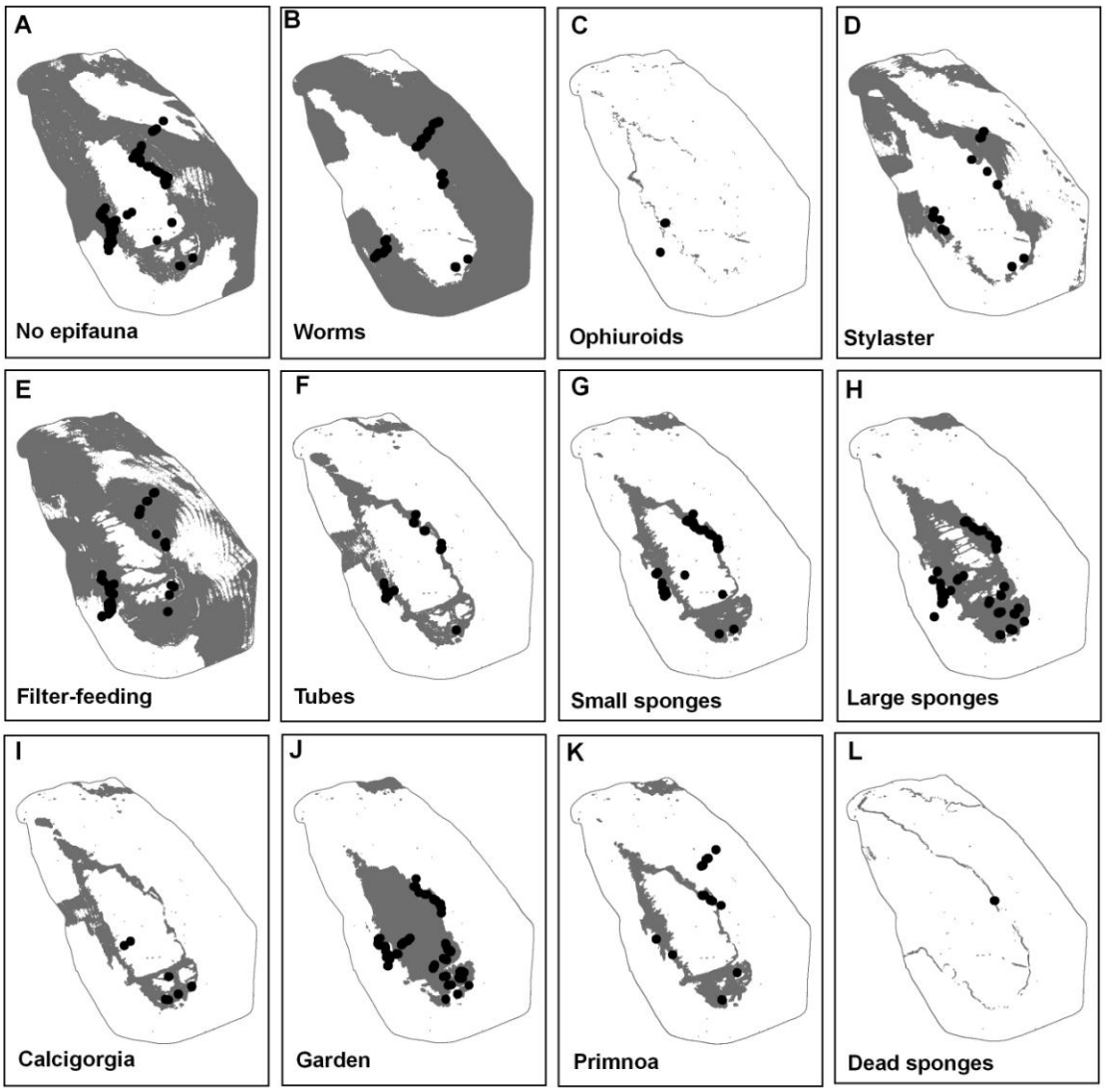

Figure F.7. Predicted individual distribution of biotopes at Learmonth Bank using bathymetry, backscatter and slope as proxies. Black dots in each map represent the correspondent class as observed in the video transects using 25% of the data.

(Figs. F.6, F.8A). Using the adopted classification criteria, the substrates map left 27% of Learmonth (~278 km^2) unclassified. Fine sediment was generally found in deep water, although its predicted distribution based upon low backscatter and low slope values

Table F.8. Uniqueness and ambiguity of the predicted substrate types and biotopes at Learmonth Bank. U%: percentage of uniquely classified points.

Substrate	**U%**	**Biotope**	**U%**	**Biotope**	**U%**
Bedrock	3.82	No epifauna	3.75	Sm. sponges	0.03
Boulder	2.67	Worms	30.83	Lrg. sponges	0.00
Cobble	0.0	Ophiuroids	0.02	*Calcigorgia*	0.54
Pebble	0.5	*Stylaster*	2.28	Garden	5.35
Sand	41.68	Filter-feeding	3.26	*Primnoa*	0.43
Fine sediment	1.51	Tubes	0.69	Dead sponges	0.01
Total unique	50.18	Total unique	47.20		
Two classes	15.89	Two classes	15.46		
Three or more	6.72	Three or more	12.02		
Unclassified	27.21	Unclassified	25.32		

Refer to Table F.2 for biotopes descriptions.

Table F.9. Distribution area of substrate types, coral and sponges at Learmonth Bank. MBES: Multibeam echosounder. Area is in km^2.

Substrates	**All**		**Unique**		**Biotopes**	**All**		**Unique**		**With substrate**	
	Area	**%**	**Area**	**%**		**Area**	**%**	**Area**	**%**	**Area**	**%**
Bedrock	142.90	13.98	62.52	6.12	*Primnoa*	76.01	7.44	8.78	0.86	45.61	4.46
Boulder	49.62	4.86	5.37	0.53	*Calcigorgia*	42.68	4.18	1.04	0.10	27.90	2.73
Cobble	96.53	9.45	13.63	1.33	*Stylaster*	84.14	8.24	9.31	0.91	42.79	4.19
Pebble	57.59	5.63	10.13	0.99	Garden	132.79	12.99	54.71	5.35	130.86	12.80
Sand	520.26	50.91	435.66	42.63	Sm. sponges	59.35	5.71	0.33	0.03	50.04	4.90
Fine	82.01	8.02	15.40	1.51	Lrg. sponges	83.11	8.12	0.16	0.02	65.74	6.43
Totals	948.90	92.85	542.71	53.10	**Totals**	460.49	45.06	74.33	7.27	342.01	33.47

Areas in the columns “All” and “With substrate” were calculated for each individual map, not taking into account the existence of overlap between cells of different classes. Refer to Table F.2 for biotope descriptions.

included local areas in shallower water than the actual depth observed in the videos (Figs. F.6, F.8A). These small areas are unevenly shaped depressions among dominantly bedrock or boulder substrates, where finer sediment could accumulate, protected from the influence of wave or current scour. Even though the distribution of Fine sediment

extrapolates the bathymetric range in which it was observed as primary substrate, in the video analysis Fine sediment as secondary substrate (data not shown) was observed from 182 to 445 m depth. When the calculations of substrate coverage were made using uniquely classified cells only, not much difference was observed for Sand while the other categories had their coverage area highly reduced, leading to an increase of unclassified areas (Table F.9).

Most of the biotopes were predicted to be distributed on Learmonth itself and around it, although Worms and No epifauna were mostly found on the deepest areas of the bank (the basin) where, according to the substrate map, Sand was the dominant substrate type (Figs. F.6, F.8A). Using the adopted classification criteria the biotopes map had 25.32% (~260 km^2) of unclassified areas. When the uniquely classified cells of corals and sponges were analyzed, the coverage area of these biotopes was greatly reduced, leading to a total coverage of ~74 km^2 or 7% of the Learmonth area (Table F.9).

Taking into consideration the area under dispute, the basin of Learmonth occupies the largest portion of disputed area, with Learmonth itself occupying approximately 26% of the disputed area (see Fig. F.1). Therefore, in the area under dispute the predicted dominant primary substrate is Sand, with Worms as the dominant biotope. On the other hand, looking at the bank itself Bedrock and Boulder are the dominant substrates within the shallower portions of the disputed area, with corals and sponges as the dominant biotopes (Fig. F.8).

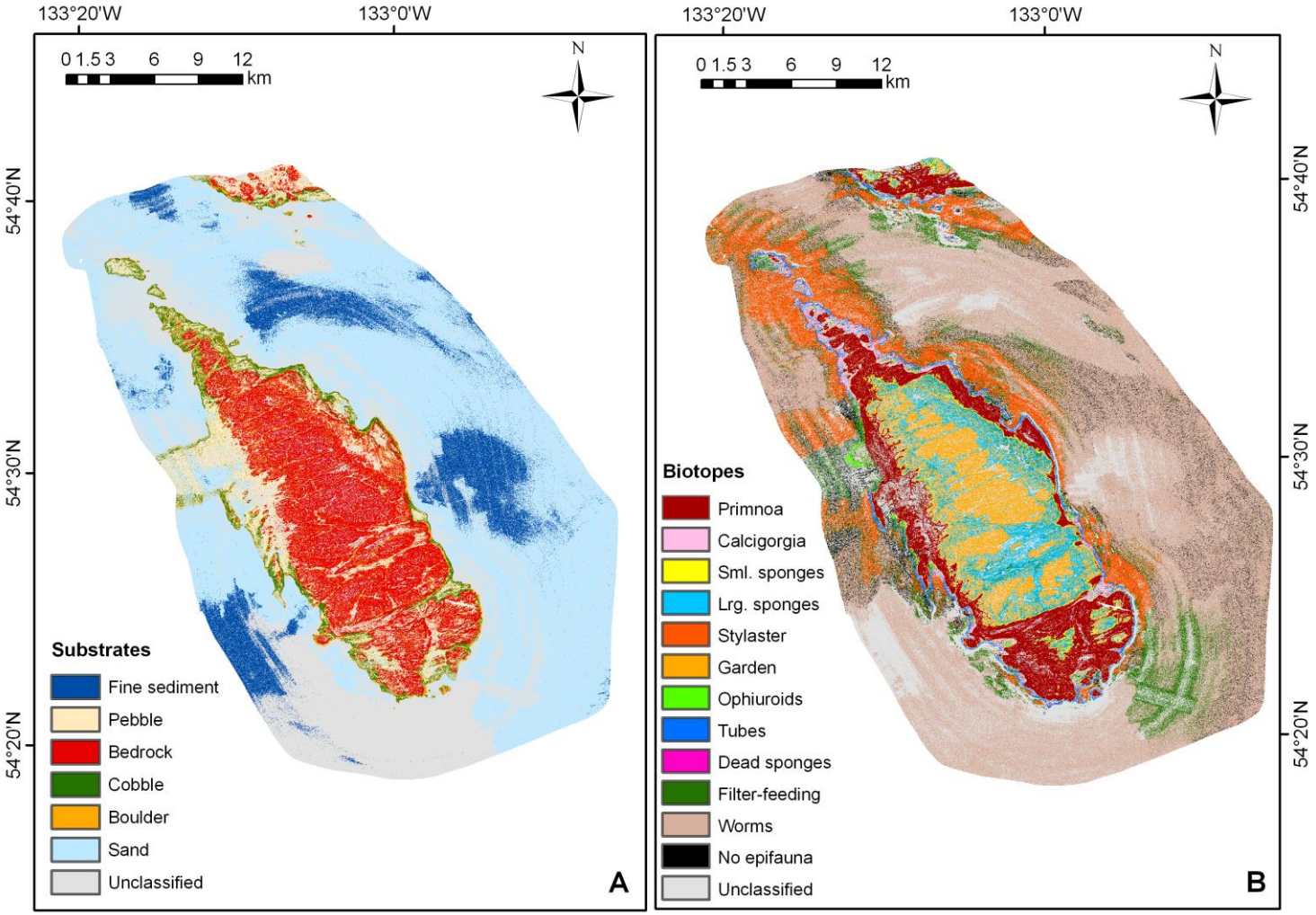

Figure F.8. Predicted distribution of substrate types (A) and biotopes (B) at Learmonth Bank using a combination of video data, backscatter, bathymetry and slope as proxies.

Based on the results from the correspondence analysis a map of biotopes distribution using MBES and the two substrate types most strongly associated to each biotope was generated (Fig. F.9). When the substrate types were added to determine biotope distributions the area classified as corals and sponges was reduced again, with exception of the class Garden, which showed a very similar area in both situations (see Table F.9).

4. Discussion

4.1. Using the inter-quartile range method to map biotopes and substrate types

The use of multibeam data for distinguishing substrate types is already well recognized (e.g. Collier and Brown, 2005 and Collins and Galloway, 1998). In this study Bedrock, Pebble, Sand, and Fine sediment could be readily distinguished using multibeam data, but Boulder and Cobble were not easily distinguished from each other using the adopted classification criteria. The high accuracy of the former substrates can be explained by their distinctive backscatter values: rougher/harder surfaces produce a stronger echo, while finer sediment classes and smoother bottoms absorb more sound (Harris and Baker, 2012). Whitmire et al. (2007) found accuracies varying from 40 to 73%, with mud and sand presenting the highest accuracies. Copeland et al. (2011), in the fjord example that produced the classification approach tested here, obtained an accuracy of 69% of the testing dataset for the substrate map. Conversely, Rooper and Zimmermann (2007) found that their worst classification rates were observed in substrate containing cobble. These authors suggest that the accuracy of sediment types may be compromised when using video to classify them. They found that 84% of their ground-trusted samples had larger

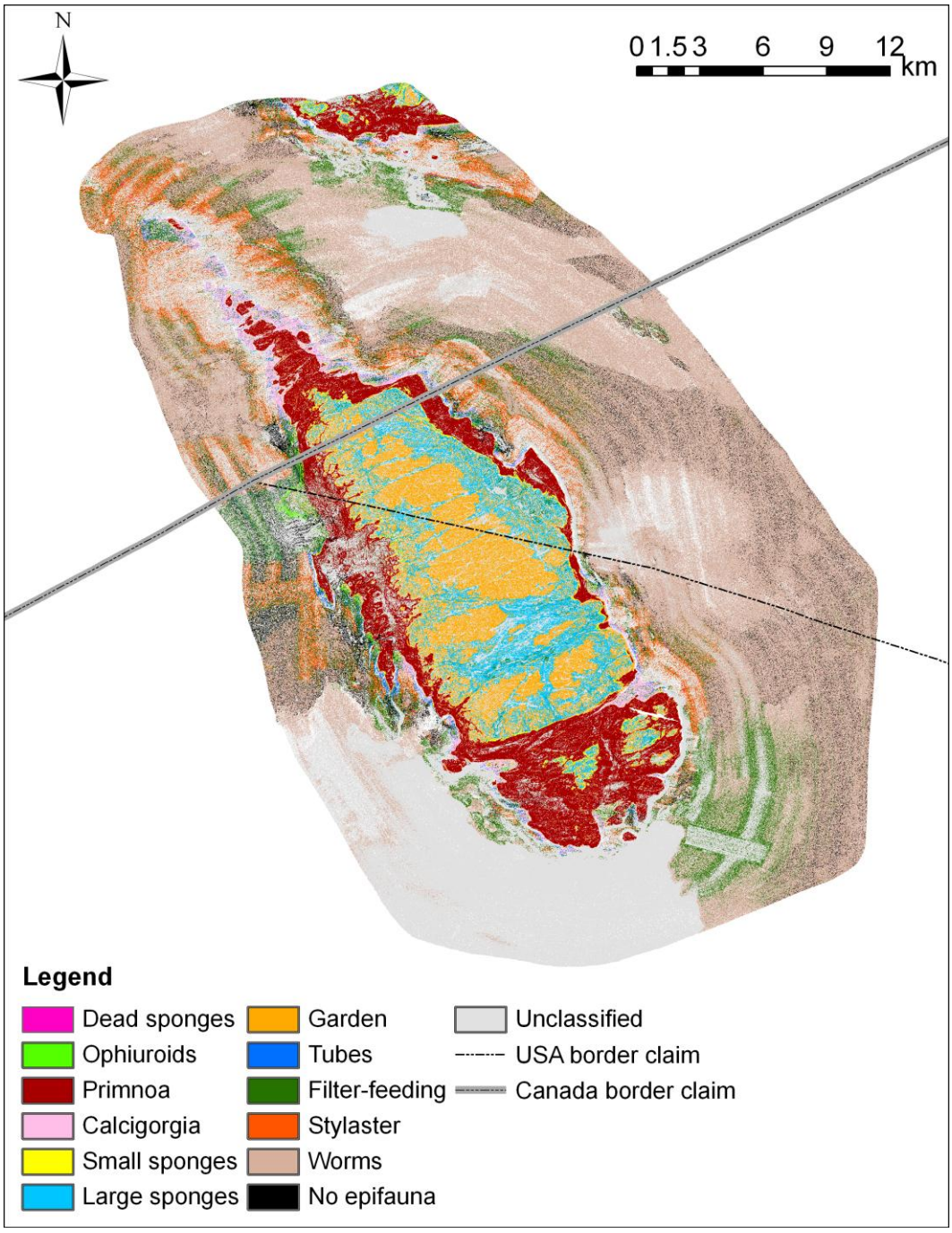

Figure F.9. Predicted distribution of biotopes at Learmonth Bank using a combination of video data, backscatter, bathymetry, slope and predicted substrate types as proxies. The triangular area at center-right experiences relatively little fishing, due to a border dispute between Canada and the USA.

mean grain size than that defined as sand (2 mm) using the video, meaning that most of this sediment could have been classified as gravel or pebble. Although sediment was not sampled for ground-truthing we feel confident about the visual identification of the grain sizes, in which sediment particles too fine to visually distinguish were classified as fine sediment (cf. Sameoto et al., 2008).

The use of multibeam data through the IQR method for determining the distribution of the biotopes identified in this study was more challenging than for substrate types. Backscatter, which is an important predictor of substrate types (Harris, 2012), showed high degrees of overlap between biotopes (see Fig. F.4), showing that most of the biotopes identified in this study did not present a distinctive acoustic signature (backscatter) that could be used to distinguish them from the surrounding environment. By contrast, biotopes that produce geological structures including cold-water coral reefs (Fosså et al., 2005 and Roberts et al., 2005), sponge reefs (Conway et al., 2005) and maerl beds (shallow water; Savini et al., 2012), tend to have characteristic bathymetric and backscatter signatures (Brown et al., 2011).

Bathymetry (i.e. depth) seemed to be the variable that best distinguished the biotopes, with Filter-feeding, Garden, No Epifauna and Worms presenting the most distinct values. Bathymetry is a key physical surrogate for benthic habitat, because a number of other variables are depth-dependent and these might have a direct influence on benthic organisms' diversity and distribution (Harris, 2012). This variable might have had an important influence on the accuracy of these biotopes, with exception of Filter-feeding, which presented a weak accuracy. Garden had the highest accuracy, followed by *Primnoa* and *Calcigorgia*. While the highest frequency of Garden along with its

distinctive bathymetric range could have had a positive impact on its accuracy, *Primnoa* and *Calcigorgia* might have been influenced by their increased range of values used in the classification criteria in relation to other biotopes (up to highest and lowest values).

We found a high ambiguity of pixels and therefore we could not detect distinct acoustic signatures for the biotopes identified in this study. The high ambiguity could be a response of the resolution used because biotopes were defined based on the number of individuals/colonies per m^2, while the multibeam cells have a resolution of 5 m×5 m (25 m^2); an area that size might support more than one biotope and substrate type within a single pixel. Another factor that could be influencing the high ambiguity for biotopes is the high number of classes (12). White et al. (2003) showed an important decrease in the accuracy of their biotope maps with increased resolution (number of classes): 85% at coarse resolution (three classes), and 28% at fine resolution (10 classes). Copeland et al. (2011) had 61% of the pixels uniquely classified on a study based on six substrate classes. Although one looks for the uniqueness of classes in order to produce a map, the ambiguity of biotopes and substrate types at the scale used in this study must be regarded as normal and even expected. The individual maps illustrate well this ambiguity and should not be disregarded when considering the distribution of biotopes and substrate types at Learmonth.

Slope is recognized as an important predictor of benthic habitat at intermediate to broad scales in the deep sea (Bryan and Metaxas, 2006, Bryan and Metaxas, 2007, Guinan et al., 2009, Harris and Baker, 2012,Rengstorf et al., 2012, Wilson et al., 2007, Woodby et al., 2009 and Yesson et al., 2012). In this study, slope alone was not

very useful for distinguishing biotopes at a local scale: all substrates and all biotopes had overlapping slope values, although Bedrock and Boulder showed a higher range of slope values than the other substrate types. Slope variation among biotopes was too small to distinguish most of the biotopes identified in this study, but each biotope has its own range of slope that mostly characterizes it. For example, although using the IQR method at Learmonth slope could not be used to distinguish the class *Primnoa* from all other biotopes, IQR slope values for *Primnoa* biotope at Learmonth (which comprises the species *Primnoa pacifica*) ranges from 3.7 to 9.3° (full range 1.44–18.2°, 5% to 95% percentiles, respectively) matched the broad-scale slope values for primnoid corals (not only the genus *Primnoa*) in the Pacific continental margin of North America, which ranged from 0 to 10.0° (Bryan and Metaxas, 2007). Bryan and Metaxas used slope as a proxy for coarse substrates (Metaxas and Bryan, 2007). Slope may be more useful as a predictor of local distributions for steep or near-vertical bedrock outcrops, which often host unique assemblages such as the solitary scleractinian *Desmophyllum dianthus* (Baker et al., 2012).

4.2. Distribution of biotopes and substrate types

The final biotopes and substrates maps showed a strong visual matching with the results of the correspondence analysis and the use of substrate as a surrogate for biotopes distribution (Harris, 2012) was statistically corroborated by the results of the correspondence analysis. Although most of the biotopes were observed on more than one substrate type (see Table F.4), the substrate types in this study represent the dominant, but not exclusive substrate. Corals and sponges were frequently observed on substrate dominated by sand, with cobbles, boulders, or bedrock as secondary substrates, while the

coral and sponge taxa included in this study were growing on a hard substrate (required for larvae settlement and subsequent growth). That the class *Stylaster* showed a strong association with Sand does not mean that these corals were growing on this substrate, but rather on a secondary hard substrate such as pebble or cobble since *Stylaster* larvae require a hard substrate for settlement and development (Cairns, 1986). Similarly, where the biotope *Primnoa* was observed on Sand, the corals were growing on cobbles or boulders, present as secondary substrates. Colonies of *Primnoa pacifica* (the main species in this biotope) at Learmonth can reach 2 m high (Du Preez and Tunnicliffe, 2011), limiting them to large hard substrate surfaces or particles such as bedrock, boulders and cobbles (Edinger et al., 2008, Edinger et al., 2011, Mortensen and Buhl-Mortensen, 2004 and Tunnicliffe and Syvitski, 1983). Other studies also showed gorgonians being recorded on sand and other soft substrates, where these organisms were assumed to have settled on a hard substrate amid the soft substrate (Bryan and Metaxas, 2006 and Mortensen et al., 2001). These results exemplify the limitations of using primary substrate only in marine habitat mapping: the attachment structure used by a coral or sponge might not be the dominant or even the secondary substrate in a particular location (Baker et al., 2012).

The influence of the substrate on the distribution of corals and sponges could also be observed when substrate types were also used as a classification criterion. The coverage area of Garden showed almost no reduction, probably reflecting again its high frequency and accuracy. As for the other sponges and coral biotopes, *Stylaster* was the class showing the highest difference, having its area reduced from 8.24 to 4.19% of the surveyed area. The reduced area of the *Stylaster* biotope is probably more accurate, more

closely matching the observed frequency of *Stylaster* in the video observations. The addition of substrate as a criterion on determining the distribution of biotopes can be seen as an effective filter for reducing ambiguous classifications, although it must be done carefully considering the limitations of using primary substrate only, as mentioned above. Dead sponges were found exclusively on Sand, which functions as a depositional substratum. Drifted accumulations of dead sponges were observed in a narrow bathymetric range, on sand, but near the boundary between bedrock and boulder substrates and finer substrates further from Learmonth itself. In the Dead sponges' individual map, the distribution of this biotope contours the predicted hard-substrate areas mostly composed of Bedrock (see Fig. F.6). Although current data were not included in this study, considering that at Learmonth bottom currents can reach more than 90 cm s^{-1} (Crawford and Thomson, 1991), it is plausible that strong bottom currents have an important influence on the transport of these sponges, which are then stopped by the physical barrier formed by the hard substrate.

Finally, distribution of three substrates on deep-water flat bottoms, Complex, Worms, and No epifauna, appear striped in the final biotope maps (Fig. F.8 and Fig. F.9) due to artifacts in the processing of the multibeam backscatter data (Hellequin et al., 2003). These artifacts do not affect the predicted distributions of the coral- and sponge-dominated biotopes in the rest of the map area.

Although the distribution of benthic organisms can be highly influenced by the type of substrate (e.g. Baker et al., 2012, Greene et al., 2011, Edinger et al., 2011 and Zajac et al., 2000), very often corals and sponges are not observed in areas with apparently suitable substrate (e.g. Brooke and Young, 2009 and Watanabe et al., 2009), likely due to the

influence of other environmental and biological factors that refrain colonization and/or growth in certain locations (e.g. Mortensen and Buhl-Mortensen, 2004, Mienis et al., 2007, Dullo et al., 2008, Roberts et al., 2009 and Wulff, 2012). Nevertheless, if on one hand the presence of suitable substrate is not a guarantee of the presence of an organism, on the other hand it can be used as a proxy to determine the suitability of a given location to the presence of certain organisms, since if environmental conditions are met but the required substrate is unavailable, colonization cannot occur. Therefore, although in this study the classification used resulted in low accuracies and high ambiguity for biotopes, the substrate types had more distinct acoustic signatures and better accuracies, implying that the multibeam data alone through the IQR method could be used to map substrate types, and then use substrate as a surrogate variable to help determining the highest probabilities of biotope distributions. However, the integration of ecological information with acoustic data on habitat mapping is a very important point that should not be ignored (Hewitt et al., 2004 and Stevens and Connolly, 2004), especially if the map is produced for management purposes.

4.3. Implications for MPA design

Although it was proposed that Learmonth should be recognized as a protected area (Ardron et al., 2007), it remains exploited and unprotected, with exception of the area under boundary dispute. The existing dispute could be seen as an opportunity for creating a trans-boundary MPA at Learmonth. Taking advantage of trans-boundary disputes to create MPA's has been suggested previously in several other regions of the world (e.g. Nilsson et al., 2012), and Canada and the USA have several examples of cross-border terrestrial parks (see Timothy, 1999).

Since the designation of an area as an effective MPA takes in consideration other factors than the protection of biodiversity (e.g. social and economic; Agardy, 2000), the results of this study can contribute to the final goal of protecting biodiversity of Learmonth. In a hypothetical situation where only a portion of Learmonth can be designated as MPA, unexplored areas in the bank itself and in the northern part of Learmonth should be considered for ground-truthing, considering the predicted high concentration of corals and sponges at these locations and its predicted hard substrate nature. Corals and sponges are emphasized here because their sessile nature and morphology make them particularly vulnerable to bottom trawling, whose consequences have been documented in by-catch data at Learmonth (e.g. Ardron et al., 2007). However, dominantly soft substrate areas should also be considered because often secondary substrates in dominantly soft bottom environments provide important habitat for corals and sponges. A MPA should include all the predicted distribution of the two most sensitive biotopes (*Primnoa*, Garden) and representation of all other biotopes to maximize habitat diversity within an eventual MPA (Nowlis and Friedlander, 2005 and Copeland et al., 2011). Although deep-sea corals and sponges are considered most sensitive to fishing impacts, other epibenthic organisms, living on hard and/or soft substrates, are also impacted by trawling and other fishing methods (Hutchings, 1990, Jones, 1992 and Thrush and Dayton, 2002). Action should be taken to prevent further fisheries damage to sponges and corals in the Learmonth area, rather than relying solely on the boundary dispute to “freeze the footprint” of fishing activities in the region (Reiser et al., 2013).

5. Conclusions

In the Learmonth Bank area, the inter-quartile ranges of backscatter, bathymetry and slope derived from multibeam sonar were effective in distinguishing bottom substrates. MBES-derived backscatter, bathymetry, and slope were much less effective for distinguishing biotopes directly than for substrates. A significant correspondence between substrate types and biotopes showed that substrate distributions were useful as surrogates for most biotope distributions. Because of the limitations of using dominant substrates only in the classification and the influence of other variables on biotope distribution, the use of substrates as a surrogate should be cautious, and should incorporate presence of subordinate hard substrates in dominantly soft-substrate environments. This study indicated the locations with the highest probabilities of corals and sponges distribution at Learmonth Bank, which gives directions for future management of this location. Our video analysis and map results on the distribution of corals, sponges, and other biotopes at Learmonth Bank will be useful to help managers in designing an international MPA for this region.

Acknowledgments

We thank the field team for data collection and advice, especially J. Boutillier and S. Davis (Chief Scientists), V. Tunnicliffe, J. Rose, J. Chu, H. Reiswig and J. Pegg. Personnel of the Canadian Scientific Submersible Facility, the Pacific Biological Station ROV department and the Canadian Coast Guard Ship (CCGS) *John P. Tully* and *Vector* aided field operations. Canadian Hydrographic multibeam bathymetry is courtesy of J.V. Barrie. Canadian Hydrographic Service, Geological Service of Canada,

Kim Picard for backscatter processing, Fisheries and Oceans Canada (ship time, 2009 data), Memorial University of Newfoundland, University of Victoria, NSERC. We thank David Mercer and Vincent Lecours for the help with ArcMap, Stephanie Robinson for the initial analyses of multibeam data and Jeff Reynolds for the video footage annotation. Research is sponsored by the Natural Sciences and Engineering Research Council (NSERC) through the Canadian Healthy Oceans Network, a university–government partnership dedicated to biodiversity science for the sustainability of Canada's three oceans.

Literature cited

Agardy, T., 2000. Information needs for marine protected areas: scientific and societal. Bull. Mar. Sci. 66, 875-888.

Althaus, F., Williams, A., Schlacher, T., Kloser, R., Green, M., Barker, B., Bax, N., Brodie, P., Hoenlinger-Schlacher, M., 2009. Impacts of bottom trawling on deep-coral ecosystems of seamounts are long-lasting. Mar. Ecol. Prog. Ser. 397, 279-294.

Anderson, T.J., Nichol, S.L., Syms, C., Przeslawski, R., Harris, P.T., 2011. Deep-sea bio-physical variables as surrogates for biological assemblages, an example from the Lord Howe Rise. Deep-Sea Res. II 58, 979-991.

Andrews, A.H., Cordes, E.E., Mahoney, M.M., Munk, K., Coale, K.H., Cailliet, G.M., Heifetz, J., 2002. Age, growth and radiometric age validation of a deep-sea, habitat-forming gorgonian (*Primnoa resedaeformis*) from the Gulf of Alaska. Hydrobiologia. 471, 101-110.

Aranha, R.S., Edinger, E.N., Layne, G.D., Piercy, G., 2014. Growth rate variation and potential paleoceanographic proxies in *Primnoa pacifica*: insights from high-resolution trace element microanalysis. Deep-Sea Res. II 99, 213–226.

Ardron, J.A., Jamieson, G.S., Hangaard, D., 2007. Spatial identification of closures to reduce the by-catch of corals and sponges in the groundfish trawl fishery, British Columbia, Canada. Bull. Mar. Sci. 81, 157-167.

Auster, P., 2005. Are deep-water corals important habitats for fishes?, in: Freiwald, A., Roberts, J.M., (Eds.), Cold-Water Corals and Ecosystems. Springer Berlin Heidelberg, pp. 747-760.

Ballantyne, V.A., Foreman, M.G.G., Crawford, W.R., Jacques, R., 1996. Three-dimensional model simulations for the north coast of British Columbia. Cont. Shelf Res. 16, 1655-1682.

Barrie, J.V., Bornhold, B.D., Conway, K.W., Luternauer, J.L., 1991. Surficial geology of the northwestern Canadian continental shelf. Cont. Shelf Res. 11, 701-715.

Barrie, J.V., Conway, K.W., 1999. Late Quaternary glaciation and postglacial stratigraphy of the Northern Pacific margin of Canada. Quatern. Res. 51, 113-123.

Brooke, S., Young, C., 2009. In situ measurement of survival and growth of *Lophelia pertusa* in the northern Gulf of Mexico. Mar. Ecol. Prog. Ser. 397, 153-161.

Brown, C.J., Smith, S.J., Lawton, P., Anderson, J.T., 2011. Benthic habitat mapping: A review of progress towards improved understanding of the spatial ecology of the seafloor using acoustic techniques. Estuar. Coast. Shelf Sci. 92, 502-520.

Bryan, T.L., Metaxas, A., 2006. Distribution of deep-water corals along the North American continental margins: Relationships with environmental factors. Deep-Sea Res. I 53, 1865-1879.

Bryan, T., Metaxas, A., 2007. Predicting suitable habitat for Paragorgiidae and Primnoidae on the Atlantic and Pacific continental margins of North America. Mar. Ecol. Prog. Ser. 330, 113-126.

Chu, J.W.F., Leys, S.P., 2010. High resolution mapping of community structure in three glass sponge reefs (Porifera, Hexactinellida). Mar. Ecol. Prog. Ser. 417, 97-113.

Cogan, C.B., Todd, B.J., Lawton, P., Noji, T.T., 2009. The role of marine habitat mapping in ecosystem-based management. ICES J. Mar. Sci. 66, 2033-2042.

Collier, J.S., Brown, C.J., 2005. Correlation of sidescan backscatter with grain size distribution of surficial seabed sediments. Mar. Geol. 214, 431-449.

Collins, W.T., Galloway, J.L., 1998. Seabed classification and multibeam bathymetry: tools for multidisciplinary mapping. Sea Technol. 39, 45-49.

Conway, K.W., Barrie, J.V., Krautter, M., 2005. Geomorphology of unique reefs on the western Canadian shelf: sponge reefs mapped by multibeam bathymetry. Geo-Mar. Lett. 25, 205-213.

Copeland, A., Edinger, E., Devillers, R., Bell, T., LeBlanc Philippe, Wroblewski, J., 2011. Marine habitat mapping in support of Marine Protected Area management in a subarctic fjord: Gilbert Bay, Labrador, Canada. J. Coast. Conserv., DOI: 10.1007/s11852-011-0172-1.

Costello, M., McCrea, M., Freiwald, A., Lundälv. T., Jonsson, L., Bett, B., Weering, T., Haas, H., Roberts, J., Allen, D., 2005. Role of cold-water *Lophelia pertusa* coral reefs as fish habitat in the NE Atlantic, in: Freiwald, A., Roberts, J.M., (Eds.), Cold-Water Corals and Ecosystems. Springer Berlin Heidelberg, pp. 771-805.

Courtney, R., Shaw, J., 2000. Multibeam bathymetry and backscatter imaging of the Canadian continental shelf. Geosci. Can. 27 (1), 31-42.

Crawford, W.R., Thomson, R.E., 1991. Physical oceanography of the western Canadian continental shelf. Cont. Shelf Res. 11, 669-683.

Danovaro, R., Gambi, C., Dell'Anno Antonio, Corinaldesi, C., Fraschetti, S., Vanreusel, A., Vincx, M., Gooday, A.J., 2008. Exponential decline of deep-sea ecosystem functioning linked to benthic biodiversity loss. Curr. Biol. 18, 1-8.

Davies, A.J., Guinotte, J., 2008. Predicting suitable habitat for the cold-water coral *Lophelia pertusa* (Scleractinia). Deep-Sea Res. I 55, 1048-1062.

Dolan, M.F.J., Grehan, A.J., Guinan, J.C., Brown, C., 2008. Modelling the local distribution of cold-water corals in relation to bathymetric variables: Adding spatial context to deep-sea video data. Deep-Sea Res. I 55, 1564-1579.

Du Preez, C., Tunnicliffe, V., 2011. Shortspine thornyhead and rockfish (Scorpaenidae) distribution in response to substratum, biogenic structures and trawling. Mar. Ecol. Prog. Ser. 425, 217-231.

Dullo, W.C., Flögel, S., Rüggeberg, A., 2008. Cold-water coral growth in relation to the hydrography of the Celtic and Nordic European continental margin. Mar. Ecol. Prog. Ser. 371, 165-176.

Edinger, E.N., Boutillier, J., Workman, G., 2008. Coral distributions around Learmonth Bank, Northern British Columbia, Canada: influence of surficial geology and tidal currents. In: Proceedings of the Fourth International Symposium on Deep-Sea Corals, Wellington, New Zealand, abstracts, p. 98.

Edinger, E.N., Sherwood, O.A., Piper, D.J.W., Wareham, V.E., Baker, K.D., Gilkinson, K.D., Scott, D.B., 2011. Geological features supporting deep-sea coral habitat in Atlantic Canada. Cont. Shelf Res. 31, S69-S84.

Ehrlich, H., 2010. Biological materials of marine origin: invertebrates. Springer, Dordrecht.

Fössa, J., Lindberg, B., Christensen, O., Lundalv, T., Svellingen, I., Mortensen, P., Alvsvag, J., 2005. Mapping of *Lophelia* reefs in Norway: experiences and survey methods. Springer-Verlag Berlin, Berlin; Heidelberger Platz 3, D-14197 Berlin, Germany.

Gonzalez-Mirelis, G., Lindegarth, M., 2012. Predicting the distribution of out-of-reach biotopes with decision trees in a Swedish marine protected area. Ecological Applications. 22, 2248-2264.

Gray, D.H. 1997. Canada's unresolved maritime boundaries. IBRU Boundary Security Bull Autumn 1997, 61-71.

Greene, G.H., O'Connell V. M., Brylinsky, C.K., 2011. Tectonic and glacial related seafloor geomorphology as possible demersal shelf rockfish habitat surrogates—Examples along the Alaskan convergent transform plate boundary. Cont. Shelf Res. 31, S39-S53.

Guinan, J., Grehan, A.J., Dolan, M.F.J., Brown, C., 2009. Quantifying relationships between video observations of cold-water coral cover and seafloor features in Rockall Trough, west of Ireland. Mar. Ecol. Prog. Ser. 375, 125-138.

Hall–Spencer, J., Allain, V., Fosså, J.H., 2002. Trawling damage to Northeast Atlantic ancient coral reefs. Proc. R. Soc. Lond. B. 269, 507-511.

Harris, P.T., Baker, E.K., 2012. Why map benthic habitats?, in: Peter T. Harris, Elaine K. Baker. Seafloor geomorphology as benthic habitat. Elsevier, London, pp. 3-22.

Heifetz J., Stone R.P., Shotwell, S.K., 2009. Damage and disturbance to coral and sponge habitat of the Aleutian Archipelago. Mar. Ecol. Prog. Ser. 397, 295-303.

Hetherington, R., Barrie, J.V., Reid, R.G.B., MacLeod, R., Smith, D.J., 2004. Paleogeography, glacially induced crustal displacement, and Late Quaternary coastlines on the continental shelf of British Columbia, Canada. Quat. Sci. Rev. 23, 295-318.

Hewitt, J.E., Thrush, S.F., Legendre, P., Funnell, G.A., Ellis, J., Morrison, M., 2004. Mapping of marine soft-sediment communities: integrated sampling for ecological interpretation. Ecol. Appl. 14, 1203-1216.

Hogg, M.M., Tendal, O.S., Conway, K.W., Pomponi, S.A., van Soest, R.W.M., Gutt, J., Krautter, M., Roberts, J.M., 2010. Deep-sea sponge grounds: reservoirs of biodiversity. UNEP-WCMC Biodiversity Series No. 32. UNEP-WCMC, Cambridge, UK.

Huang, Z., Brooke, B., Li, J., 2011. Performance of predictive models in marine benthic environments based on predictions of sponge distribution on the Australian continental shelf. Ecological Informatics. 6, 205-216.

Hutchings, P., 1990. Review of the effects of trawling on macrobenthic epifaunal communities. Mar. Freshwat. Res. 41, 111-120.

Jones, J.B., 1992. Environmental impact of trawling on the seabed: A review. N.Z.J. Mar. Freshwat. Res. 26, 59-67.

Kenny, A. J., Cato, I., Desprez, M., Fader, G., Schüttenhelm, R. T. E., Side, J., 2003. An overview of seabed-mapping technologies in the context of marine habitat classification. ICES J. Mar. Sci. 60, 411-418, doi:10.1016/S1054–3139(03)00006-7.

Kostylev, V.E., Todd, B.J., Gordon, B.J.F., Courtney, R.C., Gordon, D.M.C., Pickrill, R.A., 2001. Benthic habitat mapping on the Scotian Shelf based on multibeam bathymetry, surficial geology and sea floor photographs. Mar. Ecol. Prog. Ser. 219, 121-137.

Metaxas, A., Bryan, T., 2007. Predictive habitat model for deep gorgonians needs better resolution: reply to Etnoyer & Morgan. Mar. Ecol. Prog. Ser. 339: 313-314.

Mienis, F., de Stigter, H.C., White, M., Duineveld, G., de Haas, H., van Weering, T.C.E., 2007. Hydrodynamic controls on cold-water coral growth and carbonate-mound development at the SW and SE Rockall Trough Margin, NE Atlantic Ocean. Deep-Sea Res. I 54, 1655-1674.

Mortensen, P.B., Buhl-Mortensen, L., 2004. Distribution of deep-water gorgonian corals in relation to benthic habitat features in the Northeast Channel (Atlantic Canada). Mar. Biol. 144, 1223-1238.

Mortensen, P.B., Hovland, T., Fosså, J.H., Furevik, D.M. 2001. Distribution, abundance and size of *Lophelia pertusa* coral reefs in mid Norway in relation to seabed characteristics. J. Mar. Biol. Assoc. UK., 81, 581-597, doi:10.1017/S002531540100426X.

Nilsson, H., Povilanskas, R., Stybel, N. 2012. Transboundary management of Transitional Waters - Code of conduct and good practice examples. Coastline Reports 19, ISSN 0928-2734, ISBN 978-3-939206-04-0. Available at: http://www.eucc-d.de/coastline-reports-19-2012.html

Pickrill, R.A., Todd, B.J., 2003. The multiple roles of acoustic mapping in integrated ocean management, Canadian Atlantic continental margin. Ocean & Coast. Manag. 46, 601-614.

Rengstorf, A.M., Grehan, A., Yesson, C., Brown, C., 2012. Towards high-resolution habitat suitability modeling of vulnerable marine ecosystems in the deep-sea: resolving terrain attribute dependencies. Mar. Geod. 35, 343-361.

Reiser, A., Watlint, L., Guinotte, J., 2013. Trawl fisheries, catch shares, and the protection of benthic marine ecosystems: has ownership generated incentives for seafloor stewardship? Marine Policy 40: 75-83.

Roberts, J.M., Brown, C.J., Long, D., Bates, C.R., 2005. Acoustic mapping using a multibeam echosounder reveals cold-water coral reefs and surrounding habitats. Coral Reefs. 24, 654-669.

Roberts, J.M., Wheeler, A., Freiwald, A., Cairns, S. 2009. Cold-water corals: the biology and geology of deep-sea coral habitats. Cambridge University Press, Cambridge, UK; New York.

Rooper, C.N., Zimmermann, M., 2007. A bottom-up methodology for integrating underwater video and acoustic mapping for seafloor substrate classification. Cont. Shelf Res. 27, 947-957.

Ross, R.E., Howell, K.L., 2012. Use of predictive habitat modelling to assess the distribution and extent of the current protection of "listed" deep-sea habitats. Divers. Distrib., 1-13.

Sameoto J.A., Lawton P, Strong M.B., 2008. An approach to the development of a relational database and GIS applicable scheme for the analysis of video-based surveys of benthic habitats. Can. Tech. Rep. Fish. Aquat. Sci. 2818.

Savini, A., Basso, D., Bracchi, V. A., Corselli, C., Pennetta, M., 2012. Maerl-bed mapping and carbonate quantification on submerged terraces offshore the Cilento peninsula (Tyrrhenian Sea, Italy). Geodiversitas 34 (1), 77-98. http://dx.doi.org/105252/g2012n1a5

Sherwood, O.A., Heikoop, J.M., Scott, D.B., Risk, M.J., Guilderson, T.P., McKinney, R.A., 2005. Stable isotopic composition of deep-sea gorgonian corals *Primnoa* spp.: a new archive of surface processes. Mar. Ecol. Prog. Ser. 301, 135-148.

Sherwood, O.A., Lehmann, M.F., Schubert, C.J., Scott, D.B., McCarthy, M.D., 2011. Nutrient regime shift in the western North Atlantic indicated by compound-specific $\delta^{15}N$ of deep-sea gorgonian corals. Proc. Natl. Acad. Sci. 108, 1011-1015.

Sinclair, A.F., Conway, K.W., and Crawford, W.R., 2005. Associations between bathymetric, geologic and oceanographic features and the distribution of the British Columbia bottom trawl fishery. ICES CM 2005/L:25 Available at: www.ices.dk/products/CMdocs/2005/L/L2505.pdf

Stevens, T., Connolly, R., 2004. Testing the utility of abiotic surrogates for marine habitat mapping at scales relevant to management. Biol. Conserv. 119, 351-362.

Sundar, V.C., Yablon, A.D., Grazul, J.L., Ilan, M., Aizenberg, J., 2003. Fibre-optical features of a glass sponge. Nature. 424, 899-900.

Thomson, R.E., 1981. Oceanography of the British Columbia coast. Canadian Special Publication of Fisheries and Aquatic Sciences 56, National Research Council, Ottawa, 291 pp.

Thrush, S.F., Dayton, P.K., 2002. Disturbance to marine benthic habitats by trawling and dredging: implications for marine biodiversity source. Annu. Rev. Ecol. Syst. 33, 449-473.

Timothy, D.J., 1999. Cross-border partnership in tourism resource management: international parks along the US-Canada border. J. Sustain. Tour. 7, 182-205.

Tittensor, D.P., Baco, A.R., Brewin, P.E., Clark, M.R., Consalvey, M., Hall-Spencer, J., Rowden, A.A., Schlacher, T., Stocks, K.I., Rogers, A.D., 2009. Predicting global habitat suitability for stony corals on seamounts. J.Biogeogr. 36, 1111-1128.

Tong, R., Purser, A., Unnithan, V., Guinan, J., 2012. Multivariate statistical analysis of distribution of deep-water gorgonian corals in relation to seabed topography on the Norwegian margin. PLoS One. 7, e43534.

Tunnicliffe, V., Syvitski, J.P.M., 1983. Corals Move Boulders: An unusual mechanism of sediment transport. Limnol. Oceanogr. 28, 564-568.

Wassenberg, T.J., Dews, G., Cook, S.D., 2002. The impact of fish trawls on megabenthos (sponges) on the north-west shelf of Australia. Fish. Res. 58, 141-151.

Watanabe, S., Metaxas, A., Sameoto, J., Lawton, P., 2009. Patterns in abundance and size of two deep-water gorgonian octocorals, in relation to depth and substrate features off Nova Scotia. Deep-Sea Res. I 56, 2235-2248.

Watling, L., Norse, E.A., 1998. Disturbance of the seabed by mobile fishing gear: a comparison to forest clearcutting. Conserv. Biol. 12, 1180-1197.

Wentworth, C.K., 1922. A scale of grade and class terms for clastic sediments. J. Geol. 30, 377-392.

White, W.H., Harborne, A.R., Sotheran, I.S., Walton, R., Foster-Smith, R., 2003. Using an acoustic ground discrimination system to map coral reef benthic classes. Int. J. Remote Sens. 24, 2641-2660.

Whitmire, C.E., Embley, R.W., Wakefield, W.W., Merle, S.G., Tissot, B.N., 2007. A quantitative approach for using multibeam sonar data to map benthic habitats, in: Todd, B.J., Greene, H.G. (Eds.), Mapping the Seafloor for Habitat Characterization. Geol. Assoc. Can., Special Paper 47, pp. 111-126.

Wilson, M.F.J., O'Connell Brian, Brown, C., Guinan, J.C., Grehan, A.J., 2007. Multiscale terrain analysis of multibeam bathymetry data for habitat mapping on the continental slope. Mar. Geod. 30, 3-35.

Wulff, J., 2012. Advances in sponge science: phylogeny, systematics, ecology ecological interactions and the distribution, abundance, and diversity of sponges. Adv. Mar. Biol., 273-344.

Yesson, C., Taylor, M.L., Tittensor, D.P., Davies, A.J., Guinotte, J., Baco, A., Black, J., Hall-Spencer, J.M., Rogers, A.D., 2012. Global habitat suitability of cold-water octocorals. J. Biogeogr. 39, 1278-1292.

Zajac, R.N., Lewis, R.S., Poppe, L.J. et al (2000) Relationships among sea-floor structure and benthic communities in Long Island Sound at regional and benthoscape scales. J. Coastl. Res. 16:627–640.